UNIVERSIDAD COMPLUTENSE DE MADRID

FACULTAD DE CIENCIAS FÍSICAS

DEPARTAMENTO DE ASTROFÍSICA Y CIENCIAS DE LA ATMÓSFERA

TESIS DOCTORAL

Simulating the impact of the 11 year solar cycle on climate

MEMORIA PARA OPTAR AL GRADO DE DOCTOR

PRESENTADA POR

Gabriel Chiodo

Directores

Ricardo García Herrera
Natalia Calvo Fernández

Madrid, 2014

UNIVERSIDAD COMPLUTENSE DE MADRID
Facultad de Ciencias Físicas
Departamento de Astrofísica y Ciencias de la Atmósfera

Simulating the impact of the 11 year solar cycle on climate

Tesis doctoral

Gabriel Chiodo

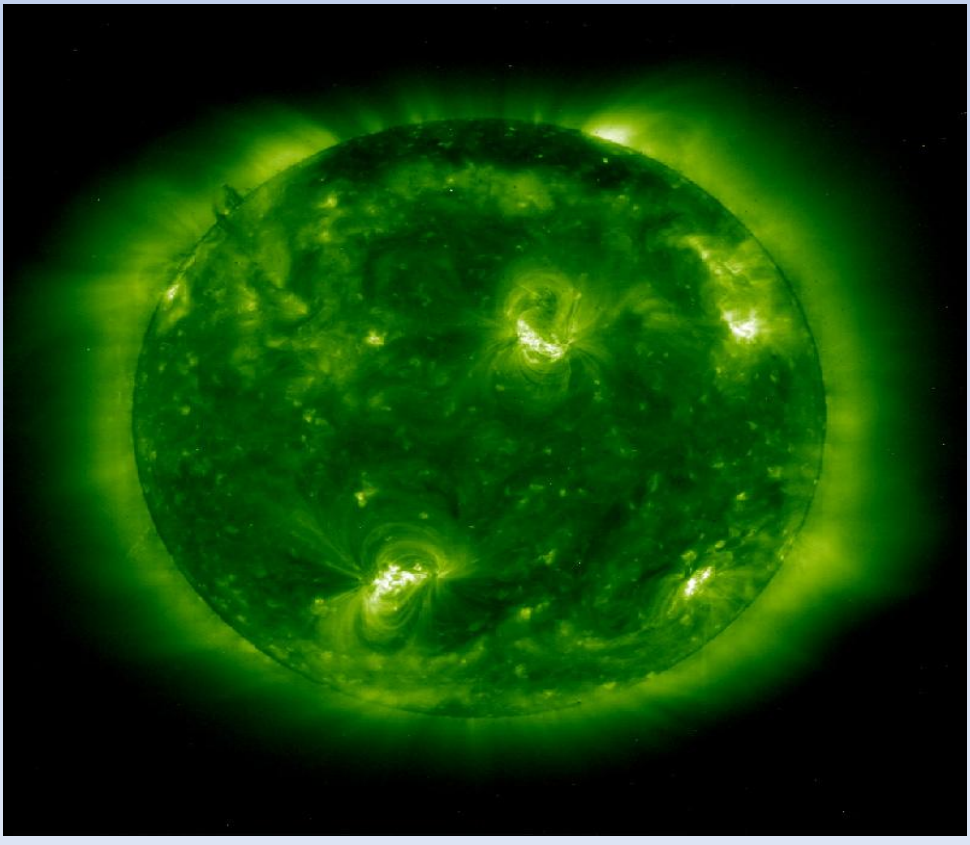

Madrid, 2014

UNIVERSIDAD COMPLUTENSE DE MADRID

DEPARTAMENTO DE ASTROFÍSICA Y CIENCIAS DE LA ATMÓSFERA

Tesis Doctoral

Gabriel Chiodo

Simulating the impact of the 11 year solar cycle on climate

Dirigida por:

RICARDO GARCÍA HERRERA
NATALIA CALVO FERNÁNDEZ

Ricardo García Herrera, Profesor Catedrático del Departamento de Astrofísica y Ciencias de la Atmósfera de la Universidad Complutense de Madrid y Natalia Calvo Fernández, Profesora Titular del Departamento de Astrofísica y Ciencias de la Atmósfera de la Universidad Complutense de Madrid

CERTIFICAN:

Que la presente memoria “Simulating the impact of the 11 year solar cycle on climate” ha sido realizada bajo nuestra dirección en el Departamento de Astrofísica y Ciencias de la Atmósfera de la Facultad de Ciencias Físicas de la Universidad Complutense de Madrid por D. Gabriel Chiodo y que constituye su tesis para optar al grado de Doctor en Ciencias Físicas.

Y para que conste, firman la presente certificación en Madrid, a 29 de Agosto de 2014

Prof. Dr. Ricardo García Herrera

Prof. Dra. Natalia Calvo

A mio padre, Luciano,
per avermi insegnato a inseguire i miei sogni.

Your guiding hand on my shoulder will remain with me forever.

Acknowledgments

Foremost, I am deeply grateful to my supervisors, Ricardo and Natalia for their enduring support, guidance, encouragement and invaluable advise throughout the research and writing of this thesis.

I wish to manifest a special thank to Daniel Marsh, who has hosted me during my visits at NCAR in Boulder (CO), USA. His suggestions and discussions have greatly contributed to the quality and contents of this work.

I would also want to express my gratitude to Hauke Schmidt and Katja Matthes, who gave me the opportunity of visiting them at MPI in Hamburg and GFZ in Berlin. Together with Kunikho Kodera, they have shown great interest in my research and provided insightful comments.

I thank my fellow labmates in the STREAM research group in Madrid and, particularly, David Barriopedro. I have also benefited from fruitful discussions with them.

I acknowledge the Spanish Ministry of Education for the FPU PhD fellowship, and the CONSOLIDER project for my funding during the first year. I also thank the Barcelona Supercomputing Center, CENITS, CESGA and the Moncloa cluster of excellence for the extensive computing resources, which have been provided to me to carry out the model simulations on different supercomputers across the country.

I would also like to acknowledge the European COST Action ES1005 for providing travel grants, through which I could attend many conferences, where I had the chance to share and discuss my results with scientists from all over Europe.

Last but not least, a very special mention goes to my mother Tiziana and my brother Ivan, for the unconditional support they have provided me through my entire life and remarkably, to my beloved wife Eva, who has been standing by my side through the good and the bad times with love and patience. Also a final thank goes to all relatives and friends in Madrid, Bolzano and elsewhere, who were always there to cheer me up.

Without the encouragement from the persons mentioned above, none of this would have been possible.

Contents

1 Introduction

1.1 Background

The solar radiation is the primary source of energy for the climate system. The pole-to-equator temperature gradient, which is maintained by differential absorption of solar radiation, is the driving force for Atmosphere dynamics and the general circulation. Accordingly, variations in solar activity can exert a great influence on the Earth's climate. Assessing the impact of solar variability on climate is a crucial step in the task of understanding natural and anthropogenic forced climate variability and change.

The most useful variable to determine the forcing exerted by solar variability on climate is the total solar irradiance (hereafter TSI); i.e., the spectrally integrated shortwave energy flux density in units W/m^2 reaching the top of the atmosphere. Fig. 1 shows the evolution of the TSI sampled since 1979 by compositing measurements from different satellites. The record shows a clear 11-yr oscillation of roughly 1 W/m^2, which makes up a relative change of 0.1% in the TSI. This is the so-called 11-yr solar cycle, and will be referred as "solar cycle" (SC) throughout this thesis. Strong fluctuations in the TSI also occur at shorter time scales. They are related to the 27-days rotational period of the Sun [*Le Mouël et al.*, 2007] (the "rotational cycle"). While short term variations over the rotational cycle can exceed the 11-yr SC (0.3%), the latter is of greater interest for climatic studies.

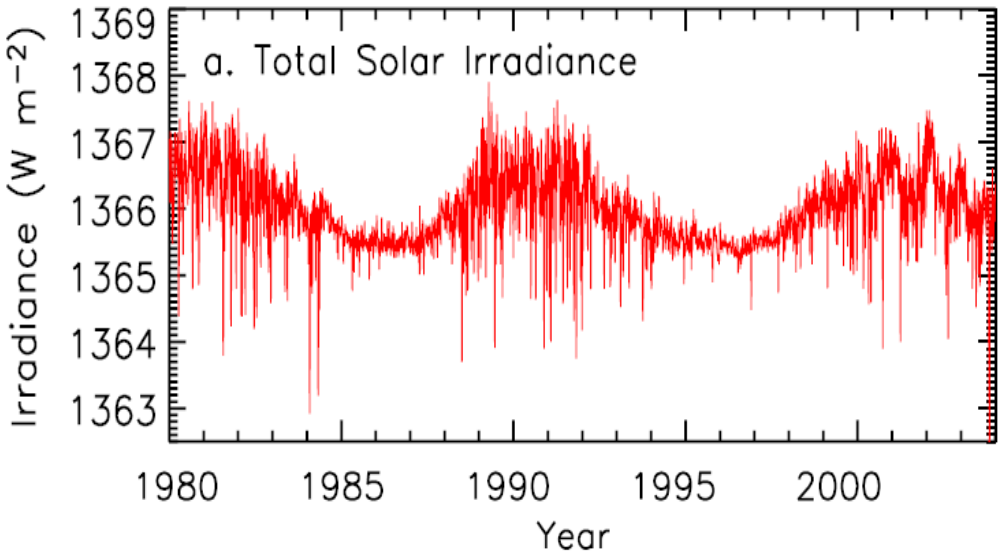

Figure 1: Daily values of the total solar irradiance (TSI) from radiometers aboard different satellites from November 1978 to December 2004. Source: `http://www.pmodwrc.ch/pmod.php?topic=tsi/composite/SolarConstant`

The SC is also commonly referred as "sunspot cycle", as it can be clearly tracked in the sunspot number. Sunspots are dark areas visible on the Sun's surface, whose number, on average, increases to 100-200 units during peaks of the 11-yr cycle. Fig. 2 shows the Sun's surface

in the years 2000 and 2009, which represent the maximum and minimum of cycle number 23. In year 2000, the surface was covered by more than 100 sunspots, while it was completely spotless in 2009. The increase in the sunspot number causes a reduction of the visible light emitted by the Sun. However, sunspots are also surrounded by brighter areas, the so-called "faculae", that can be better spotted in extreme ultraviolet (EUV) images of the Sun, as shown in Fig. 3. On time scales of the 27-days solar rotation, the sunspot "darkening" causes sudden reductions in the TSI [*Fröhlich and Lean*, 2004]. This effect is mostly seen around maxima of the 11-yr cycle, which is when the sunspot number maximizes (see Fig. 1). However, on interannual time scales, the faculae brightening over-compensates for the sunspot darkening, giving rise to an in-phase 11-yr oscillation in the sunspot number and TSI. Hence, TSI and sunspots are highly correlated on decadal time scales.

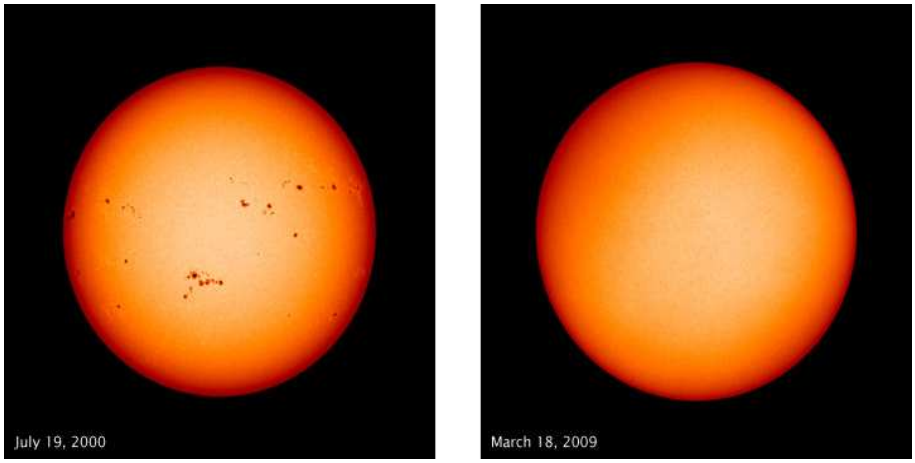

Figure 2: Images of the solar disk in the year 2000 (left), and 2009 (right). Source: `http://earthobservatory.nasa.gov/IOTD/view.php?id=37575`

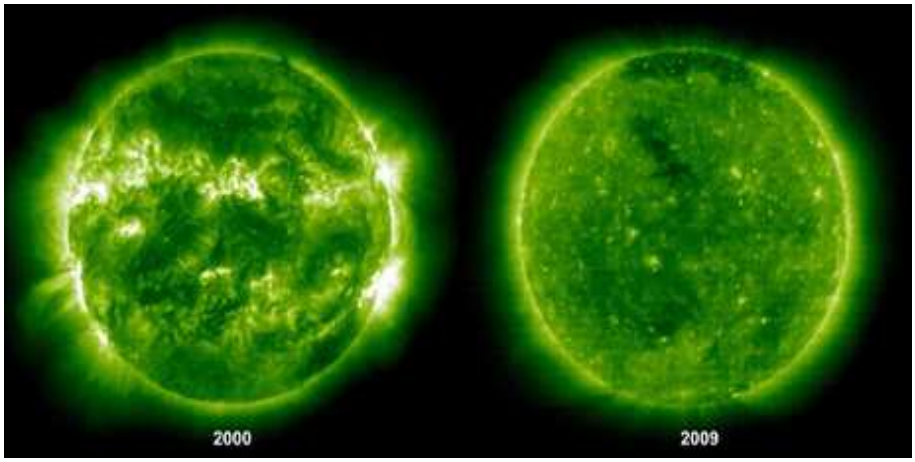

Figure 3: As Fig. 2, taken in the EUV range. Source: `http://stereo.gsfc.nasa.gov/`

A relation with solar activity has not only been observed in sunspots but also in other phenomena, such as the galactic cosmic rays and the geomagnetic activity. The incidence of geomagnetic storms and peaks in galactic cosmic rays predominantly occurs during the descending

phase of the 11-yr solar cycle, and is associated with high-frequency phenomena such as solar energetic particles and coronal mass ejections, rather than decadal scale changes in solar irradiance.

The galactic cosmic rays are better correlated with TSI on decadal time scales than the geomagnetic activity, such that their variations are inversely correlated with the 11-yr sunspot cycle. This is due to a modulation of the heliospheric "shielding" of cosmic rays by the solar magnetic field, which varies in-phase with the 11-yr cycle in TSI and sunspots. The observed negative TSI-cosmic rays correlation is the basis for the reconstruction of solar activity with cosmogenetic isotopes. Millennium long reconstructions of solar activity were derived from isotopes, such as e.g. Beryllium-10, although their relationship with the TSI is highly uncertain due to atmospheric mixing processes and wet and dry deposition from the atmosphere to the ice [*Steinhilber et al.*, 2012].

Due to its easy detection and direct relation to solar magnetic activity, the sunspot number is considered a more reliable proxy for solar activity than isotopes, although its records only reach back to the 17th century. The sunspot number and other broad characteristics of sunspots (i.e., spatial distribution on Sun's disk) were routinely documented by astronomers, making sunspots the longest direct indicator of the solar activity [*Fröhlich and Lean*, 2004]. Fig. 4 shows the evolution of the sunspot number, derived from the Zurich and group sunspot number definitions [*Vaquero et al.*, 2011; *Hoyt and Schatten*, 1998]. The amplitude and duration of the sunspot cycle are not uniform, which gives rise to cycle-to-cycle variability. In addition to the 11-yr cycle, the sunspot records also exhibit a 80/90-yr periodic modulation of the cycles amplitude [*Yousef*, 2000].

Secular scale variations are uncertain due to the use of different definitions of the sunspot number in historical records [*Hathaway et al.*, 2002]. However, there is multiple evidence of a prolonged sunspot minimum during the second half of the 17th century, which is called "Maunder Minimum" [*Eddy*, 1976]. During this period, solar activity was likely to be below average. Climatic proxies in the Northern Hemisphere show a concurrent cold phase in the 17th century, which is commonly referred to as the "Little Ice Age" [*Shindell et al.*, 2001]. This indicates a clear Sun-climate relationship on time scales longer than the 11-yr cycle. However, the exact TSI forcing during the Maunder Minimum is unknown, as the sunspot number always returns to zero near the minimum phase of all 11-yr cycles on records. Thus, even though there is also some evidence of variations at time scales beyond the 11-yr, the SC is the best documented type of solar variability.

While TSI changes over the SC of 1 W/m^2 directly translate into a top of the atmosphere (TOA) radiative forcing for the climate system of 0.25 W/m^2, the spectral dependence of irradiance changes determines the vertical and spatial distribution of the forcing within the atmosphere. For instance, the ultraviolet (UV) part of the spectrum is absorbed in the stratosphere, while the visible (VIS) penetrates to the surface [*Mohanakumar*, 2008]. Unlike the TSI for which an uninterrupted record exists since 1978 (see Fig. 1), the solar spectral irradiance (SSI) measurements are intermittent due to the termination of the satellite operations aboard which

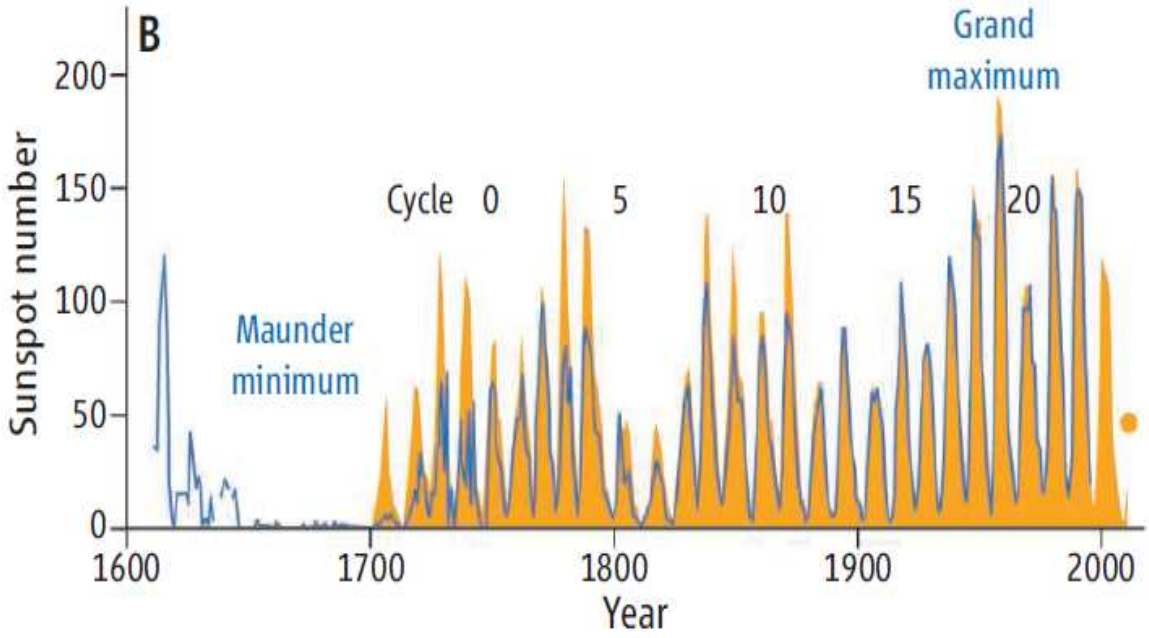

Figure 4: Yearly averaged Zurich (orange) and group (blue) sunspot number. Before around 1880, group sunspot number is thought to be a more robust representation of actual levels of activity. The Zurich number (also called the Wolf number) was introduced in the 1840s by Rudolf Wolf as an objective measure of the number of sunspots. The group sunspot number is a later improvement. The solid orange circle marks the average over the year 2011. From *Solanki and Krivova* [2011]

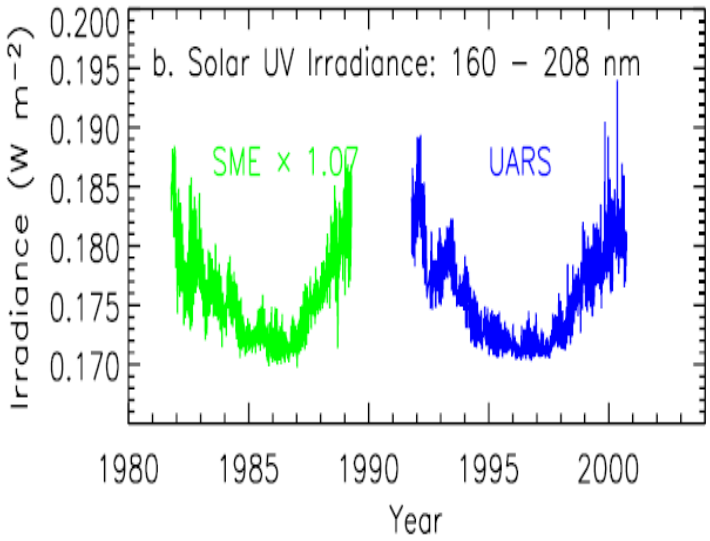

Figure 5: Time series of the solar spectral irradiance, integrated in the UV range (160-208 nm), from radiometers aboard different satellites. From *Fröhlich and Lean* [2004]

the radiometers were deployed. In addition, sampling was limited to specific UV bands. This is shown in Fig. 5, which depicts the evolution of the SSI integrated over the far UV range (160-208 nm) over cycles 22 and 23, measured by radiometers aboard the Solar Mesosphere

Explorer (SME) and the Upper Atmspheric Research Satellite (UARS). Note that while the radiant energy in the UV range is low (less than 0.2 W/m^2), the 11-yr peak-to-trough variation is stronger than in TSI (5-10 % compared to 0.1 %).

Given the prominent role of the UV radiation in the 11-yr solar variability, long-term records of the SSI with sufficient spectral resolution and temporal accuracy (i.e., to a few %) would be needed to determine reliable estimates of the radiative forcing and its spectral dependence. Unfortunately, in addition to the inhomogeneity of measurements, instrument degradation and stability limit the accuracy of such measurements to a few %, close to the relative variation in the UV range [*Rottman et al.*, 2003]. This motivates the development of empirical models of the SSI using physically-based proxies of solar irradiance, for which uninterrupted records are available.

As noted earlier, sunspots are a proxy for solar activity, although their relationship with spectral irradiance in the UV part of the spectrum is indirect. Other more objective indicators of UV irradiance are the Mg-II core to wing index, the Lyman-α and the 10.7cm flux. The Mg-II core to wing index, and the Lyman-α flux are related to the emission lines in the EUV (λ=121 nm) and in the mid UV (λ=280 nm), respectively, which are the highest variable wavelengths in the UV (10%). Another commonly used indicator of UV variability is 10.7cm radio emission flux (also referred to as the F10.7cm index), for which a continuous database covering more than 50 years is available. The F10.7cm flux primarily reflects brightness changes in the corona, and is thus considered a reliable indicator of UV variability.

Long-term records of the SSI were constructed with the empirical model developed by *Lean et al.* [1997]. They used a combination of proxies of sunspot darkening and facular brightening, constructed with information from the aforementioned indices, such as the Mg-II index, ground and space-based measurements. By using the same model, the SSI record was extended back to the 17th century [*Lean*, 2000], and has undergone a recent update [*Lean et al.*, 2005; *Wang et al.*, 2005]. Even though modeled SSI data are useful in solar cycle studies due to their extension and spectral resolution, they are based on empirical relationships. For the first time, a comprehensive sampling of the SSI across the whole spectrum was possible with the launch of the SORCE satellite mission in 2003, which included a Spectral Irradiance Monitor (SIM) instrument measuring the solar radiation from X-ray to the near-IR. The recorded SSI variations over the 2004-2008 period are shown in Fig. 6 for both SIM observations and the Lean model [*Lean*, 2000]. Unexpected features were found, such as the solar cycle out-of-phase change of VIS radiation, and the stronger UV variation (by an order of magnitude) compared to empirical models of SSI [*Harder et al.*, 2009]. These estimates suggest that the radiative forcing of the UV on climate may be much stronger than previously thought. In addition, VIS radiation directly alters the surface energy budget; thus, the understanding of the impact of the 11-yr solar cycle on climate would need to be revisited [*Haigh et al.*, 2010]. However, estimates from SORCE-SIM are limited to part of solar cycle 23, and must be thus deemed as provisional before further validation is done with additional observational evidence [*Garcia*, 2010]. It can be thus concluded that the SC is mostly prominent in the UV wavelengths, even though the precise magnitude of

the 11-yr variability is still uncertain.

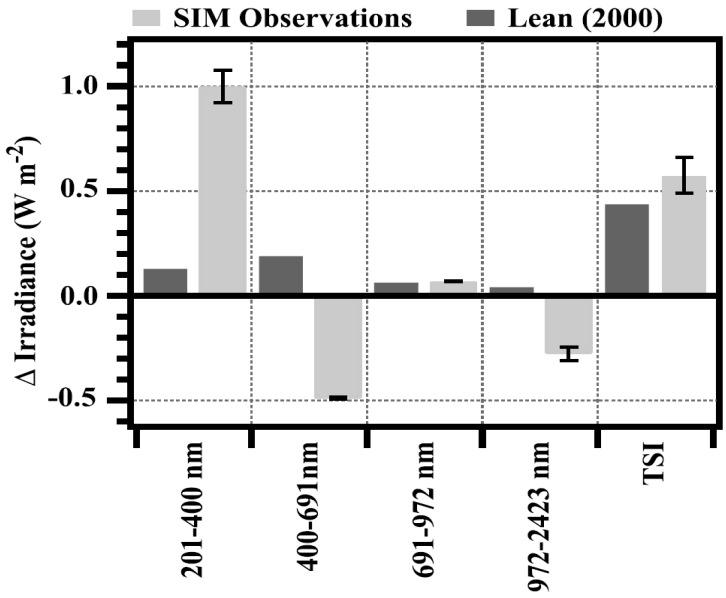

Figure 6: Comparison of SSI changes from SORCE-SIM measurements, and the empirical SSI model of *Lean* [2000] during the 2004-2008 period, which corresponds to the descending phase of the solar cycle number 23. From *Harder et al.* [2009]

1.1.1 The impact of UV radiation on stratospheric ozone

Even though the 11-yr variability in UV radiation is much stronger than at other wavelengths, the UV part of the spectrum is primarily absorbed in the stratosphere by oxygen and ozone. As depicted in Fig. 7, the molecular oxygen is most effective in the far UV (below 200 nm) due to the Shumann-Runge continuum, which is most significant between 40 and 95 km altitude. Ozone becomes the major UV absorber in the mid UV (200-300 nm) due to the Hartley-Huggins bands, which are responsible for ozone photodissociation below 50 km, peaking at 30 km where ozone concentration is greatest [*Mohanakumar*, 2008].

The UV radiation plays a key role in the photochemical production of ozone in the stratosphere, which is described by the "Chapman cycle" [*Mohanakumar*, 2008]. In brief, molecular oxygen is dissociated by high-energy UV photons ($\lambda < 250$ nm) into atomic oxygen (step 1). Oxygen atoms quickly react with oxygen molecules to form ozone (step 2). Ozone absorbs UV radiation ($\lambda < 310$ nm), whereby ozone molecules are dissociated into molecular and atomic oxygen (step 3). Through absorption in steps 1 and 3, the energy of UV photons are turned into thermal energy, which explains why the stratosphere is generally warmer than the upper troposphere. Due to the different absorptivity of oxygen and ozone, ozone is photochemically produced in the far UV (steps 1-2), and destroyed by radiation at somewhat longer wavelengths (i.e., in the mid UV). Variations in the UV radiation, such as those observed during the SC, can have a profound impact on the Chapman cycle. Hence, assuming that the absorption of solar radiation by the ozone layer is directly thermalized, a strong signature of the solar cycle should

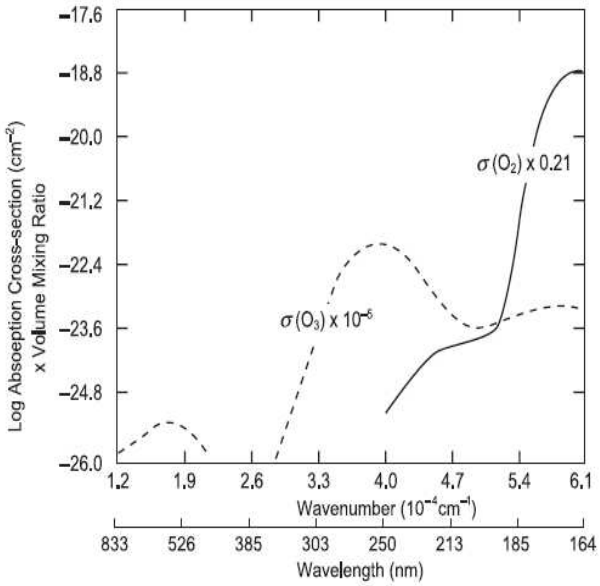

Figure 7: Absorption cross sections of molecular oxygen and ozone in the UV range

be found in the tropical stratosphere, where the ozone concentration is highest, and where the Sun is overhead. As shown in the next section, observational evidence supports this expectation.

1.2 The 11-yr solar signal in observations

The hypothesis that variations in solar irradiance could alter Earth's climate was first raised by *Eddy* [1976]. This view seemed to be supported by other contemporaneous studies showing a statistical relationship between meteorological variables and solar variability [*Pittock*, 1978]. A number of papers reported apparent correlations on both 11-yr and shorter time scales between data from individual weather stations and the sunspot number. However, many of these findings are statistically questionable [*Pittock*, 1978]. Limitations in early observational studies were posed by the poor quality and sparsity of the observations, and the methods used to diagnose the solar signals [*Pittock*, 1978].

The advent of global reanalysis and satellite products allowed for an improved characterization of the 11-yr solar signal throughout the atmosphere, from the stratosphere to the surface. The observed SC signal in stratospheric ozone (0.5-50 hPa) is shown in Fig. 8. It was diagnosed by *Soukharev and Hood* [2006] as solar regression coefficient from the analysis of ozone retrievals from the Solar Backscatter Ultraviolet (SBUV) instrument over the 1979-2003 period. The values in percentage indicate the relative variation during peaks of solar activity, compared to solar cycle minima. At low latitudes, there is a vertical double peak structure, indicating a significant ozone increase, reaching 2% in the stratopause region (at about 50 km) and in the lower stratosphere (around 20 km). In addition, there are two mid-latitude regions showing a significant increase in ozone in the middle stratosphere around 30-40km. This structure is confirmed in other two independent satellite datasets [*Soukharev and Hood*, 2006], and it is also reproduced using a different analysis technique on a longer satellite dataset, albeit with

weaker maxima [*Randel and Wu*, 2007]. Thus, a clear signature of the SC is observed in stratospheric ozone, in agreement with the expectations based on the role of the UV in the Chapman Cycle outlined in Section 1.1.1. While the upper stratospheric ozone increase is well established in terms of UV impacts on photochemistry, the increase in the tropical lower stratosphere is possibly linked to dynamical transport changes, as ozone is in approximate photochemical equilibrium in this region [*Hood*, 1997].

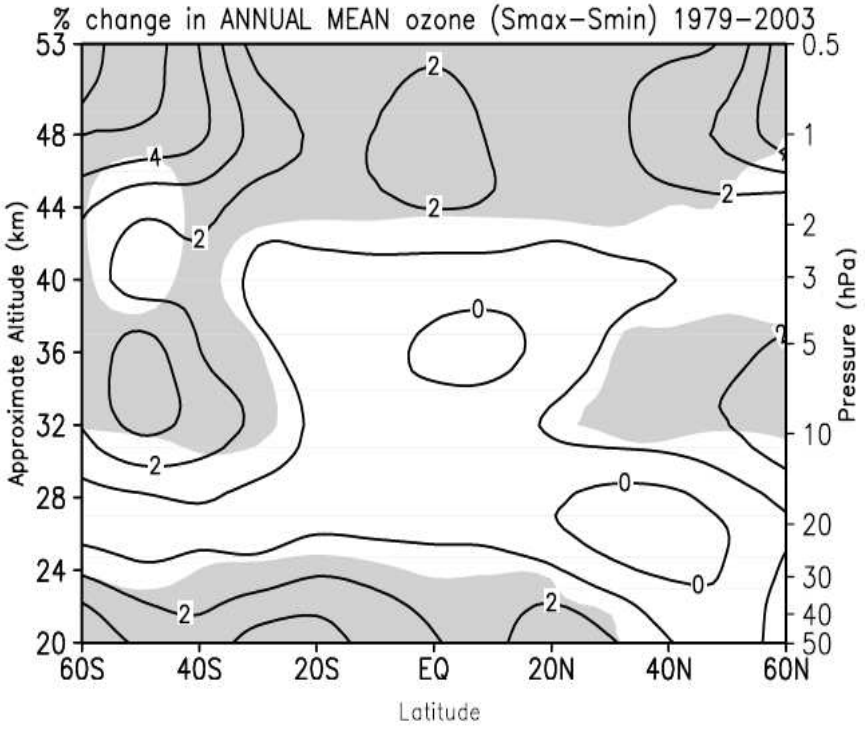

Figure 8: Solar regression coefficient in zonal mean ozone from SBUV data (1979-2003), displayed in terms of % relative values. Shaded areas are statistically significant at the 95% confidence level. From *Soukharev and Hood* [2006]

The solar signal in zonal mean temperature is shown in Fig. 9, as diagnosed by *Frame and Gray* [2010] from re-analysis data over the 1979-2008 period. Warming is localized in the tropical stratopause, suggesting a temperature increase of 1.5 K during peaks of solar activity. As it will be shown in the next section, this signature is robust and agrees with theoretical expectations. In the tropical stratosphere, no solar response is present at 30-40 km, while a weaker maximum around 0.5 K is placed at 20 km. These responses give rise to a vertical double peak structure, similar to that observed in zonal mean ozone. While it is reasonably well established that radiative processes drive the solar response in the tropical stratopause, the observed signals in other atmospheric regions are far less understood, and require the existence of dynamical mechanisms. This especially applies to temperature increase in the tropical lower stratosphere, which is possibly linked to changes in upwelling related to the Brewer Dobson circulation [*Gray et al.*, 2010].

In addition to the tropical signals, regions with significant warming are also found in the

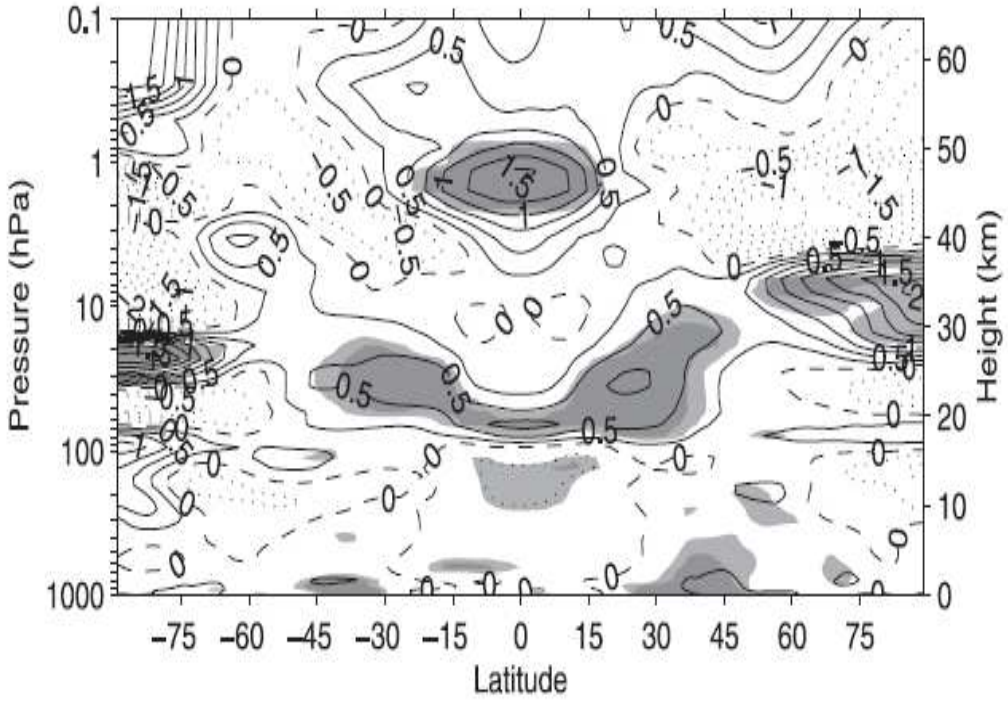

Figure 9: Solar regression coefficient in zonal mean temperature from a merged ERA-40/ERA-Interim dataset for the 1979-2008 period. Shaded areas are statistically significant at the 95% confidence level. From *Frame and Gray* [2010]

polar stratosphere in both hemispheres, and in the mid-latitude (30-45°) lower troposphere. The warming in the polar stratosphere is a late winter feature of each hemisphere, which still stands out in the annual mean due to its large amplitude. In the Northern Hemisphere, the late winter (February) warming in the polar stratosphere is mainly observed during solar maximum winters that coincide with the westerly phase of the Quasi Biennal Oscillation (QBO), when anomalies can be larger than 4 K, while cooling is found during solar maximum and QBO east conditions. This QBO modulation of the solar signal was first observed by *Labitzke* [1987], and was later confirmed adding 20 more years of data [*Labitzke and Kunze*, 2009]. This signal could also be part of a solar cycle modulation of the extratropical effect of the QBO, known as the Holton-Tan relationship [*Holton and Tan*, 1980], which predicts a cold (warm) vortex under QBO west (east) conditions. The high statistical significance of the polar vortex warming under QBO west and solar maximum conditions was confirmed by *Camp and Tung* [2007]. They suggested that this signal is possibly linked to the predominant occurrence of Sudden Stratospheric Warmings (SSWs) in these winters. *Camp and Tung* [2007] also proposed that the cooling observed during QBO east and solar maximum winters is indicative of a non-linear behavior, as the vortex is already disturbed in the east phase of the QBO, the solar maximum conditions do not lead to any further warming. Similar non-linearities are also observed in other combination of forcings, such as warm ENSO events and QBO east conditions [*Calvo et al.*, 2009]. These studies highlighted the importance of QBO-solar interactions in shaping the solar

signal at high latitudes 9.

In the lower troposphere, the warming bands observed in mid-latitudes are due to circulation changes associated with the observed poleward expansion of the tropospheric jets during peak years of solar activity, as reported by *Haigh* [2003]. These changes are consistent with the stronger zonality at mid latitudes during years of maximum activity, which in turn, is linked to a more zonal NAO pattern [*Kodera*, 2003], and a more extended NAO influence on European temperatures [*Gimeno et al.*, 2003]. In addition, blocking activity is less prominent over the European continent, being relegated to the West Atlantic sector [*Barriopedro et al.*, 2008]. Other observed changes during peaks of solar activity also include an eastward shift and weakening of the Aleutian Low [*Christoforou and Hameed*, 1997; *Roy and Haigh*, 2010].

There is also evidence for 11-yr solar signals in the ocean, as e.g., in upper oceanic temperature [*White et al.*, 1997]. In the tropical Pacific, peaks of solar activity might lead to a La-Niña like response [*van Loon and Meehl*, 2008], which is followed by a warm El-Niño a few years later [*Meehl and Arblaster*, 2009]. There are also indications of an increase in off-equatorial precipation [*Meehl et al.*, 2009], a weakening of the Hadley cell [*Kodera and Shibata*, 2006], and a modulation of the Indian Monsoon system, with higher precipitation over Arabia and India during solar maxima [*Kodera*, 2004].

To summarize, there is ample observational evidence of a SC signal in different compartments of the climate system. Considering the small amplitude of the SC radiative forcing (0.25 W/m^2), dynamical feedbacks are needed to explain the magnitude of the observed signals. Next, we review the main mechanisms that have been proposed in the literature.

1.3 Mechanisms

General consensus has been reached on the radiative nature of the solar signal in the stratopause region (Fig. 9). An increase in the UV radiation during peaks of the 11-yr cycle affects the Chapman cycle by enhancing both oxygen and ozone photolysis. As described in Section 1.2, radiometric measurements and irradiance modeling indicate that the increase is stronger in wavelengths affecting the molecular oxygen photolysis (far UV, 200 nm) than at those in which ozone is photolyzed (i.e., at 250 nm, see e.g., *Rottman et al.* [2003]). The resulting fast recombination of oxygen atoms leads to a net ozone production, resulting in the observed ozone increase in the tropical stratopause (Fig. 8). The additional ozone further increases the stratospheric heating caused by absorption of the UV radiation, thus providing a positive feedback mechanism that amplifies the temperature response to the 11-yr solar cycle [*Gray et al.*, 2010]. Idealized modeling studies indicate that the induced "UV-ozone" feedback contributes to 50% of the warming observed in the tropical stratopause region [*Gray et al.*, 2009].

On the other hand, it is also well established that radiative processes play little role in the polar stratospheric warming seen in Fig. 9, since this pattern is mainly observed during late winter in each hemisphere [*Frame and Gray*, 2010]. The polar signal is also part of the solar-induced change in the wintertime stratospheric polar night jet (PNJ). Fig. 10 shows the composite differences (MAX-MIN) in zonal mean wind for boreal winter months, obtained from NCEP re-

analysis, as displayed by *Matthes et al.* [2004]. Peaks of solar activity induce an acceleration of the stratospheric westerly flow in December. The westerly wind anomalies then propagate poleward and downward, following a pattern resembling the PNJ oscillation [*Kodera and Kuroda*, 2002]. The westerly wind anomalies reach the troposphere during January, and induce stronger zonality in the Atlantic sector [*Kodera*, 2003]. In the polar stratosphere, westerly anomalies are then replaced by easterlies in February-March.

Kodera and Kuroda [2002] proposed a conceptual model to explain the response found in the extratropical winter stratosphere. According to them, anomalous heating in the stratopause region induces (by the thermal wind relation) a stronger westerly flow in the subtropics. The wind anomalies then propagate poleward and downward through processes involving wave propagation and deposition, following the pattern seen in Fig 10. Suppressed wave deposition in the polar stratosphere then leads to a weakening of the Brewer-Dobson circulation, which in turn induces warming in the tropical lower stratosphere, consistent with the observed secondary maximum in Fig. 9. It was also argued that the suppressed upwelling in the tropical stratosphere can affect the Monsoon systems [*Kodera*, 2004]. This chain of processes provides a propagation pathway for the solar signal to reach the troposphere, which is mainly operative during boreal winter and is usually know as the "polar route".

However, the applicability of this theory in observations becomes difficult because of the dependence of the late winter solar signal onto the QBO phase, as described in the previous section [*Labitzke*, 1987; *Labitzke and Loon*, 1989; *Labitzke*, 2004; *Labitzke et al.*, 2006]. This feature involves a non-linear interaction of the SC forcing and the QBO, with the QBO exerting the strongest influence on the polar vortex through the Holton-Tan mechanism [*Holton and Tan*, 1980].

However, other studies studies based on idealized simulations showed that a similar solar response in the troposphere is obtained if a heating source is applied in the tropical lower stratosphere [*Haigh et al.*, 2005; *Haigh and Blackburn*, 2006], with synoptic-scale waves playing a dominant role in the poleward shift of the tropospheric jet [*Simpson et al.*, 2009]. The applied diabatic heating in the tropical lower stratosphere mimics the observed secondary maximum seen in Fig. 9, and thus provides a "tropical route" for solar signals to be transferred from the stratosphere to the troposphere, in contrast with the "polar route" discussed above. Even though the postulated pathways involve different mechanisms (i.e., planetary-waves dissipation in the "polar route", and synoptic-scale wave dissipation in the "tropical route"), they have the UV heating in common as a triggering mechanism for the chain of indirect effects leading to a "top-down" propagation of the solar signal from the stratosphere to the troposphere and surface.

On the other hand, the SC signal in TSI has been suggested to induce changes in the surface energy balance in the subtropical Pacific region, which initiate a chain of processes leading to a modulation of the ENSO cycle [*Meehl and Arblaster*, 2009]. Similarly, the solar response in SSTs may also drive the poleward shift in tropospheric jets [*Misios and Schmidt*, 2013]. These results indicate the existence of a "bottom-up" mechanism for the solar signal to propagate from the ocean to the atmosphere, in which the 11-yr TSI forcing and surface heating play a more

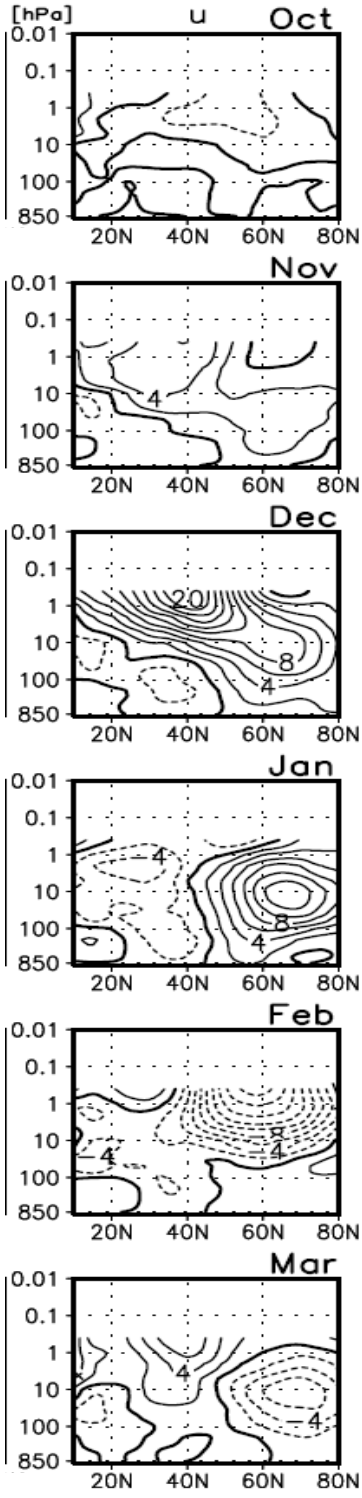

Figure 10: Composite differences (MAX-MIN) in zonal mean wind from NCEP reanalysis. From *Matthes et al.* [2004]

important role than UV changes through the stratosphere. However, there is great controversy in the sign of the SSTs response in the Eastern Tropical Pacific, and hence, in the details of the mechanisms driving the "bottom-up" pathway. While some studies point at a La-Niña like

response [*Meehl and Arblaster*, 2009; *Meehl et al.*, 2009; *Bal et al.*, 2011], others suggest a basin-wide warming of the Tropical Pacific during peaks of solar activity [*Misios and Schmidt*, 2012], which could be the result of a non-linear modulation of ENSO cycles [*White and Liu*, 2008]. In addition, a possible ENSO contamination of the apparent solar response in Tropical Pacific SSTs has also been suggested [*Tung and Zhou*, 2010; *Roy and Haigh*, 2012]. Hence, the lack of robust observational and modeling evidence of an ENSO modulation by the 11-yr solar cycle cautions against interpretation of the "bottom-up" pathway. It is also very plausible that "bottom-up" and "top-down" pathways are not mutually exclusive, and may act together in shaping the tropospheric response to the SC [*Meehl et al.*, 2009].

Fig. 11 displays a schematic diagram of the pathways that have been proposed in the literature, whereby solar variability affects the climate system. Apart from the mechanisms outlined above for the TSI and UV radiation, other variations related to solar variability are found in galactic cosmic rays and solar energetic particles. The cosmic rays flux exhibits an 11-yr cycle, which is in opposite phase compared to TSI, as explained in Section 1.1. Based on an apparently strong correlation between cosmic rays and low clouds, *Marsh and Svensmark* [2000] proposed a microphysical mechanism involving a cosmic rays modulated ionization enhancing aerosol formation. However, the statistical cosmic rays-clouds relationship has been proven to fail in more rigorous analysis procedures [*Laken et al.*, 2012].

High frequency fluctuations in solar activity are reflected in solar energetic particle events, bringing about strong changes in energetic particle fluxes at polar latitudes. These phenomena induce ionization and dissociation, primarily influencing chemical constituents, such as NOx, which in turn induce ozone loss. In this way, energetic particles may contribute to the solar signal in stratospheric ozone. However, there is little evidence indicating that such short term variations could lead to cumulative effects on decadal time scales (i.e., decadal-scale changes in NOx that could modulate ozone changes on the same time scales). Moreover, the impact of energetic particles is restricted to a limited region in the polar stratopause [*Gray et al.*, 2010].

To summarize, several mechanisms have been proposed to explain both decadal and short term relations between climate and solar variability, and it is still not clear which are dominant and how they operate. This thesis will focus on the link between decadal climate variability and the 11-yr SC.

1.4 Solar influence, or statistical problem?

Some of the solar signals detected in observations and discussed in the previous Sections are highly sensitive to details in the methodology used to diagnose them. One example is the SC signal in the tropical Pacific SSTs, whose sign critically depends on the index used for solar activity (sunspot number, or the F10.7cm), or the analyzed period [*Roy and Haigh*, 2010]. A weakening of the Aleutian Low is also known to be part of the extratropical ENSO signature, raising the possibility that ENSO contaminates the analysis of the SC signal [*Roy and Haigh*, 2010].

In the polar stratosphere, the solar signals critically depend on the phase of the QBO as dis-

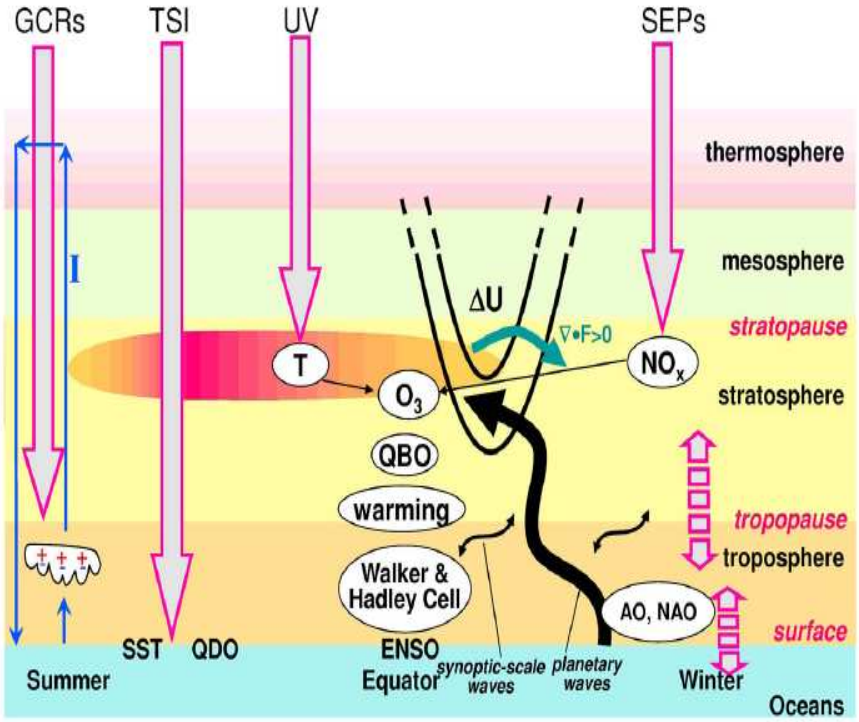

Figure 11: Schematic of the possible pathways through which solar variability affects the climate system. From *Gray et al.* [2010]

cussed in Section 1.2 [*Labitzke*, 1987; *Labitzke and Loon*, 1989; *Labitzke*, 2004]. This may suggest a non-linear interaction of the solar signal with the QBO, or a decadal scale modulation of the high-latitude QBO signal [*Lu et al.*, 2008], or even contamination of the apparent solar signal by the extratropical effect of the QBO [*Holton and Tan*, 1980]. In addition, the large interannual variability associated with the occurrence of sudden stratospheric warmings (SSWs) in the polar stratosphere gives rise to large scatter in data in both QBO phases [*Anstey and Shepherd*, 2014], as seen in Fig. 12. This raises the possibility that correlations used as basis for the QBO-solar modulation postulated by *Labitzke et al* are due to chance occurrence.

Uncertainties also appear in the winter solar response, regardless of the QBO phase, questioning the conceptual model proposed by *Kodera and Kuroda* [2002]. During peaks of solar activity, the PNJ does not always follow the poleward-downward evolution shown in Fig. 10. This is due to strong interannual variability caused by SSWs, which cause dramatic perturbations in the zonal flow in the polar stratosphere. In addition, other forcings that exert a strong influence on the polar vortex, such as ENSO and the QBO [*Calvo et al.*, 2007, 2009], may map into the composite differences of MAX and MIN conditions, which are typically used to diagnose the solar signal in the polar stratosphere, such as in Fig. 10.

While composite analysis is mainly used to investigate the solar signal in the polar regions, most observational studies diagnosed the solar signal in the tropical stratosphere with aid of multiple linear regression analysis (MLR), such as in temperature and ozone (see Figs. 8-9). If the forcing indices used in the MLR are orthogonal, the solar signal can be separated from

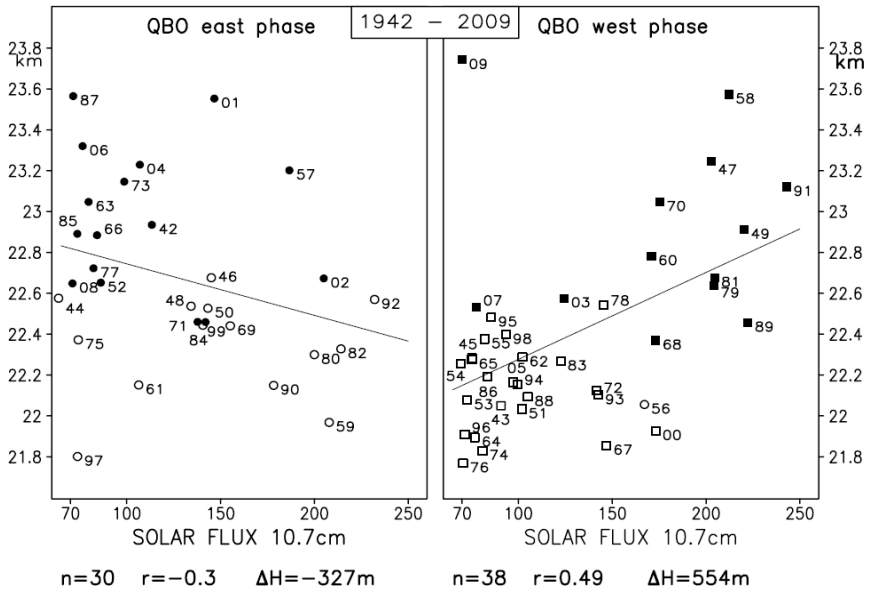

Figure 12: Scatter diagram of the February mean 30-hPa geopotential height at the North Pole versus the solar flux in QBO east (left) and QBO west (right) conditions. The numers indicate the respective years; solid symbols indicate major SSWs. From *Labitzke and Kunze* [2009]

the variability associated with other indices, as e.g. ENSO, QBO, linear trends due to GHG forcing, and volcanic eruptions. However, forcings are not orthogonal in the observational record in part due to their limited extension. In timely limited records, spurious correlations ("multicollinearity") between the forcing indices can arise, such as the case of ENSO and the F10.7cm indices over the 1979-2003 period. Due to this correlation, part of the secondary maximum at 20 km in the tropical lower stratospheric ozone in Fig. 8 can be associated with ENSO, and would thus be erroneously attributed to the 11-yr SC in a MLR analysis over a short record [*Marsh and Garcia*, 2007]. The double-peak structure in the tropics seen in temperature and ozone has also been suggested to be due to irregularities in the QBO, which spuriously map into the 11-yr SC [*Smith and Matthes*, 2008]. A similar effect was also attributed to volcanic eruptions [*Lee and Smith*, 2003]. Additionally, significant autocorrelation is found in monthly mean meteorological variables [*Tiao et al.*, 1990], a property called "persistence", which implies that individual data points in the predictand are not independent. In the presence of multicollinearity, the MLR yields biased regression coefficient values, while persistence in the data leads to overestimation of the significance [*Wilks*, 2011].

It is therefore clear that unambiguous separation of the SC contribution is hampered by the shortness of the currently available observational records, which only span over three 11-yr cycles, and by the relatively small magnitude of the putative signals compared to other sources of variability. This complicates the separation of the 11-yr solar signal from other sources of natural variability, such as ENSO and the QBO in the stratosphere. As the attribution of the 11-yr signal in observations is challenging, the robustness of the Sun-climate relationship is often called into question, and needs to be revisited.

1.5 Model simulations of the 11-yr solar signal

General circulation models (GCMs) are a fundamental tool to investigate the solar influences on climate. First, idealized GCM experiments can shed light on the mechanisms whereby the SC affects the climate system. In addition, GCMs can be used to assess the robustness of the solar signal, as it is feasible to run simulations extending over more cycles than those covered by observational records, improving the reliability of significance testing. A wide range of atmospheric models was employed in the past to simulate the stratospheric and tropospheric response to the SC. Next, the modeling studies aimed at simulating the tropical and extratropical signals outlined in Section 1.2 and the mechanisms detailed in Section 1.3 are reviewed.

1.5.1 The tropical stratospheric signal

One key aspect in the Sun-climate relationship is the response of the tropical stratosphere to the 11-yr solar cycle, which is where the strongest signature is detected in observations (see Fig. 9). To simulate the equatorial stratopause signal, it is essential to capture the ozone-UV feedback, for which models need to incorporate fully interactive photochemistry [*Haigh,* 1994]. Pioneering work in this regard was performed by *Brasseur* [1993]; *Huang and Brasseur* [1993]; *Haigh* [1994], who employed interactive ozone modules in 2-D chemistry transport models. These studies reproduced the broad features of the observed solar signal in the upper stratosphere consisting of temperature and ozone increase during peaks of solar activity, albeit they underestimate their magnitude, possibly because of the simplified dynamics.

The advances in computing power and in 3-D modeling lead to the development of a more sophisticated type of GCMs with interactive chemistry: the Chemistry Climate Models (CCMs). These models have been extensively used to simulate the atmospheric response to solar variability [*Tourpali et al.,* 2003; *Rozanov et al.,* 2004; *Egorova et al.,* 2004; *Marsh et al.,* 2007; *Schmidt et al.,* 2010; *Matthes et al.,* 2010]. The CCMs typically consider the spectral variations between different phases of the 11-yr SC through the use of SSI forcing rather than TSI, and are for this reason able to reasonably reproduce the upper stratospheric response [*Matthes et al.,* 2003]. However, despite the increase in complexity, there were only limited improvements over 2-D models in reproducing the double-peak structure in tropical stratospheric temperature and ozone depicted in Figs. 8-9. Like 2-D models, most CCMs fail to simulate the secondary maximum in the tropical lower stratosphere, even though they incorporate an improved representation of wave-mean flow interactions that have been proposed to be the origin of this signal [*Kodera and Kuroda,* 2002]. Possible reasons for this failure could be the absence of an internally generated nor assimilated QBO, as in the models used by *Tourpali et al.* [2003]; *Rozanov et al.* [2004]; *Egorova et al.* [2004], or the use of perpetual maximum and minimum solar activity, and climatological SSTs as boundary conditions as in the models used by *Schmidt et al.* [2010] and *Marsh et al.* [2007].

On the other hand, a multi-model assessment of the solar signal in CCMs participating to the first Coupled Chemistry Climate Validation activity (CCMVal-1) revealed that the models using transient forcings broadly reproduce the tropical lower stratospheric increase in ozone

and temperature [*Austin et al.*, 2008], which suggests a potential non-linear interaction between the solar cycle and other sources of variability. However, the apparent secondary maximum in models was very sensitive to the analysis period, which indicates a non-stationarity of this feature, and potential attribution issues (Section 1.4). Along the same lines, other studies suggested that quasi-decadal variations in ozone and temperature in the tropical lower stratosphere, such as those attributed to the SC, could be due the result of misattribution in the MLR analysis [*Lee and Smith*, 2003; *Marsh and Garcia*, 2007; *Smith and Matthes*, 2008], thus pointing at the possibility that the secondary maximum may be a false signal. However, their use of 2-D models (e.g., [*Lee and Smith*, 2003; *Smith and Matthes*, 2008]) limits the potential implications of their results.

These uncertaintites highlight the need to explore the nature of the tropical lower stratospheric SC response. To this end, the role of boundary conditions needs to be examined in model simulations using more realistic forcings, as these may elucidate potential non-linearities and/or statistical attribution issues. The solar signal in the tropical lower stratosphere is a key feature in the "tropical route" for transmission of the stratospheric signal to the troposphere as outlined in Section 1.3. Thus, a correct attribution of the quasi-decadal variability has also implications for correct understanding of the top-down mechanism and the tropospheric solar signal.

1.5.2 The extratropical boreal winter signal

Many of the aforementioned modeling studies also explored the boreal winter response in the Northern Hemisphere polar vortex. By using a simple GCM without interactive ozone chemistry, *Matthes et al.* [2004] and *Ineson et al.* [2011] were able to simulate the observed strengthening of the vortex, and the poleward-downward migration of zonal wind anomalies observed in Fig. 10. In their simulations, this pattern also propagates to the troposphere in mid-latitudes, projecting onto a positive phase of the AO and NAO patterns. A similar stratospheric response was also reproduced in other CCMs [*Rozanov et al.*, 2004; *Schmidt et al.*, 2010]. In addition, the models incorporating a QBO also seem to reproduce the QBO-solar modulation of the polar vortex, albeit only qualitatively [*Matthes et al.*, 2004; *Schmidt et al.*, 2010; *Matthes et al.*, 2013]. These studies showed modeling evidence in support of the dynamical mechanism proposed by *Kodera and Kuroda* [2002].

However, the observed magnitude and seasonal march of the extratropical signals in zonal wind and temperature were not reproduced. This was the case in the model simulations performed by *Schmidt et al.* [2010], where the downward propagation of high latitude wind anomalies occurred too late (i.e., in spring months). Simulations of the SC response in boreal winter were typically forced with idealized forcings, as e.g., the fixed QBO phase profiles by *Matthes et al.* [2004, 2006], or the perpetual maximum and minimum solar activity used by *Rozanov et al.* [2004] and *Schmidt et al.* [2010], the repetition of the observed QBO and 11-yr cycles by *Matthes et al.* [2013], or idealized UV forcing used by *Ineson et al.* [2011]. Non-solar forcings such as GHGs and ENSO were excluded, as performing solar-only experiments facilitates the detection of the

solar signal. On the other hand, such procedure also leads to an overestimation of the significance of the putative solar signals, as the underlying variability is small due to the absence of forcings other than solar variability.

One problem common to many GCMs is the too low frequency of major SSWs [*Charlton et al.*, 2007], which implies that the natural variability of the polar vortex in most models is underestimated. In addition, CCMs tended to simulate a too strong stratospheric vortex, as e.g. WACCM3.1 in *Marsh et al.* [2007]; *Tsutsui et al.* [2009]; *Matthes et al.* [2013]. Biases in either the background climatology or variability of the stratospheric jet hinder a realistic representation of wave-mean flow interactions [*Matthes et al.*, 2010], which are key in transferring the solar influence from the upper tropical stratosphere to the high latitudes according to the conceptual model of *Kodera and Kuroda* [2002].

The Northern Hemispheric boreal winter climate response to the SC still needs to be explored in simulations driven with a more realistic set-up of forcings than that used in previous studies. To this end, models with a more realistic representation of stratospheric basic state and variability are required. Such exercise would provide robust modeling evidence of the mechanisms operating in the polar winter stratosphere, which drive the propagation of the signal from the upper stratosphere to the lower stratosphere, and troposphere (Fig. 11).

1.5.3 The future evolution of the solar forcing

In addition to a better understanding of the solar signals and the underlying mechanisms, another interesting open question is the future behavior of the SC and its impact on a changing climate, as GHGs are projected to continue to increase in the next decade. The anomalous behavior during the current solar cycle 24 has shown that the 11-yr solar cycle is far from being a quasi-periodic forcing. Hence, repeating the solar cycle number number 23, or the sequence of the last four observed cycles (20-23), as it is done in the IPCC models, might not be the best approach. The range of solar predictions is limited to a few years by the lack of understanding of the linkage between the solar dynamo and magnetic field, which shape the solar activity and its fluctuations [*Solanki and Krivova*, 2011]. Thus, future solar activity represents a source of uncertainty, which was underestimated in previous IPCC assessment reports.

Using statistical analysis of long-term solar indicators, solar physicists have recently raised suggestions regarding the Sun entering a period of reduced activity (see e.g., [*Abreu et al.*, 2008]). These conditions may resemble the grand Maunder Minimum [*Lockwood et al.*, 2011]; i.e., the 1650-1710 period characterized by an extended minimum in the sunspot activity shown in Fig. 4, during which the solar forcing was reduced compared to current levels [*Eddy*, 1976]. Since the future evolution of solar forcing is hard to predict in the long term, a future solar minimum cannot be ruled out [*Solanki and Krivova*, 2011]. In such context, it is of primary importance to explore whether such scenario could modulate the projected global warming driven with the steady increase in GHGs loadings.

One possible approach would be to assume a future TSI forcing like the one which oc-

curred during the Maunder Minimum. However, reconstructions of historical irradiance from the Maunder Minimum to present show large uncertainties, as shown in Fig. 13 (bottom). These datasets assume the existence of a long-term source of irradiance variability in addition to the 11-yr cycle, i.e., a variable background component. Two reconstructions reach back to the Maunder Minimum years, showing a TSI reduction ranging from 0.2% in [*Lean*, 2000] to 0.3% [*Lean et al.*, 1995]. Another recently published reconstruction suggests a more extreme reduction up to 0.4% [*Shapiro et al.*, 2011]. The reconstructed background changes in the TSI are very uncertain, since they are based on indirect proxies of solar irradiance, such as variations in Sun-like stars [*Lean et al.*, 1995; *Lean*, 2000] and cosmogenic isotopes [*Shapiro et al.*, 2011]. In addition, the TSI values in the Maunder Minimum may resemble those recorded during SC minima [*Schrijver et al.*, 2011], which would imply the absence of a long term trend in the TSI since the 17th century, as shown in Fig. 13 (top panel).

A number of recent modeling studies have investigated the climate impact of a period of reduced solar activity on projections of the 21st century. The employed models range from intermediate complexity [*Feulner and Rahmstorf*, 2010], box-diffusion [*Jones et al.*, 2012], to fully coupled ocean-atmosphere models with interactive chemistry [*Meehl et al.*, 2013; *Anet et al.*, 2013]. Given the uncertainty in the Maunder Minimum reconstructions, different amplitudes of TSI reductions were used. Most of these studies used rather extreme reductions in TSI (as e.g., 0.25% in *Meehl et al.* [2013], and 0.4% in *Jones et al.* [2012]), which are in the upper-end range of TSI reconstructions shown in Fig.13 (bottom). Despite the differences in the modeling framework, they consistently show a 0.2-0.3 K reduction of the global mean temperature rise of 2 K by 2100, relative to simulations with unperturbed SC activity.

Even though these findings were instructive in showing that a new Maunder-like state would sligthly reduce warming from anthropogenic GHGs, their focus was limited to the global scale response. Moreover, it was recently shown that extreme reconstructions of the TSI during the Maunder Minimum, such as those used the aforementioned modeling studies, are too large [*Stocker et al.*, 2013]. In addition, models using spectral irradiance changes used a uniform scaling across all wavelengths (see e.g., [*Meehl et al.*, 2013]), neglecting the dominance of UV variability over other wavelengths in the spectrum.

Thus, the impact of a future solar minimum under climate change projections needs to be investigated using a model driven with a more realistic solar minimum forcing than those used in previous studies. In addition, effects on regional scales need to be quantified, as they are critically important for climate change adaptation strategies.

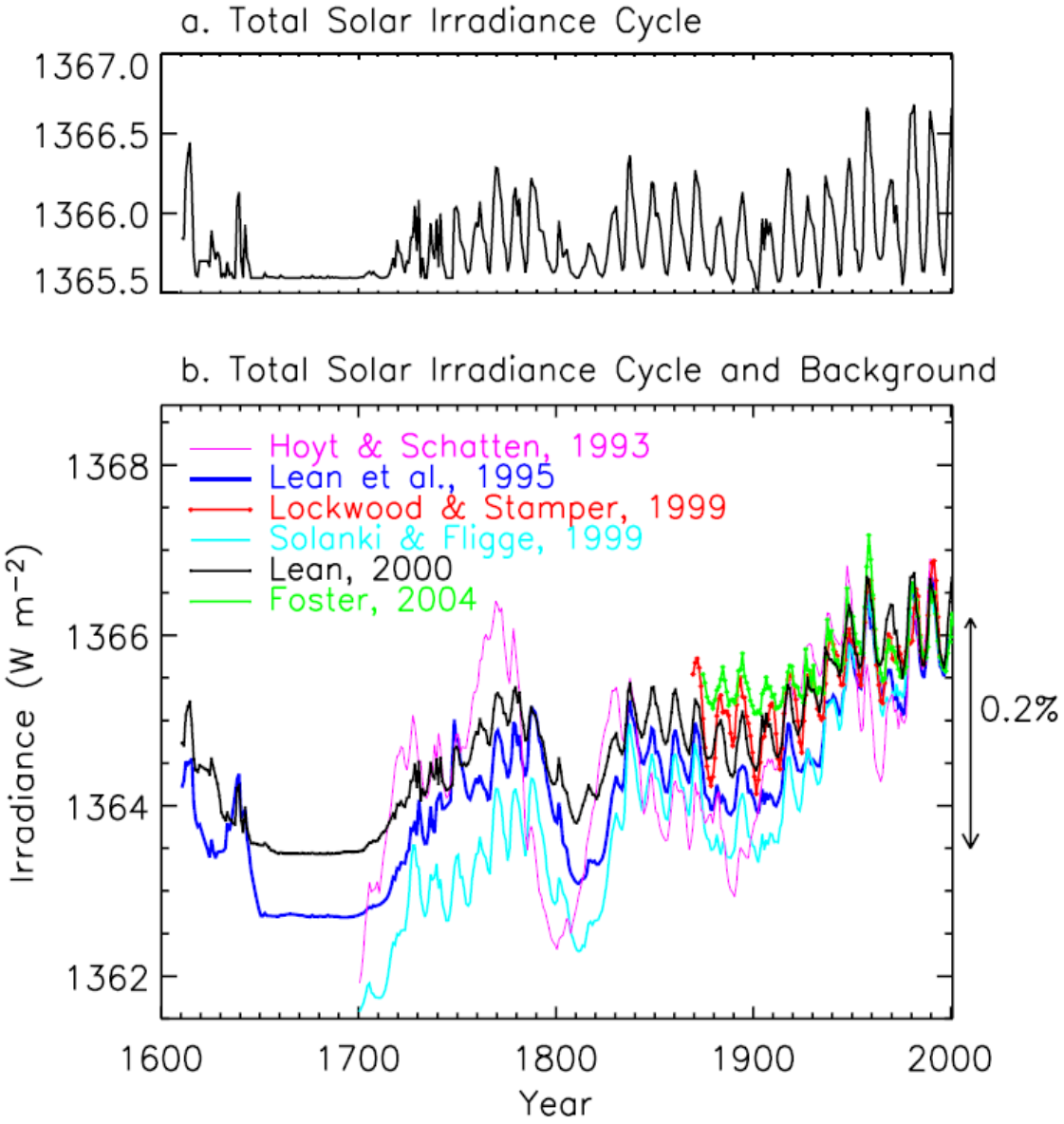

Figure 13: (Top) Evolution of the TSI based on the correlation of the annual means of observed TSI and sunspot number. (Bottom) Reconstructions of TSI over the last centuries. The different long-term trends reflect different assumptions about the irradiance reduction during the Maunder Minimum relative to the present. For comparison, the absolute scales of the various reconstructions have been adjusted by constant offsets to agree during the contemporaneous epoch. From *Fröhlich and Lean* [2004]

1.6 Science questions

The limitations of models previously used to investigate the atmospheric response to the SC, the issue of the attribution of quasi-decadal variability in observational records, and the possible descent of solar activity into a prolonged phase of minimum activity, lead to the following scientific questions:

1. **Can we simulate a realistic Northern Hemispheric boreal winter climate response in a model with improved physics, driven with more realistic forcings than in previous studies?**

2. **Can we unambiguously attribute quasi-decadal variability in the tropical stratosphere to the solar cycle?**

3. **What is the impact of a plausible future minimum in solar activity under a climate change scenario?**

These questions represent the three main goals of this thesis. By exploring the first issue, the robustness of the "top-down" pathway shown in Fig. 11 can be tested in a more realistic modeling framework, thereby also exploring the tropospheric impacts of the solar signal to understand potential implications for seasonal to decadal predictions [*Chiodo et al.*, 2012]. Answers to the second issue will provide insight into the feasibility of extracting a robust 11-yr solar signal by using regression analysis in records that cover a few solar cycles, such as state-of-the-art reanalysis products, and provide answers to the long-standing debate on the nature of the secondary maximum in the tropical lower stratosphere [*Chiodo et al.*, 2014]. Addressing the third question allows to quantify the impact of a hypothetical but plausible scenario of future solar activity [*Chiodo et al.*, 2014, submitted]. In this way, it is possible to determine whether a reduction in solar activity could modulate the regional distribution of climate change patterns. Such exercise would also shed some light onto the possible mechanisms operating in the transient response to the SC on longer (i.e., centennial) time scales.

2 Methods

The primary tool to accomplish the proposed goals is the Whole Atmosphere Community Climate Model (WACCM), developed at the National Center for Atmospheric Research. It is a fully coupled CCM, with an interactive stratospheric chemistry module developed by *Kinnison et al.* [2007]. Different versions of the model have participated in CCMVal-1, CCMVal-2 and CMIP5 intercomparison activities. It has 66 vertical levels which extend from the surface to the thermosphere (145 km) and are based on a hybrid pressure sigma coordinate system, with a variable vertical resolution, ranging from approximately 1 km in the mid troposphere to about 3.5 km in the upper mesosphere. The underlying GCM is based on CAM3 [*Collins et al.*, 2004] and uses a finite-volume dynamical core [*Lin*, 2004] with 1.9° longitude by 2.5° latitude horizontal resolution. In WACCM, the height of the model top, along with the good resolution in the middle atmosphere allows for an adequate representation of the stratospheric dynamics and variability (e.g., *CCMVal-2* [2010]). The chemistry module calculates in-line photolysis rates due to UV radiation and photoionization by the EUV flux. The model also includes ionization by energetic particle precipitation events in the auroral regions, as explained in *Marsh et al.* [2007]. These features are key for a realistic simulation of the UV-ozone feedback in the stratosphere, which involves the interaction of the UV variability with the Chapman Cycle, as described in Section 1.3.

As input for chemistry and radiation calculations, the SSI forcing from *Lean et al.* [2005] is used, as in most modeling studies discussed in Section 1.5. This popularity among modeling groups is due to the longer extension of this record compared to direct measurements. This allows for simulation of solar effects on climatic time scales, bearing in mind the potential underestimation of the UV variability in light of the recent SORCE-SIM estimates shown in Fig. 6. Since the solar flux from *Lean et al.* [2005] is available in relatively high spectral resolution, it can properly be used in WACCM without the need to interpolate to the bands included in the radiation code. In addition, the underlying CAMRT radiation code solves for 7 bands in the UV range, which is a reasonable resolution for accurate calculation of solar heating rates [*CCMVal-2*, 2010]. The offline performance of the CAMRT radiation code has been validated for stratospheric ozone changes since 1850 with the PORT radiative transfer tool [*Conley et al.*, 2012]. It was found that output from the radiation code compares well that obtained from more complex transfer schemes. Even though the offline performance has not been checked for maximum and minimum solar cycle conditions, the shortwave heating rate increase of 0.2 K/day calculated during peaks of solar activity in the transient simulations (Fig.8.12 in Chapter 8 of *CCMVal-2* [2010]) agree well with CCMVal models that perform well in this test (e.g., the EMAC model).

WACCM versions 3.5 and 4 are used in this thesis. The only major difference among them is the ability of WACCM4 to be coupled to the full ocean model Parallel Ocean Program (POP). The main improvements of WACCM3.5 and WACCM4 over their previous version WACCM3.1, used in CCMVal-1 [*Austin et al.*, 2008] and previous solar studies (e.g. *Marsh et al.* [2007]), are described next. A parameterization of turbulent mountain stress (TMS) is included

to estimate surface stress due to unresolved orography. This inclusion has been proved to bring the simulated frequency of sudden stratospheric warmings (SSWs) in very good agreement with observations [*Richter et al.*, 2009]. The parameterization of gravity waves has been updated based on a more physically related parameterization of the sources, which leads to a more realistic winter stratospheric jet [*Richter et al.*, 2009]. Failure in simulating realistic winds in this region is a common issue in many CCMs used for the simulation of the solar signal, as mentioned in Section 1.5.2. Both changes in gravity wave paramterization and the inclusion of turbulent mountain stress improved the winter mean climatology of the zonal mean zonal wind in the middle and high latitudes of the Northern Hemisphere [*Richter et al.*, 2009].

The implementation of the solar forcing is also improved in WACCM3.5 and WACCM4. In these versions, for wavelengths greater than 121 nm in the solar spectrum (Lyman-a), photolysis and photoionization rates are calculated directly using the SSI input, according to the recommendations for *CCMVal-2* [2010]. The radiative flux is obtained by integrating the spectral irradiance data over specific bands, and is used as input for both the chemistry and radiation modules. This replaces the implementation of the spectral irradiance in the WACCM3.1, in which the solar radiation shortward of 350 nm was inferred from the F10.7 index for radiative calculations, while a different forcing was used for the photolysis calculation (the details are given by *Marsh et al.* [2007]. In this way, heating and photolysis rates are calculated in a more self-consistent manner in WACCM3.5 and WACCM4.

Other novel aspects in WACCM3.5 and WACCM4 are the possibility of including a realistic QBO by means of an assimilation of observed tropical stratospheric winds [*Matthes et al.*, 2010], and both radiative and chemical effects of volcanic eruptions [*Tilmes et al.*, 2009].

2.1 Simulating solar cycle effects in WACCM

To simulate the 11-yr solar signal, and the boreal winter response in the Northern Hemisphere (objective 1 in Section 1.6), an ensemble of four WACCM3.5 simulations over the 1960-2005 period is used. The simulations were part of the CCMVal-2 activity [*CCMVal-2*, 2010] and are listed in Table 1. The design of the four members differs only in the initial conditions, as all other observed forcings are identical. These comprise a transient 11-yr solar cycle in spectral irradiance from *Lean et al.* [2005], observed SSTs and sea ice concentrations from *Hurrell et al.* [2008], and loadings of GHGs and ozone depleting substances from observations [*Eyring et al.*, 2008]. Volcanic forcing is implemented by prescribing the observed Aerosol Surface Area Densities (SADs) from *Thomason et al.* [1997].

name (n members)	SSTs	QBO	volcanoes	solar
refb1.x (4)	obs [*Hurrell et al.*, 2008]	assim [*Matthes et al.*, 2010]	SAGE II [*Thomason et al.*, 1997]	[*Lean et al.*, 2005]

Table 1: Forcings used to perform the WACCM3.5 ensemble, which is aimed at simulating the atmospheric response to the 11-yr solar cycle (task 1).

The solar response is diagnosed using two different statistical methods of common use in the

literature: multiple linear regression (MLR) and composite analysis. The standard MLR technique is used to diagnose the 11-yr signal in temperature and ozone in the tropical stratosphere. In the regression equation, predictors which are consistent with the design of the WACCM3.5 simulations are included. These comprise a long-term trend, the F10.7cm index for solar activity, two orthogonal QBO indices, and a ENSO and volcanic terms. The autocorrelation of the residuals is taken into account in the regression analysis by including an autoregressive noise model of first order in the regression equation, following the procedure formulated by *Garny et al.* [2007].

The same MLR technique is applied to the ERA-40 re-analysis dataset for the 1979-2001 period to compare with the model results. A more direct comparison with results from *Frame and Gray* [2010] is not possible as the MLR they used to extract the temperature response (Fig. 9) contains more predictors than those considered in this thesis. In addition, the tropical signal in ozone is compared to that obtained from three satellite datasets, shown in Fig. 8 (see *Soukharev and Hood* [2006] for details).

In the NH high latitudes, the solar signal is diagnosed by means of composite differences between maximum and minimum (MAX-MIN) conditions of the 11-yr cycle. Composites are preferred over the MLR analysis, as responses in the polar stratosphere are expected to be nonlinear, as outlined in Section 1.2. Zonal wind changes track the response of the PNJ to the solar cycle. Shortwave heating differences identify the direct impact of solar MAX conditions in the upper tropical stratosphere. Transformed Eulerian Mean diagnostics are calculated to diagnose changes in wave-mean interaction patterns, which explain the solar cycle signal in the PNJ.

The inclusion of all types of observed forcings in a model simulation allows for a more direct comparison with observations than in previous related work. In addition, the availability of four members enables a proper quantification of the internal variability. This aspect was underestimated in previous modeling studies, which only used single realizations. The improved stratospheric variability, along with the improved implementation of UV variability makes the WACCM3.5 model an ideal testbed for the "top-down" mechanism.

With the simulations outlined here, we determine whether a realistic Northern Hemispheric boreal winter climate response can be simulated in a model with improved physics, driven with more realistic forcings than in previous studies (question 1 in Section 1.6). The first paper included in this thesis, entitled "The 11 year solar cycle signal in transient simulations from the Whole Atmosphere Community Climate Model" [*Chiodo et al.*, 2012] describes the main findings.

2.2 The robustness of the 11-yr signal in the tropical stratosphere

The use of more realistic forcings is crucial to the aim of providing robust modeling evidence for the solar signal. However, this practice can complicate the task of attributing 11-yr signals, as more sources of variability potentially generate quasi-decadal variations. This issue is especially relevant when the solar signal is diagnosed by means of MLR techniques, such as the case of the tropical stratosphere.

In the second part of the thesis, the robustness of the solar signal in the lower stropical stratosphere is assessed together with the potential aliasing from non-solar forcings.

As outlined in Section 1.4, the MLR methods can give unrealiable estimates in the presence of (i) persistence in the predictand time series (i.e., the meteorological variable used as input for regression), and (ii) multicollinearity between predictors. Thus, a novel MLR approach was formulated. It reduces both persistence and multicollinearity effects by filtering the data with a Box-Jenkins pre-whitening technique [*Box and Jenkins,* 1980], and by using an optimal lag in the predictors.

To answer question 2, four ensembles of transient experiments from WACCM3.5 over the 1960-2004 period were investigated. They are listed in Table 2. The four sets differ in the combination of forcings. One ensemble is driven with all observed forcings, using the same set-up employed in the simulations analyzed in the first part of this thesis. This set is referred to as "all forcings", and represents a reference case in this study. In addition, three idealized sets of experiments were performed, each of them excluding one of the non-solar forcings. Thus, in the "noQBO" set, the observed tropical zonal winds are not assimilated. Since WACCM3.5 is not able to spontaneously generate a QBO, weak easterlies are simulated in the tropical lower stratospheric region instead, excluding QBO variability. In the "fixedSSTs" set, ENSO variability is excluded by prescribing climatological values of the SSTs. Finally, the "noVOLC" set excludes the volcanic forcing by imposing climatological values of sulphate aerosols. These idealized experiments are enlightening to assess the impact of boundary conditions on the simulated solar signal.

name (n members)	SSTs	QBO	volcanoes	solar
all forcings (2)	obs [*Hurrell et al.*, 2008]	assim [*Matthes et al.*, 2010]	SAGE II [*Thomason et al.*, 1997]	[*Lean et al.*, 2005]
fixedSSTs (2)	climatological	assim [*Matthes et al.*, 2010]	SAGE II [*Thomason et al.*, 1997]	[*Lean et al.*, 2005]
noQBO (2)	obs [*Hurrell et al.*, 2008]	none (weak east)	SAGE II [*Thomason et al.*, 1997]	[*Lean et al.*, 2005]
noVOLC (2)	obs [*Hurrell et al.*, 2008]	assim [*Matthes et al.*, 2010]	climatological	[*Lean et al.*, 2005]

Table 2: Table of the performed WACCM3.5 ensembles to assess the impact of aliasing in the analysis of the 11-yr solar cycle signal (objective 2).

The 11-yr signal in tropical stratospheric temperature and ozone is diagnosed by applying the novel MLR approach described above to the four model ensembles. Differences in the apparent solar signal between the reference case ("all forcings") and the idealized experiments quantify the aliasing caused by the missing forcing.

The feasibility of extracting a robust 11-yr component from timely limited records, such as the case of state-of-the-art observational records, is also explored. For this purpose, the sensitivity of the SC signal to the extension of the input record in the "all forcings" set is studied. This suggests the number of years needed to extract a robust 11-yr signal. To get insight into the feasibility of extracting a robust signal from observational records, the same exercise is repeated with NASA's reanalysis MERRA [*Rienecker et al.*, 2011] for the 1979-2004 period.

Previous work on the potential aliasing in the tropical signal was either performed with idealized 2-D models (e.g. [*Lee and Smith*, 2003; *Smith and Matthes*, 2008], or with older versions of WACCM [*Marsh and Garcia*, 2007]. The novelty of the present work lies in the use of an improved version of WACCM, a more realistic set-up, and in the development of an improved regression method, which is less prone to aliasing. Results from this analysis shed light on the origin of the secondary maximum in ozone and temperature in the tropical lower stratosphere, thus answering the question 2 defined in Section 1.6, and are described in the paper entitled "On the detection of the solar signal in the tropical stratosphere" [*Chiodo et al.*, 2014], whose Appendix contains the technical details of the novel MLR approach.

2.3 Solar forcing in climate change projections

In the third part of this thesis, the climatic impact of a more realistic future minimum scenario compared to those used in previous modeling studies (e.g., *Anet et al.* [2013]; *Meehl et al.* [2013]. is explored. WACCM4 is used in this part instead of WACCM3.5, as it allows for production of coupled ocean-atmosphere-chemistry climate simulations.

The experiments performed within this part are listed in Table 3. A three-member ensemble over the 2005-2065 period, referred as "MIN" case, is forced with a mid-range scenario of GHGs emissions according to the Representative Concentration Pathway 4.5 (RCP4.5) [*Stocker et al.*, 2013], and a realistic minimum scenario for solar irradiance. The MIN simulations are compared with a three-member ensemble "RCP4.5" from the same model driven with the same GHGs concentrations, but repeating the last four observed solar cycles (19-23). The three members of each ensemble only differ in the initial conditions.

For the MIN simulations, the spectral irradiance is compiled from records of years of minimum activity within the 11-yr solar cycle [*Wang et al.*, 2005]. According to *Schrijver et al.* [2011], this represents a more plausible scenario of solar activity than those used in previous studies. As a result, a reduction in spectral irradiance is applied, which is mostly prominent in the UV wavelengths (120-319 nm) with a relative variation of 2-5%, while it is considerably weaker in the VIS part of the solar spectrum (320-700 nm), with a variation of 0.1-0.5%.

name (n members)	GHGs + ODS	solar
MIN (3)	RCP4.5	solar MIN
RCP4.5 (3)	RCP4.5	11y SC
MINuv (1)	RCP4.5	solar MIN [UV] // 11y SC [VIS]
MINvis (1)	RCP4.5	11y SC [UV] // solar MIN [VIS]

Table 3: Table of the performed CESM-WACCM4 experiments to explore the impact of a future minimum under climate change scenarios (question 3).

First, the evolution of global mean temperature is evaluated in both ensembles to assess the impact of the MIN forcing on the simulated global warming tendency over the 2005-2065

period. Next, the impact of the MIN forcing on surface climate is explored by taking differences between the MIN and RCP4.5 climatologies. Emphasis is given on the boreal winter surface climate responses. The reason for the focus on the boreal winter is two-fold; (1) this is the season during which high latitudes in the NH experience the largest GHG-warming compared to other parts of the globe (also referred to as Arctic Amplification), and (2) this is the season that shows the strongest impact due to "top-down" mechanisms, as evidenced in the first part of this thesis.

The use of a constant MIN forcing allows using climatological differences for diagnosing the simulated response, with a modified t-test significance test to take autocorrelation into account [*Zwiers and von Storch*, 1995]. Thus, the use of MLR analysis is avoided, thereby circumventing problems related to aliasing, as described in the second part of this thesis. In addition, the availability of three members for each ensemble allows for accurate quantification of the natural (internal) variability and a more stringent significance test, since the t-test statistics of the MIN minus RCP4.5 differences are based on two relatively large samples (61 x 3 = 183 years).

Additional simulations are performed to separate the contribution of "top-down" and "bottom-up" mechanisms to the surface response simulated in the MIN ensemble. The simulations are listed in Table 3. In one of them, the MIN forcing is imposed in the UV only (MINuv), while a time varying solar cycle is imposed elsewhere, as it is done in the RCP4.5 ensemble. This simulation limits the direct impact of the MIN forcing to the stratosphere. The second simulation is driven with solar MIN forcing in the VIS (MINvis), being the rest of the spectrum common to the RCP4.5 case. In MINvis, the direct impact of the MIN forcing is limited to the surface. This study is described in the third part of this thesis [*Chiodo et al.*, 2014, submitted].

3 The 11 year solar cycle signal in transient simulations from the Whole Atmosphere Community Climate Model

The 11 year solar cycle signal in transient simulations from the Whole Atmosphere Community Climate Model

G. Chiodo,[1] N. Calvo,[2] D. R. Marsh,[2] and R. Garcia-Herrera[3]

Received 13 June 2011; revised 3 February 2012; accepted 9 February 2012; published 29 March 2012.

[1] The atmospheric response to the 11 year solar cycle (SC) and its combination with the quasi-biennal oscillation (QBO) are analyzed in four simulations of the Whole Atmosphere Community Climate Model version 3.5 (WACCM3.5), which were performed with observed sea surface temperatures, volcanic eruptions, greenhouse gases, and a nudged QBO. The analysis focuses on the annual mean response of the model to the SC and on the evolution of the solar signal during the Northern Hemispheric winter. WACCM3.5 simulates a significantly warmer stratosphere under solar maximum conditions compared to solar minimum. The vertical structure of the signal in temperature and ozone at low latitudes agrees with observations better than previous versions of the model. The temperature and wind response in the extratropics is more uncertain because of its seasonal dependence and the large dynamical variability of the polar vortex. However, all four simulations reproduce the observed downward propagation of zonal wind anomalies from the upper stratosphere to the lower stratosphere during boreal winter resulting from solar-induced modulation of the polar night jet and the Brewer-Dobson circulation. Combined QBO-SC effects in the extratropics are consistent with observations, but they are not robust across the ensemble members. During boreal winter, solar signals are also found in tropospheric circulation and surface temperature. Overall, these results confirm the plausibility of proposed dynamical mechanisms driving the atmospheric response to the SC. The improvement of the model climatology and variability in the polar stratosphere is the basis for the success in simulating the evolution and magnitude of the solar signal.

Citation: Chiodo, G., N. Calvo, D. R. Marsh, and R. Garcia-Herrera (2012), The 11 year solar cycle signal in transient simulations from the Whole Atmosphere Community Climate Model, *J. Geophys. Res.*, *117*, D06109, doi:10.1029/2011JD016393.

1. Introduction

[2] The influence of the solar cycle (SC) on climate is a research topic of high scientific relevance because of the need of estimating and separating natural variability from anthropogenic climate change. This challenge is hampered by the lack of understanding in the physical mechanisms involved in the atmospheric response to variations in solar flux, such as those over the 27 day rotational period, and the 11 year SC.

[3] The measured total change in solar irradiance during the 11 year SC is around 0.1%, translating into a radiative forcing of 0.2–0.3 W m^{-2} in the total solar irradiance (TSI). Although the net forcing in the TSI is small, measurements from space indicate large variations (4%–8%) in the UV range of 200–250 nm from solar minima to maxima conditions [*Lean et al.*, 1997]. The increase in UV irradiance modulates stratospheric ozone and oxygen photolysis, in a way that ozone concentration increases in the upper and middle stratosphere during solar maximum. Strong absorption of UV radiation by the additional ozone augments the temperature response in the upper stratosphere, thus providing an amplification mechanism for the response in temperature [*McCormack and Hood*, 1996; *Shindell et al.*, 1999].

[4] Satellite observations and reanalysis data show that the strongest variations in ozone associated with the 11 year SC occur in the upper tropical stratosphere [*Hood et al.*, 1993; *McCormack and Hood*, 1996; *Soukharev and Hood*, 2006; *Randel and Wu*, 2007]. In addition, a significant increase is also found in the lower tropical stratosphere. This leads to a double-peak structure in the vertical profile of the ozone response at low latitudes [*Soukharev and Hood*, 2006]. The impact of the 11 year SC has also been observed in zonal mean temperature and winds. Satellite and reanalysis data sets show a significant warming in the upper tropical stratosphere [*Frame and Gray*, 2010; *Gray et al.*, 2010]. However, the signals in temperature are not confined to the upper stratosphere. A warming response was also observed in the lower tropical stratosphere [*Labitzke and Van Loon*, 1995]. These responses were also evident when data

[1]Departamento Fisica de la Tierra II, Facultad de Ciencias Fisicas, Universidad Complutense de Madrid, Madrid, Spain.
[2]Atmospheric Chemistry Division, National Center for Atmospheric Research, Boulder, Colorado, USA.
[3]Agencia Estatal de Meteorologia, Madrid, Spain.

0148-0227/12/2011JD016393

covering an additional solar cycle became available [*Crooks and Gray*, 2005], and when the effect of volcanic eruptions was adequately separated [*Frame and Gray*, 2010]. Solar signals in temperature and zonal wind were also documented during boreal winter in the extratropical lower stratosphere [*Crooks and Gray*, 2005; *Frame and Gray*, 2010]. In addition, NCEP reanalysis and model simulations suggest that peaks of solar activity lead to a poleward shift of the subtropical tropospheric jet and to a broadening of the Hadley circulation [*Haigh and Blackburn*, 2006].

[5] The solar-induced temperature changes in the upper tropical stratosphere are caused by a direct response to the increase in UV radiation. The response in the other atmospheric regions (e.g., in the lower equatorial and extratropical stratosphere) is an indirect result of dynamical changes in stratospheric and tropospheric circulation. During boreal winter, a poleward and downward propagation of solar signals in zonal wind has been observed in the extratropical stratosphere [*Kuroda and Kodera*, 2002]. Accordingly, it seems plausible that the radiatively driven signal in the upper tropical stratosphere propagates to the lower stratosphere and to the troposphere via dynamical processes, so that the 11 year SC can influence the lower atmosphere via a "top-down" pathway [*Matthes et al.*, 2006; *Meehl et al.*, 2009]. In addition, *Meehl et al.* [2009] suggest that the impact of the SC in the troposphere could also be originated by a "bottom-up" pathway involving ocean-atmosphere feedbacks in the Pacific region.

[6] Although a unique and definitive mechanism has not been identified yet for both pathways, for the top-down response, there is general consensus on two hypothesized processes controlling the downward propagation of the SC signals in temperature and zonal wind [*Kodera and Kuroda*, 2002]: (1) the modulation of the polar night jet (PNJ) oscillation and (2) changes of the Brewer-Dobson circulation. These processes are driven by a combination of direct (radiative) and indirect (dynamical) effects in the stratosphere, which operate during winter months in both hemispheres.

[7] However, interactions between the SC and other modes of stratospheric variability, e.g., the quasi-biennial oscillation (QBO) and El Niño–Southern Oscillation (ENSO), complicate the overall picture. Several observational studies indicated that correlations of solar activity with winter temperatures in the lower extratropical stratosphere increase substantially in February when the data is stratified according to the QBO phase [*Labitzke*, 1987; *Labitzke and Van Loon*, 1989; *Labitzke*, 2004]. A similar QBO-SC relationship was also found in the low equatorial stratosphere [*Labitzke*, 2005]. These combined QBO-SC effects seem to depend on the state of the winds in the upper stratosphere, as suggested by *Gray et al.* [2004], where QBO and solar influences may enhance or counteract each other. Nevertheless, the detailed physical mechanism which originates this relationship remains unclear.

[8] Additionally, the characterization of the observed solar signal is hampered by limitations in the length and quality of the observational data sets and the statistical analysis. Reanalysis from NCEP-NCAR [*Kalnay et al.*, 1996; *Kistler et al.*, 2001] and ERA-40 [*Uppala et al.*, 2005] cover the last five solar cycles (1950–2009). However, reliable satellite data covering altitudes above 10 hPa became available for assimilation in 1978. Hence, the assimilation systems have only been constrained with stratospheric observations for a time span covering the last three cycles (1978–2009).

[9] Such a limited reference period might complicate the attribution of decadal variability to the SC because of the contamination of the solar signal with that from other sources of variability as, e.g., volcanic aerosols [*Lee and Smith*, 2003], ENSO [*Marsh and Garcia*, 2007], and QBO [*Smith and Matthes*, 2008]. In addition, previous observational studies were generally based on linear statistical methods like regression models, which are methods that cannot, by definition, account for the nonlinear interactions mentioned above.

[10] A whole range of atmospheric models has been used in the past to simulate the stratospheric and tropospheric response to solar variability. Pioneering work was done with 2-D models with interactive photochemistry [*Huang and Brasseur*, 1993; *Haigh*, 1994; *Fleming et al.*, 1995]. Improved versions of 2-D models with interactive photochemistry and dynamics were used to determine possible aliasing effects in the observed 11 year SC signals in ozone and temperature in the lower stratosphere due to the QBO and volcanic events [*Lee and Smith*, 2003; *Smith and Matthes*, 2008]. However, these models lacked a full description of wave-mean flow interactions that have been proposed to be the origin of these signals.

[11] Further improvements were made by using GCMs with interactive chemistry (hereafter chemistry-climate models (CCMs)) [*Tourpali et al.*, 2003; *Rozanov et al.*, 2004; *Egorova et al.*, 2004; *Marsh et al.*, 2007; *Schmidt et al.*, 2010; *Matthes et al.*, 2010]). Despite advances in model physics, the improvement of CCMs over 2-D models in reproducing the observed solar signal in temperature and ozone was only partial [*Labitzke et al.*, 2002], particularly in the tropical lower stratosphere. The reasons for this are still unclear, although CCMs still presented limitations, as the absence of an internally generated QBO (e.g., the models used by *Tourpali et al.* [2003], *Egorova et al.* [2004], and *Marsh et al.* [2007]), the use of perpetual maximum and minimum solar activity conditions [e.g., *Marsh et al.*, 2007; *Schmidt et al.*, 2010], or climatological SSTs as boundary conditions [e.g., *Tourpali et al.*, 2003; *Egorova et al.*, 2004; *Matthes et al.*, 2004]. Some of the CCMs simulate a significant response in the polar vortex during boreal winter in the NH [*Matthes et al.*, 2004; *Rozanov et al.*, 2004; *Schmidt et al.*, 2010]. However, the observed magnitude and seasonal march of the extratropical signals in zonal wind and temperature were not reproduced by these models.

[12] Another limitation of most previous modeling studies, when the analysis was extended to the extratropics and focused on the seasonal evolution of the solar signal in zonal wind and temperature, was the use of single simulations instead of an ensemble [e.g., *Matthes et al.*, 2004; *Tsutsui et al.*, 2009; *Schmidt et al.*, 2010]. The significance of the simulated solar signals is then generally small because of the high levels of variability, especially at high latitudes. In an experimental design with transient forcings, the use of ensembles leads to a better estimate of the model variability, and thus of the significance of the solar signal.

[13] In this paper we present the analysis of the 11 year solar signal in four-member ensemble of simulations from a "whole atmosphere" CCM incorporating an assimilated QBO: version 3.5 of the Whole Atmosphere Community

Climate Model (WACCM3.5). The simulations were performed with all observed forcings for the reference period 1960–2005, including prescribed SSTs as boundary conditions, which allows for direct comparison with observations. The model has a well resolved stratosphere and a vertical domain extending to 145 km, which leads to better representation of wave-mean flow interactions, and makes the model particularly suited for investigating the top-down solar-induced response. Accordingly, analysis of both the composited ensemble mean and each ensemble member reveals a robust solar signal in the upper stratosphere that propagates to the troposphere via wave-mean flow interactions during Northern Hemisphere (NH) winter, consistent with previously proposed mechanisms. Our results show that the simulated response in the tropical lower stratosphere is linked to the evolution of the extratropical SC signal.

[14] The paper is arranged as follows. Section 2 provides a description of the model, the experimental design and the statistical methods employed to extract the SC signal in different fields (e.g., ozone). The simulated annual mean response to the SC is presented in section 3. In section 4, the analysis is refined to monthly timescales, and dynamical mechanisms are explored. Section 5 summarizes the main results and conclusions.

2. Data and Methodology

2.1. Model and Experimental Design

[15] WACCM3.5 is an improved version of the WACCM3.1 global circulation model [*Garcia et al.*, 2007]. It has 66 vertical levels which extend from the surface to the thermosphere (145 km). Since the vertical model layers are based on a hybrid pressure–sigma coordinate system, the vertical resolution is variable, and ranges from approximately 1 km in the mid troposphere to about 3.5 km in the upper mesosphere. The underlying GCM is based on CAM3 [*Collins et al.*, 2004] and uses a finite-volume dynamical core [*Lin*, 2004] with 1.9° longitude by 2.5° latitude horizontal resolution. In the simulations analyzed here, WACCM3.5 was run coupled with a fully interactive chemistry module (details are given by *Kinnison et al.* [2007]) that includes neutral and ionized species. In addition to photoionization by extreme ultraviolet radiation, the model includes ionization by energetic particle precipitation events in the auroral regions, as explained by *Marsh et al.* [2007]. This leads to a more accurate representation of thermospheric nitric oxide, which might also be transported to the upper stratosphere, affecting ozone concentrations and heating rates [*Marsh et al.*, 2007].

[16] The major code changes from WACCM3.1 to WACCM3.5 relate to the gravity wave (GW) physics. The triggering of GW near the tropopause is driven by a more physically based parameterization [*Richter et al.*, 2009] than in WACCM3.1. *Richter et al.* [2009] showed that the change in GW physics leads to a more realistic winter stratospheric jet in WACCM3.5 compared to the previous version WACCM3.1. Furthermore, they showed that the inclusion of a turbulent mountain stress term to estimate surface stress due to unresolved orography has a large impact on the simulated frequency of major sudden stratospheric warmings (SSWs). The frequency of major SSWs in WACCM3.5 simulations is reported to be 0.6 events per year (yr^{-1}), which is in agreement with ERA-40 (0.6 yr^{-1}), while WACCM3.1 shows a much lower frequency (0.1 yr^{-1}) [*Richter et al.*, 2009].

[17] For the solar spectral irradiance at wavelengths greater than 121 nm (Lyman-α), photolysis and photoionization rates are calculated directly using the spectral irradiance modeled by *Lean et al.* [2005], according to the recommendations for the second CCM Validation Activity (CCMVal-2) from the Stratospheric Processes and their Role in Climate (SPARC) project. The radiative flux is obtained by integrating the spectral irradiance data over specific bands, and is used as input for both the chemistry and radiation modules. This replaces the implementation of the spectral irradiance in the WACCM3.1 model, in which the solar radiation shortward of 350 nm was inferred from the $F_{10.7}$ index (the details are given by *Marsh et al.* [2007]). For the extreme ultraviolet spectral range (wavelengths between 0.05 nm and 121 nm), the Solomon and Qian parameterization [*Solomon and Qian*, 2005] is used to calculate the solar irradiance and the solar variability factor, as in WACCM3.1. More details of the parameterization, along with the photochemistry of the model, are given by *Marsh et al.* [2007].

[18] We use an ensemble of four simulations of the WACCM3.5 model run from 1960 to 2005, whose design differs only in the initial conditions. The simulations were run with observed forcings, which comprise spectrally resolved solar variability, observed SSTs and sea ice concentrations, loadings of GHG and ozone depleting substances. Model equatorial stratospheric winds were relaxed toward observed winds to obtain a realistic time-varying QBO oscillation [*Matthes et al.*, 2010]. The effects of volcanic eruptions are simulated by prescribing the surface area density of sulphate aerosols. The assumed aerosol mass distribution is then used along with all other radiatively active gases for the calculation of heating and cooling rates (more details are given by *Tilmes et al.* [2009]).

[19] The imposed SSTs and zonal winds in the tropical stratosphere that follow observations may contain decadal perturbations, which are not related to solar variability. Thus, the responses attributed to the SC may contain signals arising from other sources of variability (i.e., aliasing from decadal changes in ENSO and QBO). On the other hand, nonlinear interactions between changes due to solar variability and other sources of variability would only be captured in such an approach. The inclusion of observed SSTs and QBO variations leads to a more realistic representation of the variability in the simulated climate, particularly in the extratropical stratosphere [*Sassi et al.*, 2004]. This also possibly leads to a higher level of realism in the simulation of solar signals, as part of natural variability in the climate system.

[20] The simulations are part of the CCMVal-2. The results of this activity revealed that the WACCM3.5 climatological global mean temperature and its long-term trends in the stratosphere are in good agreement with observations, and the model accurately represents the annual mean and the annual cycle in ozone and global column ozone [*Austin et al.*, 2010]. WACCM3.5 is also successful in reproducing the stratospheric mean state of the NH, while in the Southern Hemisphere (SH) problems were reported concerning the strength of the stratospheric jet and the cold bias in SH

spring. This bias in the SH is linked to a late vortex breakdown, which indicates that the winter state in this hemisphere lasts too long [*Butchart et al.*, 2010; *Eyring et al.*, 2010]. In the NH, both the shape and the interannual variability of the stratospheric jet are improved in WACCM3.5 compared to previous versions of the model, and the bias in strength was reduced from 20 to 10 m/s [*Richter et al.*, 2009]. The report also showed that WACCM3.5 reproduces a realistic solar signal in temperature and ozone. However, their work on the solar signal was only based on one of the four ensemble realizations (K. Matthes, personal communication 2010), and the annual mean model response was only analyzed in the tropics [*Manzini et al.*, 2010].

2.2. Statistical Methods

[21] The inclusion of all types of observed forcings in a model simulation, as outlined above for WACCM3.5, allows direct comparison with observations but complicates the task of attributing certain signals to solar variability. For this reason, we examined the solar-induced response with two different statistical methods which are in common use in the literature: multiple linear regression (MLR) and composite analysis. Nonlinear interactions with other sources of variability have been reported to occur in the extratropics [*Calvo et al.*, 2009; *Calvo and Marsh*, 2011]. Therefore, composites are preferred over the regression for the analysis of the signal in the extratropical stratosphere during winter.

2.2.1. Multiple Linear Regression

[22] The solar signal is often calculated in observations and model simulations by means of linear regression methods, in which the predictors represent the forcings included in the simulations. For comparison purposes with previous studies, we also adopt the standard MLR technique, and regress monthly and annual mean fields onto different predictors, which are consistent with the design of the WACCM3.5 simulations:

$$\mathrm{Var} = b_0 + b_1 t + b_2 \mathrm{AOD} + b_3 F_{10.7a} + b_4 \mathrm{QBO}_1(\mathrm{EOF1}) + b_5 \mathrm{QBO}_2(\mathrm{EOF2}) + b_6 N3.4(t - \mathrm{lag}_{\mathrm{ENSO}}) \quad (1)$$

[23] We include a constant factor (b_0), a long-trend term, the 11 year SC, the QBO, an ENSO-term and a volcanic aerosol term in the statistical fit. A least squares linear trend is used to compute the long-term trend, while a 80 days centered mean of the daily values of the solar radio flux ($F_{10.7a}$) is used as input for the 11 year SC. The QBO term is calculated with two indexes, which are based on the first and second EOF in the QBO vertical domain [see *Randel and Wu*, 1996], orthogonal by construction. In the regression equation, the aerosol optical depth index (AOD index) is used as a predictor for volcanic effects. We used the data from *Sato et al.* [1993]; since no major eruptions occurred from 2000 until the end of our simulations (2005), no update of the AOD index has been necessary. N3.4 is the NIÑO 3.4 index, which is used as predictor for the ENSO effects. A 3 month lag is chosen to allow for the ENSO signal to propagate to the lower tropical stratosphere [*Garcia-Herrera et al.*, 2006].

[24] The autocorrelation of the residuals is taken into account in our regression analysis by including an autoregressive noise model of first order in the regression equation. The original data set (left-hand side of equation (1)) and the basis function (i.e., the matrix including all regressors) are corrected with the autocorrelation coefficient of the residuals, which is estimated from a first application of the MLR model (more details are given by *Garny et al.* [2007]). The use of this correction leads to more accurate estimates of the regression coefficients and of the 2σ uncertainty level of the fits [*Tiao et al.*, 1990]. We use the 2σ uncertainty from the corrected regression coefficients as a parametric test to assess significance of the solar regression fits.

[25] Even though a separation of the response to the whole set of forcings can be obtained, only the SC signature will be analyzed here. The regression method is only able to capture the linear solar signal. Therefore, nonlinear interactions between QBO and SC, which may be important contributors to the indirect dynamical effects observed in the lower stratosphere at high latitudes [*Labitzke and Van Loon*, 1989], cannot be accounted for.

[26] For better comparison with past observational [*Frame and Gray*, 2010] and modeling [*Austin et al.*, 2008] studies, we use the $F_{10.7}$ flux even though it has not been used to drive the solar variability in the WACCM3.5 model. The solar regression coefficient has also been normalized throughout the figures to a forcing of 100 units of the $F_{10.7}$ radio flux (100 sfu).

2.2.2. Composite Analysis

[27] All months and years in solar maximum and minimum conditions have been grouped together in the same monthly or annual composite whenever the monthly and annual mean observed F10.7 cm radio flux (downloaded from NOAA data service http://www.ngdc.noaa.gov/stp/solar/solardataservices.html) was higher than 145 (for solar maximum) or lower than 95 (for solar minimum).

[28] To examine the combined QBO-SC effects, the model data were also stratified according to the QBO phase. To do so, the equatorial zonal mean zonal wind at 30 hPa was used to define a QBO index. The same criteria used by *Calvo et al.* [2007] to analyze the QBO signature in ERA-40 data were used here. Monthly and annual mean model output were merged into the QBO/WEST or QBO/EAST phase whenever the average of the modeled equatorial zonal mean zonal wind at 30 hPa is higher than 5 m/s, or lower than −10 m/s. Positive values indicate westerly winds, while negative values indicate easterly winds. When studying the SC-QBO signal in the extratropics, an important requisite is that the model reproduces the observed extratropical QBO signal, known as the Holton-Tan (HT) relationship [*Holton and Tan*, 1980]. With the chosen threshold values of zonal wind for QBO/WEST and QBO/EAST conditions, a significant QBO signal computed as difference between QBO/WEST and QBO/EAST months is found during boreal winter in the NH polar vortex (not shown). As shown in Figure 1, the asymmetry of the threshold values for the QBO index follows that in the zonal wind values at the 30 hPa level, where easterly phases are stronger than westerly phases. The monthly mean composites for each solar and QBO phase have been computed as the average of all months included in each group, and differences between composites have been taken to analyze the respective signals. MAX-MIN differences are computed to investigate the pure SC signal, where MAX and MIN stand for solar maximum and

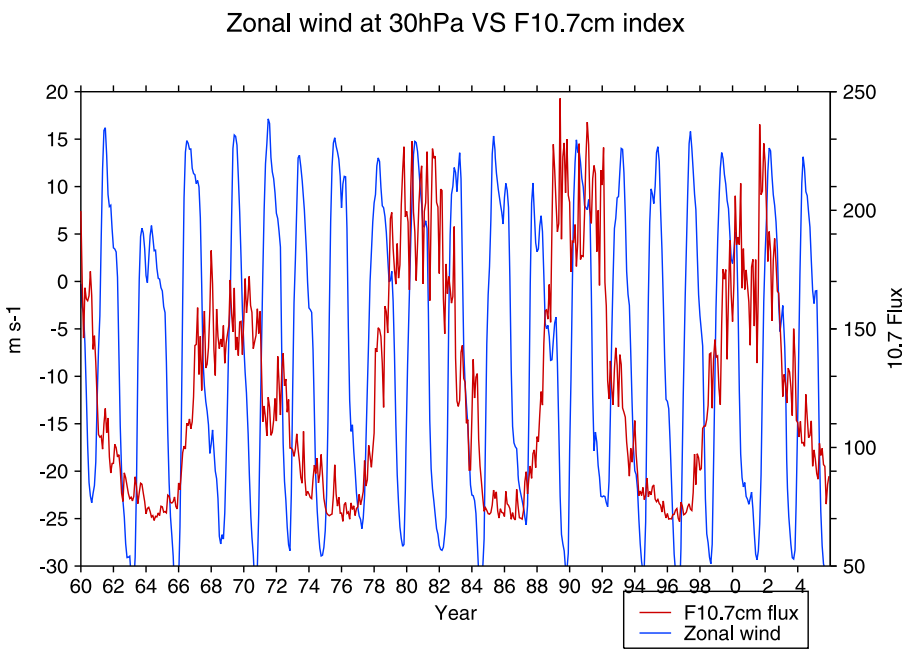

Figure 1. Time series of the zonal mean zonal wind (m/s) at 30 hPa and $F_{10.7}$ flux index during the simulated period (1960–2005).

minimum, respectively. Similarly, MAX-MIN differences have been stratified according to QBO/WEST and QBO/EAST conditions for the study of the SC-QBO signal.

[29] Tables 1 and 2 show the selected years for each SC and for all combinations of QBO and SC phase, respectively. To study the combined SC-QBO effects during NH winter, December has been used as a reference for the QBO phase, so that all winter months were grouped together according to the solar phase and the December zonal wind at 30 hPa. This was done to track the temporal evolution of the solar signal and its modulation by the QBO throughout the NH winter. Before compositing, data were linearly detrended between 1960 and 2005. Furthermore, years with major volcanic eruptions (1982 and 1991) were excluded to avoid aliasing of volcanic signals in the solar response [*Lee and Smith*, 2003]. Since a significant temperature signal caused by the Pinatubo eruption is still detectable approximately 16 months after the eruption event in 1991, the 1992 year was also excluded from the analysis. However, no significant anomalies related to other volcanic eruptions (e.g., Agung in 1963) were detectable in tropical lower stratospheric temperature, thus no more years were excluded from the calculation of composites. Statistical significance of the composite differences has been computed using a Student's *t* test. Throughout this paper, significant values correspond to the 95% confidence level.

Table 1. Years Selected to Compute the Composites for the Maximum (MAX) and Minimum (MIN) Solar Phases in WACCM3.5[a]

	Years
MAX	1960, 1968, 1969, 1970, 1979, 1980, 1981, 1989, 1990, 1999, 2000, 2001, 2002
MIN	1962, 1963, 1964, 1965, 1973, 1974, 1975, 1976, 1977, 1985, 1986, 1987, 1994, 1995, 1996, 1997, 2005

[a]The years 1982, 1991, and 1992 have been excluded from the MAX composite.

3. The Annual Mean Solar Signal

[30] The simulated ensemble mean annual zonal mean temperature and zonal wind responses to the SC have been calculated by means of the regression model described by equation (1). Results for the full reference period, 1960–2005, are shown for both variables in Figures 2a and 2b, respectively. In temperature, a statistically significant warming is evident throughout the stratosphere, characterized by a maximum in the upper stratosphere–lower mesosphere region of up to 0.6 ± 0.2 K/100 sfu at low latitudes, with peak values of 1.4 ± 1.0 K at high latitudes. As it will be shown later, the significant increase in annual mean stratospheric ozone (shown as vertical profile in Figure 4) and the shortwave heating anomalies of 0.2 K/d (not shown) over the upper stratospheric region indicate that the positive temperature signal in the upper stratosphere–lower mesosphere is radiatively driven. In the tropical stratosphere, the

Table 2. Years Selected to Compute the Composites for All Four Combinations of Solar (MAX and MIN) and Quasi-biennial Oscillation (QBO) (QBO/WEST and QBO/EAST) Phases in WACCM3.5

	Years
MAX+QBOW	1969, 1978, 1980, 1988, 1990, 1999, 2002
MIN+QBOW	1964, 1973, 1975, 1985, 1995, 1997
MAX+QBOE	1968, 1970, 1979, 1981, 1989, 2001
MIN+QBOE	1962, 1963, 1965, 1974, 1977,1994, 1996, 2005

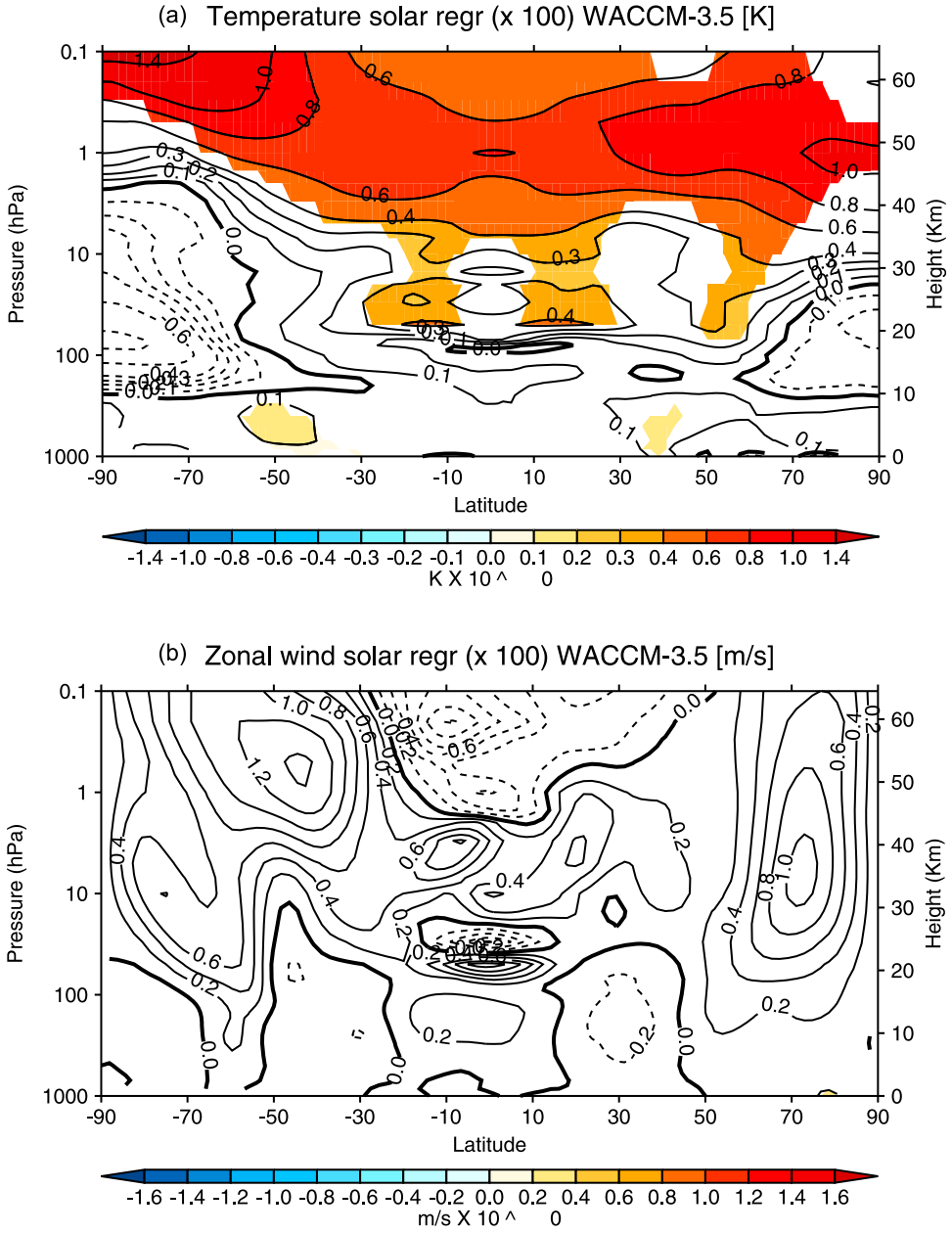

Figure 2. Solar cycle response in (a) zonal mean temperature and (b) zonal mean zonal wind, represented as solar regression coefficient (× 100 sfu) for the full reference period 1960–2005 in WACCM3.5. Colored fields are greater than 2σ. Contours are drawn every 0.1 K. Solid contour lines are drawn to indicate positive values (i.e., warming in Figure 2a and westerly anomalies in Figure 2b), while dashed contours indicate negative values (cooling in Figure 2a and easterly anomalies in Figure 2b).

magnitude of the response gradually decreases with decreasing height, although a statistically significant secondary maximum is found at 20 km. At this altitude, the structure of the response is composed by two separate maxima at subtropical latitudes, with values reaching 0.4 ± 0.1 K/100 sfu. Weaker, but significant, warming areas are also found in the midlatitude troposphere in both hemispheres. In the polar regions the model simulates a weak cooling, though not significant.

[31] It is apparent in Figure 2b that in the annual mean, peaks of solar activity lead to stronger westerlies in both hemispheres. This type of response is expected from the simulated warming at low latitudes on the basis of thermal wind balance. However, the simulated changes are not significant, which is due to the large dynamical variability in the extratropical stratosphere. Weak easterly anomalies are also found in the subtropical troposphere of both hemispheres. As it will be shown in section 4, the tropospheric changes, and the response in the extratropical stratosphere are both seasonally dependent and so lead to a signal in temperature and zonal wind that is only marginally significant in the ensemble mean annual mean.

[32] The results shown above have been calculated on the full available period to obtain a better signal to noise ratio. Nevertheless, the period for which reliable observational data sets exist is more limited than the one analyzed in the model. Even though more than 50 years of reanalysis data have become available [*Uppala et al.*, 2005], past observational studies focused on the 1979–2001 period, because it is the period during which satellite data have been assimilated in the reanalysis [*Crooks and Gray*, 2005]. A set of simulations was run with the preceding version of WACCM, WACCM3.1 at the same horizontal resolution, and transient forcings, although without the inclusion of a nudged QBO and volcanic eruptions. We compare the solar signal in temperature obtained from WACCM3.5 with that from its preceding version (WACCM3.1) and ERA-40 data sets over the 1979–2001 period [e.g., *Crooks and Gray*, 2005]. The regression model applied to ERA-40 data uses the same QBO regressors as in WACCM3.5 (see (1)), which are based on the first and second EOFs in the QBO domain. To account for the differences in the experimental design, we exclude the QBO and volcanic regressors from the model applied to WACCM3.1. Figure 3 plots solar regression coefficients in temperature from WACCM3.5 (Figure 3a), WACCM3.1 (Figure 3b), and ERA-40 (Figure 3c).

[33] Figure 3c reproduces the same structure shown by *Crooks and Gray* [2005] and *Frame and Gray* [2010], although the regression model applied here is not identical. It is evident from Figures 3a and 3b that both WACCM versions simulate a statistically significant response throughout the stratosphere, characterized by a maximum in the upper stratosphere–lower mesosphere region. At these altitudes, the solar-induced warming peaks at high latitudes, and the warming at low latitudes reaches 0.80 $\pm$ 0.10 K/100 sfu, with slightly higher values in WACCM3.5. These results do not differ from previous equilibrium simulations using WACCM3.1 [*Marsh et al.*, 2007; *Matthes et al.*, 2010] and other CCMs [*Tourpali et al.*, 2003; *Egorova et al.*, 2004; *Austin et al.*, 2008; *Schmidt et al.*, 2010], which suggests that other sources of variability do not affect the results in this region. Figure 3c reveals that a strong warming in the tropical stratopause is also present in ERA-40 data, although the warming in this data set is stronger and limited to low latitudes. In the tropical stratosphere, ERA-40 shows a relative minimum at 30 km, and a significant warming in the lower stratosphere (20 km), with a threefold structure composed by a maximum in the equatorial tropopause, and 2 distinct maxima at a slightly higher altitude in the subtropics with values of 0.80 $\pm$ 0.25 K/100 sfu.

[34] The SC temperature response in WACCM3.5 (Figure 3a) at 20 km is in better agreement with ERA-40 than WACCM3.1 (Figure 3b). In this region, we note that the amplitude of the solar signal in WACCM3.5 is stronger than in the full period (Figure 2a). A similar sensitivity of the response to the analyzed period was noted in WACCM3.1 for tropical ozone [*Marsh and Garcia*, 2007]. They showed that over a relatively short period (e.g., 1979–2003), ENSO may contaminate the solar signal in ozone. However, a separate analysis revealed that excluding the ENSO term in the regression model for WACCM3.5 does not alter our results, which differs from *Marsh and Garcia*'s [2007] results.

[35] Unlike ERA-40 and WACCM3.5, the temperature response in WACCM3.1 in the middle tropical stratosphere is significant. This is probably due to the absence of the QBO in these simulations, which reduces the variability of the temperature field in this region. The WACCM3.1 model shows a weak secondary maximum at 20 km, but there is not evidence of a threefold structure found in ERA-40.

[36] In WACCM3.1, the warming in the lower tropical stratosphere did not appear in previous equilibrium simulations [*Marsh et al.*, 2007; *Tsutsui et al.*, 2009]. With the inclusion of a QBO in the same model version, *Matthes et al.* [2010] reproduced a secondary maximum, whose amplitude is modulated by the QBO phase. However, the magnitude and the structure of the solar signal in temperature at low latitudes in their simulations are not in agreement with that obtained with ERA-40 data shown in Figure 3c.

[37] In the troposphere, both the WACCM ensemble and ERA-40 data show significant warming bands with values of approximately 0.20 $\pm$ 0.05 K/100 sfu at midlatitudes in the NH. The structure of the solar signal in tropospheric in temperature obtained by the regression method in WACCM3.5 is a robust feature since it appears in all ensemble members (not shown).

[38] Figure 4 shows the tropical mean (25°N–25°S) vertical profile of the relative ozone solar regression coefficients in both WACCM ensembles (red and black lines), and the weighted average of three independent satellite instruments presented by *Soukharev and Hood* [2006] (blue line), along with standard error bars for each data set. The satellite data show a relative ozone increase, with a two peak structure with maxima of approximately 2.5% $\pm$ 1.0%/100 sfu at 45 km, a relative minimum at 30 km, and a peak ozone response of more than 3% $\pm$ 2%/100 sfu in the lower tropical stratosphere at 50 and 70 hPa. *Lee and Smith* [2003] showed that the relative minimum response in the middle stratosphere may be due to aliasing of QBO and volcanic signals in ozone. This artifact may affect the results from WACCM3.5 since QBO and volcanoes are included in the simulations but not in WACCM3.1. Both WACCM models show an ozone response, which is broadly similar to that obtained from satellite data, although the structure in the middle and upper stratosphere is slightly shifted toward lower levels with respect to the satellite data.

[39] Interestingly, 2-D and general circulation models show the same discrepancy in the vertical profile of the tropical ozone response [*Rozanov et al.*, 2004; *McCormack et al.*, 2007; *Austin et al.*, 2008], as WACCM runs have revealed. It was speculated that this could be due to the coarse vertical resolution of satellite retrievals for ozone [*Austin et al.*, 2008]. At upper and middle stratospheric levels, the increase in UV radiation during peaks of solar activity favors chemical reactions, which in turn lead to an increase in ozone production [*Pap et al.*, 2003].

[40] The ozone response in WACCM3.5 at 50–70 hPa reaches values up to 3.2%–3.5% $\pm$ 1.0%/100 sfu, which is close to the observed values, while WACCM3.1 simulates a much weaker ozone response, as already shown in Figure 3b for temperature. This improvement of WACCM3.5 over WACCM3.1 is robust at the 50 hPa level, whereas at 70 hPa the uncertainty in the satellite data overlaps the range given by both WACCM models. It should be noted that the satellite data also show high levels of uncertainty. Most of the 2-D models do not show any evidence of a tropical secondary maximum [*Lee and Smith*, 2003; *Smith and Matthes*, 2008],

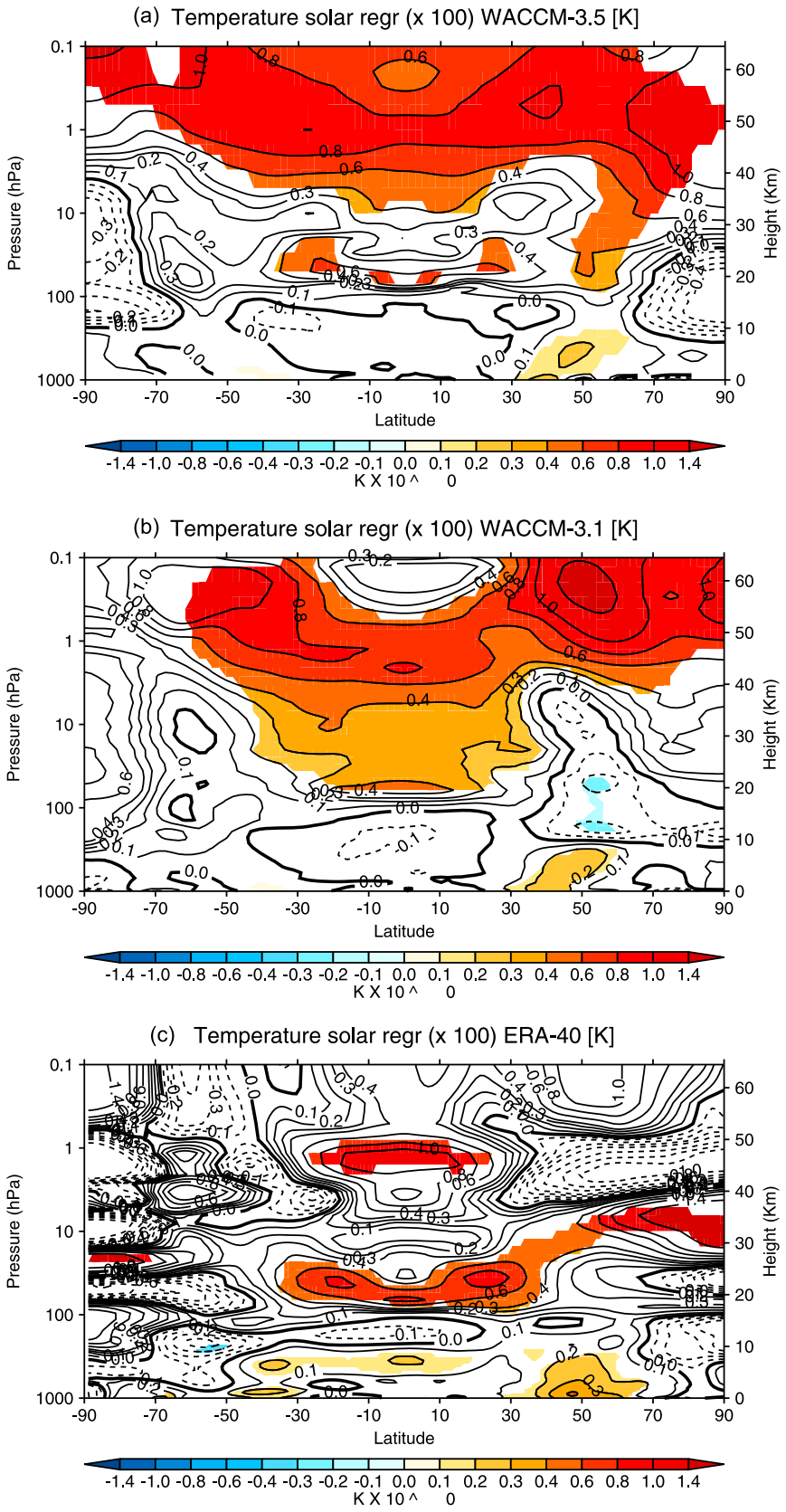

Figure 3. Solar cycle response in zonal mean temperature, displayed as solar regression coefficient ($\times$ 100 sfu) for the period 1979–2001 in (a) WACCM3.5, (b) WACCM3.1, and (c) ERA-40. Colored fields are greater than 2σ. Contours are drawn every 0.1 K. Solid contour lines are drawn to indicate positive values (i.e., warming), while dashed contours indicate negative values (i.e., cooling).

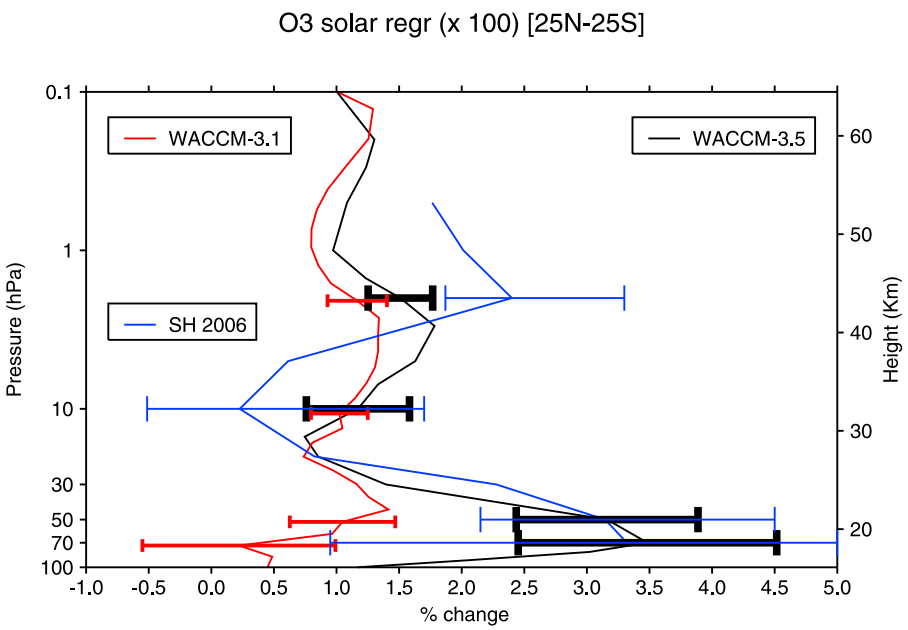

Figure 4. Relative SC response in ozone, displayed as solar regression coefficient of the ensemble mean zonal mean ozone concentration in WACCM3.5 (black), WACCM3.1 (red), and satellite data (blue). The response in satellite data represents the error-weighted mean of three different data sets from *Soukharev and Hood* [2006]. Error bars are drawn to display the 2σ uncertainty in the WACCM simulations and the standard error in satellite data.

while CCMs with comprehensive representation of stratospheric dynamics (e.g., the models used by *Marsh and Garcia* [2007] and *Schmidt et al.* [2010]) simulate a rather weak SC signal in ozone (of the order of 1%–1.5%). At such low stratospheric levels, ozone has a long lifetime, so the increase may be dynamically controlled through changes in vertical upwelling and transport during NH winter, which are investigated in section 4. Hence, the lack of response in some models (especially in 2-D models) could be originated by the missing dynamical feedback in the winter stratosphere.

[41] We tested the possibility of aliasing in the results in the tropical lower stratosphere, as shown by *Marsh and Garcia* [2007]. WACCM3.5 shows some sensitivity of the lower stratospheric ozone response to the reference period, as it occurs in zonal mean temperature. However, the ozone response in WACCM3.5 is stronger than in WACCM3.1 regardless of the length of the data set used in the regression analysis, and of the inclusion of the ENSO term in the regression model.

[42] In addition, the QBO modulation of the solar signal in the ensemble mean zonal mean temperature and ozone in the tropical lower stratosphere (30–50 hPa) is especially noticeable in the easterly phase of the QBO (not shown). The sign and the magnitude of the modulation agrees well with NCEP/NCAR reanalysis [*Labitzke*, 2004]. However, this modulation is not reproduced in all realizations, which indicates that this effect is not a robust feature in the WACCM3.5 simulations.

[43] Figure 5 shows the annual cycle of the solar regression coefficient in the lower stratosphere at 70 hPa as a function of latitude, calculated with ensemble mean zonal mean temperature in WACCM3.5. It is evident that the solar-induced warming of the lower stratosphere seen in Figure 2a has a seasonal cycle, with maximum values in September and December over the equator. Weaker but significant values are also found between 30°N and 45°N from October to January. No evidence of such seasonality in the SC signal in the lower tropical stratospheric temperature is found in the WACCM3.1 simulations (not shown). In the NH, cooling is found at high latitudes from October to January, and from April to June, although it is not statistically significant. A similar pattern is found in the SH between July and December.

[44] These results suggest that in WACCM3.5 the simulated SC signal in the tropical lower stratosphere is linked to

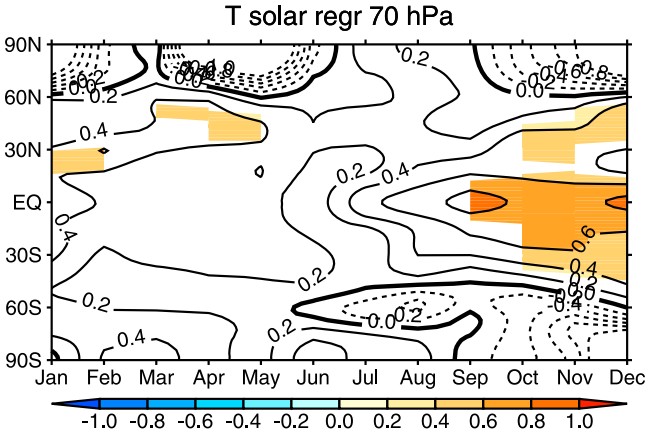

Figure 5. Annual cycle of the zonal mean temperature solar regression coefficient at 70 hPa. Colored fields are greater than 2σ. Contours are drawn every 0.2 K. Solid contour lines are drawn to indicate positive values (i.e., warming), while dashed contours indicate negative values (i.e., cooling).

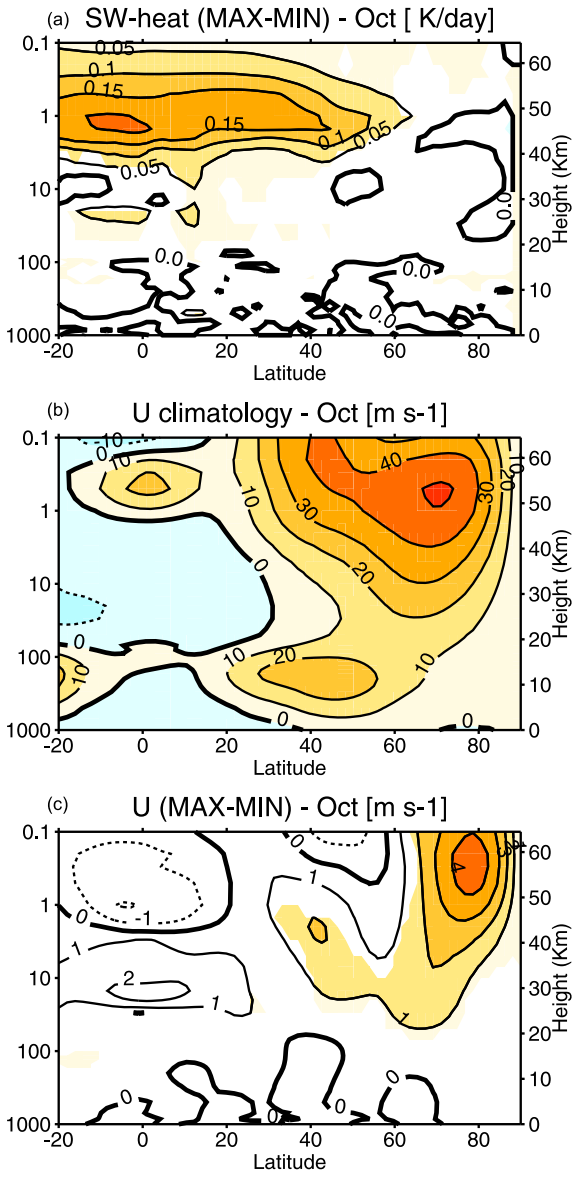

Figure 6. (a) Composite differences (MAX-MIN) of the ensemble mean October monthly mean of zonal mean shortwave heating rate in K/d, (b) zonal wind climatology of the 1960–2005 period in m/s, and (c) as in Figure 6a for zonal mean zonal wind. Shading denotes 95% significant areas; MAX and MIN stand for solar maximum and minimum, respectively.

the SC response at polar latitudes during NH winter and SH spring. For this reason, a detailed analysis of the seasonal evolution of the extratropical solar signal is key in understanding the dynamics of the response at low latitudes shown in this section, and will be shown next.

4. The Solar Signal During Northern Hemisphere Winter

[45] In this section, we present the analysis of the evolution of the SC signal in zonal wind and temperature through the course of the winter season in both hemispheres, with qualitative distinction between direct and indirect responses of the middle atmosphere to the SC.

[46] Figure 6a shows the ensemble mean MAX-MIN composite differences of the model shortwave heating in October. This field is useful to identify the direct model response to the solar forcing. In the upper stratosphere–lower mesosphere (50 km), the solar heating is mainly due to UV absorption by ozone, and it is limited to the tropics and the SH, where the Sun elevation is the highest during the NH fall season (not shown). At low latitudes, the shortwave heating increases by 0.2 K/d during MAX compared to MIN conditions. This is also true during the other fall months (September and November, not shown). This response enhances the meridional temperature gradient at approximately 60°N, where the core of the lower mesospheric jet is located (see Figure 6b). Because of thermal wind balance, the jet significantly increases by around 4 m/s (Figure 6c) during the same month. This is in line with NCEP reanalysis results [*Kuroda and Kodera*, 2001, 2002] and is consistent with the early winter direct solar-induced response mentioned in section 1.

[47] Figures 7 and 8 show MAX-MIN ensemble mean composite differences of the zonal mean zonal wind and temperature from November to February. In November (Figure 7a), the zonal wind anomaly of up to 5 m/s, which was initiated earlier in October by the anomalous UV forcing in the tropical stratopause region, starts to propagate downward to the middle polar stratosphere. The significant zonal wind signal attains its largest magnitude of 6 m/s in the middle polar stratosphere during December (Figure 7b), and negative anomalies appear in the subtropical upper stratosphere, although they are not significant. Weaker (2–4 m/s) but significant positive zonal wind anomalies migrate in January further down into the troposphere with a negative anomalies aloft (Figure 7c), which encompasses the whole polar stratosphere in February (Figure 7d) and March (not shown).

[48] As expected, the response in zonal mean wind is related to that in temperature. In the ensemble zonal mean temperature field (Figure 8), significant warming of up to 4 K develops in November in the polar lower mesosphere (Figure 8a) and propagates downward with height during the following winter months (December, January, and February, shown in Figures 8b, 8c, and 8d, respectively). This is accompanied by cooling at lower levels. Together, they form a vertical dipole structure, which propagates downward. In February (Figure 8d), the warming response is found at 40 km, with weak cooling above and below. The high-latitude temperature response is not significant during most of the winter months because of the high variability caused by the winter SSWs simulated in the model. During November (Figure 8a) and December (Figure 8b), a warming of up to 1 K is also found at low latitudes in the lower stratosphere.

[49] The evolution of the zonal wind signal mostly resembles the observed internal mode of variation of the PNJ [*Kuroda and Kodera*, 2001; *Kodera and Kuroda*, 2002], which indicates that the SC influences the extratropical stratosphere-troposphere system through a modulation of the PNJ oscillation. However, the observed poleward migration of the signal in zonal wind from November to December in the upper stratosphere [see *Kodera and Kuroda*, 2002, Figure 12] is missing in WACCM3.5 and only the downward propagation at polar latitudes is simulated. This is due to the biased position of the lower mesospheric jet in October, which is placed too far toward the pole at 60°N (Figure 6b)

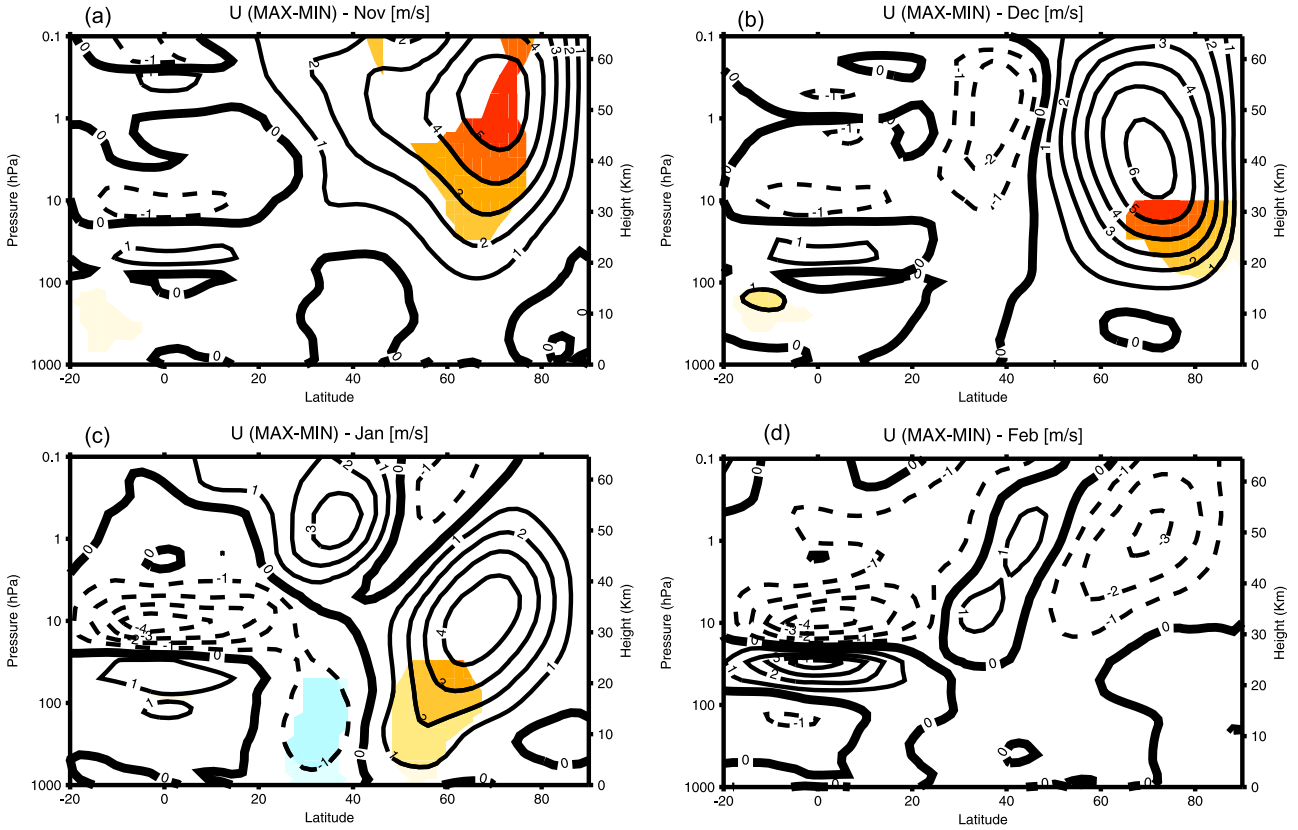

Figure 7. Composite differences (MAX-MIN) of the ensemble mean monthly mean zonal mean zonal wind for (a) November, (b) December, (c) January, and (d) February. Contours are drawn every 1 m/s. Solid contour lines are drawn to display positive (i.e., westerly) values, and dashed contours indicate negative (i.e., easterly) values. Shading denotes 95% significant areas.

compared to observations (not shown). Consequently, the zonal wind anomaly is triggered at midlatitudes instead of in the subtropical upper stratosphere, and propagates downward during the course of the NH winter.

[50] The individual response in zonal wind in the PNJ region (average between 60 and 80°N) can be seen in Figure 9 for each simulation (color lines), which shows the vertical profile of the zonal mean zonal wind MLR solar coefficient for November (Figure 9, top), December (Figure 9, middle), and January (Figure 9, bottom). The same figure also shows the solar regression coefficient of the ensemble mean zonal wind, along with error bars at the 2σ at each vertical model level (black lines). During MAX phases, an increase in zonal mean zonal wind in November (Figure 9, top) is simulated in all ensemble runs, although the magnitude of the wind response and the timing of its subsequent downward propagation varies significantly in each run. This is due to strong variability in some realizations (particularly in run 1 and 4) in December and January, which also explains why the regions of the ensemble mean composite differences are not significant during these months (see Figures 7c and 7d). These are also ensemble members which show a larger number of SSWs (L. De La Torre, personal communication, 2011). The strongest response and the fastest downward propagation of the westerly wind anomaly is found in run 3. Other runs (e.g., run 4) show stronger westerlies during December (Figure 9, middle), but the propagation of the anomalies to the lower levels is slow compared to run 3. Negative (i.e., easterly) anomalies start to appear in January (Figure 9, bottom) in the upper levels (1 hPa) in 2 of the 4 runs, and propagate to the lower levels in February–March (not shown). The strengthening of the PNJ is hence a robust feature of the SC signal in zonal wind in these simulations. Nevertheless, the magnitude of the zonal wind anomalies is uncertain because of large variability of the polar vortex, which is in turn related to the realistic experimental design which includes all observed forcings in the simulations.

[51] These results suggest that maxima of solar activity lead to a stronger polar vortex in November and December. The solar signal in zonal mean zonal wind is initially triggered by stronger UV heating in the upper subtropical stratosphere, and propagates down with the PNJ. In February–March during MAX conditions, the polar vortex weakens. The winter solar signal in zonal wind and temperature in the NH extratropical stratosphere is thus characterized by a transition between different states of the polar vortex. Solar-induced changes in wave-mean flow interactions drive the downward propagation of the stratospheric signal from early to mid winter and the opposite signal in late winter, as explained by *Kodera and Kuroda* [2002] in their conceptual model.

[52] The analysis of the Eliassen-Palm flux (EPF; more details are given by *Andrews et al.* [1987]) and its divergence provides a framework to diagnose and quantify

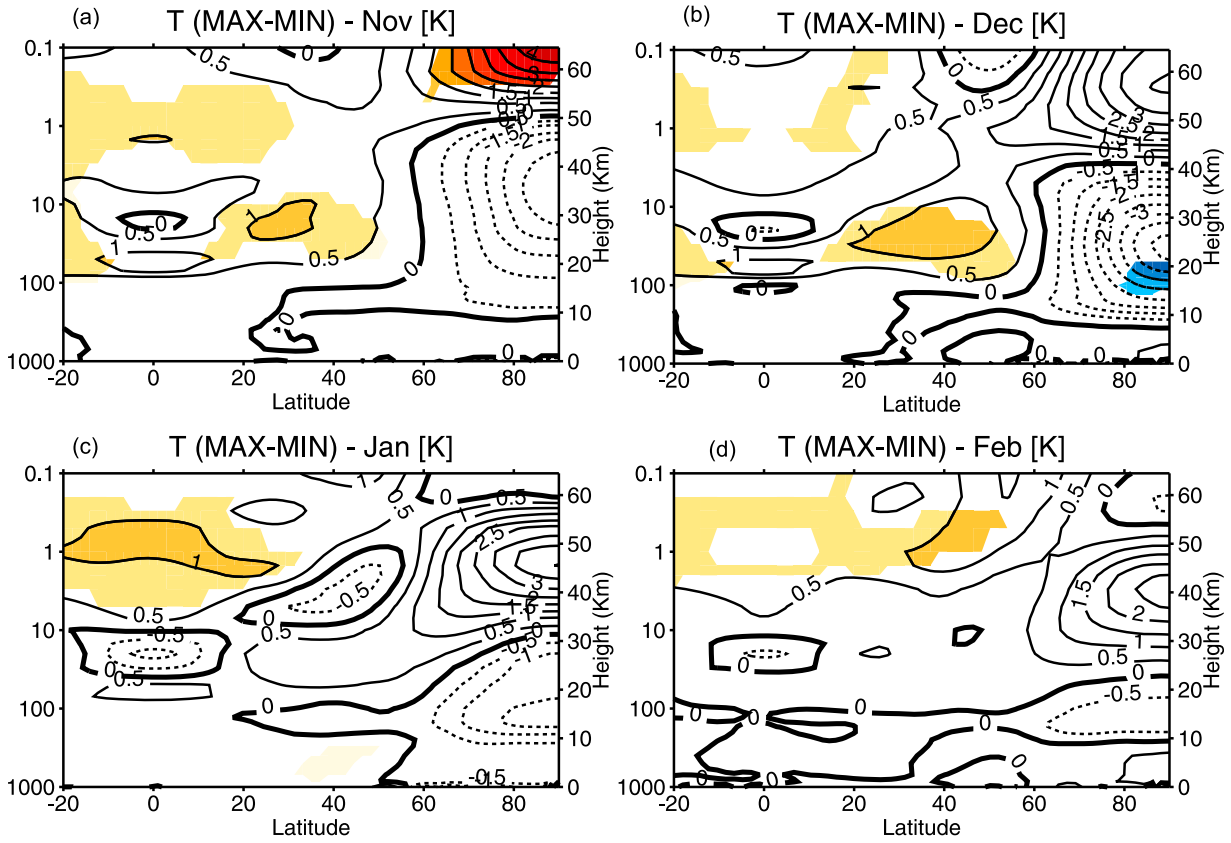

Figure 8. As in Figure 7 for ensemble mean zonal mean temperature. Contour intervals are 0.5 K.

changes in the planetary wave propagation and dissipation, respectively, and therefore to test the mechanisms proposed by *Kodera and Kuroda* [2002]. As a measure for planetary wave activity and wave-mean flow interactions, Figure 10 shows composite differences between MAX and MIN conditions for EPF and its divergence during November (Figure 10a) and December (Figure 10c). Figures 10b and 10d show the composites differences of the transformed Eulerian mean (TEM) meridional ($\bar{v}^*$) and vertical ($\bar{w}^*$) velocities for the same months, which represent the stratospheric mean meridional circulation. During MIN winters, there is upward wave propagation at 60°N from the troposphere into the stratosphere. In the stratosphere, the waves are then refracted toward lower latitudes, and strongly dissipated at higher levels (not shown). During MAX winters, the stronger westerly flow in the middle stratosphere at 60°N observed in November (Figure 7a) reduces the upward propagation of planetary waves in the region, and their equatorward deflection. These anomalies appear as a poleward and downward anomaly (relative to MIN conditions) in the composite differences (Figure 10a). Therefore, less dissipation occurs in this area as indicated by significant positive anomalies in the EPF divergence (2–2.5 m/s/d) simulated at midlatitudes at 50 km (color contours in Figure 10a). This leads in turn to anomalous relative counterclockwise motion in the middle and upper stratosphere, as seen in the TEM velocity vectors in Figure 10b, which act against the characteristic boreal winter stratospheric circulation. This implies that MAX conditions lead to weaker stratospheric residual circulation in November. Less meridional heat transport (not shown) and relative upwelling motion are simulated throughout the whole polar stratosphere (indicated by significant positive anomalies in $\bar{w}^*$ of 0.8 mm/s; color contours in Figure 10b), consistent with the significant cooling which develops in the lower polar stratosphere during November and December (Figures 8a and 8b). At low latitudes, relative downwelling motion during MAX conditions causes the weak warming in the subtropical lower stratosphere in November (Figure 8a).

[53] In December, the positive zonal wind anomalies move downward to the polar lower stratosphere (Figure 7b), and equatorward propagation of waves is enhanced in the lower stratosphere between 40 and 60°N in December (Figure 10c). Further aloft in the polar stratosphere, composite differences indicate an increase in upward and equatorward EPF propagation, and significantly stronger EPF convergence at 40 km during MAX conditions. The enhanced wave dissipation forces a negative westerly anomaly at these levels, which propagates poleward and downward in January–February (see Figures 7c and 7d) and reaches the lower stratosphere in March (not shown). The stronger EP flux convergence also leads to relative clockwise residual motion (which implies stronger Brewer-Dobson circulation) in the middle stratosphere during December (Figure 10d) and following late winter months (not shown). Consequently, relative downwelling in the upper polar stratosphere (indicated by negative anomalies in $\bar{w}^*$, which are drawn as color contours) leads to adiabatic warming

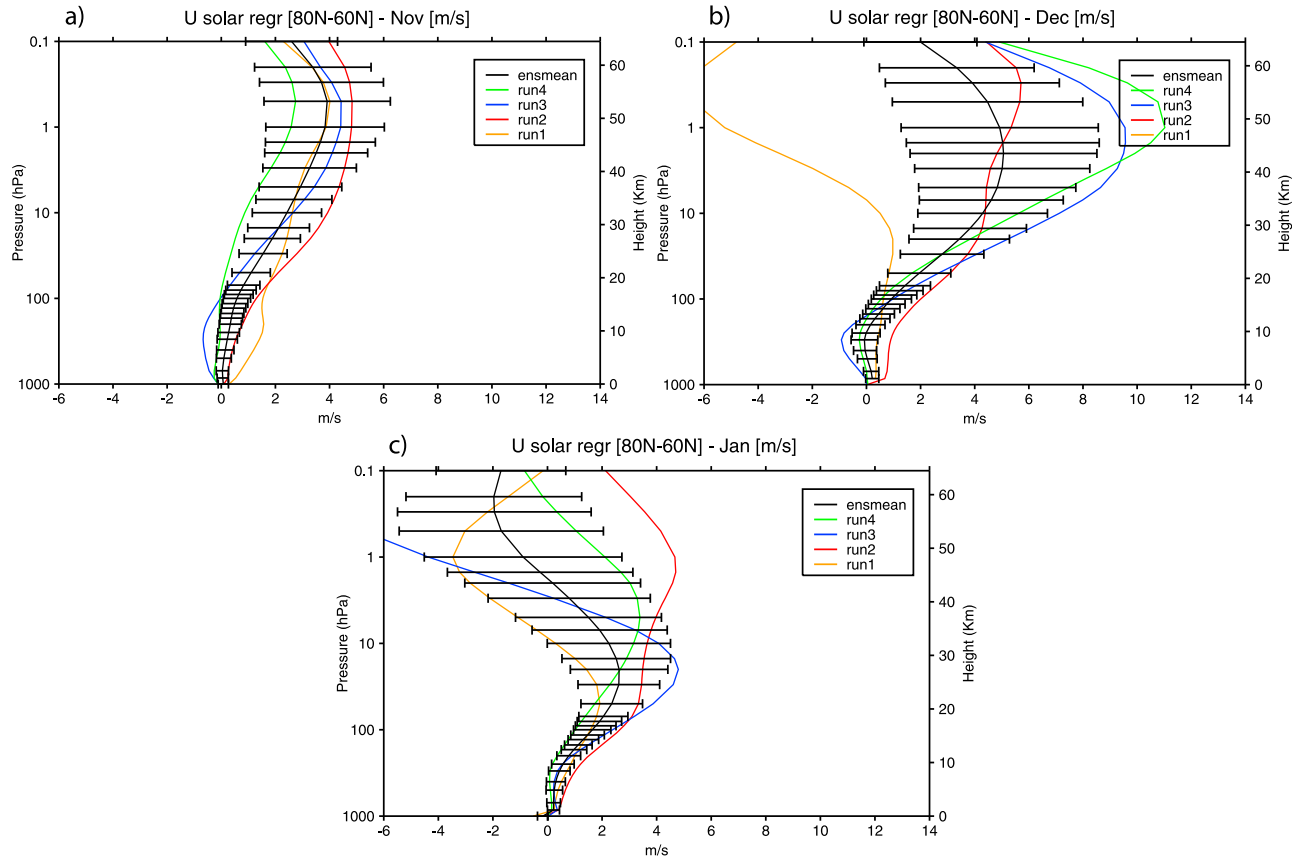

Figure 9. Vertical profile of the polar average (60°N–80°N) zonal wind solar multiple linear regression coefficient for all ensemble runs (colored lines) and ensemble mean (black line) for (a) November, (b) December, and (c) January. Error bars represent the sigma uncertainty range of the regression coefficient for the ensemble mean zonal wind.

in these regions in December. The entire structure propagates downward to the lower stratosphere in late winter (January and February, see Figures 8c and 8d), while stronger upwelling (although weak and not significant) at low latitudes causes slight cooling during MAX conditions between 1 and 10 hPa at midlatitudes and over the Equator during January–February (Figures 7c and 7d). This late winter pattern of warming at high latitudes and equatorial cooling in the stratosphere agrees qualitatively with observations [*Claud et al.*, 2008], although the magnitude of the changes simulated by WACCM3.5 at low latitudes is weaker and not significant.

[54] To summarize, MAX conditions lead to a stronger PNJ in November. The stronger westerlies suppress upward and equatorward planetary wave propagation, and wave dissipation, which in turn leads to a weaker Brewer-Dobson circulation and cooling of the polar stratosphere. In December, when the westerly wind anomaly reaches the lower extratropical stratosphere, upward and equatorward wave propagation is enhanced, along with wave dissipation in the middle stratosphere, leading to a stronger Brewer-Dobson circulation, which stays until March (not shown). Accordingly, the SC signal in the polar stratosphere during winter exhibits a seasonality, which is controlled by changes in wave propagation and dissipation patterns.

[55] Simulations of the SC response with the previous WACCM3.1 model version [*Calvo and Marsh*, 2011] showed a zonal wind anomaly in the equatorial stratopause similar to that in WACCM3.5 (Figure 6c). However, the anomaly did not migrate poleward and downward, thus leading to a weak response in the polar vortex. This was also found by *Tsutsui et al.* [2009]. During October and November, the structure of the PNJ in WACCM3.5 is more realistic than in WACCM3.1, particularly at the polar stratopause (not shown). In WACCM3.1, the PNJ shows a slanted tilt between the subtropical and the high-latitude stratosphere, which is not seen in ERA40 [see *Calvo and Marsh*, 2011, Figure 6]. The more pronounced vertical tilt of the PNJ in WACCM3.5 favors more effective upward propagation of planetary waves in the polar stratopause than in WACCM3.1. The solar-induced changes in zonal wind affect the vertical propagation of planetary waves as shown by *Calvo and Marsh* [2011], which is better represented in WACCM3.5 because of the improved wind climatology in the stratopause region, where the initial change in zonal wind is triggered (Figure 6c).

[56] Furthermore, *Richter et al.* [2009] showed that the stratospheric jet in WACCM3.1 is too strong. Moreover, the overall frequency of major SSWs in this version is low compared to ERA-40 and WACCM3.5. It is thus plausible that an overly strong stratospheric westerly jet might suppress dynamically induced solar changes in WACCM3.1. In the WACCM3.5 simulations presented here, the ensemble mean number of major SSWs agrees with ERA-40 (29.2 in

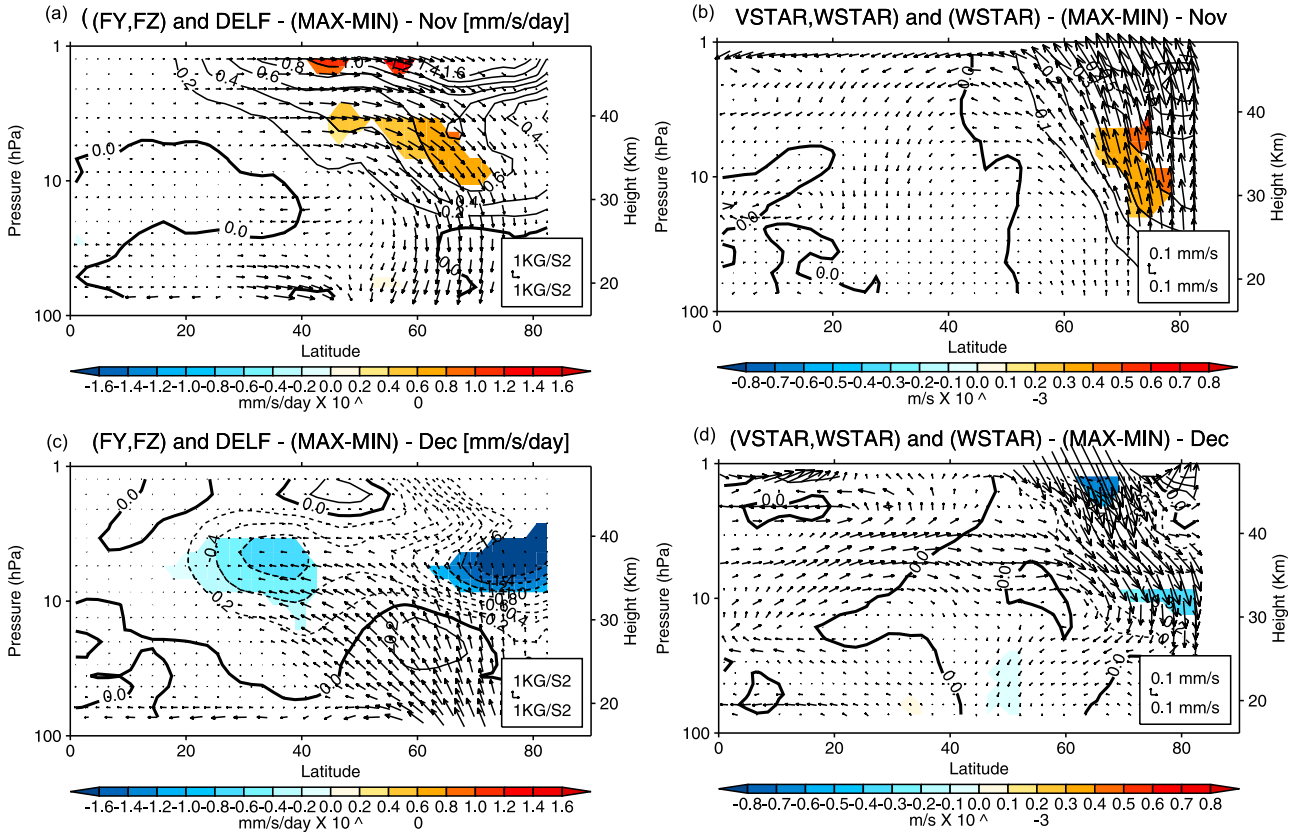

Figure 10. Left panels show the composite differences (MAX-MIN) of the ensemble mean Eliassen-Palm fluxes (EPF) (arrows; Fy and Fz) and EPF divergence for (a) November and (c) December. Units are kg/s for EPF and mm/s/d for EPF divergence. Contours are drawn for the EPF divergence. The composite differences (MAX-MIN) of the ensemble mean transformed Eulerian mean (TEM) velocity vectors (arrows; $\bar{v}^*$ and $\bar{w}^*$) and $\bar{w}^*$ as contours (positive values indicate upwelling, and negative values indicate downwelling) for (b) November and (d) December. Units are mm/s for $\bar{w}^*$. Shading denotes 95% significant areas.

WACCM3.5, and 29 in ERA-40). Notwithstanding the uncertainty in the response of each ensemble member, the more realistic representation of the stratospheric jet and of its variability in the NH polar region is likely to be the basis for the simulation of a realistic solar signal during boreal winter in the newer version of WACCM.

[57] *McCormack et al.* [2007] reproduced a similar SC signal to WACCM3.5 during NH winter. However, since their model cannot incorporate wave-mean flow feedbacks, the changes in the propagation properties of planetary waves due to changes in the mean flow are not accounted for in their model. Previous modeling studies based on CCMs [*Rozanov et al.*, 2004; *Schmidt et al.*, 2010] showed a stronger polar vortex throughout the boreal winter. Other authors simulated the detailed evolution of the boreal winter signal in zonal wind and temperature [*Tourpali et al.*, 2003; *Matthes et al.*, 2004]. However, these simulations were performed with idealized constant forcings. Unlike these past modeling studies, WACCM3.5 reproduces the observed evolution of the winter signal in detail using a set of transient (observed) forcings. This means that the solar-induced response can be reproduced in a model which simulates a more realistic dynamical variability of the winter stratosphere.

[58] In the SH, MAX conditions lead to a meridional dipole of stronger and weaker westerlies at the stratopause during austral winter months (not shown). The dipole propagates downward during austral spring and a weakening of the Brewer-Dobson circulation is found in the SH similar to that found in November and December in the NH. This originates the significant warming in the low tropical stratosphere during September (Figure 5). However, the wind anomalies in the SH are smaller than those simulated in the NH during winter and not statistically significant. Furthermore, they do not penetrate to the lower stratospheric and tropospheric levels, in contrast with observations [*Kuroda and Kodera*, 2002].

[59] This may be a consequence of the biases in the background climatology of the winter stratospheric jet, which were mentioned in section 1. It is plausible that too strong westerlies in the SH modify wave mean flow interactions, and suppress dynamically induced solar changes.

4.1. Influence of the QBO on the Extratropical Solar Signal

[60] In section 3, we investigated the QBO modulation of the SC signal in the tropics in annual mean temperature by using the composite analysis technique, and stratifying the data by both QBO and solar activity phases. A number of studies have analyzed the SC-QBO interactions in the extratropics in observations [*Labitzke*, 1987; *Labitzke and*

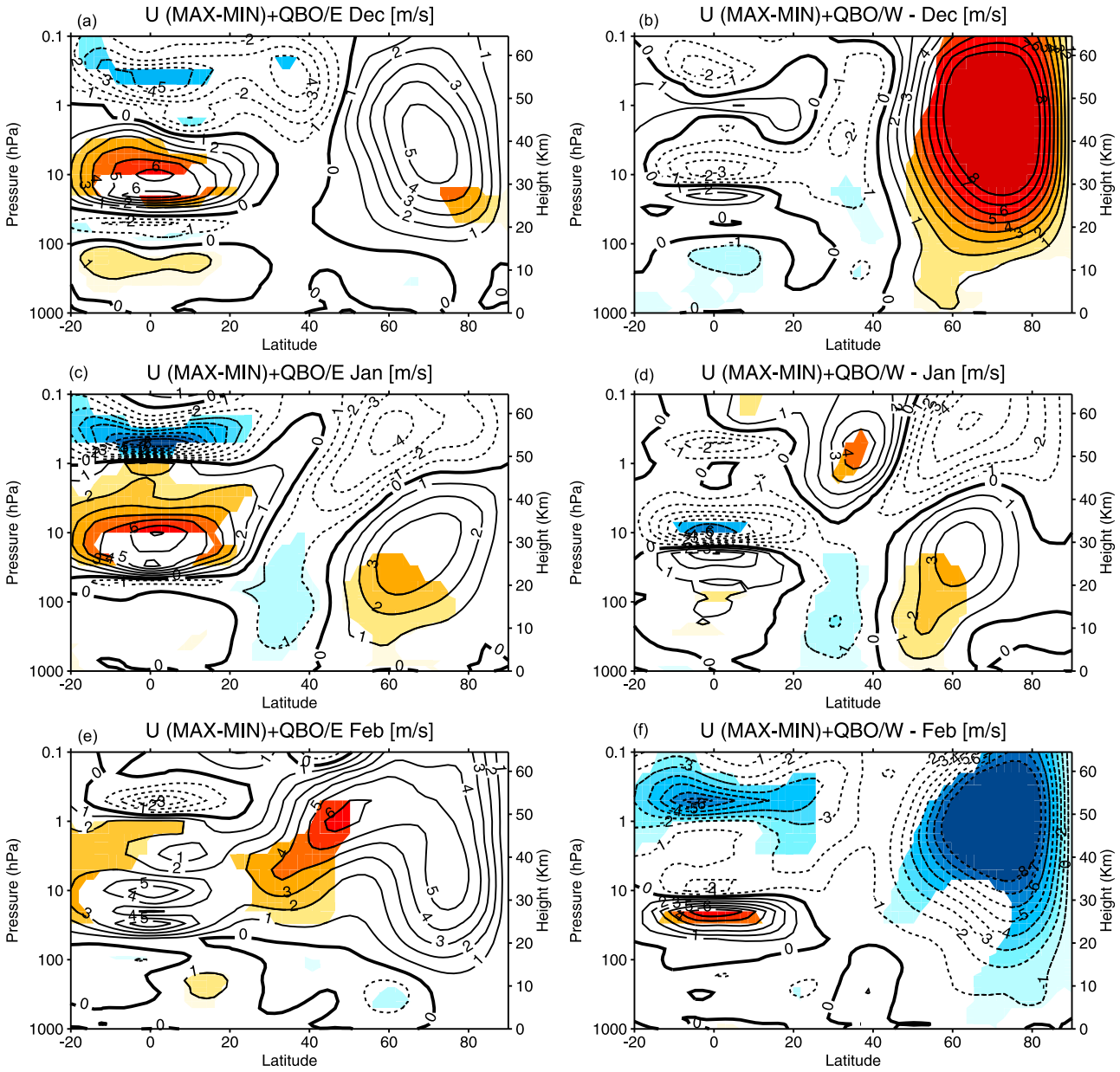

Figure 11. Ensemble mean composite differences (MAX-MIN) of zonal mean zonal wind for (left) QBO/EAST and (right) QBO/WEST winters. Composite differences are shown for (a, b) December, (c, d) January, and (e, f) February. Solid contour lines are drawn to display positive (i.e., westerly) values, and dashed contours indicate negative (i.e., easterly) values. Contour interval is 1 m/s.

Van Loon, 1989] and models of various complexity [*Gray et al.*, 2004; *Schmidt et al.*, 2010; *Matthes et al.*, 2010], and in the context of idealized simulations [*McCormack et al.*, 2007; *Ito et al.*, 2009]. The modeling results concerning combined SC-QBO effects in the polar vortex do not always agree, which may in part be related to the experimental design.

[61] Before analyzing the SC-QBO interactions, we first study the QBO signature in the extratropical stratosphere. To do so, we composited the model anomalies with respect to the ensemble mean climatology according to their QBO phase (QBO/WEST and QBO/EAST), without stratifying data by the solar phase, and selecting winters according to the QBO index in December, as explained in section 2.2. During boreal winters in QBO/WEST phase, the polar vortex is found to be stronger in the ensemble mean, and the opposite occurs during QBO/EAST winters. This indicates that the observed HT relationship [*Holton and Tan*, 1980] is well reproduced in these simulations. However, this pattern was only found in November and December (not shown). During January, February and March the QBO signal in the ensemble mean zonal mean zonal wind switches sign, and therefore a stronger and colder polar vortex is simulated during QBO/EAST (not shown). The modulation of the extratropical QBO signature by the SC can be analyzed when the QBO signal in zonal wind is stratified by the solar phase. We found that the HT relationship is true regardless of the solar phase during early winter. During late winter, the relationship holds true

only in MIN winters, suggesting that the SC does modulate the late winter QBO signal in the polar vortex.

[62] To investigate the modulation of the SC signal in zonal wind by the QBO, ensemble mean composite MAX-MIN differences have been computed for QBO/WEST and QBO/EAST phases throughout the winter, and are shown in Figure 11 from December to February. The SC signal does not depend on the QBO during December (Figures 11a and 11b). This means that MAX conditions lead to stronger ensemble mean zonal wind (i.e., stronger polar vortex) during early winter, regardless of the QBO phase. In January, the westerly wind anomaly propagates to the lower stratospheric levels in both QBO phases (Figures 11c and 11d). In February, MAX conditions lead to significantly stronger ensemble mean zonal wind in QBO/EAST winters (Figure 11f), while easterly anomalies (i.e., weaker polar vortex) are found in QBO/WEST winters (Figure 11e). Therefore, the solar signal in the boreal polar vortex, and its switch from westerly to easterly anomalies (seen in Figures 7b and 7d) is modulated by the QBO phase in late winter. This means that the polar vortex is stronger throughout winters in QBO/EAST phase. No evidence of such QBO modulation of the SC signal during winter is found in the SH (not shown).

[63] In observations, several studies found a similar modulation of the SC by the QBO in the NH [*Labitzke*, 1987; *Labitzke and Van Loon*, 1989]. *McCormack et al.* [2007] obtained similar results to the present study with a 2-D model for QBO/EAST conditions, though their model does not show a clear weakening of the vortex in QBO/WEST conditions (see their Figure 11). The results from the WACCM3.5 simulations were obtained when compositing the ensemble mean zonal wind data, but could not be confirmed in each of the four ensemble simulations. An analysis of the single ensemble runs revealed that only two show differences in the solar signal (MAX-MIN) in zonal wind between both QBO phases during middle and late winter. This indicates that the combined QBO and SC signals in the polar vortex are smaller than internal variability. This occurs even though the statistical *t* test on the ensemble mean fields could indicate a significant modulation of the SC by the QBO, which is close to observations. In addition, the possibility of contamination from the QBO signal cannot be excluded in the SC signal shown in Figures 11e and 11f since a QBO-like structure appears in the tropical stratosphere. Since the tropical winds are assimilated, this could also indicate that a modulation of the QBO itself by the SC [*Salby and Callaghan*, 2000] may intrinsically be introduced in the model simulations. However, further exploration of this modulation is beyond of the scope of this paper.

4.2. Tropospheric Response to the Solar Signal

[64] In the troposphere, Figure 2b showed a dipole of zonal wind anomalies in the ensemble annual mean in the NH as a response to peaks of solar activity. This dipole structure has stronger westerlies at midlatitudes and weaker westerlies in the subtropics, which suggests a weakening and northward shift of the subtropical tropospheric jet. The pattern is prominent in the NH during January (see Figure 7c), although a similar pattern is also simulated in the SH but it is weaker in intensity (not shown). All runs show that this pattern attains its largest magnitude in the upper troposphere–lower stratosphere region in January at 30°N (which is evident as a significant ensemble mean composite difference of −1 m/s in Figure 7c). The structure of the zonal wind response in the troposphere is similar to that found in ERA-40 data in both hemispheres [*Frame and Gray*, 2010]. However, reanalysis data show a larger weakening of the subtropical jets, particularly in the SH during boreal winter [*Frame and Gray*, 2010].

[65] *Haigh and Blackburn* [2006] suggested that the tropospheric wind response may be caused by a weakening in the eddy momentum flux convergence during MAX conditions but a definitive mechanism for the downward propagation of the solar signal to the troposphere has not been provided yet. Although a clear causal relationship cannot be given here, the enhanced meridional planetary wave propagation and dissipation in the tropopause region at midlatitudes during December (Figure 10c) is likely to be related to the tropospheric zonal wind anomalies in January, which lag the mid winter stratospheric SC signal. This suggests a link in the extratropics between the stratospheric and tropospheric solar response, with the stratosphere leading, which agrees well with earlier modeling studies [e.g., *Kodera and Kuroda*, 2000; *Matthes et al.*, 2006].

[66] The SC responses (MAX-MIN) in the ensemble mean surface pressure and temperature during boreal winter are shown in Figures 12a and 12b, respectively. In the NH, the signature is evident as a meridional dipole structure of negative pressure anomalies over the pole, and positive anomalies at midlatitudes. The meridional pressure gradient is particularly strong in the Atlantic and Pacific sectors at approximately 60°N, where Aleutian and Atlantic Low systems normally dominate the synoptic pressure distribution. This pattern is statistically significant, and reminiscent of a positive Arctic Oscillation (AO) response [*Thompson and Wallace*, 1998]. The surface temperature response shows significant warming over Northern Europe, large parts of Siberia, and the Eastern United States. Strong cooling is found over Northern Canada and the West coast of Canada and Alaska. The temperature patterns are broadly consistent with the surface pressure response, and in agreement with other CCMs [*Rozanov et al.*, 2004]. The stronger westerlies in the Atlantic sector advect mild air masses to the Eurasian continent, while the colder temperatures over Northern Canada are linked to the stronger polar vortex. Hence, the solar activity in the WACCM model influences the NH surface climate through projection onto a typical wintertime variability mode of surface pressure. This is consistent with the reported effect of solar variability on the North Atlantic Oscillation and on blocking activity [*Barriopedro et al.*, 2008], which may be a mechanism by which solar-induced changes in the stratosphere influence European weather regimes [*Lockwood et al.*, 2010]. The timing of the solar modulation of NH surface pressure patterns occurs in conjunction with the downward propagation of the SC signal in zonal wind from the stratosphere to the troposphere that we discussed above, and again indicates a link between the solar-induced changes in the stratosphere and troposphere. In the SH, the late winter SC signals in surface pressure and temperature are less persistent and significant, which may be related to the weaker stratospheric response to the SC in this hemisphere (not shown).

[67] The response in zonal mean vertical (pressure) velocity and precipitation during boreal winter are shown in

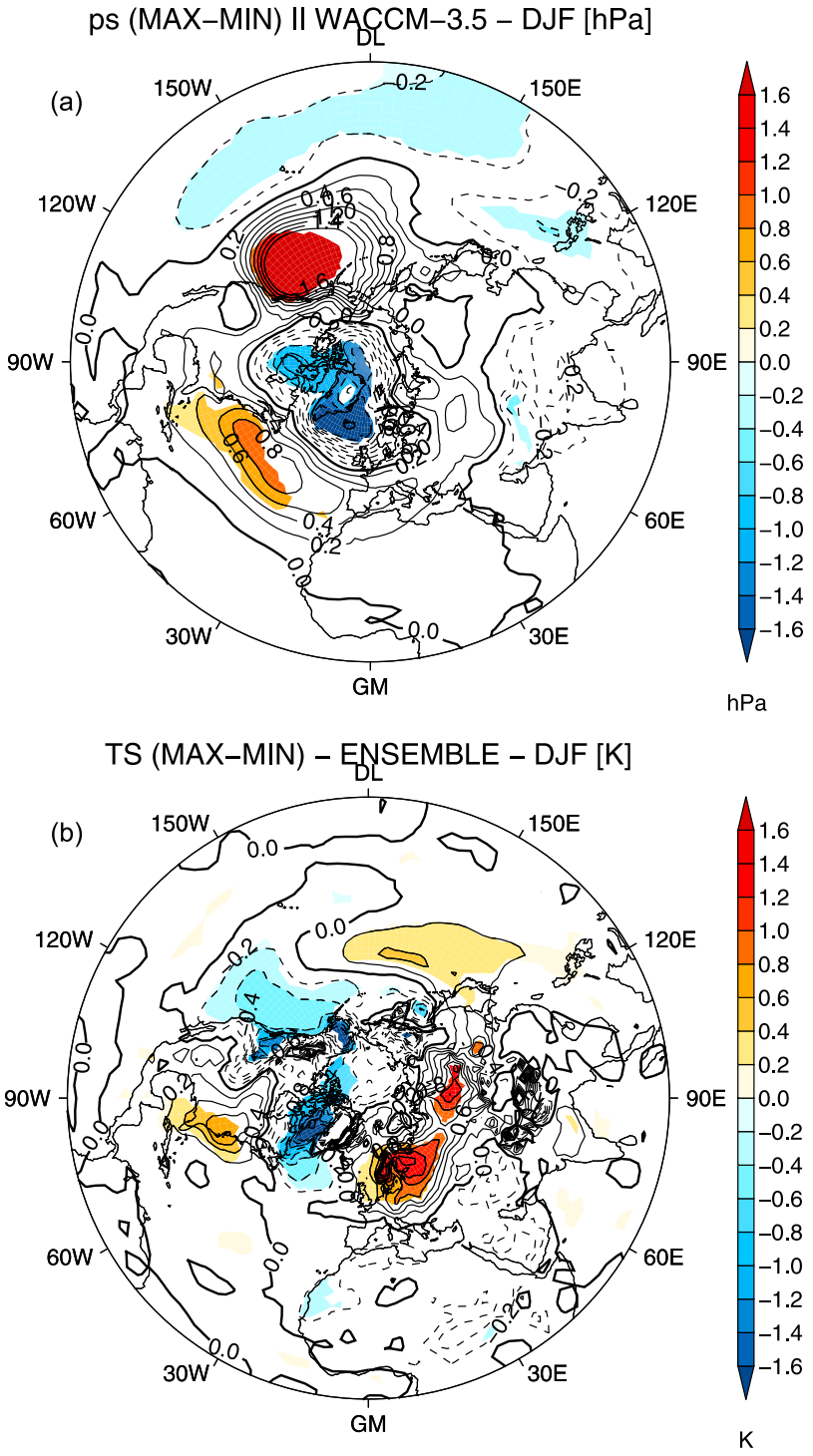

Figure 12. NH winter (DJF) composite differences (MAX-MIN) of (a) ensemble mean surface pressure in Pa and (b) surface temperature in K. Solid contour lines are drawn to indicate positive values (i.e., increase in surface pressure in Figure 12a and surface warming in Figure 12b), while dashed contours indicate negative values (surface pressure decrease in Figure 12a and surface cooling in Figure 12b). Shading denotes 95% significant areas.

Figures 13a and 13b, respectively. Figure 13a shows significant changes in the ensemble mean vertical motion in the tropical middle and lower troposphere. Negative ensemble mean vertical pressure velocity values imply upward changes. The opposite is true for positive changes. We speculate that the simulated warming of the lower stratosphere, which is observed in Figure 2a, leads to an increase of the static stability at the tropopause level. The changes in stability have a strong impact on convection and tropospheric vertical motion, particularly during NH winter. The significant

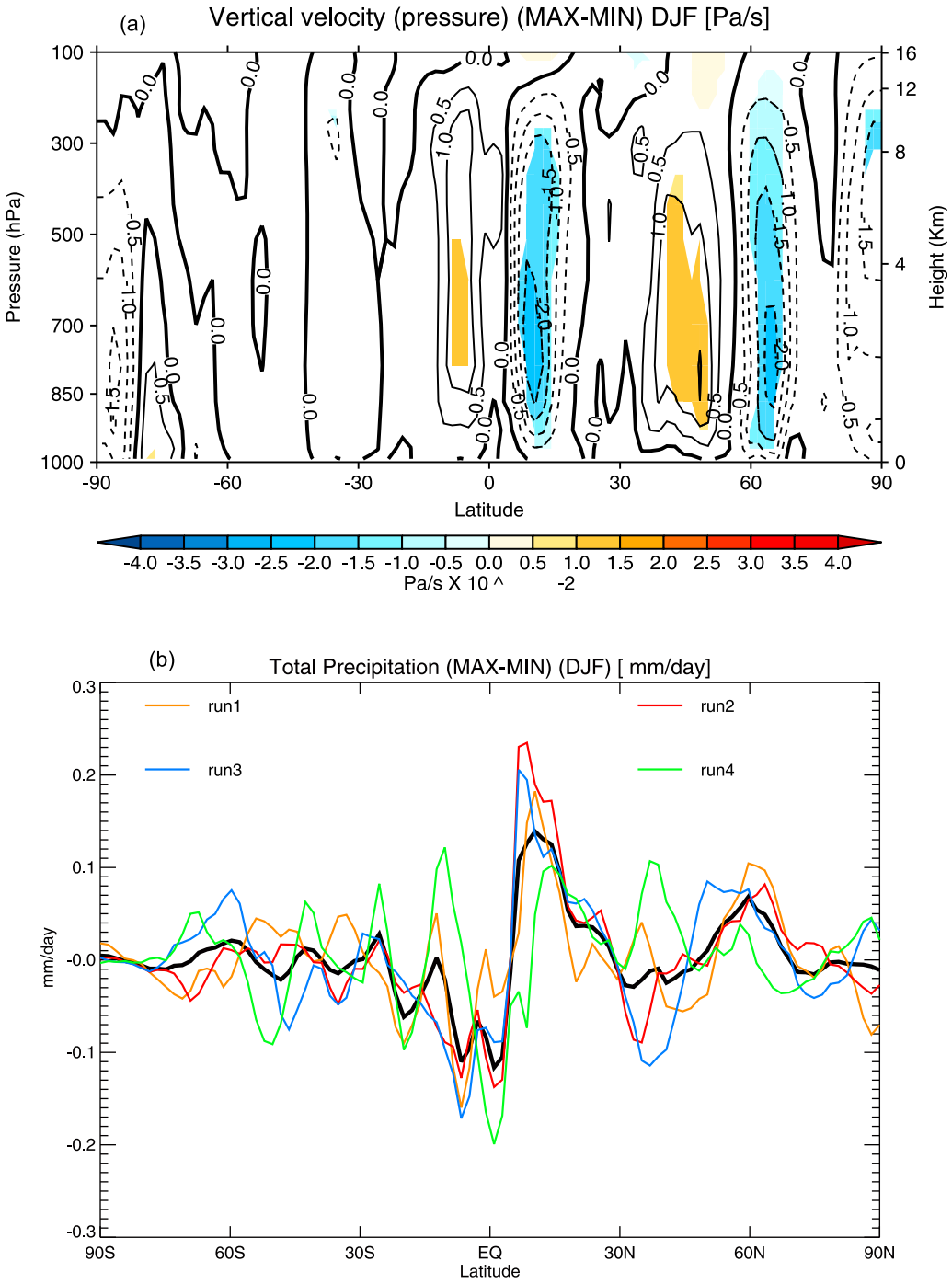

Figure 13. (a) Northern Hemisphere winter (December–February) composite differences (MAX-MIN) of zonal mean pressure velocity (dP/dt) in Pa/s. Solid contour lines are drawn to indicate positive values (i.e., downward anomalies), while dashed contours indicate negative values (i.e., upward anomalies). Shading denotes 95% significant areas. (b) Northern Hemisphere winter (December–February) composite differences (MAX-MIN) of zonal mean total precipitation (convective plus stratiform) for the ensemble mean (black line) and for the single simulations (colored lines) in mm/d.

warming simulated during November in the low equatorial stratosphere supports this hypothesis (Figure 7a). Significant positive changes in the mid troposphere (500–850 hPa) at 10°S indicate a weakening of the climatological upwelling south of the equator during boreal winter, while positive anomalies north of the equator (10–20°N) indicate less downwelling in the downward branch of the Hadley cell. Positive changes at 40–50°N also suggest a northward shift of the downward branch of the Hadley cell in the NH.

[68] These changes occur in conjunction with changes in zonal mean total precipitation, which are shown for the ensemble mean and for each simulation in Figure 13b. The

weaker upwelling leads to less precipitation in the Intertropical Convergence Zone (ITCZ), which lies south of the equator during NH winter at 0°–10°S. The off-equatorial precipitation (10°N) is also intensified during solar maximum conditions. This response in the tropical region is evident in all simulations (although the magnitude of the SC signal in precipitation varies in each one) and suggests that during winters in MAX conditions, the ITCZ is weaker and slightly shifted northward, which agrees well with previous model simulations [*Matthes et al.*, 2006; *Meehl et al.*, 2009]. A similar pattern in tropical precipitation is also found in the NH between July and September, which coincides with a warming in the equatorial lower stratosphere (Figure 5). The weakening and northward shift of the subtropical jet, along with the signals in precipitation and vertical velocity, indicate that in WACCM3.5, MAX conditions lead to a weakening and broadening of the Hadley cell during boreal winter.

[69] Nevertheless, some inconsistency between observational and modeling studies exists concerning the solar-induced response in the tropical circulation [*Gray et al.*, 2010]. Tropospheric solar-induced changes are generally difficult to attribute because of their small size compared to those linked to other sources of variability (e.g., ENSO). The use of observed SSTs implies that ENSO signals may also alias on the decadal response attributed to the SC, as it is the case in tropical SSTs [*White and Liu*, 2008]. A deeper analysis of ENSO aliasing will be discussed in a future study with a more idealized set of forcings.

5. Conclusions

[70] We have analyzed the dynamical SC response in an ensemble of four simulations of the WACCM3.5 chemistry climate model run from 1960 to 2005, which were performed within the coordinated CCMVal-2 activity. Analysis of an ensemble reduces uncertainty in the derived solar signals, which is often larger in transient simulations. In addition, the difference between the ensemble members is a useful metric to assess model uncertainty and robustness of the findings. This improves the detection of the SC signals in various meteorological fields in the stratosphere-troposphere system compared to past GCM studies, particularly in the extratropical region, where indirect solar effects are masked by dynamical variability during the winter season. The main findings are as follows.

[71] 1. The solar signal in annual mean temperature and ozone shows a double-peak response structure in the tropical stratosphere, consisting of warming and ozone increase in the upper and lower levels during solar maximum conditions compared to solar minimum. The signal in the lower stratosphere is closer to observations than in the previous WACCM version.

[72] 2. During solar maximum years, the model simulates a strengthening of the polar vortex in the NH during boreal winter compared to solar minimum conditions. The SC signal in zonal wind and temperature at high latitudes is weak in magnitude, but significant during most of the winter months.

[73] 3. The evolution of the solar signal in zonal wind and temperature in the NH is broadly consistent with observations and conceptual studies. The solar signal in zonal wind shows a downward propagation during early boreal winter in the NH. The response in the polar vortex in late winter is opposite. This is due to opposite changes in planetary wave propagation in early and late winter and related to a different response of the Brewer-Dobson circulation during winters in solar maximum conditions. The winter signal is more realistic than in previous WACCM versions. Part of the improvement is due to the more realistic vertical structure and climatology of the stratospheric jet during winter, and of its variability.

[74] 4. In the polar region, solar maximum conditions lead to a stronger polar vortex in QBO/EAST winters in February, and to a weaker vortex in QBO/WEST winters. The QBO modulation of the tropical and extratropical solar cycle signals in zonal wind agrees well with observations [*Labitzke*, 1987; *Labitzke et al.*, 2006], although it is not reproduced in all ensemble members.

[75] 5. The solar-induced stratospheric anomalies are transmitted to the troposphere in the tropics and extratropics during boreal winter months. In the troposphere, the response to the SC manifests itself as a strong positive AO pattern in the NH midlatitudes, a warming over the Eurasian continent, and as a weakening and broadening of the tropical Hadley circulation.

[76] Overall, WACCM3.5 simulates a realistic solar signal in the tropics and in the NH polar vortex, in better agreement with observations and conceptual studies than WACCM3.1. To our knowledge, no CCM was able, to date, to reproduce the observed solar signal in such agreement in a transient simulation with an evolving solar cycle.

[77] We note that the response to the SC in the upper stratosphere is generally reproduced by a wide range of different models, while more disagreement exists concerning the response in the lower stratosphere, particularly at low latitudes. We have shown indications that solar-induced changes in the polar and low latitude stratosphere are linked through a modulation of the Brewer-Dobson circulation. The better performance of WACCM3.5 compared to WACCM3.1 in both regions is likely to be due to the improvements in the simulation of the boreal winter circulation response. Thus, it is possible that the uncertainty in simulating the solar signal in most models is related to the representation of wave-mean flow interaction processes taking place in the polar stratosphere, which are highly dependent on the background climatology and variability of the polar vortex.

[78] Nevertheless, the simulated changes in the Brewer-Dobson circulation in WACCM3.5 mainly originate high-latitude stratospheric temperature anomalies, whereas the model temperature response at lower latitudes (which would be expected from changes in the upward branch of the residual circulation) is weak and limited to the subtropics. This may be due to the relaxation procedure of observed stratospheric winds in the low equatorial stratosphere (see *Matthes et al.* [2010, section 3.1.1] for details), which forces a secondary QBO circulation that operates independently from the Brewer-Dobson circulation, thus limiting any solar signal in temperature to the extratropics.

[79] This study verifies that the WACCM3.5 model is a suitable model for solar cycle studies, particularly when focusing on the boreal winter circulation response, and on the tropical stratospheric region. The mechanisms responsible for the observed response are well captured by the

model, although a clear causality is still to be determined. The tropospheric signals in different meteorological variables are detectable, although they are small and additional evidence from idealized experiments is still needed.

[80] This study also shows that efforts are still needed to achieve a more realistic simulation of the controversial combined QBO-SC effects in the extratropics. The latter issue could be solved only in future versions of the model where a full interaction between QBO and solar cycle can be investigated by internally generating a QBO in WACCM.

[81] **Acknowledgments.** The authors thank Katja Matthes for instructive comments and fruitful discussions. G. Chiodo was supported by the Spanish Project CONSOLIDER (grant CSD2007-00050-II-PR4/07), TRODIM (grant CGL2007-65891-CO5-02), and the Spanish Ministry of Education in the framework of the "FPU" doctoral fellowship (grant AP2009-0064). N. Calvo was partially supported by the Advanced Study Program (ASP) at NCAR.

References

Andrews, D., J. Holton, and C. Leovy (1987), *Middle Atmosphere Dynamics*, Academic, Orlando, Fla.

Austin, J., et al. (2008), Coupled chemistry climate model simulations of the solar cycle in ozone and temperature, *J. Geophys. Res.*, *113*, D11306, doi:10.1029/2007JD009391.

Austin, J., et al. (2010), Chemistry-climate model simulations of spring Antarctic ozone, *J. Geophys. Res.*, *115*, D00M11, doi:10.1029/2009JD013577.

Barriopedro, D., R. García-Herrera, and R. Huth (2008), Solar modulation of Northern Hemisphere winter blocking, *J. Geophys. Res.*, *113*, D14118, doi:10.1029/2008JD009789.

Butchart, N., A. Charlton-Perez, I. Cionni, S. Hardiman, and K. Krüger (2010), Stratospheric dynamics, in *SPARC Report on the Evaluation of Chemistry-Climate Models*, *SPARC Rep. 5*, pp. 109–147, World Meteorol. Organ., Geneva, Switzerland.

Calvo, N., and D. Marsh (2011), The combined effects of ENSO and the 11-year solar cycle on the Northern Hemisphere polar stratosphere, *J. Geophys. Res.*, *116*, D23112, doi:10.1029/2010JD015226.

Calvo, N., M. Giorgetta, and C. Peña-Ortiz (2007), Sensitivity of the boreal winter circulation in the middle atmosphere to the quasi-biennial oscillation in MAECHAM5 simulations, *J. Geophys. Res.*, *112*, D10124, doi:10.1029/2006JD007844.

Calvo, N., M. Giorgetta, R. Garcia-Herrera, and E. Manzini (2009), Nonlinearity of the combined warm ENSO and QBO effects on the Northern Hemisphere polar vortex in MAECHAM5 simulations, *J. Geophys. Res.*, *114*, D13109, doi:10.1029/2008JD011445.

Claud, C., C. Cagnazzo, and P. Keckhut (2008), The effect of the 11-year solar cycle on the temperature in the lower stratosphere, *J. Atmos. Sol. Terr. Phys.*, *70*(16), 2031–2040.

Collins, W., et al. (2004), Description of the NCAR community atmosphere model (CAM 3.0), *NCAR Tech. Note NCAR/TN-464+ STR*, Natl. Cent. for Atmos. Res., Boulder, Colo.

Crooks, S., and L. Gray (2005), Characterization of the 11-year solar signal using a multiple regression analysis of the ERA-40 dataset, *J. Clim.*, *18*, 996–1015, doi:10.1175/JCLI-3308.1.

Egorova, T., E. Rozanov, E. Manzini, M. Haberreiter, W. Schmutz, V. Zubov, and T. Peter (2004), Chemical and dynamical response to the 11-year variability of the solar irradiance simulated with a chemistry-climate model, *Geophys. Res. Lett.*, *31*, L06119, doi:10.1029/2003GL019294.

Eyring, V., et al. (2010), Multi-model assessment of stratospheric ozone return dates and ozone recovery in CCMVal-2 models, *Atmos. Chem. Phys.*, *10*(19), 11,659–11,710.

Fleming, E., S. Chandra, C. Jackman, D. Considine, and A. Douglass (1995), The middle atmospheric response to short and long term solar UV variations: Analysis of observations and 2D model results, *J. Atmos. Terr. Phys.*, *57*(4), 333–365.

Frame, T., and L. J. Gray (2010), The 11-year solar cycle in ERA-40 data: An update to 2008, *J. Clim.*, *23*, 2213–2222, doi:10.1175/2009JCLI3150.1.

Garcia, R., D. Marsh, D. Kinnison, B. Boville, and F. Sassi (2007), Simulation of secular trends in the middle atmosphere, 1950–2003, *J. Geophys. Res.*, *112*, D09301, doi:10.1029/2006JD007485.

Garcia-Herrera, R., N. Calvo, R. Garcia, and M. Giorgetta (2006), Propagation of ENSO temperature signals into the middle atmosphere: A comparison of two general circulation models and ERA-40 reanalysis data, *J. Geophys. Res.*, *111*, D06101, doi:10.1029/2005JD006061.

Garny, H., G. Bodeker, and M. Dameris (2007), Trends and variability in stratospheric mixing: 1979–2005, *Atmos. Chem. Phys.*, *7*(3), 6189–6228.

Gray, L., S. Crooks, C. Pascoe, S. Sparrow, and M. Palmer (2004), Solar and QBO influences on the timing of stratospheric sudden warmings, *J. Atmos. Sci.*, *61*(23), 2777–2796.

Gray, L., et al. (2010), Solar influences on climate, *Rev. Geophys.*, *48*, RG4001, doi:10.1029/2009RG000282.

Haigh, J. (1994), The role of stratospheric ozone in modulating the solar radiative forcing of climate, *Nature*, *370*(6490), 544–546.

Haigh, J., and M. Blackburn (2006), Solar influences on dynamical coupling between the stratosphere and troposphere, *Space Sci. Rev.*, *125*(1), 331–344, doi:10.1007/s11214-006-9067-0.

Holton, J., and H. Tan (1980), The influence of the equatorial quasi-biennial oscillation on the global circulation at 50 mb, *J. Atmos. Sci.*, *37*, 2200–2208.

Hood, L., J. Jirikowic, and J. McCormack (1993), Quasi-decadal variability of the stratosphere: Influence of long-term solar ultraviolet variations, *J. Atmos. Sci.*, *50*(24), 3941–3958.

Huang, T., and G. Brasseur (1993), Effect of long-term solar variability in a two-dimensional interactive model of the middle atmosphere, *J. Geophys. Res.*, *98*(D11), 413–420, doi:10.1029/93JD02187.

Ito, K., Y. Naito, and S. Yoden (2009), Combined effects of QBO and 11-year solar cycle on the winter hemisphere in a stratosphere-troposphere coupled system, *Geophys. Res. Lett.*, *36*, L11804, doi:10.1029/2008GL037117.

Kalnay, E., et al. (1996), The NCEP/NCAR 40-year reanalysis project, *Bull. Am. Meteorol. Soc.*, *77*(3), 437–471.

Kinnison, D., et al. (2007), Sensitivity of chemical tracers to meteorological parameters in the MOZART-3 chemical transport model, *J. Geophys. Res.*, *112*, D20302, doi:10.1029/2006JD007879.

Kistler, R., et al. (2001), The NCEP-NCAR 50-year reanalysis: Monthly means CD-ROM and documentation, *Bull. Am. Meteorol. Soc.*, *82*(2), 247–268.

Kodera, K., and Y. Kuroda (2000), A mechanistic model study of slowly propagating coupled stratosphere-troposphere variability, *J. Geophys. Res.*, *105*(D10), 361–370.

Kodera, K., and Y. Kuroda (2002), Dynamical response to the solar cycle, *J. Geophys. Res.*, *107*(D24), 4749, doi:10.1029/2002JD002224.

Kuroda, Y., and K. Kodera (2001), Variability of the polar night jet in the Northern and Southern Hemispheres, *J. Geophys. Res.*, *106*(D18), 20,703–20,713.

Kuroda, Y., and K. Kodera (2002), Effect of solar activity on the polar-night jet oscillation in the Northern and Southern Hemisphere winter, *J. Meteorol. Soc. Jpn.*, *80*(4B), 973–984.

Labitzke, K. (1987), Sunspots, the QBO, and the stratospheric temperature in the north polar region, *Geophys. Res. Lett.*, *14*(5), 535–537, doi:10.1029/GL014i005p00535.

Labitzke, K. (2004), On the signal of the 11-year sunspot cycle in the stratosphere and its modulation by the quasi-biennial oscillation, *J. Atmos. Sol. Terr. Phys.*, *66*(13–14), 1151–1157, doi:10.1016/j.jastp.2004.05.011.

Labitzke, K. (2005), On the solar cycle-QBO relationship: A summary, *J. Atmos. Sol. Terr. Phys.*, *67*(1–2), 45–54, doi:10.1016/j.jastp.2004.07.016.

Labitzke, K., and H. Van Loon (1989), Association between the 11-Yr Solar Cycle, the QBO, and the Atmosphere. Part III: Aspects of the association, *J. Clim.*, *2*(6), 554–565, doi:10.1175/1520-0442(1989)002<0554:ABTYSC>2.0.CO;2.

Labitzke, K., and H. Van Loon (1995), Connection between the troposphere and stratosphere on a decadal scale, *Tellus, Ser. A*, *47*(2), 275–286, doi:10.1034/j.1600-0870.1995.t01-1-00008.x.

Labitzke, K., J. Austin, N. Butchart, J. Knight, M. Takahashi, M. Nakamoto, T. Nagashima, J. Haigh, and V. Williams (2002), The global signal of the 11-year solar cycle in the stratosphere: Observations and models, *J. Atmos. Sol. Terr. Phys.*, *64*(2), 203–210, doi:10.1016/S1364-6826(01)00084-0.

Labitzke, K., M. Kunze, and S. Broennimann (2006), Sunspots, the QBO and the stratosphere in the North Polar region—20 years later, *Meteorol. Z.* [Berlin], *15*(3), 355–364, doi:10.1127/0941-2948/2006/0136.

Lean, J., G. Rottman, H. Kyle, T. Woods, J. Hickey, and L. Puga (1997), Detection and parameterization of variations in solar mid-and near-ultraviolet radiation (200–400 nm), *J. Geophys. Res.*, *102*(D25), 29,939–29,956, doi:10.1029/97JD02092.

Lean, J., G. Rottman, J. Harder, and G. Kopp (2005), SORCE contributions to new understanding of global change and solar variability, *Sol. Phys.*, *230*, 27–53, doi:10.1007/s11207-005-1527-2.

Lee, H., and A. Smith (2003), Simulation of the combined effects of solar cycle, quasi-biennial oscillation, and volcanic forcing on stratospheric ozone changes in recent decades, *J. Geophys. Res.*, *108*(D2), 4049, doi:10.1029/2001JD001503.

Lin, S. (2004), A vertically Lagrangian finite-volume dynamical core for global models, *Mon. Weather Rev.*, *132*, 2293–2307, doi:10.1175/1520-0493(2004)132<2293:AVLFDC>2.0.CO;2.

Lockwood, M., R. Harrison, T. Woollings, and S. Solanki (2010), Are cold winters in Europe associated with low solar activity?, *Environ. Res. Lett.*, *5*(2), 024001, doi:10.1088/1748-9326/5/2/024001.

Manzini, E., et al. (2010), Natural variability, in *SPARC Report on the Evaluation of Chemistry-Climate Models*, *SPARC Rep. 5*, pp. 306–346, World Meteorol. Organ., Geneva, Switzerland.

Marsh, D., and R. Garcia (2007), Attribution of decadal variability in lower-stratospheric tropical ozone, *Geophys. Res. Lett.*, *34*, L21807, doi:10.1029/2007GL030935.

Marsh, D., R. Garcia, D. Kinnison, B. Boville, F. Sassi, S. Solomon, and K. Matthes (2007), Modeling the whole atmosphere response to solar cycle changes in radiative and geomagnetic forcing, *J. Geophys. Res.*, *112*, D23306, doi:10.1029/2006JD008306.

Matthes, K., U. Langematz, L. Gray, K. Kodera, and K. Labitzke (2004), Improved 11-year solar signal in the Freie Universitaet Berlin climate middle atmosphere model (FUB-CMAM), *J. Geophys. Res.*, *109*, D06101, doi:10.1029/2003JD004012.

Matthes, K., Y. Kuroda, K. Kodera, and U. Langematz (2006), Transfer of the solar signal from the stratosphere to the troposphere: Northern winter, *J. Geophys. Res.*, *111*, D06108, doi:10.1029/2005JD006283.

Matthes, K., D. Marsh, R. Garcia, D. Kinnison, F. Sassi, and S. Walters (2010), Role of the QBO in modulating the influence of the 11 year solar cycle on the atmosphere using constant forcings, *J. Geophys. Res.*, *115*, D18110, doi:10.1029/2009JD013020.

McCormack, J., and L. Hood (1996), Apparent solar cycle variations of upper stratospheric ozone and temperature: Latitude and seasonal dependences, *J. Geophys. Res.*, *101*(D15), 20,933–20,944, doi:10.1029/96JD01817.

McCormack, J., D. Siskind, and L. Hood (2007), Solar-QBO interaction and its impact on stratospheric ozone in a zonally averaged photochemical transport model of the middle atmosphere, *J. Geophys. Res.*, *112*, D16109, doi:10.1029/2006JD008369.

Meehl, G., J. Arblaster, K. Matthes, F. Sassi, and H. van Loon (2009), Amplifying the Pacific climate system response to a small 11-year solar cycle forcing, *Science*, *325*(5944), 1114–1118, doi:10.1126/science.1172872.

Pap, J., P. Fox, C. Fröhlich, H. S. Hudson, J. Kuhn, J. McCormack, G. North, W. Sprigg, and S. T. Wu (Eds.) (2003), *Solar Variability and Its Effects on Climate*, *Geophys. Monogr. Ser.*, vol. 141, AGU, Washington, D. C., doi:10.1029/GM141.

Randel, W., and F. Wu (1996), Isolation of the ozone QBO in SAGE 2 data by singular-value decomposition, *J. Atmos. Sci.*, *53*(17), 2546–2560, doi:10.1175/1520-0469(1996)053<2546:IOTOQI>2.0.CO;2.

Randel, W., and F. Wu (2007), A stratospheric ozone profile data set for 1979–2005: Variability, trends, and comparisons with column ozone data, *J. Geophys. Res.*, *112*, D06313, doi:10.1029/2006JD007339.

Richter, J., F. Sassi, and R. Garcia (2009), Towards a physically based gravity wave source parameterization in a general circulation model, *J. Atmos. Sci.*, *67*, 136–156, doi:10.1175/2009JAS3112.1.

Rozanov, E., M. Schlesinger, T. Egorova, B. Li, N. Andronova, and V. Zubov (2004), Atmospheric response to the observed increase of solar UV radiation from solar minimum to solar maximum simulated by the University of Illinois at Urbana-Champaign climate-chemistry model, *J. Geophys. Res.*, *109*, D01110, doi:10.1029/2003JD003796.

Salby, M., and P. Callaghan (2000), Connection between the solar cycle and the QBO: The missing link, *J. Clim.*, *13*(14), 2652–2662, doi:10.1175/1520-0442(1999)012<2652:CBTSCA>2.0.CO;2.

Sassi, F., D. Kinnison, B. Boville, R. Garcia, and R. Roble (2004), Effect of El Niño–Southern Oscillation on the dynamical, thermal, and chemical structure of the middle atmosphere, *J. Geophys. Res.*, *109*, D17108, doi:10.1029/2003JD004434.

Sato, M., J. Hansen, M. McCormick, and J. Pollack (1993), Stratospheric aerosol optical depths, 1850–1990, *J. Geophys. Res.*, *98*(D12), 22,987–22,994, doi:10.1029/93JD02553.

Schmidt, H., G. Brasseur, and M. Giorgetta (2010), Solar cycle signal in a general circulation and chemistry model with internally generated quasi-biennial oscillation, *J. Geophys. Res.*, *115*, D00I14, doi:10.1029/2009JD012542.

Shindell, D., D. Rind, N. Balachandran, J. Lean, and P. Lonergan (1999), Solar cycle variability, ozone, and climate, *Science*, *284*(5412), 305–308, doi:10.1126/science.284.5412.305.

Smith, A., and K. Matthes (2008), Decadal-scale periodicities in the stratosphere associated with the solar cycle and the QBO, *J. Geophys. Res.*, *113*, D05311, doi:10.1029/2007JD009051.

Solomon, S., and L. Qian (2005), Solar extreme-ultraviolet irradiance for general circulation models, *J. Geophys. Res.*, *110*, A10306, doi:10.1029/2005JA011160.

Soukharev, B., and L. Hood (2006), Solar cycle variation of stratospheric ozone: Multiple regression analysis of long-term satellite data sets and comparisons with models, *J. Geophys. Res.*, *111*, D20314, doi:10.1029/2006JD007107.

Thompson, D., and J. Wallace (1998), The Arctic Oscillation signature in the wintertime geopotential height and temperature fields, *Geophys. Res. Lett.*, *25*(9), 1297–1300, doi:10.1029/98GL00950.

Tiao, G., G. Reinsel, D. Xu, J. Pedrick, X. Zhu, A. Miller, J. DeLuisi, C. Mateer, and D. Wuebbles (1990), Effects of autocorrelation and temporal sampling schemes on estimates of trend and spatial correlation, *J. Geophys. Res.*, *95*(D12), 20,507–20,517, doi:10.1029/JD095iD12p20507.

Tilmes, S., R. Garcia, D. Kinnison, A. Gettelman, and P. Rasch (2009), Impact of geoengineered aerosols on the troposphere and stratosphere, *J. Geophys. Res.*, *114*, D12305, doi:10.1029/2008JD011420.

Tourpali, K., C. Schuurmans, R. Van Dorland, B. Steil, and C. Brühl (2003), Stratospheric and tropospheric response to enhanced solar UV radiation: A model study, *Geophys. Res. Lett.*, *30*(5), 1231, doi:10.1029/2002GL016650.

Tsutsui, J., K. Nishizawa, and F. Sassi (2009), Response of the middle atmosphere to the 11-year solar cycle simulated with the Whole Atmosphere Community Climate Model, *J. Geophys. Res.*, *114*, D02111, doi:10.1029/2008JD010316.

Uppala, S., et al. (2005), The ERA-40 re-analysis, *Q. J. R. Meteorol. Soc.*, *131*(612), 2961–3012, doi:10.1256/qj.04.176.

White, W., and Z. Liu (2008), Non-linear alignment of El Nino to the 11-yr solar cycle, *Geophys. Res. Lett.*, *35*, L19607, doi:10.1029/2008GL034831.

N. Calvo and D. R. Marsh, Atmospheric Chemistry Division, National Center for Atmospheric Research, PO Box 3000, Boulder, CO 80307, USA.

G. Chiodo, Departamento Fisica de la Tierra II, Facultad de Ciencias Fisicas, Universidad Complutense de Madrid, E-28040 Madrid, Spain. (gchiodo@fis.ucm.es)

R. Garcia-Herrera, Agencia Estatal de Meteorologia, E-28040 Madrid, Spain.

4 On the detection of the solar signal in the tropical stratosphere

Atmos. Chem. Phys., 14, 5251–5269, 2014
www.atmos-chem-phys.net/14/5251/2014/
doi:10.5194/acp-14-5251-2014

Atmospheric Chemistry and Physics
Open Access

On the detection of the solar signal in the tropical stratosphere

G. Chiodo[1], D. R. Marsh[2], R. Garcia-Herrera[1,3], N. Calvo[1], and J. A. García[4]

[1]Dpto. de Astrofísica y CC de la Atmósfera, Universidad Complutense de Madrid, Madrid, Spain
[2]Atmospheric Chemistry Division, National Center for Atmospheric Research, Boulder, CO, USA
[3]Instituto de Geociencias IGEO (CSIC-UCM), Madrid, Spain
[4]Dpto. de Física, Universidad de Extremadura, Badajoz, Spain

Correspondence to: G. Chiodo (gchiodo@ucm.es)

Received: 8 October 2013 – Published in Atmos. Chem. Phys. Discuss.: 18 November 2013
Revised: 21 March 2014 – Accepted: 14 April 2014 – Published: 2 June 2014

Abstract. We investigate the relative role of volcanic eruptions, El Niño–Southern Oscillation (ENSO), and the quasi-biennial oscillation (QBO) in the quasi-decadal signal in the tropical stratosphere with regard to temperature and ozone commonly attributed to the 11 yr solar cycle. For this purpose, we perform transient simulations with the Whole Atmosphere Community Climate Model forced from 1960 to 2004 with an 11 yr solar cycle in irradiance and different combinations of other forcings. An improved multiple linear regression technique is used to diagnose the 11 yr solar signal in the simulations. One set of simulations includes all observed forcings, and is thereby aimed at closely reproducing observations. Three idealized sets exclude ENSO variability, volcanic aerosol forcing, and QBO in tropical stratospheric winds, respectively. Differences in the derived solar response in the tropical stratosphere in the four sets quantify the impact of ENSO, volcanic events and the QBO in attributing quasi-decadal changes to the solar cycle in the model simulations. The novel regression approach shows that most of the apparent solar-induced lower-stratospheric temperature and ozone increase diagnosed in the simulations with all observed forcings is due to two major volcanic eruptions (i.e., El Chichón in 1982 and Mt. Pinatubo in 1991). This is caused by the alignment of these eruptions with periods of high solar activity. While it is feasible to detect a robust solar signal in the middle and upper tropical stratosphere, this is not the case in the tropical lower stratosphere, at least in a 45 yr simulation. The present results suggest that in the tropical lower stratosphere, the portion of decadal variability that can be unambiguously linked to the solar cycle may be smaller than previously thought.

1 Introduction

The Sun–climate connection is a topic of high relevance since solar variability is one source of natural variability in the climate system. The 11 yr solar cycle is a well-documented mode of variation of solar activity. To date, observations have shown decadal variations in the climate system that are commonly attributed to the 11 yr solar cycle (see review by Gray et al., 2010). A well-established decadal variability can be found in reanalysis data of stratospheric temperature (Crooks and Gray, 2005). An extended reanalysis data set from the European Centre for Medium-Range Weather Forecasts seems to confirm this pattern (Frame and Gray, 2010). A similar variability has also been found in stratospheric ozone in three independent satellite data sets (Soukharev and Hood, 2006).

In the tropical stratospheric domain (25° N–25° S), these studies show that zonal mean temperature and ozone vary in phase with solar activity (i.e., a warming and an ozone increase are found during peaks in solar activity). The vertical structure of the observed positive response is composed of a double peak, with maxima in the upper stratosphere at 1–3 hPa and tropical lower stratosphere (hereafter TLS) at 50–70 hPa, along with a minimum response in the middle stratosphere at 10–20 hPa (e.g., see Fig. 1 in Frame and Gray, 2010, for temperature, and Fig. 5 in Soukharev and Hood (2006)). While the upper stratospheric peak is well established and in agreement with theoretical expectations, the structure of the signal in the middle stratosphere and TLS is more uncertain, and far less understood. It has been suggested that a solar cycle modulation of tropical upwelling may be the dynamical mechanism originating the response in

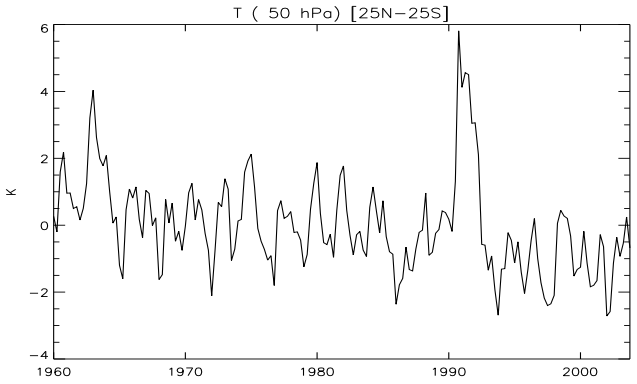

Figure 1. Time series of the simulated seasonal mean temperature anomalies at 50 hPa, averaged over the tropics [25° N–25° S] in the reference "all forcings" set. Unit: K.

the TLS in ozone (Hood, 1997; Hood and Soukharev, 2003) and temperature (Kodera and Kuroda, 2002). However, this mechanism is linked to changes in wave driving of extratropical circulation, and it is mainly operative in the winter stratosphere, where the strong variability therein makes the detection of such changes extremely challenging.

Chiodo et al. (2012) reported good agreement in the simulated vertical profile of the solar signal from the Whole Atmosphere Community Climate Model (WACCM), version 3.5, and observations. WACCM3.5 is a general circulation model with a well-resolved stratosphere and interactive chemistry. Reasonable agreement was also found in other models of similar characteristics (Austin et al., 2008; Schmidt et al., 2010). However, the ability of the models in reproducing the signal in the TLS appears to depend on the boundary conditions, and the elements necessary to reproduce such a signal are model dependent. For this reason, the role of additional sources of variability (e.g., El Niño–Southern Oscillation (ENSO), or quasi-biennial oscillation (QBO) in those models that assimilate it) in the tropical lower-stratospheric solar signal is far from being understood. The detection of solar signals is also difficult considering their relatively small amplitude compared with other sources of variability. This is especially true in the TLS, where a substantial portion of interannual variability is controlled by the QBO in both ozone (Randel and Wu, 2007) and temperature (Randel et al., 2009b). Another important driver for interannual variability in the TLS is ENSO (Calvo-Fernández et al., 2004; Randel et al., 2009a). Volcanic eruptions also lead to strong temperature and ozone changes in this region, where decreases of 5–10 % in ozone and a warming of more than 1 K after the Mt. Pinatubo eruption in 1991 were reported (Randel et al., 1995).

Solar signals in observations and transient simulations are usually quantified with multiple linear regression (MLR) models that include a linear trend term, and proxies for ENSO, QBO, and volcanic eruptions. Unambiguous attribution using a MLR model requires the predictors to be orthogonal (i.e., that they are not cross correlated) and predictand time series to be serially uncorrelated. However, serial correlation in temperature and ozone exists within seasonal timescales (Tiao et al., 1990). Additionally, cross correlations between proxies may arise during certain epochs. This is the case for the QBO, which is characterized as the vertical profile of the equatorial zonal mean zonal wind. The zonal wind in the tropical stratosphere can potentially be affected by ENSO and in situ heating caused by volcanic aerosol. Thus, volcanic and ENSO signals are embedded in the QBO index. Hence, deviations from the basic assumptions limit the reliability of estimates from regression models, especially when using data that only cover a few solar cycles, as in the case of reanalysis and satellite data sets.

The only feasible approach to quantify aliasing in observational data is to assess the sensitivity of the derived solar regression coefficients to the formulation of the regression model. This is the method used by some authors (Frame and Gray, 2010; Soukharev and Hood, 2006; Hood et al., 2010), who claimed that their solar regression coefficient is not affected by aliasing because of the very small changes when including ENSO, QBO, and volcanic terms in their regression model.

On the other hand, when using a climate model, the sensitivity of the simulated solar signal to the presence of other boundary conditions can be directly tested. This was done in simulations with a 2-D chemistry transport model (Smith and Matthes, 2008; Lee and Smith, 2003). Smith and Matthes (2008) showed that the simulated solar signal in tropical ozone strongly depends on the presence of the QBO. They showed that this dependence is indicative of a contamination of the solar signal by the QBO, and that the aliasing is mainly due to irregularities (i.e., departures from a sinusoidal function) in the observed QBO. In an earlier study using the same 2-D model, Lee and Smith (2003) found that volcanic eruptions have a similar effect, and that both QBO and volcanic signals equally alias on the observed structure of the ozone solar response. However, one may argue that such simplified 2-D models lack a full description of wave–mean-flow interactions that have been proposed to explain the origin of the decadal changes in the TLS.

Marsh and Garcia (2007) used a more comprehensive model to investigate tropical ozone decadal variability (WACCM3.1, Garcia et al., 2007). They found that the ozone solar signal in the TLS could only be reproduced by WACCM3.1 when observed SSTs were prescribed. They demonstrated that part of the ozone solar signal simulated in transient WACCM simulations was due to spurious correlation between the index for the solar cycle and ENSO over the 1979–2003 period. These conclusions were obtained by contrasting transient WACCM3.1 simulations performed with observed SSTs with time-slice experiments performed with climatological SSTs. Nevertheless, neither of these simulations included the radiative effects of volcanic eruptions,

or a QBO. Thus, their results cannot be directly compared to observations.

There is clearly a need for a quantitative estimate of the portion of the decadal signals in the stratosphere that can unambiguously be linked to the solar cycle. It has been demonstrated that a warming in the TLS, such as that commonly attributed to the solar cycle, can trigger changes in tropospheric circulation (Haigh and Blackburn, 2006). Consequently, a correct attribution of changes in the TLS may in turn improve our understanding of the role of external forcings on tropospheric and surface climate that propagate downward from the stratosphere.

In this paper, we quantify the impact of the presence of other forcings on the detection of the 11 yr solar cycle signal in simulations of the WACCM3.5 version including more realistic forcing than in previous studies. WACCM3.5 is a valuable tool for this exercise, since it has been previously shown that this model version is able to reproduce most features of the apparent 11 yr solar cycle observed in the tropical stratosphere over the last several decades (Chiodo et al., 2012).

We compare the amplitude of the solar signal in simulations with all observed forcings to those where a single forcing has been excluded. Differences between the simulations quantify the impact of the exclusion of each forcing on the apparent solar signal, and thus the potential aliasing from the respective sources. The solar signal is diagnosed using a novel MLR approach, which reduces the autocorrelation and improves the accuracy of the regression fit through the use of an optimal lag in the predictors.

The paper is arranged as follows. Section 2 provides a description of the model and the experimental setup, along with the statistical methods employed in the analysis. The results are outlined in Sect. 3. Section 3.1 is dedicated to the relationship between each forcing and the simulated temperature and ozone variations. In Sect. 3.2, focus is then directed towards the 11 yr solar cycle signal. The robustness of the apparent solar signal in the reference case is assessed in Sect. 3.3. A general discussion of the results and their implications is given in Sect. 4, while Sect. 5 summarizes the main results and conclusions.

2 Data and methodology

2.1 Model simulations

WACCM3.5 is an improved version of the WACCM3.1 general circulation model (Garcia et al., 2007). The standard resolution of 66 vertical levels ranging up from the surface to the thermosphere (140 km) and 1.9° latitude by 2.5° longitude in the horizontal was used in this work. This is the same model version that participated in the CCMVal-2 activity (CCMVal-2, 2010). Details of the model relevant for simulating the 11 yr solar cycle are discussed in Chiodo et al. (2012).

We performed pairs of simulations of WACCM3.5 model run from 1960 to 2004. The setup of one pair is identical to the REFB1 type of simulation presented in Eyring et al. (2010) for a comparison with other chemistry climate models and in Chiodo et al. (2012) for a detailed analysis of the 11 yr solar cycle signal. This ensemble is referred to as "all forcings" due to the inclusion of all known natural and anthropogenic forcings. The forcings include observed SSTs and sea-ice concentrations (Hurrell et al., 2008), loadings of GHGs and ozone-depleting substances. Model equatorial stratospheric winds are relaxed toward observed winds to obtain a realistic time-varying QBO (Matthes et al., 2010). The effects of volcanic eruptions are included by prescribing aerosol surface area densities (SAD), compiled from a combination of Stratosphere Aerosol and Gas Experiment (SAGE) measurements (Thomason et al., 1997) and Solar Mesosphere Explorer (SME) instruments from 1979 onward. Aerosol data before 1979 are constructed based on assumptions of background aerosol (CCMVal-2, 2010). The impact on the heating rates in the stratosphere is explicitly calculated (Tilmes et al., 2009). The 11 yr solar cycle in solar irradiance is introduced in the model by prescribing spectral irradiance data modeled by Lean et al. (2005), integrated over specific model bands for radiation and chemistry calculations. This set of simulations is aimed at closely reproducing observed interannual variations in the tropical stratosphere, and serves as a reference case.

In the second set of experiments, named "fixedSSTs", a climatological seasonal cycle of the SSTs is prescribed, thus removing ENSO from possible sources of variability in the stratosphere. In the next set, called "noQBO", the tropical stratospheric winds are not relaxed towards observations. Since the model version used in this work does not spontaneously generate a QBO, permanent weak easterlies in the tropical stratosphere are simulated. Finally, the fourth set, named "noVOLC", is forced with a constant seasonal cycle of SAD, thus excluding peaks in sulfate aerosol concentrations in the stratosphere due to volcanic eruptions. The list of experiments is given in Table 1.

2.2 Analysis method

Monthly mean output is averaged over the two realizations done for each of the four sets, season (DJF, MAM, JJA, SON), longitude, and the 25° N–25° S latitude band. The tropical average seasonal mean anomalies are used as input for an improved MLR technique, whose formulation is novel in the context of solar cycle studies. Details are described in the Appendix and are briefly outlined below.

First, the autocorrelation is removed following a Box–Jenkins prewhitening procedure (Box and Jenkins, 1980). This is applied to the time series of the seasonal means of the simulated ozone and temperature and of the predictors (i.e., the forcings used in each set). Next, lags are calculated that maximize the absolute value of the correlation between

Table 1. Table of the WACCM3.5 ensembles performed.

Name	SSTs	QBO	Volcanoes	Solar
"all forcings" (2)	observed, Hurrell et al. (2008)	assimilated, Matthes et al. (2010)	SAGE II, Thomason et al. (1997)	Lean et al. (2005)
"fixedSSTs"(2)	climatological	assimilated, Matthes et al. (2010)	SAGE II, Thomason et al. (1997)	Lean et al. (2005)
"noQBO" (2)	observed, Hurrell et al. (2008)	none (weak east)	SAGE II, Thomason et al. (1997)	Lean et al. (2005)
"noVOLC" (2)	observed, Hurrell et al. (2008)	assimilated; Matthes et al. (2010)	climatological	Lean et al. (2005)

the prewhitened field variable and the forcings. In this way, the projection of the field variable onto the forcings in each set is maximized. These steps have been extensively used in the formulation of multiple linear regression models in other fields (e.g., in biometeorology (Diaz et al., 2002a, b) and economic forecasting (Bisgaard and Kulahci, 2011)), though they are new in the analysis of the 11 yr solar signal.

The suitable lag for each predictor must be chosen with care. Ideally, the lag correlations should represent a physically consistent relationship between the predictand and predictors. On the other hand, such lags should not bring different predictors into phase, thereby increasing collinearity. With these criteria in mind, an optimal window, over which the suitable lag is searched for, is identified.

In our analysis, we use zonal wind time series at 30 and 10 hPa, which serve as QBO indices in the regression. By using the residual of a regression of the zonal wind onto other indices, the QBO indices become orthogonal to the other predictors. We exclude any lags in the QBO term itself in order to keep the mutual phase relationship in both indices (see Appendix). We find that by using this technique, the cross correlation among the QBO indices and the other predictors never exceeds 0.06, which ensures that the null hypothesis of no correlation cannot be rejected at the 99 % confidence level.

Principal component analysis (PCA) has been used in previous studies to derive orthogonal QBO indices (Randel and Wu, 1996; Crooks and Gray, 2005; Frame and Gray, 2010). The mathematical orthogonality constraint can potentially limit the physical realism of the principal component associated with the QBO. For this reason, we believe that the residuals from a MLR at 30 and 10 hPa are more directly linked to the original wind field at both heights, and thus more suited than principal components for representing the QBO variability in the MLR.

This procedure is repeated for each of the simulation sets for both temperature and ozone. The regression model formulated in Eq. (A6) is applied at constant pressure levels of the tropical stratospheric domain (0.1–100 hPa).

The MLR includes only predictors for those forcings included in the specific set of experiments (e.g., no QBO term is used in the analysis of the noQBO set). Since the main focus of this paper is the detection of the solar signal in the tropical stratosphere, results from the regression analysis are only presented for the UV coefficient (β'_{uv} in Eq. A6). The coefficient has been scaled at all isobaric levels by 0.175. This scaling factor is the 2-σ value of the UV radiation index used in the MLR, which represents the peak-to-trough solar cycle variation in units of $W\,m^{-2}\,nm^{-1}$.

3 Results

Figure 1 shows the time series of the tropical average (25° N–25° S) seasonal mean anomalies of the zonal mean temperature at the 50 hPa level from the "all forcings" set. A long-term cooling trend is evident, and the amplitude of approximately −0.5 K per decade agrees with observations (Randel et al., 2009b). The trend is interrupted by positive peaks over 2 K in 1964 and 5 K in 1992, which are caused by two major volcanic eruptions, i.e., Agung and Mt. Pinatubo. Among these events, the Mt. Pinatubo eruption is the best-characterized eruption on records. These records show a 1–2 K warming in 1992 in the 50 hPa global mean (Randel et al., 2009b), while anomalies over the tropical belt reach 3 K (see Fig. 1 in Tilmes et al., 2009). Compared to these values, WACCM tends to overestimate the heating caused by the sulfate aerosols associated with the Mt. Pinatubo eruption.

Before applying the MLR, the variables and the forcings are prewhitened with the autocorrelation coefficient of the field variables. Since the choice of the lag for the predictors is crucial to improve the regression fit, we first analyze the lag correlation between forcings and the simulated field variables temperature and ozone.

3.1 Lag correlation analysis

The optimal lag must ensure a physically consistent relationship between the prewhitened field variables and the forcings. For this purpose, the vertical structure of the lag correlation is analyzed in detail in order to identify a window representing a realistic timescale for the response in the selected variable to each of the applied forcings.

Figure 2 shows the vertical profile of the correlation of the tropical average seasonal mean temperature with UV radiation from the all forcings set, plotted as a function of the time lag in a window of 10 yr (−5 to +5), thus covering an almost complete solar cycle. Correlations at positive lag values mean that variations in UV lead temperature changes. Although the prewhitening of the time series considerably

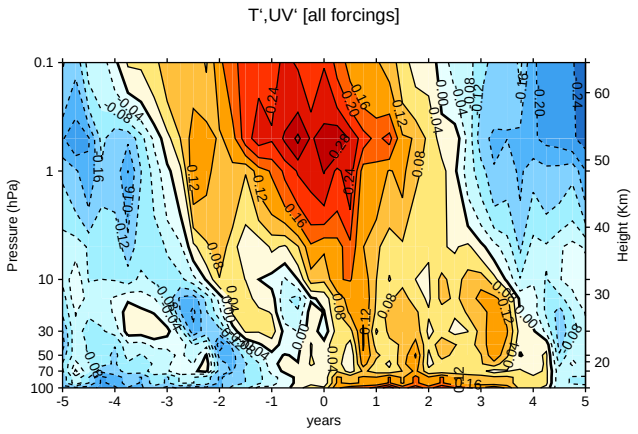

Figure 2. Lag correlation between the tropical average [25° N–25° S] prewhitened seasonal mean temperature from the all forcings case and the UV radiation index. Positive lags mean that UV predictor leads temperature changes. Solid contours and red colors denote positive correlations, while dashed contours and blue colors indicate negative correlations. Contours are drawn every 0.04.

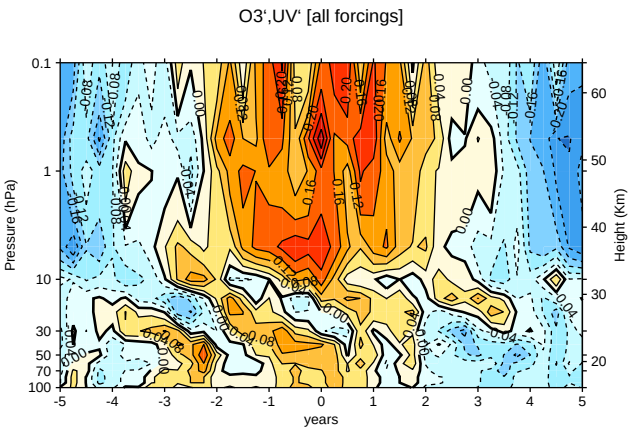

Figure 3. As in Fig. 2, for tropical mean zonal mean ozone from the all forcings case.

reduces the magnitude of the correlations, a well-defined positive temperature–UV relation is found at 1 hPa, which lingers for 2 yr around the peak of solar activity (that is, from lag −1 yr to 1 yr). Negative values can be seen 5 yr before and after the peak in UV radiation, indicating a cooling around minima of solar activity. Between 10 and 70 hPa, we identify positive maxima at lags of 0.75, 1.75, and 3.25 yr. Among them, the peak at 0.75 yr corresponding to three seasons (or 9–11 months) seems to be connected to the upper stratosphere. This suggests that the warming induced by maxima in solar activity is instantaneous and longer-lasting in the upper stratosphere, whereas it is slightly weaker and delayed by a few seasons in lower layers.

Overall, the lag correlation to the UV in the WACCM simulations depicts a downward propagation of the solar signal. This is consistent with the "top-down" mechanism involving a downward pathway (which is thus mediated by the stratosphere) for solar influences to impact surface climate, as hypothesized in previous studies (Meehl et al., 2009; Gray et al., 2010). The broad time span of the maximum at 1 hPa is most likely due to absorption of UV radiation whose peaks, on average over the recorded 11 yr cycles 19–23, last for about 2–3 yr (Lean et al., 2005). In lower levels, the intermittency of the positive correlations suggests a seasonality in the apparent downward propagation of the temperature signal. One candidate mechanism for such propagation is the strengthening of the wintertime polar night jet during solar maxima, which causes suppressed tropical upwelling (Kodera and Kuroda, 2002). This mechanism is captured by WACCM (Chiodo et al., 2012), and the timescales for the downward propagation are consistent with the lags found in the positive correlations of the 0–1 yr window.

The lag correlation of UV radiation with tropical mean ozone is shown in Fig. 3. As it occurred in zonal mean temperature, a broad structure of positive ozone–UV correlations appears around lag 0 in the upper stratosphere (0.1–10 hPa), with two peaks at 1 and 5 hPa. A more complex structure in the lag correlations is found in lower levels. At 10–50 hPa, there is a small region with negative values around lag 0, while positive correlations appear at lags of 0.75–1 yr. At 50–100 hPa, positive correlations are found between 0 and 1 yr, maximizing at a lag of 0.25 yr, equal to one season. Except for the negative correlations at 30 hPa, there is good correspondence between temperature and ozone in the 0–1 yr window.

The in-phase ozone–UV relationship in the middle and upper stratosphere is likely due to the UV-induced photolysis of molecular oxygen and recombination with atomic oxygen (Pap and Fox, 2004). This process is instantaneous, and extends for the 2–3 yr of peak solar activity. As in temperature, the intermittency in the correlations at lower levels suggests a seasonality in the lower-stratospheric ozone response. In the 0–1 yr span, the correspondence in the temperature and ozone correlations suggests that the same mechanism is controlling ozone and temperature responses in this window. Unlike in temperature, there is less evidence of a delayed response at lags larger than 1 yr throughout the 30–100 hPa region. This indicates that at such lags, it is difficult to link both temperature and ozone responses through a common mechanism.

Once we have analyzed the structure of the correlations, we next identify the optimal lag that maximizes the absolute value of the cross correlation with the UV index. We constrain the window over which the optimal lag is identified to the 0–1 yr time span, motivated by the finding that a coherent variation in correlations with temperature and ozone was present in that interval. An added benefit of limiting the lag in the 0 to 1 yr window is that the cross correlation between

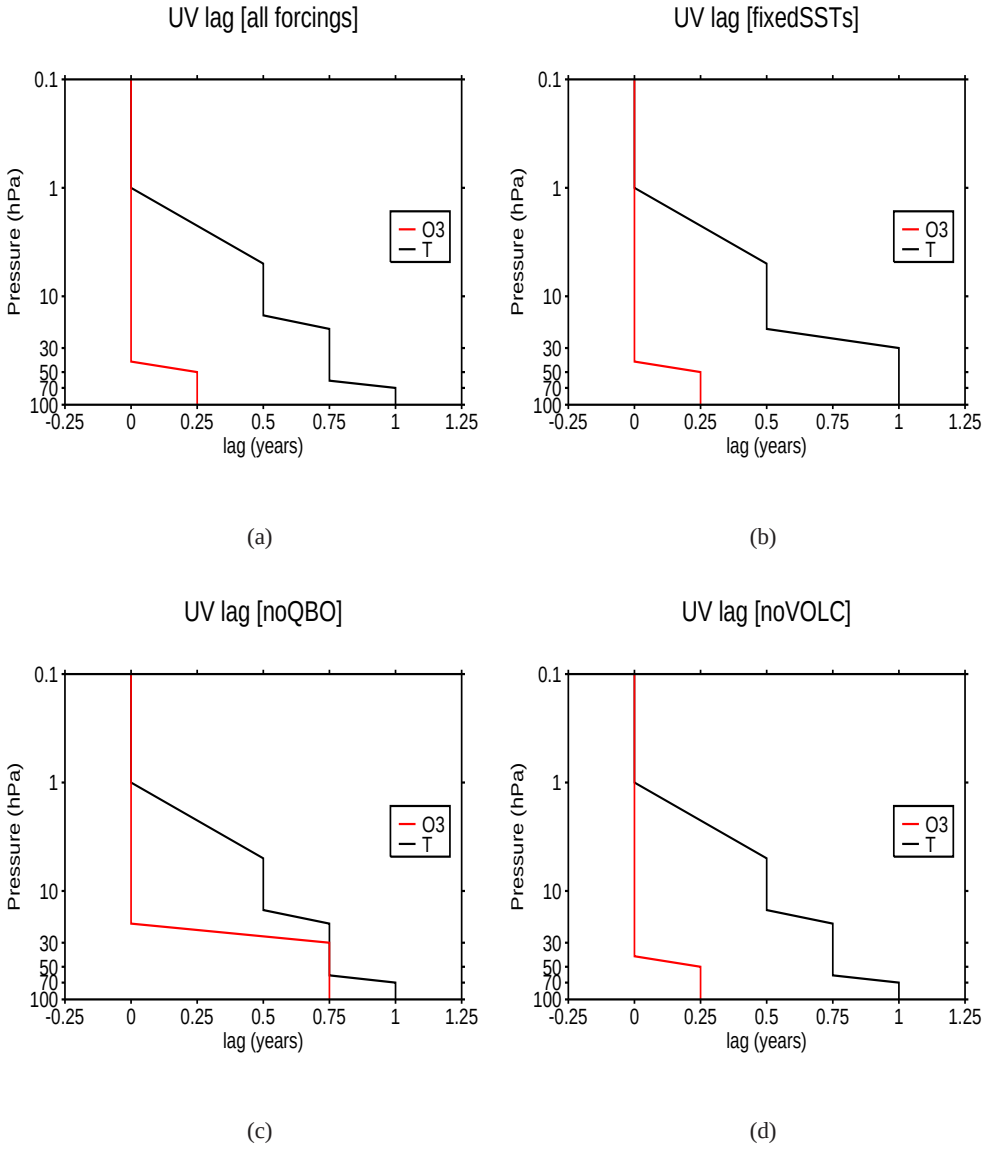

Figure 4. Vertical profile of the lag that maximizes the absolute value of the correlation (in the 0–1 years window) between UV radiation and prewhitened seasonal mean temperature (black) and ozone (red) from **(a)** the all forcings, **(b)** fixedSSTs, **(c)** noQBO, and **(d)** noVOLC sets. The values are introduced as $\tau_{i=uv}$ in Eq. (A6) for regression of tropical average temperature and ozone.

the UV index and the other predictors is minimized. Hence, the optimal UV lag (τ_{uv}) to be used in Eq. (A6) is chosen in this window.

The vertical profile of τ_{uv} is shown in Fig. 4 for zonal mean temperature and ozone. We show the values obtained for the all forcings case (a) and for the three idealized sets (b–d). Overall, the temperature–UV and the ozone–UV correlation patterns are found to be qualitatively similar in the three simulation sets excluding single forcings (not shown), which explains the similarity in the vertical profile of the optimal lag. In the case of zonal mean temperature, the profile shows a downward progression in all four cases, with a lag of 0.5 yr (or two seasons) at 10 hPa, 0.75 yr (or three seasons) between 20 and 70 hPa, and 1 yr between 80 and 100 hPa, consistent with the lagged positive correlation in this region seen in Fig. 2. In tropical ozone, the lag needed to maximize the correlation in the TLS is slightly smaller than in temperature, as seen in Fig. 3.

We also analyzed the lag correlation for the other terms included in Eq. (A6): the two QBO indices, N3.4 and SAD. As the present paper is focused on the solar response, we discuss it without showing additional figures. The cross correlation of temperature and ozone with $u30'$ and $u10'$ shows a downward-propagating pattern associated with the meridional secondary circulation of the imposed QBO (Baldwin et al., 2001). For the N3.4 index, negative correlations of

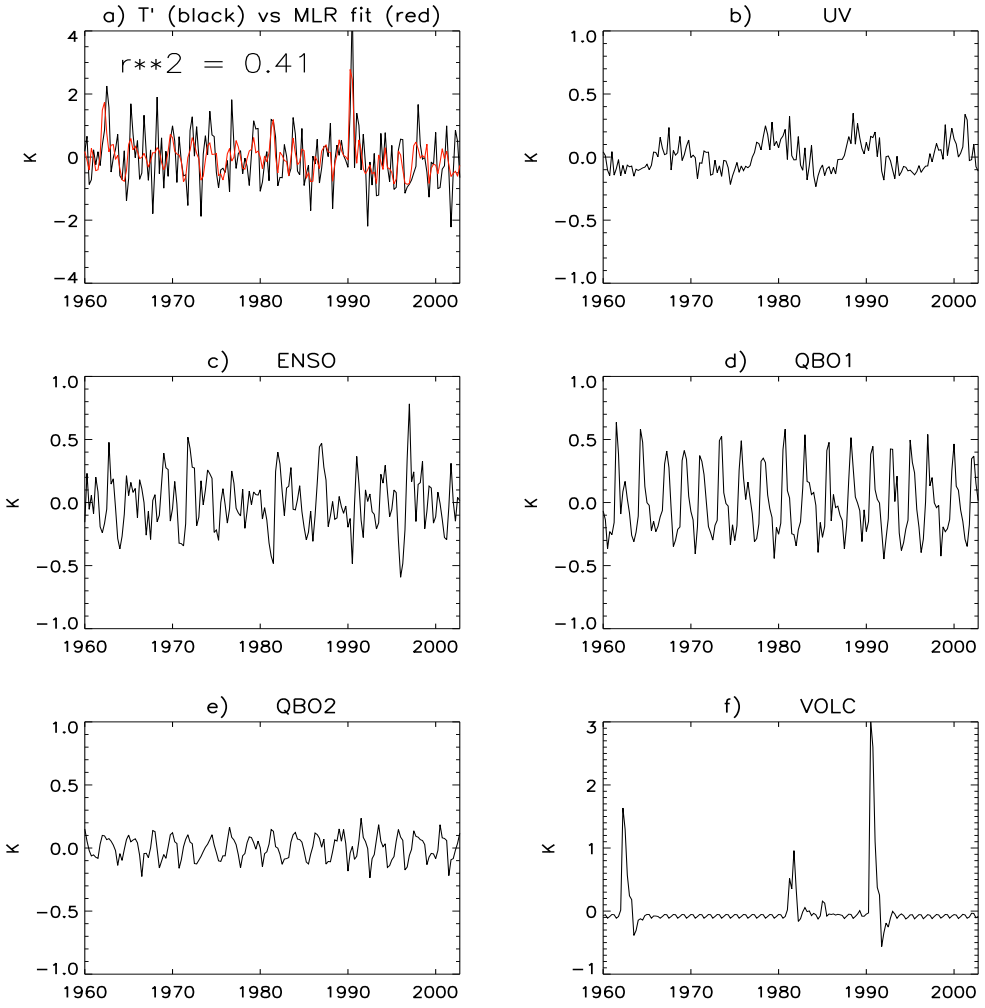

Figure 5. (a) Time series of tropical average seasonal mean zonal mean temperature anomalies at 50 hPa after prewhitening (black), along with the regression fit from Eq. (A6) (red). **(b–f)** Contribution of each of the terms on the right-hand side of Eq. (A6) to the regression fit.

ozone and temperature maximize at 0.5 yr (6–8 months, or two seasons) and 0.25 yr (3–5 months, or one season), respectively, consistent with the lagged impact of El Niño on the TLS through an increase in tropical upwelling (Marsh and Garcia, 2007; Calvo et al., 2010). For the SAD index, we find positive correlations in temperature and negative values in ozone, both peaking at zero lag, and decaying as the lag increases to around 1.5 yr.

We constrained the optimal lag in the N3.4 and SAD indices to be no more than 1 yr, as was done for the UV index. This is motivated by the fact that at lags longer than 1 yr, spurious interference with the QBO appears in the form of downward-propagating QBO structures in both ozone and temperature correlations with N3.4 and SAD indices. Also, the cross correlation between N3.4, SAD, and QBO indices in the 0 to 1 yr window is minimized. Hence, the optimal lag maximizing the correlation with these indices (i.e., τ_{enso} and τ_{volc} in Eq. A6) is chosen in this window.

We do not use a lag for the SAD index for the regression of both temperature and ozone, as the strongest correlation is found at zero lag. This implies that $\tau_{\text{volc}} = 0$ at all levels in Eq. (A6). For the N3.4 index, we use $\tau_{\text{enso}} = 0.25$ yr (or one season) for the regression of temperature, while a value of 0.5 yr (or two seasons) is used for ozone. No lags are used in $u10'$ and $u30'$, as the optimal fit is obtained by adjusting the relative weighting (i.e. regression coefficients) of these roughly sinusoidal variations. With these values for τ_{enso}, τ_{volc} and those for τ_{uv} displayed in Fig. 4, a regression of the time series of zonal mean wind at 10 and 30 hPa ($u10'$ and $u30'$) is performed (see Eq. (A5)). The residuals are then taken as QBO indices (i.e., $u10^*$ and $u30^*$ in Eq. (A6)).

An example of the application of the MLR procedure employed in this paper is given for the tropical average zonal mean temperature at 50 hPa, which is the time series shown in Fig. 1. Figure 5a shows the temperature time series after prewhitening, along with the fit output from the MLR

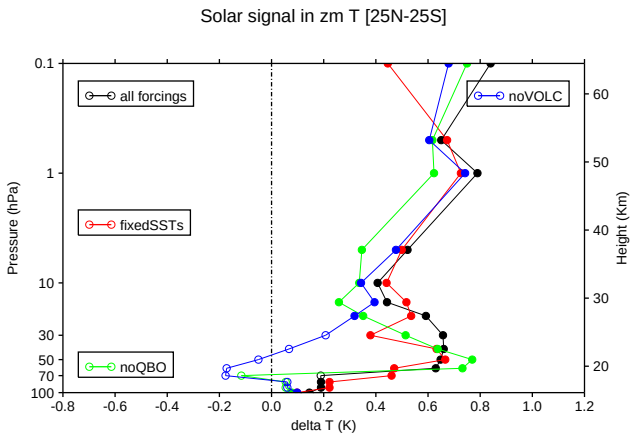

Figure 6. Solar signal in tropical average zonal mean temperature, estimated as the UV regression coefficient (β'_{UV} in Eq. (A6)) multiplied by 0.175, which represents the 2-σ variation of the UV index used in the MLR. Delta K units denote the relative solar cycle peak to trough change in kelvin. Filled dots indicate that the derived regression coefficients are significantly different from 0 at the 2-σ significance level. The lags used for the UV index in each experiment set is the black line shown in Fig. 4.

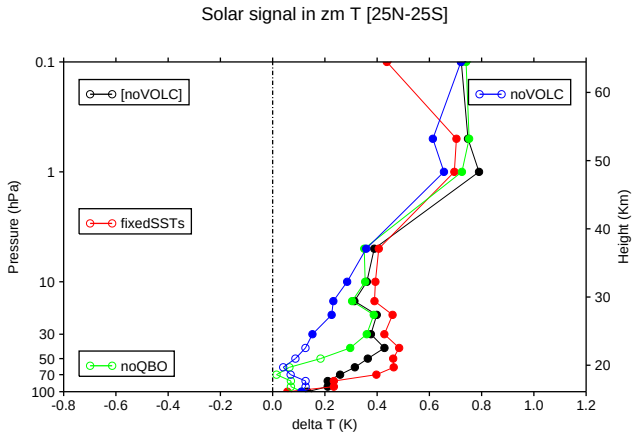

Figure 7. As in Fig. 6, calculated as the UV regression coefficient from a standard MLR (β_{uv} in Eq. (A1)) multiplied by 0.175, which represents the 2-σ variation of the UV index used in the MLR.

model formulated in Eq. (A6). As seen in Fig. 4, the optimal UV lag (τ_{uv}) used at this level is 0.75 yr (or three seasons), while τ_{enso}=0.25 yr (or one season). It is found that while the prewhitening smooths part of the variability, the peaks of the original time series shown in Fig. 1 are preserved. The r^2 value of 0.4 implies that 40 % of the variability in the prewhitened temperature time series can be explained by the regression fit. Note that if no optimal lag is used for the predictors, the r^2 value would be 0.2 (not shown), which indicates a less accurate fit. Figure 5b–f plot the contribution of each term on the right-hand side of Eq. (A6) to the regression fit shown in Fig. 5a. The strongest temperature changes are caused by volcanic eruptions, with Mt. Pinatubo generating a 3 K anomaly (Fig. 5f). Changes of 0.5–1 K are associated with the first QBO term ($u30^*$, i.e., the filtered zonal wind at 30 hPa) and ENSO (Fig. 5c, d). On the other hand, the 11 yr solar cycle signal is smaller, with temperature deviations of a few tenths of a kelvin (Fig. 5b).

3.2 The 11 yr solar cycle signal

The vertical profile of the solar signal, shown as the UV regression coefficient (β'_{uv}) of the tropical average (25° N–25° S) zonal mean temperature scaled by 2σ of UV radiation (0.175), is shown in Fig. 6. The profile is shown for the reference all forcings set, and the idealized experiments, using the optimal lag for the UV index shown in Fig. 4.

In the all forcings set (black line in Fig. 6), a statistically significant UV-induced warming is found throughout the tropical stratosphere, with maximum values of 0.8 K at 1 hPa and a secondary maximum of 0.6–0.7 K at 40–50 hPa. It is interesting to note that a statistically significant solar signal is also extracted in the middle stratosphere at 10 and 20 hPa, even though this is a region of relative minimum response. The lag used for the UV index is 0 at 1 hPa, 6–8 months (or two seasons) at 10 hPa, and 9–11 months (or three seasons) between 20 and 70 hPa (see Fig. 4).

In the fixedSSTs case (red line in Fig. 6), the simulated temperature solar signal is similar to the reference case, although the secondary maximum at 50 hPa is obtained at a slightly larger lag compared to the other sets ($\tau_{\mathrm{uv}} = 1$ yr; see Fig. 4). The strong similarity in the derived UV regression coefficient in temperature suggests that the ENSO contribution to the apparent solar signal is negligible. The low sensitivity of the UV regression coefficient to the inclusion of ENSO is not due to the removal of the serial correlation, as similar results are obtained without prewhitening the data (not shown). The noQBO set (green line in Fig. 6) shows a significant solar response throughout the stratosphere above 60 hPa, with a peak of 0.7 K at 50 hPa. Overall, this profile resembles the reference all forcings case, although a slighly stronger magnitude of the warming is evident at 50 hPa. In the noVOLC set (blue line), a significant regression coefficient is obtained at all levels above 20 hPa, with a peak of 0.7 K at 1 hPa. However, below 20 hPa the signal becomes weak and statistically insignificant. Thus, no robust solar response in temperature is obtained in the TLS in the WACCM simulations that do not include volcanic eruptions. The absence of response indicates that the apparent lagged temperature solar signal in the TLS diagnosed in all other simulation sets is associated with the effect of volcanic aerosols.

For comparison, the UV coefficient was also estimated from a standard MLR (β_{uv} in Eq. (A1)). Figure 7 shows the vertical profile scaled by 0.175. The temperature response in the upper stratosphere between 1 and 5 hPa is very similar to that obtained with the new technique (Fig. 6); that

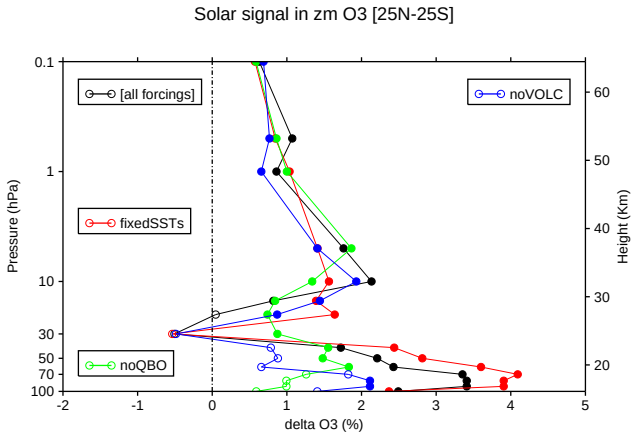

Figure 8. Solar signal in tropical average zonal mean ozone, estimated as the UV regression coefficient (β'_{UV} in Eq. (A6)) multiplied by 0.175, which represents the 2-σ variation of the UV index used in the MLR. Delta % units denote the relative solar cycle peak to trough change in percent (i.e., relative change in mixing ratio). Filled dots indicate that the derived regression coefficients are significantly different from 0 at the 2-σ significance level. The lags used for the UV index in each experiment set is the red line shown in Fig. 4.

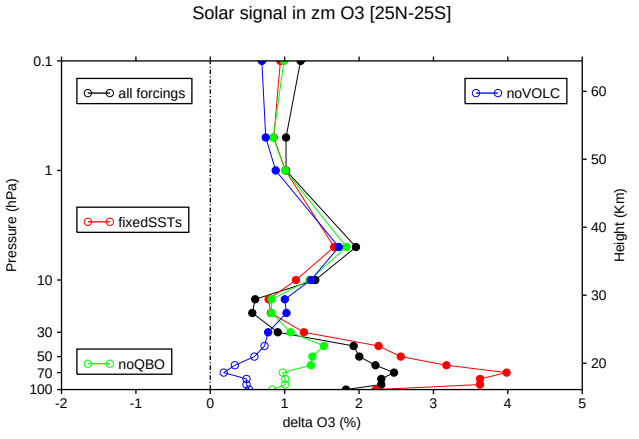

Figure 9. As in Fig. 8, calculated as the UV regression coefficient from a standard MLR (β_{uv} in Eq. (A1)) multiplied by 0.175, which represents the 2-σ variation of the UV index used in the MLR.

is, a significant warming of 0.6–0.8 K in all experiments. In the lower layers, there is less agreement between the ensembles. A secondary maximum is evident in the all forcings and fixedSSTs sets, with a peak of 0.4–0.5 K at 50 hPa. A similar response is also seen in the noQBO set, although the region of statistical significance is limited to higher altitudes (20 hPa). Below 30 hPa, no significant response is seen in the noVOLC and noQBO ensembles. Comparing both techniques (i.e., Figs. 7 and 6), it is evident that the secondary maximum in the TLS extracted from the new regression technique, when statistically significant (i.e., in the all forcings and fixedSSTs sets), is stronger in magnitude than when using the standard MLR. Also, the new technique yields a secondary maximum in the noQBO set, whereas no response is seen in the standard MLR. Thus, in the TLS region the new regression method allows for better separation of the temperature solar signal from the QBO. The new method also shows a stronger reduction of the solar signal in the noVOLC set.

The new method was also applied to the tropical mean ozone mixing ratio. The vertical profile of β'_{uv} scaled by 0.175 is shown in Fig. 8 in terms of relative solar cycle (%) peak to trough change in the mixing ratio using the lag values for the UV index shown in Fig. 4. In the all forcings case, there is a well-defined double peak structure, with statistically significant ozone increase in the middle and upper stratosphere peaking at 2 % at 10 hPa, a relative minimum at 30 hPa, and a significant increase at 40 hPa and below, peaking at 3.5 % between 70 and 90 hPa.

Fairly good agreement across all pairs of simulations is seen in the UV-induced ozone increase of 1.5–2.0 % at 5–10 hPa, although the exact height of the maximum varies. At 20 hPa, the solar cycle ozone response in the noVOLC and noQBO case is slightly stronger than in the all forcings case. Reasonable agreement is also evident in the weakly negative response at 30 hPa, with exception of the noQBO case, which shows a positive and significant ozone response of 1 %.

Significant differences are evident in the amplitude of the ozone increase in the stratospheric levels between 40 and 100 hPa. While the all forcings case features a significant ozone increase ranging from 2.0 % at 50 hPa to 3.5 % at 70 hPa, the response in the noVOLC case follows a similar profile, although with lower values ranging from a non-significant 0.8 % increase at 50 hPa to 1.5–2.0 % at 70–80 hPa. At 70 hPa and below, a different response is also observed in the noQBO case, where a non-significant 1.0 % ozone increase is obtained. On the other hand, the ozone response at 70–80 hPa is increased to 4.0 % in the fixedSSTs case, although the difference between this set and the all forcings pair of simulations is not statistically significant. Among all experiments, the profile of β'_{uv} obtained from the fixedSSTs set is the one that most closely resembles the all forcings case in the lower stratosphere. Those calculated from the noVOLC and noQBO exhibit the largest differences to the reference case, with a weaker response throughout the lower stratosphere below 40 hPa in the noVOLC case, and below 70 hPa in the noQBO case. This suggests that part of the apparent lower-stratospheric ozone signal obtained from the all forcings case is due to QBO and volcanic aliasing, with the largest spurious contribution coming from volcanic aerosol.

Figure 9 shows the ozone UV regression coefficient obtained from a standard MLR (β_{uv} in Eq. (A1)). The ozone increase of approximately 2 % at 5 hPa is similar to the response obtained from the new technique (Fig. 8). The relative minimum at 20 hPa is statistically significant, while, using

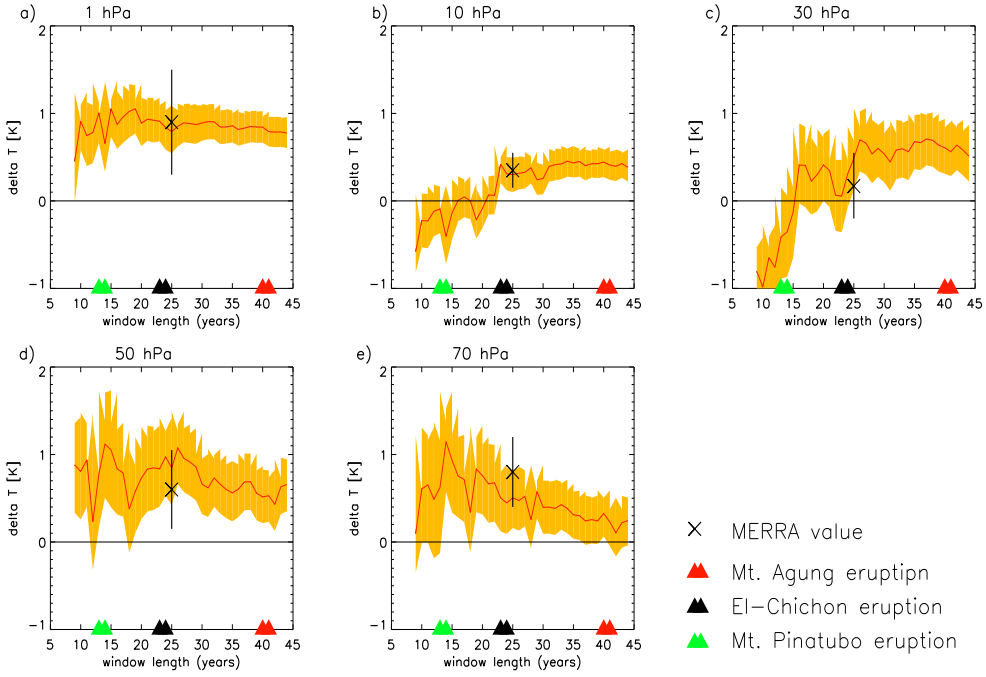

Figure 10. UV regression coefficient (β'_{UV} in Eq. (A6)) in tropical mean zonal mean temperature (red line) along with the 2-σ uncertainty (yellow shading) from the all forcings case, plotted as a function of the window used (in years). The endpoint of the window is the last available year in the ensembles, i.e., 2004. Results are shown for **(a)** 1 hPa, **(b)** 10 hPa, **(c)** 30 hPa, **(d)** 50 hPa, and **(e)** 70 hPa. Crosses show the values obtained from MERRA reanalysis at 30, 50, and 70 hPa using the window overlapping the simulation period (1979–2004). Unit: K.

the new MLR, this response is not significant and lower in altitude (30 hPa). Both techniques show differences between ensembles in the region below 40 hPa, although the spread seems larger in the standard MLR. In the new MLR, the difference in the solar response between the all forcings and fixedSSTs sets at 50–70 hPa is smaller compared to the standard MLR. This indicates that the use of the new regression technique reduces the ENSO aliasing in the apparent solar response of lower-stratospheric ozone. Overall, both techniques show a reduction of the solar signal below 30 hPa in the noVOLC set compared to the all forcings set. Accordingly, the contribution of volcanic aerosol to quasi-decadal variability of tropical lower-stratospheric ozone does not depend on the type of regression analysis.

3.3 Sensitivity of the solar signal to the data window

The results from the idealized cases give useful information about the impact of other forcings on the analysis. However, these simulations might not be able to reproduce non-linear interactions between the missing forcing and the 11 yr solar cycle. The aim of this section is thus to assess aliasing in the regression of one pair of simulations driven by the combination of forcings that most closely resembles the real atmosphere, as is the all forcings case. In this way, it is possible to quantify the potential aliasing in regressing a limited record, and in turn to infer the feasibility of extracting a robust solar signal from the window covered by observational records. One method to accomplish this consists of testing the sensitivity of the diagnosed signal to the length of the data.

We calculate the UV regression coefficient (β'_{uv}) from the all forcings set for a varying data window, whose endpoint is the last year available in the simulations: 2004. A minimum of 10 yr is used to cover the last solar cycle (1995–2004), and the data window is gradually extended to the whole 45 available years, using 1 yr increments.

Figure 10 shows the estimates for tropical mean temperature, calculated at 5 different pressure levels representative of the upper stratosphere (1 hPa), middle stratosphere (10 hPa), and lower stratosphere (30, 50, and 70 hPa), scaled by the 2-σ value of the UV index. Note that the endpoint value obtained with the entire 45 yr time series is identical to that shown (on the same levels) in Fig. 6.

In the upper stratosphere at 1 hPa (Fig. 10a), a constant value of 0.8–1.0 $\pm$ 0.2 K is obtained. One can deduce that the minimum number of years necessary for extracting a significant and stable solar signal in temperature at 1 hPa is 10–15 yr, since the value obtained with such window is fairly close to that calculated with the full available period of 45 yr. At 10 and 30 hPa (Fig. 10b, c), the regression coefficient is slightly negative and not significant when less than 20 yr of data is used. It then stabilizes to a significant positive value of 0.4 $\pm$ 0.2 K at 10 hPa and 0.5 $\pm$ 0.3 K at 30 hPa when more than 25 yr of data is used.

At lower-stratospheric levels (50 and 70 hPa, shown in Fig. 10d, e), the derived values are more uncertain than in the upper stratosphere, as indicated by the wider error bars, and exhibit stronger sensitivity to the window length. Broadening the data window reduces the apparent signal at 50 and 70 hPa from 1.0 ± 0.7 K with 15 yr of data to 0.2–0.5 ± 0.3 K when using the 45 yr of data. No convergence towards a steady value is found at these levels. Thus, a stable and significant temperature response can only be detected above 30 hPa, while a different behavior is observed at 50 and 70 hPa, where no robust value can be extracted with the available 45 yr long record.

In addition, strong swings are evident in the middle and lower stratosphere (30, 50, and 70 hPa) a few years after the occurrence of the two major volcanic eruptions when using WACCM data, suggesting that volcanic and solar signals cannot be cleanly separated by the regression model at these levels. Interestingly, both Mt. Pinatubo and El Chichón eruptions appear to interfere with the solar signal at 30 and 50 hPa. This is not the case at 70 hPa, where only the former has a discernible impact (Fig. 10e). There are also perturbations of negative sign when the Agung eruption (1963) is included in the analysis. This effect is seen at 50 and 70 hPa, although the jumps are much less evident than in the case of the other two eruptions. Overall, the peaks associated with Mt. Pinatubo and El Chichón disappear after 30 yr of data is included in the regression analysis. Even when the analysis is extended using a longer window, the UV coefficient decreases at both levels, which is particularly evident at 70 hPa. This suggests that in WACCM3.5, no robust signal in temperature can be extracted in the TLS with 45 yr of simulations data.

The UV regression coefficient is also estimated using the same procedure on NASA's Modern-Era Retrospective Analysis for Research and Applications (MERRA) reanalysis data (Rienecker et al., 2011), chosen here over other reanalysis products due to the larger overlap with the simulations (1979–2004). WACCM and MERRA can be directly compared by using 26 yr as the window in the all forcings case. At this window length, the apparent solar signals at 1 hPa (Fig. 10a) and 10 hPa (Fig. 10b) of 0.8 and 0.3 K in the model simulations are in excellent agreement with MERRA estimates. Since the temperature response at these heights is related to the direct response to the UV radiation, the agreement with reanalysis suggests that the model sensitivity to the 11 yr UV forcing is realistic. There is also qualitative agreement at 30 hPa (Fig. 10c), 50 hPa (Fig. 10d), and 70 hPa (Fig. 10e) in the signals of 0.3, 0.5, and 0.7 ± 0.2 K, respectively. However, this only applies to the 26 yr window overlapping with MERRA since, as indicated above, a decrease in the diagnosed solar signal is seen as a larger analysis period is used.

It should be recalled that the warming simulated at 50 hPa after Mt. Pinatubo in 1992 is too large (see Fig. 1). This bias might contribute to the misattribution of quasi-decadal variability when using model data in the analysis. Accordingly, the impact on the detection of solar signals might depend on the size of the underlying volcanic signature. To test this possibility, we analyze the dependence of the solar signal to data windowing in the MERRA record, bearing in mind that less stability is expected due to the shorter window compared to the WACCM simulations. Figure 11 shows the regression coefficient obtained from MERRA, calculated in the same way as in Fig. 10, plotted as a function of the 26 yr window. A robust signal is found at 1 and 10 hPa, with values of 0.9 ± 0.5 K and 0.3 ± 0.2 K, respectively (Figs. 11a, b). The values at 30, 50, and 70 hPa (Figs. 11c, e) are less stable, which is in large part due to the peak coinciding with the Mt. Pinatubo eruption, especially at 50 hPa (Fig. 11d). There is also a tendency towards smaller values at these levels, as the window gets broader, although a stable value is not reached. This suggests that, as in WACCM, the solar signal extracted over the available observational record is not robust, mainly due to the heating associated with the Mt. Pinatubo eruption.

Figure 12 shows the UV regression coefficient obtained from WACCM at 50 and 70 hPa, when periods after El Chichón and Mt. Pinatubo eruptions are omitted (June 1982–November 1983 and September 1991–November 1993). During such periods, the peaks in lower-stratospheric temperature associated with the SAD index can be identified (see Fig. 5f). Convergence toward a constant value of approximately 0.1 ± 0.3 K is obtained when more than 20 yr of data is used. However, this value is not significantly different from zero. When the same years are excluded from the MERRA reanalysis data, the UV coefficient is also reduced from 0.6–0.7 ± 0.3 K to 0.2 ± 0.4 K at both 50 and 70 hPa. This indicates that when applying MLR methods on stratospheric temperature data covering 26 yr, a better separation of solar and volcanic signals can only be achieved with removal of data around both El Chichón and Mt. Pinatubo eruptions. This is consistent with the absence of a signal in the TLS in the set without volcanoes (blue line in Fig. 6). Note that the removal of the period after the Agung eruption (1963–1964) would not alter the results (not shown), which is consistent with the small impact of this event on the window sensitivity of the solar signal shown in Fig. 10.

The sensitivity to data windowing of the regression coefficient in zonal mean ozone simulated by WACCM is shown in Fig. 13. The ozone signal is robust to the extension of the data window at 1 hPa (Fig. 13a), and a constant and significant ozone increase of 0.7 ± 0.4 % is found after 10 yr of simulations data. At 10 hPa (Fig. 13b), positive and significant values of 2.2 ± 0.8 % are found for all data windows, although jumps to higher values are evident when using less than 30 yr of data. A significant positive UV coefficient is obtained at 30 hPa when using less than 15 yr of data (Fig. 13c). However, this signal is not real since no significant ozone–UV relationship is obtained with a larger data window. This is the region in which a relative minimum response in the vertical profile is obtained in all idealized experiments, although

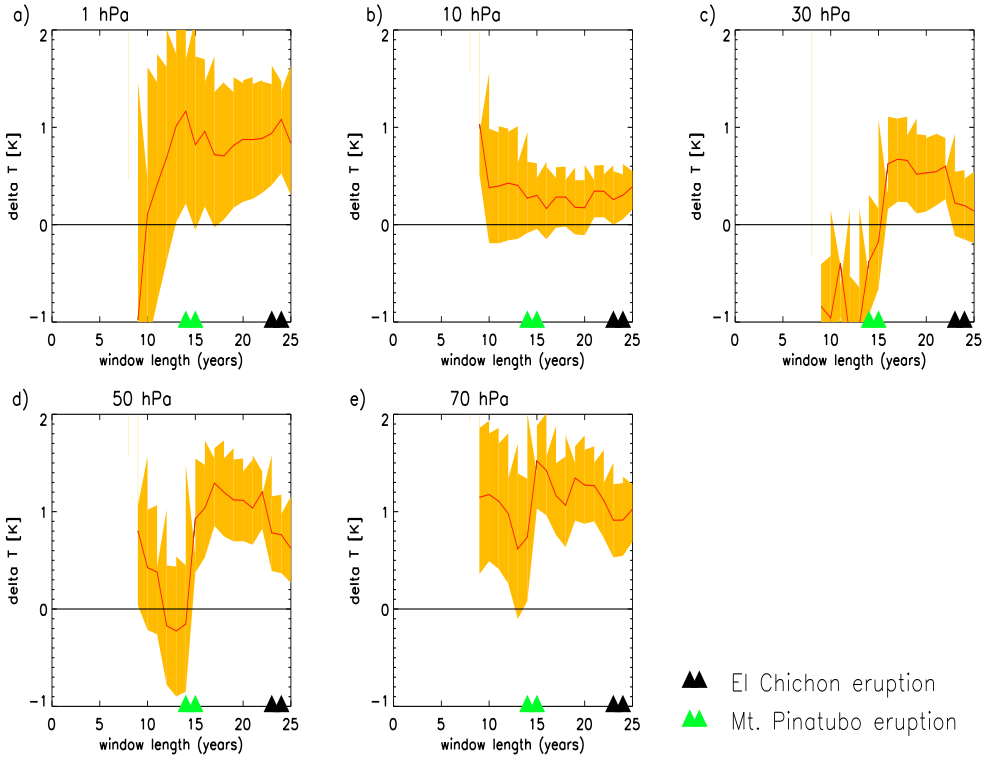

Figure 11. UV regression coefficient (β'_{UV} in Eq. (A6)) in tropical average zonal mean temperature from MERRA reanalysis, displayed as a function of the window used, which is 26 yr long. Note that the signal has been computed with the same regression technique as in WACCM. The endpoint of the window is the last available year in the WACCM simulations, i.e., 2004. Unit: K.

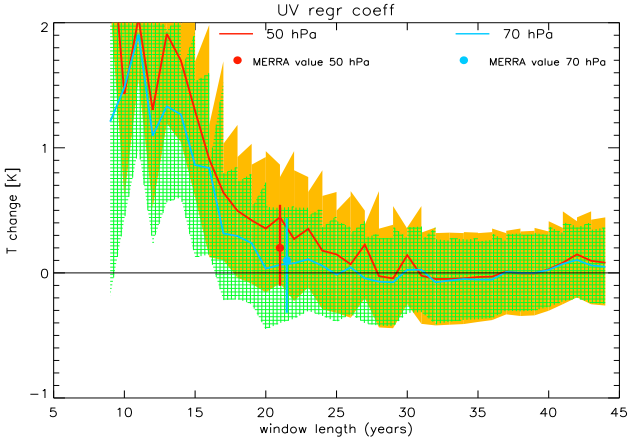

Figure 12. UV regression coefficient in tropical mean zonal mean temperature from the all forcings case, obtained when omitting post El Chichón and Mt. Pinatubo data (see exact dates indicated in the text), plotted as a function of the years included in the window. The endpoint of the window is the last available year in the ensembles, i.e., 2004. Results are shown for the 50 hPa (red) and 70 hPa (blue) levels, along with the 2-σ uncertainty (yellow for 50 hPa and green for 70 hPa). Dots indicate the values obtained from MERRA reanalysis, along with the 2-σ uncertainty. Unit: K.

with slightly different magnitudes (see Fig. 8). At 30 hPa, the noQBO experiment showed a significant ozone increase of 0.6 % (see Fig. 8), which suggests that QBO aliasing reduces the apparent 11 yr variation at this level.

At 50 and 70 hPa, a strong swing in the ozone UV response from negative to positive values is evident in proximity to the Mt. Pinatubo eruption in 1991 (Fig. 13d, e), which is indicative of the volcanic aliasing when regressing data of Mt. Pinatubo eruption. There is little evidence of aliasing in the wake of the El Chichón eruption in 1982 at 50 hPa. At this level, a rather constant and marginally significant value of 1.0–1.5 $\pm$ 1.0 % is diagnosed when more than 20 yr of data is used.

At 70 hPa (Fig. 13e), there is also a jump in proximity to the El Chichón eruption in 1982, although the strongest variation is seen in the years around Mt. Pinatubo (1991). Overall, volcanic eruptions have a stronger impact on the signal at 70 than at 50 hPa, which is consistent with the larger differences found at this level in the noVOLC set (Fig. 8). The error bars and the variations in the amplitude are larger than at higher levels, which suggests that it is not feasible with the available data to extract an accurate estimate for the ozone solar response at 70 hPa. Nevertheless, there is some evidence of a trend toward a positive signal of 3.2 $\pm$ 1.8 % as all available 45 yr of data are included in the analysis. This

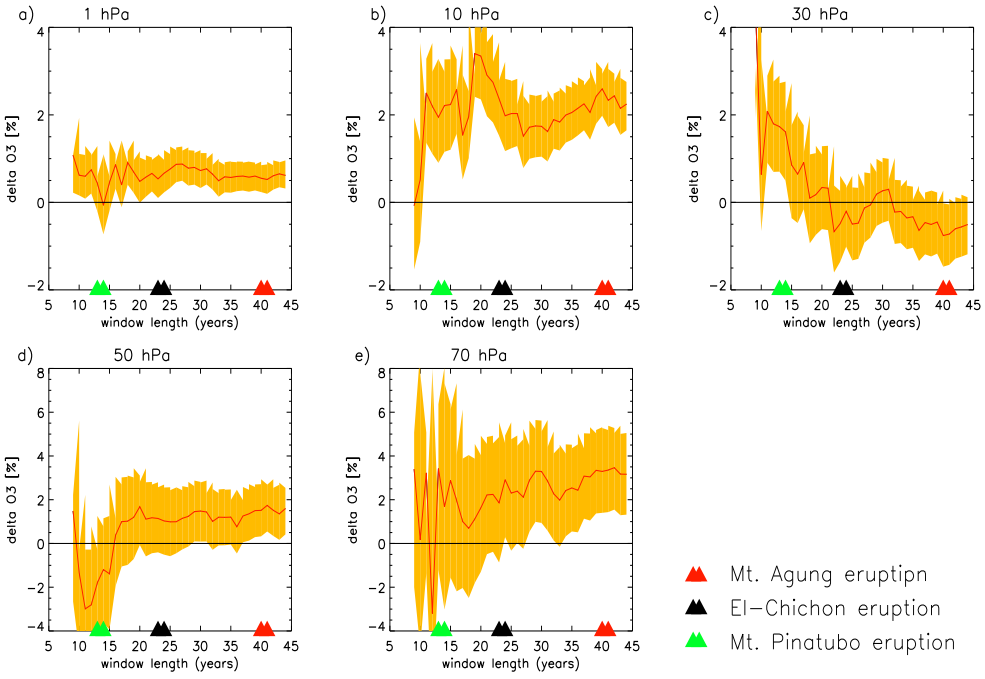

Figure 13. As in Fig. 10, for tropical mean zonal mean ozone. Unit: %(i.e., relative change in mixing ratio).

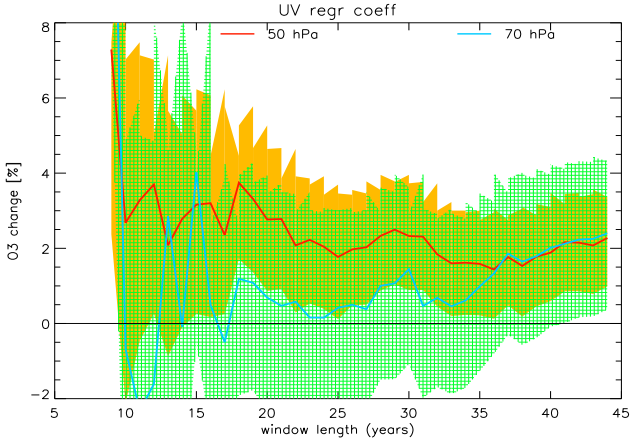

Figure 14. UV regression coefficient in zonal mean ozone from the all forcings case, omitting the post-El Chichón and Mt. Pinatubo data (June 1982 to November 1983, and September 1991 to November 1993), plotted as a function of the window used (in years) for 50 hPa (red) and 70 hPa (blue), along with the 2-σ uncertainty (yellow shading for 50 hPa and green shading for 70 hPa). The endpoint of the window is the last available year in the ensembles, i.e., 2004. Unit: percent.

behavior is unlikely to be related to the Agung eruption, since the tendency in the ozone solar signal starts at year 35, i.e., 6 yr ahead of year 41 in the window, which would correspond to the eruption year 1963.

Figure 14 shows the ozone UV coefficient calculated at 50 and 70 hPa, when the El Chichón and Mt. Pinatubo post-eruption data are omitted following the same procedure taken for temperature. A fairly constant value of 2.0 ± 1.5 % is obtained at 50 hPa when using more than 25 yr of data. These numbers are not significantly different from those shown in Fig. 13d, which were calculated with Mt. Pinatubo and El Chichón data retained. At 70 hPa, there is nearly no response at a window of 20–25 yr, and a positive trend towards positive values is evident when more than 35 yr of data is used. The value of 2.3 ± 1.9 % obtained with the full 42 yr window is lower than the 3.2 ± 1.8 %, which was diagnosed without removing post-eruption data (Fig. 13e). This is consistent with the reduction in the apparent solar signal obtained from the noVOLC experiment at this level (Fig. 8).

Overall, temperature and ozone show slightly different sensitivities to data windowing, which probably owes to the different processes controlling their variations in the tropical stratosphere. Further complication is brought by the low signal-to-noise ratio in ozone due to the relatively small ozone concentrations below 50 hPa. Nevertheless, both variables suggest that a robust solar signal can only be extracted using an MLR technique at upper- and middle-stratospheric levels.

4 Discussion

The tropical mean vertical profile of the 11 yr solar signal has been extracted from WACCM simulations using a novel MLR methodology. In the upper stratosphere, a 0.8 ± 0.2 K warming is diagnosed, which agrees with MERRA

and ERA-40/ERA-Interim estimates within the levels of uncertainty (see Fig. 1 in Frame and Gray, 2010). A robust and statistically significant signal is extracted at 1 hPa using a 15–20 yr window, which is covered by stratospheric observational records. At 10 hPa, WACCM shows a significant warming of 0.4 ± 0.2 K obtained, whereas ERA-40 and ERA-Interim data show no significant response. This difference is possibly due to the different (longer) period analyzed in our study.

Between 30 and 70 hPa a significant warming of 0.5–0.7 ± 0.3 K is diagnosed in WACCM, which agrees with values reported from ERA-40/ERA-Interim reanalysis in Frame and Gray (2010). Similar numbers are also calculated from MERRA reanalysis at 30, 50, and 70 hPa using the same MLR technique over the same period (1979–2004; see Figs. 10c–e). Almost half of the temperature increase in this region is due to the use of a 1 yr lag in the UV index, since a warming of 0.3 to 0.4 K is obtained when using a standard MLR without a lagged UV index (Fig. 7).

It is clear from Fig. 6 that the warming at 30 hPa and lower levels disappears in the set without volcanic forcing, which suggests that aliasing of the volcanic aerosol signal increases the apparent solar signal. Further evidence of this comes from the increase in the UV regression coefficient when the boundaries of the data window considered for regression analysis overlap the years of the Mt. Pinatubo and El Chichón eruptions (Fig. 10c–e). There is also a tendency towards smaller values of the UV regression coefficient in the lower stratosphere (50–70 hPa) as more years are added to the analysis, although no convergence towards a stable value is obtained even with a 45 yr window. This indicates that it is not feasible to extract a robust signal in this region over the recent past. The spurious contribution of volcanic aerosols to the UV regression coefficient is especially pronounced when using records covering two to three decades, as in MERRA reanalysis data (see Fig.11). Better separation of solar and volcanic signals in temperature can be achieved by excluding El Chichón and Mt. Pinatubo post-eruption data from the analysis, since convergence toward a stable (though non-significant) signal is obtained in this way (shown in Fig. 12). Additionally, extending the observational data record to cover solar cycles without volcanic eruptions coincident with peaks of solar activity (e.g., solar cycle 23) decreases the apparent solar-induced warming in the middle and lower tropical stratosphere. This is seen when regressing onto a 31 yr long ERA-Interim/ERA-40 merged data set of 1978–2008 instead of the 23 yr long ERA-40 data set of 1979–2001 (Frame and Gray, 2010, their Fig. 1).

The ozone increase of 2.0 ± 0.7 % in the upper stratosphere at solar maximum in the all forcings WACCM simulation agrees well with the Solar Backscatter Ultraviolet Instrument (SBUV) and Stratospheric Aerosol and Gas Experiment (SAGE) observations (Soukharev and Hood, 2006; Randel and Wu, 2007). An increase of similar magnitude is also obtained using a standard MLR (Fig. 9), which is the more akin to the technique used to extract the signal in the mentioned observational studies than the new MLR formulated here. The response at these levels is robust, since it is stable over time, and it is also diagnosed in the idealized experiments. An accurate estimate can be extracted with 20–25 yr of data, which is a window covered by satellite data. A relative minimum response in tropical ozone is diagnosed in WACCM around 30 hPa. This structure resembles the non-significant negative response seen at 10–20 hPa in SBUV and SAGE (Soukharev and Hood, 2006; Randel and Wu, 2007). The mismatch in the height of the relative minimum response from model and satellite estimates is due to the different formulation of the regression method, since the standard MLR yields a higher relative minimum (20 hPa; see Fig. 9).

A significant ozone increase is found in the lower stratosphere between 40 and 100 hPa, with values ranging from 2.2 ± 1.2 % at 50 hPa to 3.5 ± 2.0 % at 80 hPa. Similar numbers have been previously reported for the same period covered by SAGE and SBUV data (see Fig. 12a in Randel and Wu, 2007, and Fig. 8 in Soukharev and Hood, 2006), although no comparison with these studies is possible below 50 hPa, as this is the lowest boundary in the available satellite data of stratospheric ozone. Idealized experiments show that ENSO aliasing in the lower-stratospheric ozone signal is negligible. This is due to the new MLR technique, which combines the use of lagged ENSO and UV terms, and to a sufficiently large window of 45 yr, which is in line with the findings of Marsh and Garcia (2007). On the other hand, it is also found that the apparent solar cycle ozone increase in the lower stratosphere is strongly influenced by volcanic aerosols and, to a lesser extent, by the presence of the QBO. Interference with volcanic eruptions is also indicated by the increase in the UV regression coefficient when the data window overlaps periods shortly after Mt. Pinatubo and El Chichón eruptions (Fig. 13c–e). Our results confirm the findings from a study using a more simplified 2-D transport chemistry model that pointed to a strong contribution of the QBO and volcanic aliasing on the tropical ozone solar signal (Lee and Smith, 2003; Smith and Matthes, 2008).

We note that around 20 hPa a consistent bias is seen in both temperature and ozone related to the problem of volcanic heating aliasing. Specifically, it appears that a fraction of the volcanic-induced heating is misattributed to the solar cycle by the new and standard MLR techniques, thus producing warmer temperatures during solar maximum. This diabatic heating produces stronger upwelling rates in the simulations including all observed forcings compared to the set excluding volcanic forcing. Along with the chemically induced ozone depletion by the sulfate aerosols, the increased upwelling results in an ozone decrease due to the strongly positive vertical gradient in ozone mixing ratio, which the regression also attributes to the solar cycle, leading to a weaker solar cycle ozone response relative to the set excluding volcanic aerosols. On the other hand, the spurious contribution of volcanic aliasing to the apparent solar signal in both temperature

and ozone below 50 hPa is more difficult to be explained in these terms. At these levels, the simulated ozone depletion is generally much weaker than at 20–30 hPa, as was, for example, the case for the Mt. Pinatubo eruption (see Fig. 8.21 in CCMVal-2, 2010). Moreover, the regression fits from the new technique described in Eq. (A6) are carried independently for temperature and ozone. Thus, the misattribution of volcanically induced ozone and temperature changes cannot be expected to have opposite sign throughout the lower stratosphere.

Chiodo et al. (2012) showed that the temperature and ozone signal in the TLS estimated is stronger and closer to observations in the WACCM3.5 model than in the WACCM3.1 version. The improvement is likely a consequence of WACCM3.1 not assimilating a QBO and the omission of volcanic aerosol heating in the simulations (Garcia et al., 2007). Consequently, the QBO and volcanic signals did not map into the 11 yr solar cycle in the regression analysis of transient WACCM3.1 simulations, leading to a worse agreement compared to transient WACCM3.5 simulations. However, the better agreement with observations does not necessarily imply a better estimate of the solar signal. In conclusion, the present results suggest that either given a long enough window, or in idealized experiments excluding the spurious contribution of volcanic aerosols in the analysis, a consistent, though weaker than previously thought, solar response is diagnosed in the tropical lower stratosphere.

Finally, it is important to note the caveat of excessive heating caused by the Mt. Pinatubo eruption in the TLS region (see Fig.1), although the precise size of the bias is difficult to assess as the uncertainty in the response derived from observations is not known. An excessive volcanic warming could have possibly contributed to the aliasing of the apparent solar signal. However, it must also be noted that the oversized heating could be due to errors in the SAD aerosol forcing data set recommended by CCMVal (Arfeuille et al., 2013). As such, this is a common bias in many community climate models (see, for example, Fig 8.21 in CCMVal-2, 2010). Depending on how the radiative transfer is handled, this affects the models sensitivity to volcanic aerosols to a greater or lesser degree than in WACCM. Thus, while there may be caveats in comparing modeled and observed MLR-derived attribution of decadal variability, our findings are likely not limited to WACCM.

5 Summary

We have investigated the attribution of quasi-decadal variations in tropical stratospheric temperature and ozone to the 11 yr solar cycle. To do so, we perform a set of transient WACCM3.5 simulations with different combination of forcings. The solar signal is extracted from the model simulations using a new MLR approach, which (i) reduces the autocorrelation through prewhitening and (ii) improves the accuracy of the fit through the use of an optimal lag. Results are also compared to the standard MLR, which is found to be more prone to aliasing from non-solar sources than the new MLR method. The design of the model experiments employed here is more realistic than previous modeling studies on the impact of aliasing on the detection of the solar signal, e.g., Marsh and Garcia (2007). The main findings are as follows:

- A double-peak profile in both temperature and ozone with maxima in the upper and lower stratosphere is diagnosed in the WACCM3.5 simulations forced with all observed forcings. This agrees qualitatively well with reanalysis and satellite data.

- In the tropical lower stratosphere, a substantial portion of the apparent solar-induced increase in temperature and ozone is related to volcanic aerosol. This is due to alignment of two major volcanic eruptions (El Chichón and Mt. Pinatubo) with peaks of solar activity during cycles 21 and 22.

- Using 45 yr of data, a robust 11 yr solar signal can only be extracted above 10 hPa. At lower levels, longer records would be required. This occurs because the solar and volcanic signals cannot be adequately separated.

- The aliasing issue is ameliorated if windows around El Chichón and Mt. Pinatubo are excluded from the analysis (June 1982 to November 1983, and September 1991 to November 1993). This removal reduces the apparent solar signal in temperature in both modeled and observational data. In ozone, further complication is caused by interference with the QBO.

It is plausible that the observed amplitude of the solar-induced increase in the TLS in temperature and ozone (as reported in other studies, 0.8 K in reanalysis (Frame and Gray, 2010) and 4 % in satellite data (Soukharev and Hood, 2006)) is overestimated due to issues associated with the MLR analysis of a too short record that have been explored in this work.

The present results suggest that MLR techniques require the use of longer observational records for unambiguous separation of decadal changes driven by the solar cycle. When regressing reanalysis and satellite data that are available to date (e.g., MERRA reanalysis data spanning over 26 yr), both windows around El Chichón and Mt. Pinatubo should be removed for more accurate determination of the solar signal.

Appendix A:

The standard version of multiple linear regression models takes the following form:

$$Y_t = \sum_{i=1}^{n} \mathbf{X}_{i,t}\beta_i + \epsilon_t, \quad \text{(A1)}$$

where Y is the predictand (i.e., the dependent variable), t is the time dimension, $\mathbf{X}$ is a matrix with the basis functions containing n predictors, β represents the regression coefficients, and ϵ is the residual error term.

Multiple linear regression models after Eq. (A1) are commonly used in solar cycle studies. The $\mathbf{X}$ matrix typically contains a set of predictors representing possible sources of variability: a linear trend term for long-term changes due to increases in GHGs and ozone-depleting substances, and a set of proxy indices for ENSO, the 11 yr solar cycle, the QBO, and volcanic eruptions.

Valuable information about the impact of each forcing can be extracted with this method, provided that the correct portion of variance in the predictand time series is fit, along with its relative attribution to each of the predictors. However, this is not the case when the predictors in matrix $\mathbf{X}$ are cross correlated ("multi-collinearity"), and when there is autocorrelation in the predictand time series ("persistence") (Wilks, 2011). Spurious correlations with the predictors can arise due to persistence in the predictand time series, while multicollinearity leads to erroneous partitioning of the variance among predictors. Collinearity between the predictors can be significant, especially in relatively short records; an example is the correlation found between the N3.4 index and the 11 yr solar cycle (Marsh and Garcia, 2007). Additionally, significant persistence can be found within seasonal timescales in atmospheric field variables, which implies that individual data points in the predictand are not independent.

A common way to circumvent the problem associated with persistence is to treat the residual error term in the regression model as an autoregressive process (Tiao et al., 1990). This method implies correction of both the basis functions in $\mathbf{X}$ and the predictand Y with the autocorrelation coefficient of the residual error term ϵ estimated from a first application of the regression model. This intermediate step is called "prewhitening", and its application can be found in numerous papers on the solar signal in the stratosphere (e.g., Soukharev and Hood, 2006; Austin et al., 2008; Frame and Gray, 2010). Another way to account for autocorrelation is by prewhitening the predictand Y and predictors $\mathbf{X}$ with the first-order autocorrelation coefficient of the original time series of the predictand Y. This is the so-called Box–Jenkins (BJ) methodology (Box and Jenkins, 1980).

Both prewhitening techniques were carried out on the output from the WACCM model. It was found that the BJ prewhitening leads to an autocorrelation function (ACF) that is closer to white noise (not shown) and hence optimal for regression analysis (Box and Jenkins, 1980). Hence, the BJ technique was chosen for the analysis of the simulations presented in this paper.

Once the time series have been prewhitened, the regression model equation is carefully assessed upon analysis of the lagged cross-correlation structures between the predictors (i.e., the i time series in the $\mathbf{X}$ matrix) and the predictand Y. This is done to identify the lags that maximize the projection of variance onto the basis functions, improving the fit accuracy.

We performed a preliminary analysis by using both (i) deseasonalized monthly mean, (ii) seasonal mean (3-month averages), and (iii) 3-month running mean anomalies of temperature and ozone. It is found that the use of (ii) seasonal averages filters spurious cross-correlation structures showing up at high frequencies (1–2 months) that are related to internal noise rather than a causal relationship. Therefore, seasonal mean anomalies are used in this analysis. The use of seasonal averages is also justified physically. Part of the changes in stratospheric temperature and ozone due to ENSO, QBO, and solar cycle are mediated by changes in upwelling rates, especially in the TLS. Randel et al. (2002) showed that coherence between temperature and upwelling rates in the TLS is enhanced at seasonal timescales compared to higher frequencies, so that dynamically forced changes in temperature can be better captured with seasonal averages.

In the reference all forcings ensemble, the matrix $\mathbf{X}$ reads as follows:

$$\mathbf{X} = \begin{pmatrix} t \\ N3.4 \\ \mathrm{UV} \\ u30 \\ u10 \\ \mathrm{SAD} \end{pmatrix}, \quad \text{(A2)}$$

where t is the time dimension in seasons; $N3.4$ is the Niño 3.4 index (the standardized mean sea surface temperature between 5° S and 5° N latitude and between 120 and 170° W longitude) for ENSO; UV is the ultraviolet solar radiation flux integrated in the Hartley band (240–270 nm) from the Lean dataset (Lean et al., 2005), and is used as a proxy for the 11 yr solar cycle; and $u30$ and $u10$ are the equatorial zonal mean zonal winds at 30 and 10 hPa, which have the quality of being nearly orthogonal proxies for the QBO (Randel and Wu, 1996). SAD is the global mean surface area density at 50 hPa (in units of $\mu m^2\ cm^{-3}$) of sulfate aerosol taken from a combination of different datasets: SAGE I (1979–1981), SAGE II (1984–2005), and SME instruments. Aerosol data before 1979 are constructed based on assumptions of background aerosol (see Sect. 2.5.3.4 of CCMVal-2, 2010). Based on SAD, an aerosol mass distribution is assumed in WACCM3.5 for heating rate calculations (Tilmes et al., 2009). Hence, this dataset is the most appropriate proxy for the volcanic forcing in the model simulations.

When using data from the idealized ensembles, the forcings that are kept constant (following table 1) are removed from the **X** matrix. The N3.4 index is excluded in the fixedSSTs ensemble, $u10$ and $u30$ are excluded in the noQBO ensemble, while the SAD index is excluded in the noVOLC ensemble.

The first step in the formulation of the regression model is prewhitening of both sides of Eq. (A1):

$$Y'_{t,z} = Y_{t,z} - \rho_z Y_{t-1,z}$$
$$\mathbf{X}'_{t,i,z} = \mathbf{X}_{t,i,z} - \rho_z \mathbf{X}_{t-1,i,z}, \quad \text{(A3)}$$

where ρ_z is the autocorrelation coefficient of Y at lag of one season and at the level z, and i is the forcing index. Equation (A3) is applied at each discrete model level z ranging from 0.1 to 100 hPa. It is found that the use of the autocorrelation at lag 1 is enough to reduce the ACF of Y' to white noise, so that there is no need to use autoregressive models of higher order.

After prewhitening both forcings and seasonal mean anomalies of temperature and ozone, we calculate the lag τ at which the absolute value of the cross correlation between each predictor i and Y' reaches a maximum value at a given level z.

$$\tau_{i,z} = t||r(Y'_{t=0\ldots n,z}, \mathbf{X}'_{i,t=0+\tau\ldots n,z}) = \mathrm{MAX} \quad \text{(A4)}$$

A separate analysis showed that no significant cross correlation between predictors is introduced by using the 1 yr window. Furthermore, correlations arising at lags larger than the characteristic timescale of each forcing are unlikely to describe a physical link with the dependent variable. This is especially true in the stratosphere, where the responses are not modulated by the ocean.

In the case of the QBO, the indices $u30'$ and $u10'$ are approximately sinusoidal and nearly orthogonal to each other. As such, the use of different lags would introduce correlations between them, and therefore loss of orthogonality. The most accurate fit is obtained by computing the regression coefficient, and hence without using any lag in any of the QBO indices. This motivates a different treatment of the QBO in Eq. (A4) compared to the other terms, i.e. by using $\tau_{\mathrm{qbo}} = 0$.

An additional complication is posed by the separation of QBO signals from the other sources of variability. We found that the observed zonal wind that is assimilated in the ensembles including a QBO contains significant variations arising from volcanoes, ENSO, and solar cycle. For the solar cycle, this result is consistent with the reported modulation of the QBO periodicity by the solar cycle (Salby and Callaghan, 2000). We remove the collinearity by computing two filtered QBO indices. For this purpose, we regress the UV, ENSO, and SAD indices using their optimal lag τ on zonal mean wind at both 30 and 10 hPa, and take the residual as filtered QBO index, as described by Eq. (A5):

$$u30^*_{t,z} = u30'_{t,z} - (\beta_{\mathrm{uv}}\mathrm{UV}'_{t-\tau_{i=\mathrm{uv},z},z} + \beta_{\mathrm{enso}}N3.4'_{t-\tau_{i=\mathrm{enso},z},z} + \beta_{\mathrm{volc}}\mathrm{SAD}'_{t-\tau_{i=\mathrm{volc},z},z}) \quad \text{(A5)}$$
$$u10^*_{t,z} = u10'_{t,z} - (\beta_{\mathrm{uv}}\mathrm{UV}'_{t-\tau_{i=\mathrm{uv},z},z} + \beta_{\mathrm{enso}}N3.4'_{t-\tau_{i=\mathrm{enso},z},z} + \beta_{\mathrm{volc}}\mathrm{SAD}'_{t-\tau_{i=\mathrm{volc},z},z}).$$

In this way, $u30^*$ and $u10^*$ are made orthogonal with respect to the other indices while preserving their mutual orthogonality by excluding any QBO lag. This improves the accuracy of the regression analysis. The two filtered QBO indices, along with the prewhitened and lagged predictors, are then used in the target regression model for ozone and temperature.

$$Y'_{t,z} = \beta'_{\mathrm{uv}}UV'_{t-\tau_{i=\mathrm{uv},z},z} + \beta'_{\mathrm{enso}}N3.4'_{t-\tau_{i=\mathrm{enso},z},z} + \beta'_{\mathrm{qbo1}}u30^*_{t,z} + \beta'_{\mathrm{qbo2}}u10^*_{t,z} + \beta'_{\mathrm{volc}}\mathrm{SAD}'_{t-\tau_{i=\mathrm{volc},z},z} + e'_{t,z} \quad \text{(A6)}$$

For the regression of ozone, the regression coefficients β' are given in relative percentage units. First, we regress absolute values of tropical mean mixing ratio, and then the percentages are taken on the long-term climatology.

The regression model described by Eq. (A6) is used in the analysis of the reference all forcings set. In the idealized sets, the forcings that are kept fixed are excluded from Eq. (A6).

Acknowledgements. The authors thank J. Añel, K. Matthes, and J. Richter for performing two of the simulations. The authors are grateful for the support with high-performance computing from Yellowstone (ark:/85065/d7wd3xhc), provided by NCAR's Computational and Information System Laboratory, sponsored by the National Science Foundation. Computing resources were also provided by the Barcelona Supercomputing Center (BSC), Centro Extremeño de iNvestigación, Innovación Tecnológica y Supercomputacion (CENITS), and Centro de Supercomputación de Galicia (CESGA). The authors thankfully acknowledge the technical expertise and assistance provided by BSC, CENITS, and CESGA for carrying out the model simulations in the MareNostrum, Lusitania, and Finisterrae supercomputers. The authors also acknowledge the European COST Action ES1005. G. Chiodo was supported by the Spanish Ministry of Education in the framework of the FPU doctoral fellowship (grant AP2009-0064).This work was also supported by the Spanish Ministry of Science and Innovation (MCINN) through the CONSOLIDER (CSD2007-00050-II-PR4/07) and MATRES (CGL2012-34221) projects. The National Center for Atmospheric Research is operated by the University Corporation for Atmospheric Research with sponsorship of the National Science Foundation.

Edited by: P. Jöckel

References

Arfeuille, F., Luo, B. P., Heckendorn, P., Weisenstein, D., Sheng, J. X., Rozanov, E., Schraner, M., Brönnimann, S., Thomason, L. W., and Peter, T.: Modeling the stratospheric warming following the Mt. Pinatubo eruption: uncertainties in aerosol extinctions, Atmos. Chem. Phys., 13, 11221–11234, doi:10.5194/acp-13-11221-2013, 2013.

Austin, J., Tourpali, K., Rozanov, E., Akiyoshi, H., Bekki, S., Bodeker, G., Brühl, C. Butchart, N., Chipperfield, M., Deushi, M., Fomichev, V. I., Giorgetta, M. A., Gray, L., Kodera, K., Lott, F., Manzini, E., Marsh, D., Matthes, K., Nagashima, T., Shibata, K., Stolarski, R. S., Struthers, H., and Tian, W.: Coupled chemistry climate model simulations of the solar cycle in ozone and temperature, J. Geophys. Res., 113, 1–20, doi:10.1029/2007JD009391, 2008.

Baldwin, M., Gray, L. J., Dunkerton, T. J., Hamilton, K., Haynes, P. H., Randel, W. J., Holton, J. R., Alexander, M. J., Hirota, I., Horinouchi, T., Jones, D. B. A., Kinnersley, J. S., Marquardt, C., Sato, K., and Takahashi, M.: The quasi-biennial oscillation, Rev. Geophys., 39, 179–230, 2001.

Bisgaard, S. and M. Kulahci: Time Series Analysis and Forecasting by Example, vol. 815, Wiley, Singapore, 2011.

Box, G., and Jenkins, G.: Time Series Analysis. Forecasting and Control, Holder Day, San Francisco, 1980.

Calvo, N., Garcia, R., Randel, W., and Marsh, D. R.: Dynamical mechanism for the increase in tropical upwelling in the lowermost tropical stratosphere during warm enso events, J. Atmos. Sci., 67, 2331–2340, 2010.

CCMVal-2: SPARC CCMVal Report on the Evaluation of Chemistry-Climate Models, edited by: Eyring, V., Shepherd, T. G., and Waugh, D. W., Tech. rep., SPARC Report No. 5, WCRP-132, WMO/TD-1526, World Meteorological Organization, Geneva, 2010.

Chiodo, G., Calvo, N., Marsh, D. R., and Garcia-Herrera, R.: The 11 year solar cycle in transient WACCM3.5 simulations, J. Geophys. Res., 117, D06109, doi:10.1029/2011JD016393, 2012.

Crooks, S. and Gray, L.: Characterization of the 11-year solar signal using a multiple regression analysis of the ERA-40 dataset, J. Climate, 18, 996–1015, doi:10.1175/JCLI-3308.1, 2005.

Diaz, J., Garcia, R., De Castro, F. V., Hernández, E., López, C., and Otero, A.: Effects of extremely hot days on people older than 65 years in seville (Spain) from 1986 to 1997, Int. J. Biometeorol., 46, 145–149, 2002.

Diaz, J., Jordán, A., García, R., López, C., Alberdi, J., Hernández, E., and Otero, A.: Heat waves in madrid 1986–1997: effects on the health of the elderly, Int. Arch. Occ. Env. Hea., 75, 163–170, 2002.

Eyring, V., Cionni, I., Bodeker, G. E., Charlton-Perez, A. J., Kinnison, D. E., Scinocca, J. F., Waugh, D. W., Akiyoshi, H., Bekki, S., Chipperfield, M. P., Dameris, M., Dhomse, S., Frith, S. M., Garny, H., Gettelman, A., Kubin, A., Langematz, U., Mancini, E., Marchand, M., Nakamura, T., Oman, L. D., Pawson, S., Pitari, G., Plummer, D. A., Rozanov, E., Shepherd, T. G., Shibata, K., Tian, W., Braesicke, P., Hardiman, S. C., Lamarque, J. F., Morgenstern, O., Pyle, J. A., Smale, D., and Yamashita, Y.: Multimodel assessment of stratospheric ozone return dates and ozone recovery in CCMVal-2 models, Atmos. Chem. Phys., 10, 9451–9472, doi:10.5194/acp-10-9451-2010, 2010.

Calvo-Fernández, N. C., Garcia-Herrera, R., Puyol, D. G., Hernandez, E., GarcÍa, R., Gimeno, L., and Ribera, P.: Analysis of the enso signal in tropospheric and stratospheric temperatures observed by msu, 1979–2000, J. Climate, 17, 3934–3946, 2004.

Frame, T. and Gray, L.-J.: The 11-year solar cycle in era-40 data: an update to 2008, J. Climate, 23, 2213–2222, 2010.

Garcia, R., Marsh, D. R., Kinnison, D., Boville, B., and Sassi, F.: Simulation of secular trends in the middle atmosphere, 1950–2003, J. Geophys. Res., 112, D09301, doi:10.1029/2006JD007485, 2007.

Gray, L., Beer, J., Geller, M., Haigh, J. D., Lockwood, M., Matthes, K., Cubasch, U., Fleitmann, D., Harrison, G., Hood, L., Luterbacher, J., Meehl, G. A., Shindell, D., Van Geel, B., and White, W.: Solar influences on climate, Rev. Geophys., 48, RG4001, doi:10.1029/2009RG000282, 2010.

Haigh, J. and Blackburn, M.: Solar influences on dynamical coupling between the stratosphere and troposphere, Space Sci. Rev., 125, 331–344, 2006.

Hood, L.: The solar cycle variation of total ozone: Dynamical forcing in the lower stratosphere, J. Geophys. Res., 102, 1355–1370, 1997.

Hood, L. and Soukharev, B.: Quasi-decadal variability of the tropical lower stratosphere: The role of extratropical wave forcing, J. Atmos. Sci., 60, 2389–2403, 2003.

Hood, L., Soukharev, B., and McCormack, J.: Decadal variability of the tropical stratosphere: Secondary influence of the el niño–southern oscillation, J. Geophys. Res., 115, D11113, doi:10.1029/2009JD012291, 2010.

Hurrell, J. W., Hack, J. J., Shea, D., Caron, J. M., and Rosinski, J.: A new sea surface temperature and sea ice boundary dataset for the community atmosphere model, J. Climate, 21, 5145–5153, 2008.

Kodera, K. and Kuroda, Y.: Dynamical response to the solar cycle, J. Geophys. Res., 107, 4749, doi:10.1029/2002JD002224, 2002.

Lean, J., Rottman, G., Harder, J., and Kopp, G.: Sorce contributions to new understanding of global change and solar variability, The Solar Radiation and Climate Experiment (SORCE), Sol. Phys., 230, 27–53, 2005.

Lee, H. and Smith, A.: Simulation of the combined effects of solar cycle, quasi-biennial oscillation, and volcanic forcing on stratospheric ozone changes in recent decades, J. Geophys. Res., 108, D24049, doi:10.1029/2001JD001503, 2003.

Marsh, D. R. and Garcia, R.: Attribution of decadal variability in lower-stratospheric tropical ozone, Geophys. Res. Lett., 34, L21807, doi:10.1029/2007GL030935, 2007.

Matthes, K., Marsh, D., Garcia, R., Kinnison, D., Sassi, F., and Walters, S.: Role of the QBO in modulating the influence of the 11 year solar cycle on the atmosphere using constant forcings, J. Geophys. Res., 115, D18110, doi:10.1029/2009JD013020, 2010.

Meehl, G., Arblaster, J., Matthes, K., Sassi, F., and van Loon, H.: Amplifying the Pacific Climate System Response to a Small 11-Year Solar Cycle Forcing, Science, 325, 1114–1118, 2009.

Pap, J. and Fox, P.: Solar variability and its effects on climate, Washington DC American Geophysical Union Geophysical Monograph Series, 141, 356 pp., doi:10.1029/141GM, 2004.

Randel, W. J., Wu, F., Russell, J., Waters, J., and Froidevaux, L.: Ozone and temperature changes in the stratosphere following the eruption of mount pinatubo, J. Geophys. Res., 100, 16753–16764, 1995.

Randel, W. and Wu, F.: Isolation of the Ozone QBO in SAGE 2 Data by Singular-Value Decomposition, J. Atmos. Sci., 53, 2546–2560, 1996.

Randel, W. J., Garcia, R. R., and Wu, F.: Time-dependent upwelling in the tropical lower stratosphere estimated from the zonal-mean momentum budget, J. Atmos. Sci., 59, 2141–2152, 2002.

Randel, W. and Wu, F.: A stratospheric ozone profile data set for 1979–2005: Variability, trends, and comparisons with column ozone data, J. Geophys. Res, 112, D06313, doi:10.1029/2006JD007339, 2007.

Randel, W., Garcia, R., Calvo, N., and Marsh, D.: ENSO influence on zonal mean temperature and ozone in the tropical lower stratosphere, Geophys. Res. Lett, 36, L15822, doi:10.1029/2009GL039343, 2009.

Randel, W. J., Shine, K. P., Austin, J., Barnett, J., Claud, C., Gillett, N. P., Keckhut, P., Langematz, U., Lin, R., Long, C., Mears, C., Miller, A., Nash, J., Seidel, D. J., Thompson, D. W. J., Wu, F., and Yoden, S.: An update of observed stratospheric temperature trends, J. Geophys. Res., 114, D02107, doi:10.1029/2008JD010421, 2009.

Rienecker, M. M., Suarez, M. J., Gelaro, R., Todling, R., Bacmeister, J., Liu, E., Bosilovich, M. G., Schubert, S. D., Takacs, L., Kim, G.-K. Bloom, S., Chen, J., Collins, D., Conaty, A., Da Silva, A., Gu, W., Joiner, J., Koster, R.D., Lucchesi, R., Molod, A., Owens, T., Pawson, S., Pegion, P., Redder, C.R., Reichle, R., Robertson, F.R., Ruddick, A.G., Sienkiewicz, M., and Woolen, J.: Merra: Nasa's modern-era retrospective analysis for research and applications, J. Climate, 24, 3624–3648, 2011.

Robock, A.: Volcanic eruptions and climate, Rev. Geophys., 38, 191–219, 2000.

Salby, M. and Callaghan, P.: Connection between the solar cycle and the qbo: The missing link, J. Climate, 13, 2652–2662, 2000.

Schmidt, H., Brasseur, G., and Giorgetta, M.: Solar cycle signal in a general circulation and chemistry model with internally generated quasi biennial oscillation, J. Geophys. Res., 115, D00I14, doi:10.1029/2009JD012542, 2010.

Smith, A. and Matthes, K.: Decadal-scale periodicities in the stratosphere associated with the solar cycle and the QBO, J. Geophys. Res., 113, D05311, doi:10.1029/2007JD009051, 2008.

Soukharev, B. and Hood, L.: Solar cycle variation of stratospheric ozone: Multiple regression analysis of long-term satellite data sets and comparisons with models, J. Geophys. Res., 111, D20314, doi:10.1029/2006JD007107, 2006.

Thomason, L., Poole, L., and Deshler, T.: A global climatology of stratospheric aerosol surface area density deduced from stratospheric aerosol and gas experiment ii measurements: 1984–1994, J. Geophys. Res.,102, 8967–8976, 1997.

Tiao, G., Reinsel, G., Xu, D., Pedrick, J., Zhu, X., Miller, A., DeLuisi, J., Mateer, C., and Wuebbles, D.: Effects of autocorrelation and temporal sampling schemes on estimates of trend and spatial correlation, J. Geophys. Res., 95, 20507–20517, 1990.

Tilmes, S., Garcia, R., Kinnison, D., Gettelman, A., and Rasch, P.: Impact of geoengineered aerosols on the troposphere and stratosphere, J. Geophys. Res., 114, D12305, doi:10.1029/2008JD011420, 2009.

Wilks, D. S.: Statistical methods in the atmospheric sciences, vol. 100, Academic press, Oxford, 2011.

5 The impact of a future solar minimum under a climate change scenario

The impact of a future solar minimum under a climate change scenario

September 14, 2014

G. Chiodo (1), R. García-Herrera (1,2), N. Calvo (1), J.M. Vaquero (3), and J.A. Añel (4,5)

E-mail: gchiodo@ucm.es

1) Dpto. Astrofísica y CC de la Atmosfera, Fac. de Ciencias Físicas,
Universidad Complutense, Spain
2) Instituto de Geociencias (IGEO), Madrid, Spain
3) Universidad de Extremadura, Mérida, Spain
4) Smith School of Enterprise and the Environment, University of Oxford, Oxford, UK
5) EPhysLab, Universidade de Vigo, Ourense, Spain

submitted to Nature Climate Change

Abstract

Increasing evidences suggest that solar activity levels may decrease in the near future [*Abreu et al.*, 2008; *Lockwood et al.*, 2011], similar to what occurred during the grand "Maunder Minimum" in the 17^{th} century [*Eddy*, 1976]. This prompts modeling studies on the effects of a future solar minimum under climate change projections. Climate simulations have shown that a reduction in solar irradiance of 4-6 W/m^2 would diminish the projected global warming by a small, but significant, fraction [*Jones et al.*, 2012; *Meehl et al.*, 2013; *Anet et al.*, 2013]. However, a solar dimming of this magnitude is excessive according to recent evidences [*Stocker et al.*, 2013; *Feulner*, 2011], and thus, unlikely to occur. Our study examines the impact of a more plausible future minimum in coupled ocean-atmosphere-chemistry climate change simulations, driven with a mid-range emissions scenario for greenhouse-gases. While the solar minimum would have a negligible effect on global warming, it exerts a significant influence on boreal winter climate change, reducing the Arctic Amplification by 30%. For the first time, we show how dynamical (top-down) and radiative (bottom-up) mechanisms triggered respectively by ultraviolet and visible radiation contribute to the regional response to a solar minimum in a climate change scenario. According to our findings, the role of solar forcing uncertainty should be reconsidered in climate change assessments.

1 Introductory paragraph

The Sun is the fundamental source of energy for the climate system. The lack of understanding of the Sun's interior limits the range of predictability of future solar activity. Thus, solar variability represents a source of uncertainty in future forcings used in climate simulations, with a descent of solar activity into a grand minimum as one possible scenario. Hence, modeling studies are needed to quantify the effects of this hypothetical evolution on climate change projections. With aid of experiments from a state-of-the-art Earth system model, we show that a period of reduced solar activity would not alter the projected change associated with a mid-range emission scenario. However, large regional responses emerge in the winter Northern Hemisphere, involving a modulation of internal modes of variability, and a reduction of the Arctic Amplification by 30%. To understand these responses, we assess the role of amplifying mechanisms, triggered by irradiance changes at different wavelengths of the solar spectrum, and find a distinct but complementary role of ultraviolet and visible radiation. According to our findings, the role of solar forcing uncertainty should be reconsidered in climate change assessments.

2 Introduction

Space-born measurements of solar irradiance indicate a 11 years cyclicity in solar activity. Proxy evidences also suggest variations on longer time scales, such as the minimum sunspot activity in the 17^{th} century, referred as the Maunder Minimum, an epoch during which solar activity was likely to be lower than present [*Eddy*, 1976; *Vaquero et al.*, 2011]. A number of studies have recently raised the possibility of a descent of solar activity into a new grand minimum, similar to the grand Maunder Minimum [*Abreu et al.*, 2008; *Lockwood et al.*, 2011; *Roth and Joos*, 2013]. The weakness of the current solar cycle number 24, and the unusually deep minimum in 2008-2009 [*Janardhan et al.*, 2011; *Nandy et al.*, 2011; *Lockwood*, 2011] support this view. However, model projections of the 21^{st} century participating in the Fifth Coupled Model Intercomparison Project (CMIP5) did not include any type of solar variability, other

than repeating the previous solar cycle number 23 or the last four observed solar cycles [*Myhre et al.*, 2013]. Thus, the solar forcing employed in CMIP5 models may not be representative of future conditions. In this context, it is necessary to assess the potential impact of a hypothetical and realistic solar minimum on Earth's climate.

With this rationale, a number of studies have been performed with models ranging from intermediate complexity [*Feulner and Rahmstorf*, 2010], box-diffusion [*Jones et al.*, 2012], to fully coupled ocean-atmosphere models with interactive chemistry [*Meehl et al.*, 2013; *Anet et al.*, 2013]. Despite the differences in the modeling framework, the simulations perturbed by a grand minimum consistently show a 0.2-0.3 K reduction of the 2 K global mean temperature rise projected by their control RCP simulations by 2100, in which current observed levels in solar activity are assumed. These studies were instructive in showing that an idealized grand minimum state would partly reduce global warming by 10%. However, they imposed extreme reductions in solar irradiance (as e.g., 0.4% in *Anet et al.* [2013]), which are overestimated by a factor of 4 or more according to paleo reconstructions [*Feulner*, 2011; *Stocker et al.*, 2013].

Our study explores the climatic impact of a future solar minimum calculated as a mean over the minima recorded in the last four solar cycles, including the deep minimum in 2008-2009. This type of forcing represents the Maunder Minimum conditions more closely [*Schrijver et al.*, 2011; *McCracken and Beer*, 2014], providing a more plausible scenario than those used in previous modeling studies. We use the Community Earth System Model (CESM), including the Whole Atmosphere Community Climate Model atmospheric component (CESM-WACCM), which incorporates a good resolution of the stratosphere and interactive ozone chemistry [*Marsh et al.*, 2013]. The model is able to capture the "top-down" propagation of the solar signal from the stratosphere [*Chiodo et al.*, 2012] and the "bottom-up" propagation from the ocean [*Meehl et al.*, 2009]. One ensemble of three climate change simulations is driven with a solar minimum (MIN), which is constant throughout a 58 years long period (2008-2065). A second three-member ensemble is driven with the last four observed 11-yr solar cycles (RCP45) (see Fig. S1). The spectral irradiance is taken from *Wang et al.* [2005]. The MIN forcing implies a wavelength dependent decrease in solar irradiance relative to the RCP45 case of 0.36 W/m^2 (or 0.03%).

Two additional experiments are performed to clarify the mechanisms that contribute to the surface response. In these experiments, the MIN forcing is imposed separately in the ultraviolet (120-350 nm) and visible (350-700 nm) range, and are referred as MINuv, and MINvis, respectively, and implies a decrease in solar irradiance relative to the RCP45 case of 0.09 W/m^2 and 0.27 W/m^2. The MINuv forcing has a direct impact in the stratosphere due to ozone absorption of the UV radiation [*Gray et al.*, 2010]. Thus, its tropospheric and surface impacts are linked to a transmission of the solar signal from the stratosphere to the troposphere (e.g., *Kodera and Kuroda* [2002]) (known as top-down mechanism). The MINvis forcing directly affects the surface radiative balance, and is thus associated with the direct impact of the solar signal at the surface, which has been referred as bottom-up mechanism [*Meehl et al.*, 2009; *Gray et al.*, 2010].

3 Results

The simulated evolution of the globally averaged surface air temperature (SAT) is shown in Fig. 1a. A linear increase of approximately 0.2 K per decade is found over the simulated period of MIN and RCP45 simulations. The linearity of the temperature trend is associated with the steady increase in GHGs concentrations over the 2000-2065 period in the RCP4.5 scenario. Contrary to previous studies, the impact of the MIN forcing at global scales is negligible. However, there are significant differences between the MIN and RCP45 ensembles in the Northern Hemisphere (NH) high latitudes (60°N-90°N) during the boreal winter season (DJF mean, Fig. 1b). In this region, the warming trend is much larger than in the global mean, a behavior that has been reported in most of the IPCC-AR5 models as the "Arctic Amplification" [*Kirtman et al.*, 2013] (see Fig. S2a). Interestingly, the MIN forcing reduces the Arctic Amplification effect by roughly 30%.

Consequently, we explore the spatial distribution of the SAT response to MIN, computed as the difference between the 2005-2065 climatologies of the MIN and RCP45 ensemble means (Fig. 2a). A widespread cooling region is found over the Arctic, with peaks of 1.2 K in the Bering Sea. This response englobes the eastern part of the Pacific basin, and extends to the

western Tropical Pacific, resembling a horse-shoe pattern. The similarities with the Pacific Decadal Oscillation (PDO) [*Mantua et al.*, 1997] indicate that the response to the MIN forcing projects onto a negative PDO-like pattern. There is also significant cooling over Siberia up to 0.8 K, and warming of similar amplitude over eastern North America, which extends to the North Atlantic. Overall, the cooling signals are similar in magnitude to those reported by *Anet et al.* [2013] during winter (see their Fig. S3), despite the larger irradiance reduction employed in their study. It is also interesting to note that a similar regional distribution of the cooling was also observed by *Meehl et al.* [2013] at the late stages of their simulations (see their Fig. 3). This suggests that this pattern does not respond linearly to solar forcing. The cooling in the Bering Sea and the PDO-like structure are reproduced in the MINvis case (Fig. 2b), which indicates that the Pacific response is driven by direct changes in the radiative balance at the surface through the dimming in visible wavelengths. Interestingly, the negative PDO-like temperature response to the solar minimum resembles that associated with the global warming hiatus over the last decade [*Kosaka and Xie*, 2013], which coincided with the descending phase of solar cycle 23, and the deep solar minimum in 2008-2009. On the other hand, the signal over Siberia is well captured in the MINuv experiment (Fig. 2c), which points at the role of the UV forcing in this response, and suggests a contribution of the top-down mechanism (see e.g., *Matthes et al.* [2006]; *Gray et al.* [2010]). We note that the cooling up to 1-1.5 K in the NH account for as much as 30-40% of the GHG-induced warming of 3 K simulated over the 2005-2065 in the NH high latitudes (Fig. S2b). Thus, it is clear that the MIN forcing significantly modulates the regional patterns of climate change. The impact on the Arctic Amplification is mostly due to a reduction of the warming in Siberia, Alaska and the Bering Sea, while in the eastern North America and Europe the climate change effect gets amplified.

A boreal winter response to solar MIN is also seen in sea level pressure (SLP), as shown in Fig. 3a. A dipole is evident in the Pacific basin, suggesting a SLP increase in the West Pacific, and a decrease over Alaska, which is consistent with an eastward shift of the Aleutian Low pressure system observed during minima of the 11-yr solar cycle [*Christoforou and Hameed*, 1997]. The SLP increase reaches 1.4-1.6 hPa over the regions where cooling is observed in Fig. 3a, in-

dicating a link between the temperature and circulation responses. It is also reproduced in the Pacific in the MINvis experiment, although with much larger amplitude than in MIN (Fig. 3b). This SLP pattern over the Pacific in MIN and MINvis indicates a shift of the westerlies towards the North East, which inhibits the advection of mild air off the coast of western North America. In addition, stronger westerlies over the northeastern part of the North Pacific result in more southeastward transport of cooler surface water and a negative SST anomaly (see e.g., *Hartmann* [1994]), which shapes the horse-shoe cooling pattern. Taken together, the cooling over Alaska, the Pacific SLP increase and the PDO pattern in the MIN ensemble are all related to a reduction in VIS directly affecting the surface energy balance, and consequently, surface temperatures.

We note that the simulated basin-wide SLP increase in the Pacific (Fig. 3b) is not in line with the observed SLP increase during peaks of solar activity [*Roy and Haigh*, 2010]. This apparent inconsistency is possibly due to the difference in the time scales of the forcing and the associated response. In this work, a perpetual minimum in spectral irradiance is imposed over a period of 58 years, thereby involving feedback processes (as e.g., the changes in sea-ice) that are not effective over the 11-yr solar cycle due to the transient nature of the solar forcing. Imposing a solar forcing over a multi decadal period leads to responses that project onto decadal scale modes, such as the PDO. Therefore, long-lasting responses are different than those found over the 11-year solar cycle.

The surface response to the MINvis forcing is relatively large considering the small decrease in solar irradiance (0.27 W/m^2). Thus, the signal needs to be amplified by processes occurring at the surface. Fig. 4a shows the simulated boreal winter mean sea-ice concentration (SIC) response to MIN in the Pacific basin. Relative to the RCP45 ensemble, the MIN experiments show a SIC increase of 8% in the coastal regions of Alaska and Russia, which is where the sea-ice edge is placed during the first simulated decade (2005-2015). The SIC increase relative to the RCP45 enhances the cooling localized in these regions (Fig. 2a) through an increase in surface albedo, and a reduction in heat flux exchange between ocean and the overlying atmosphere. This is reproduced in the MINvis experiment (Fig. 4b), while the UV effects are much smaller

and not significant (Fig. 4c). This confirms the existence of a causal link between the reduction in VIS and the sea-ice increase. Consequently, the surface temperature signal in the Pacific basin for the MIN experiments (Fig. 2a) is mostly due to surface processes involving the sea-ice positive feedback. Contributions from this feedback amplify regional scale solar effects in regions where the sea-ice edges progressively shrink due to global warming, such as the Bering Strait. A similar effect was also argued to enhance regional scale effects of a solar minimum under a global warming scenario, compared to preindustrial conditions [*Song et al.*, 2010]. However, they applied a much stronger and spectrally uniform irradiance decrease in their simulations of 2.7 W/m^2, which is one order of magnitude stronger than the irradiance reduction employed here.

While surface feedbacks drive the MIN response in the Pacific basin, the origin of the zonally asymmetric temperature pattern that comprises cooling over Siberia, and warming over eastern North America (Fig. 2) is different. This pattern appears intensified in the first half of the simulation (2005-2035), when the MIN and MINuv responses are characterized by an anomalous SLP increase over the Arctic (Fig. S3), coherent with the above temperature response. This SLP response is reminescent of a negative Arctic Oscillation (AO), which is a leading mode of variability of the SLP in winter in the NH [*Thompson and Wallace*, 1998]. Anomalous high pressure over the Arctic fosters the development of cold anomalies in Siberia (Fig. 2). This is only reproduced in the MINuv experiment (Fig. S3c), which indicates that UV changes and their impact on the stratosphere are the main driver of this surface signal.

Changes in the AO pattern are one of the clearest manifestations of stratosphere-troposphere coupling, and in particular of the proposed top-down solar mechanism through changes in zonal mean zonal wind (e.g., *Thompson and Wallace* [1998]). To better clarify the stratospheric origin of the AO signal, the zonal mean zonal wind response to the MIN forcings over the 2005-2035 period is analyzed (Fig. 5a). Easterly and significant anomalies are simulated in the NH high latitudes, reaching 2.5 m/s at 30-40 km, and extending to the lower troposphere and surface at 60°N. These signals correspond with a weakening of the stratospheric polar vortex, in connection with the weakening of the jet stream in the troposphere and the zonal mean flow at the

surface. A significant signal in zonal mean zonal wind is also reproduced in the MINuv experiment, but not in the MINvis case (Fig. 5b-c). The weakening in stratospheric westerly winds is caused by a decrease in UV absorption by ozone at low latitudes, whereby the meridional temperature gradient slightly decreases. During the course of the boreal winter, easterly wind anomalies are sustained by dynamical processes involving more wave deposition in the polar stratosphere, which in turn favor a 35% increase in the frequency of major Sudden Stratospheric Warmings in the MIN ensemble relative to the RCP45. This is consistent with the "top-down" mechanism related to UV variability, which was first postulated by *Kodera and Kuroda* [2002], and simulated in WACCM [*Chiodo et al.*, 2012] and other models [*Matthes et al.*, 2004, 2006; *Ineson et al.*, 2011].

Interestingly, the zonal mean zonal wind response in Fig. 5 does not appear throughout the entire length of the MIN simulation (2005-2065), consistent with a less evident negative AO signal over the second half of the simulation. This is due to a weakening trend in the westerly winds simulated in RCP45 in the polar stratosphere (Fig. S4a), in response to climate change and consistent with other modeling studies [*Hinssen et al.*, 2011; *Manzini et al.*, 2014]. This weakening trend leads towards a weaker polar vortex in the latest part of the RCP45 simulation, with similar values to the weakening response to MIN. Despite being driven with the same GHGs concentrations, the MIN ensemble does not show such response (Fig. S4b). This might be due to a non-linear response and saturation machanism of the polar vortex to the presence of two forcings, solar MIN and increasing GHGs, acting both to weaken the polar vortex. These non-linear interactions have been documented among other combination of forcings such as ENSO and QBO [*Calvo et al.*, 2009], or QBO and solar forcing [*Camp and Tung*, 2007]. Our results show a causal relationship between the UV forcing and the polar vortex response in the stratosphere, leading to the surface AO and temperature signals seen in the MIN ensemble in Siberia and North America. Therefore, both bottom-up and top-down mechanisms, through changes in VIS and UV radiation, separately drive surface signals.

4 Concluding remarks

The inability to predict the long-term evolution of solar activity is a source of uncertainty in future climate projections. The solar minimum employed in this study follows a scenario of solar activity close to present levels, albeit with inhibited 11-yr sunspot cycle activity, following what recent evidences have proposed for the future [*Schrijver et al.*, 2011; *McCracken and Beer*, 2014; *Zolotova and Ponyavin*, 2014]. In this sense, our scenario is realistic than others because spectral irradiance changes are obtained during the recent solar cycle minima, rather than relying on historical reconstructions of the Maunder Minimum. While this plausible minimum would have a negligible effect on the global warming tendency under a mid-range emission scenario, it would have a significant impact on northern hemispheric winter climate. Relative to changes projected by the RCP45 scenario, the solar minimum produces a significant cooling in parts of Russia, Alaska, and over the Pacific, while warming is simulated over eastern North America. The 'so-called' Arctic Amplification effect would be reduced in winter by 30%, implying that a solar minimum would substantially delay the warming signal in wide parts of the NH continental regions, accelerating it in more confined regions such as eastern North America. In addition, the surface response in the Pacific strongly projects onto a negative PDO, suggesting that the long-lasting solar forcing modulates coupled modes of internal variability at decadal time scales.

A substantial part of the cooling in sub-Arctic regions and the PDO signal is primarily linked to the solar minimum at visible wavelengths, which trigger "bottom-up" mechanisms involving sea-ice feedbacks. On the other hand, the surface cooling signal over Eurasia is caused by dynamical changes in the polar stratospheric vortex, which are fostered by reduced stratospheric absorption of ultraviolet radiation. Changes in the stratospheric zonal flow project onto a negative Arctic Oscillation pattern at the surface. This effect is not seen over the entire simulated period, probably due to non-linear interactions between the solar and climate change forcings.

Thus, a future solar minimum would greatly modify regional scale climate change projections in the Northern Hemisphere. Even though the modeled changes in surface climate are limited geographically, they have far-reaching implications for the assessment of global warming

impacts in other components of the climate system, such as high-latitudes ecosystems [*Macias-Fauria et al.*, 2012], and permafrost [*Lawrence and Slater*, 2005]. Since the present results have been obtained from a solar minimum within the observed levels of solar irradiance, these results would also apply to a scenario in which the upcoming 11-yr solar cycle exhibit a smaller amplitude compared to the last four in the irradiance records (20-23).

The role of future solar activity as a potential source of uncertainty is underrepresented in the design of model projections participating in IPCC assessment reports [*Myhre et al.*, 2013]. We conclude that it needs to be taken into account in the future, by e.g. designing possible solar forcing scenarios, such as the experiments performed in this study. Given that both changes in the visible and ultraviolet wavelengths are equally instrumental in creating surface temperature anomalies, the present results also stress the importance for modeling groups to use spectrally resolved solar scenarios.

Acknowledgments

The authors would like to thank D. Barriopedro for helpful discussions and comments. This research has been supported by the Supercomputing Centre of Galicia (CESGA) through three ICTS projects. In addition, computing resources were also provided by the Barcelona Supercomputing Center through three RES activities, and by the EOLO cluster of excellence at Universidad Complutense de Madrid. G. Chiodo was supported by the Spanish Ministry of Education in the framework of the FPU doctoral fellowship (grant AP2009-0064). This work was supported by the Spanish Ministry of Science and Innovation (MCINN) through the CONSOLIDER (CSD2007-00050-II-PR4/07), MATRES (CGL2012-34221), and ExCirEs (CGL2011-24826) projects, and by the European Commission within the FP7 framework through the StratoClim project (Ref. 603557). J.M. Vaquero was supported by the Junta de Extremadura (Research Group Grant No. GR10131), the Ministerio de Economa y Competitividad of the Spanish Government (AYA2011-25945). The authors also aknowledge the COST Action ES1005 TOSCA (http://www.tosca-cost.eu).

Methods summary

Climate model

We use the Community Earth System Model (CESM) version 1.0.5 [*Marsh et al.*, 2013], which includes the atmospheric component from the Whole Atmosphere Community Climate Model version 4 (WACCM4), and the Parallel Ocean Program (POP) full ocean model. The atmosphere resolution is 1.9° latitude and 2.5° longitude with 66 vertical levels providing a well-resolved middle atmosphere and an upper boundary at 140 km. In this version of the model, tropical stratospheric winds are assimilated to reproduce a QBO as described by *Matthes et al.* [2010]. Incoming shortwave radiation is divided into 19 intervals from 200-5000 nm, 7 of which are centered in the ultraviolet (200-350 nm) and 2 in the visible (350-700 nm) range. Absorption of EUV radiation (i.e., below 200) nm is neglected. The atmosphere component WACCM4 is fully coupled with a chemistry module, and photolysis rates are calculated in-line using a resolution of 66 bands, covering all absorption lines from 120 nm onwards. Details on the photochemistry calculations are given by *Marsh et al.* [2007]. The ocean component POP employs a nominal latitude-longitude resolution of 1° (down to 1/4° in latitude in the equatorial tropics) and 60 levels in the vertical [*Gent et al.*, 2011].

Experiment design

We perform two ensembles of three members each over the 2005-2065 period. In both ensembles, the atmospheric loadings of GHGs and ozone depleting substances (ODSs) follow the Representative Concentration Pathway 4.5 (RCP4.5), i.e., a mid-range scenario used in the IPCC-AR5. In one ensemble, a transient 11-yr solar cycle is imposed by repeating the last four solar cycles (20-23). This ensemble, which is referred throughout the paper as RCP45, was previously run for the IPCC-AR5, and provides a reference case of climate change projections for the 21st century. The second ensemble is driven with the same RCP4.5 forcing for GHGs and ODSs, and a hypothetical minimum in future solar irradiance. A constant spectral irradiance is imposed from year 2008, which marks the minimum of solar cycle number 23 (see Fig. S1).

This ensemble is referred as MIN, since the irradiance is obtained by averaging recorded years in solar minima (1964,1965,1975,1976,1985,1986,1995,1996,2007,2008) of the spectral irradiance dataset from *Wang et al.* [2005]. The averages were calculated separately for each band, thereby adapting the solar forcing to get the best overlap with the spectral resolution of radiation code. Two idealized experiments were also performed for the same period, in which a solar minimum is separately imposed in the ultraviolet (120-350 nm) and visible (350-700 nm) range, while the rest of the spectrum contains a transient solar cycle, as in the RCP45 ensemble. These experiments are referred to as MINuv and MINvis, respectively. The radiative forcing in the MINuv is confined to the stratosphere due to ozone absorption of UV radiation, while in the MINvis, the dimming in the visible part of the solar radiation directly affects the surface radiation budget (see e.g., *Gray et al.* [2010]).

Spectral irradiance forcing

In the MIN ensemble, the decrease in spectral irradiance relative to the RCP45 ensemble is imposed in all wavelengths, as the input irradiance dataset from *Wang et al.* [2005] does not contain the compensating trends between visible and ultraviolet changes observed in the descending phase of solar cycle 23 in recent SORCE-SIM data [*Harder et al.*, 2009]. While the decrease in UV dominates in relative terms (2-10%), the integrated energy change in VIS wavelengths (0.27 W/m^2) is more than three times that obtained in the UV (0.09 W/m^2). Relative to the RCP45 ensemble, the MINuv and MINvis experiments are solely driven with the relative and energy decrease in the UV (120-350 nm) and VIS (350-700 nm) ranges.

Statistics

Statistically significant differences are computed using a Student t-test, including a correction to take serial correlation into account [*Zwiers and von Storch*, 1995]. The null hypothesis is that the difference in the climatological averages of RCP45 and MIN ensembles is not significantly different from zero. Throughout the paper, differences are considered significant when they exceed the 0.05 (95%) confidence level. Three members are performed for each MIN and

RCP45 ensembles, making a total sample size of 183 years for each case.

References

Abreu, J., J. Beer, F. Steinhilber, S. Tobias, and N. Weiss (2008), For how long will the current grand maximum of solar activity persist?, *Geophys. Res. Lett.*, *35*(20).

Anet, J., et al. (2013), Impact of a potential 21st century grand solar minimum on surface temperatures and stratospheric ozone, *Geophys. Res. Lett.*, *40*(16), 4420–4425.

Calvo, N., M. Giorgetta, R. Garcia-Herrera, and E. Manzini (2009), Nonlinearity of the combined warm ENSO and QBO effects on the Northern Hemisphere polar vortex in MAECHAM5 simulations, *J. Geophys. Res.*, *114*(D13), D13,109.

Camp, C. D., and K.-K. Tung (2007), The influence of the solar cycle and QBO on the late-winter stratospheric polar vortex, *J. Atmos. Sci.*, *64*(4), 1267–1283.

Chiodo, G., N. Calvo, D. Marsh, and R. Garcia-Herrera (2012), The 11 year solar cycle signal in transient simulations from the whole atmosphere community climate model, *J. Geophys. Res.*, *117*(D6).

Christoforou, P., and S. Hameed (1997), Solar cycle and the pacific centers of action', *Geophys. Res. Lett.*, *24*(3), 293–296.

Eddy, J. A. (1976), The maunder minimum, *Science*, *192*(4245), 1189–1202.

Feulner, G. (2011), Are the most recent estimates for maunder minimum solar irradiance in agreement with temperature reconstructions?, *Geophys. Res. Lett.*, *38*(16).

Feulner, G., and S. Rahmstorf (2010), On the effect of a new grand minimum of solar activity on the future climate on Earth, *Geophys. Res. Lett.*, *37*, 5707–+, doi:10.1029/2010GL042710.

Gent, P. R., et al. (2011), The community climate system model version 4, *J. Climate*, *24*(19), 4973–4991.

Gray, L., et al. (2010), Solar influences on climate, *Rev. Geophys.*, *48*(RG4001), 1–53, doi: 10.1029/2009RG000282.

Harder, J. W., J. M. Fontenla, P. Pilewskie, E. C. Richard, and T. N. Woods (2009), Trends in solar spectral irradiance variability in the visible and infrared, *Geophys. Res. Lett.*, *36*(7).

Hartmann, D. L. (1994), *Global physical climatology*, vol. 56, Academic press.

Hinssen, Y. B. L., C. J. Bell, and P. C. Siegmund (2011), The influence of the stratosphere on the tropospheric zonal wind response to co_2 doubling, *Atmos. Chem. Phys.*, *11*(10), 4915–4927, doi:10.5194/acp-11-4915-2011.

Ineson, S., A. A. Scaife, J. R. Knight, J. C. Manners, N. J. Dunstone, L. J. Gray, and J. D. Haigh (2011), Solar forcing of winter climate variability in the northern hemisphere, *Nature Geoscience*, *4*(11), 753–757.

Janardhan, P., S. K. Bisoi, S. Ananthakrishnan, M. Tokumaru, and K. Fujiki (2011), The prelude to the deep minimum between solar cycles 23 and 24: Interplanetary scintillation signatures in the inner heliosphere, *Geophys. Res. Lett.*, *38*(20).

Jones, G. S., M. Lockwood, and P. A. Stott (2012), What influence will future solar activity changes over the 21st century have on projected global near-surface temperature changes?, *J. Geophys. Res.*, *117*(D5).

Kirtman, B., et al. (2013), Near-term climate change: Projections and predictability, in *Climate Change 2013: The Physical Science Basis. Contribution of Working Group I to the Fifth Assessment Report of the Intergovernmental Panel on Climate Change*, edited by T. Stocker, D. Qin, G.-K. Plattner, M. Tignor, S. Allen, J. Boschung, A. Nauels, Y. Xia, V. Bex, and P. e. Midgley, Cambridge Univ Press, New York.

Kodera, K., and Y. Kuroda (2002), Dynamical response to the solar cycle, *J. Geophys. Res.*, *107*(D24), 4749, doi:10.1029/2002JD002224.

Kosaka, Y., and S.-P. Xie (2013), Recent global-warming hiatus tied to equatorial pacific surface cooling, *Nature*, *501*(7467), 403–407.

Lawrence, D. M., and A. G. Slater (2005), A projection of severe near-surface permafrost degradation during the 21st century, *Geophys. Res. Lett.*, *32*(24).

Lockwood, M. (2011), Was uv spectral solar irradiance lower during the recent low sunspot minimum?, *J. Geophys. Res.*, *116*(D16).

Lockwood, M., M. Owens, L. Barnard, C. Davis, and F. Steinhilber (2011), The persistence of solar activity indicators and the descent of the sun into maunder minimum conditions, *Geophys. Res. Lett.*, *38*(22).

Macias-Fauria, M., B. C. Forbes, P. Zetterberg, and T. Kumpula (2012), Eurasian arctic greening reveals teleconnections and the potential for structurally novel ecosystems, *Nat. Clim. Change*, *2*(8), 613–618.

Mantua, N. J., S. R. Hare, Y. Zhang, J. M. Wallace, and R. C. Francis (1997), A pacific interdecadal climate oscillation with impacts on salmon production, *Bull. Am. Met. Society*, *78*(6), 1069–1079.

Manzini, E., et al. (2014), Northern winter climate change: Assessment of uncertainty in cmip5 projections related to stratosphere-troposphere coupling, *J. Geophys. Res.*, *119*(13), 7979–7998.

Marsh, D., R. Garcia, D. Kinnison, B. Boville, F. Sassi, S. Solomon, and K. Matthes (2007), Modeling the whole atmosphere response to solar cycle changes in radiative and geomagnetic forcing, *J. Geophys. Res.*, *112*(D23306), doi:10.1029/2006JD008306.

Marsh, D. R., M. J. Mills, D. E. Kinnison, J.-F. Lamarque, N. Calvo, and L. M. Polvani (2013), Climate change from 1850 to 2005 simulated in cesm1 (waccm), *J. Climate*, *26*(19), 7372–7391.

Matthes, K., U. Langematz, L. Gray, K. Kodera, and K. Labitzke (2004), Improved 11-year solar signal in the freie universitaet Berlin climate middle atmosphere model (FUB-CMAM), *J. Geophys. Res.*, *109*(D06101), 15, doi:10.1029/2003JD004012.

Matthes, K., Y. Kuroda, K. Kodera, and L. U. (2006), Transfer of the solar signal from the stratosphere to the troposphere: Northern winter, *J. Geophys. Res.*, *111*(D6), D06,108, doi: 10.1029/2005JD006283.

Matthes, K., D. Marsh, R. Garcia, D. Kinnison, F. Sassi, and S. Walters (2010), Role of the QBO in modulating the influence of the 11 year solar cycle on the atmosphere using constant forcings, *J. Geophys. Res.*, *115*(D18), D18,110, doi:10.1029/2009JD013020.

McCracken, K., and J. Beer (2014), Comparison of the extended solar minimum of 2006–2009 with the spoerer, maunder, and dalton grand minima in solar activity in the past, *J. Geophys. Res.*, *119*(4), 2379–2387.

Meehl, G., J. Arblaster, K. Matthes, F. Sassi, and H. van Loon (2009), Amplifying the Pacific climate system response to a small 11-year solar cycle forcing, *Science*, *325*(5944), 1114–1118, doi:10.1126/science.1172872.

Meehl, G. A., J. M. Arblaster, and D. R. Marsh (2013), Could a future grand solar minimum like the maunder minimum stop global warming?, *Geophys. Res. Lett.*, *40*(9), 1789–1793.

Myhre, G., et al. (2013), Anthropogenic and natural radiative forcing, in *Climate Change 2013: The Physical Science Basis. Contribution of Working Group I to the Fifth Assessment Report of the Intergovernmental Panel on Climate Change*, edited by T. Stocker, D. Qin, G.-K. Plattner, M. Tignor, S. Allen, J. Boschung, A. Nauels, Y. Xia, V. Bex, and P. e. Midgley, Cambridge Univ Press, New York.

Nandy, D., A. Munoz-Jaramillo, and P. C. Martens (2011), The unusual minimum of sunspot cycle 23 caused by meridional plasma flow variations, *Nature*, *471*(7336), 80–82.

Roth, R., and F. Joos (2013), A reconstruction of radiocarbon production and total solar irradiance from the holocene 14 c and co 2 records: implications of data and model uncertainties, *Clim. Past Discuss.*, *9*(2), 1165–1235.

Roy, I., and J. D. Haigh (2010), Solar cycle signals in sea level pressure and sea surface temperature, *Atmos. Chem. Phys.*, *10*(6), 3147–3153.

Schrijver, C., W. Livingston, T. Woods, and R. Mewaldt (2011), The minimal solar activity in 2008–2009 and its implications for long-term climate modeling, *Geophys. Res. Lett.*, *38*(6).

Song, X., D. Lubin, and G. J. Zhang (2010), Increased greenhouse gases enhance regional climate response to a maunder minimum, *Geophys. Res. Lett.*, *37*(1).

Stocker, T. F., et al. (2013), *Climate change 2013: The physical science basis*, Cambridge Univ Press, New York.

Thompson, D., and J. Wallace (1998), The Arctic Oscillation signature in the wintertime geopotential height and temperature fields, *Geophys. Res. Lett.*, *25*(9), 1297–1300, doi: 10.1029/98GL00950.

Vaquero, J. M., M. Gallego, I. G. Usoskin, and G. A. Kovaltsov (2011), Revisited sunspot data: a new scenario for the onset of the maunder minimum, *Astrophys. J. Lett.*, *731*(2), L24.

Wang, Y.-M., J. Lean, and N. Sheeley Jr (2005), Modeling the sun's magnetic field and irradiance since 1713, *Astrophys. J.*, *625*(1), 522.

Zolotova, N. V., and D. I. Ponyavin (2014), Is the new Grand minimum in progress?, *J. Geophys. Res.*, *119*, 3281–3285, doi:10.1002/2013JA019751.

Zwiers, F. W., and H. von Storch (1995), Taking serial correlation into account in tests of the mean, *J. Climate*, *8*(2), 336–351.

5 Figures

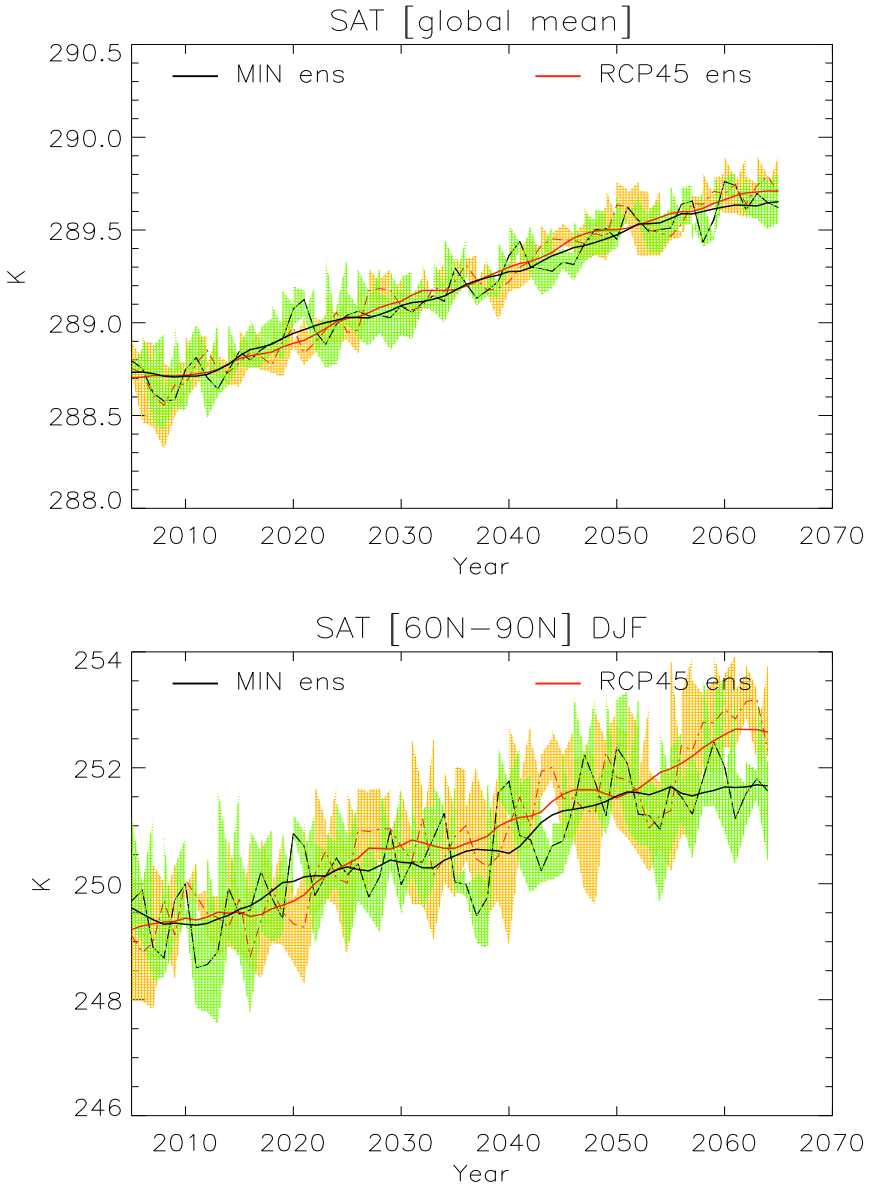

Figure 1: Time series of the surface air temperature; (a) globally averaged annual mean, (b) boreal winter mean (DJF) averaged over NH high latitudes (60°N-90°N). The stippled lines indicate the (a) annual and (b) winter mean ensemble average in the MIN (black) and RCP45 (red) simulations. The shading depicts the spread spanned by the three members of each ensemble, and is shown in green and orange for the MIN and RCP45 ensembles, respectively. Bold lines indicate the running mean obtained with a 10-yr boxcar average. Units K

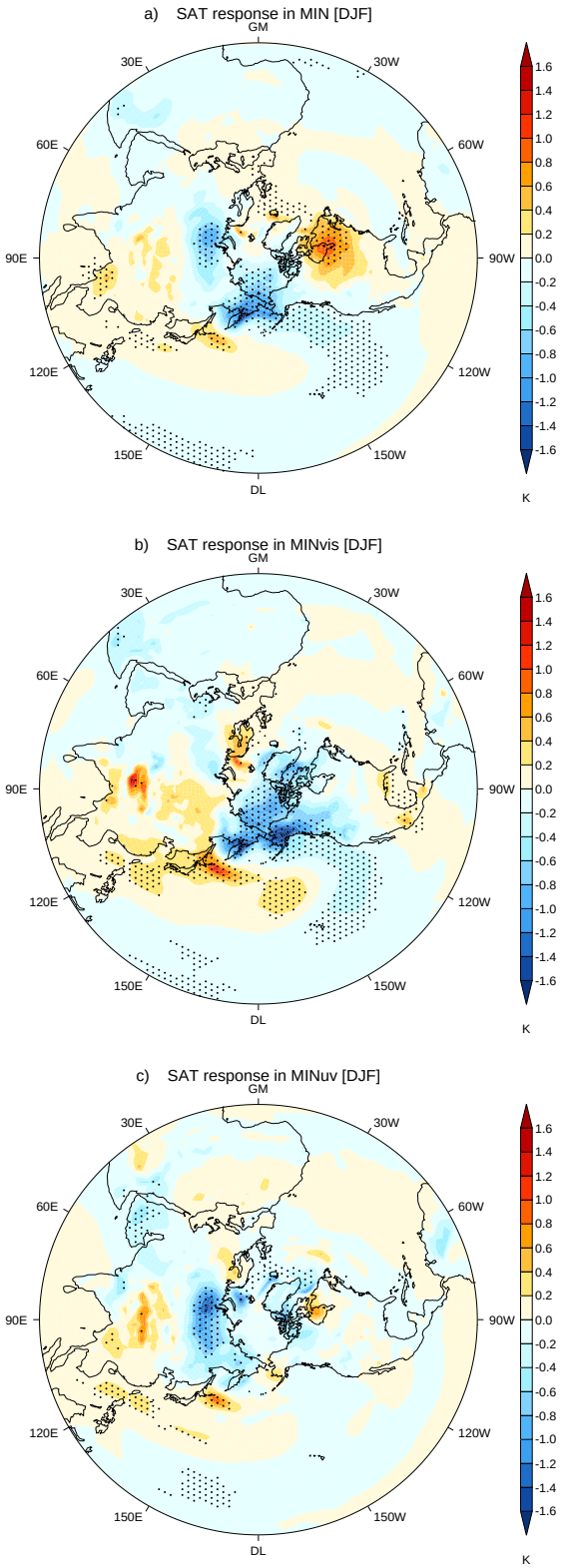

Figure 2: Polar stereographic projection of the boreal winter (DJF) MIN response in surface air temperature, calculated as the difference over the simulated period (2005-2065) between (a) MIN minus RCP45 ensemble means, (b) MINvis minus RCP45, (c) MINuv minus RCP45. Stippled areas are statistically significant at 95%. Contours are drawn every 0.2. Units K

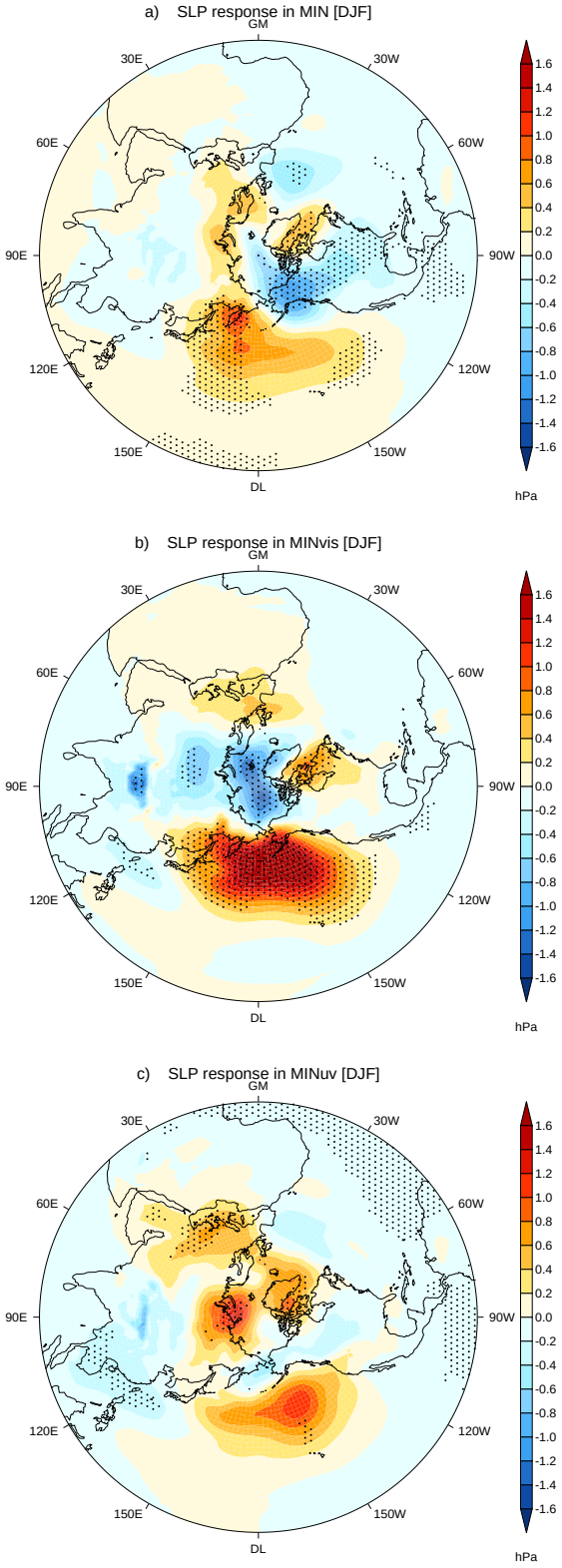

Figure 3: As in Fig. 2, for sea level pressure (SLP). Contours are drawn every 0.2 hPa. Units hPa

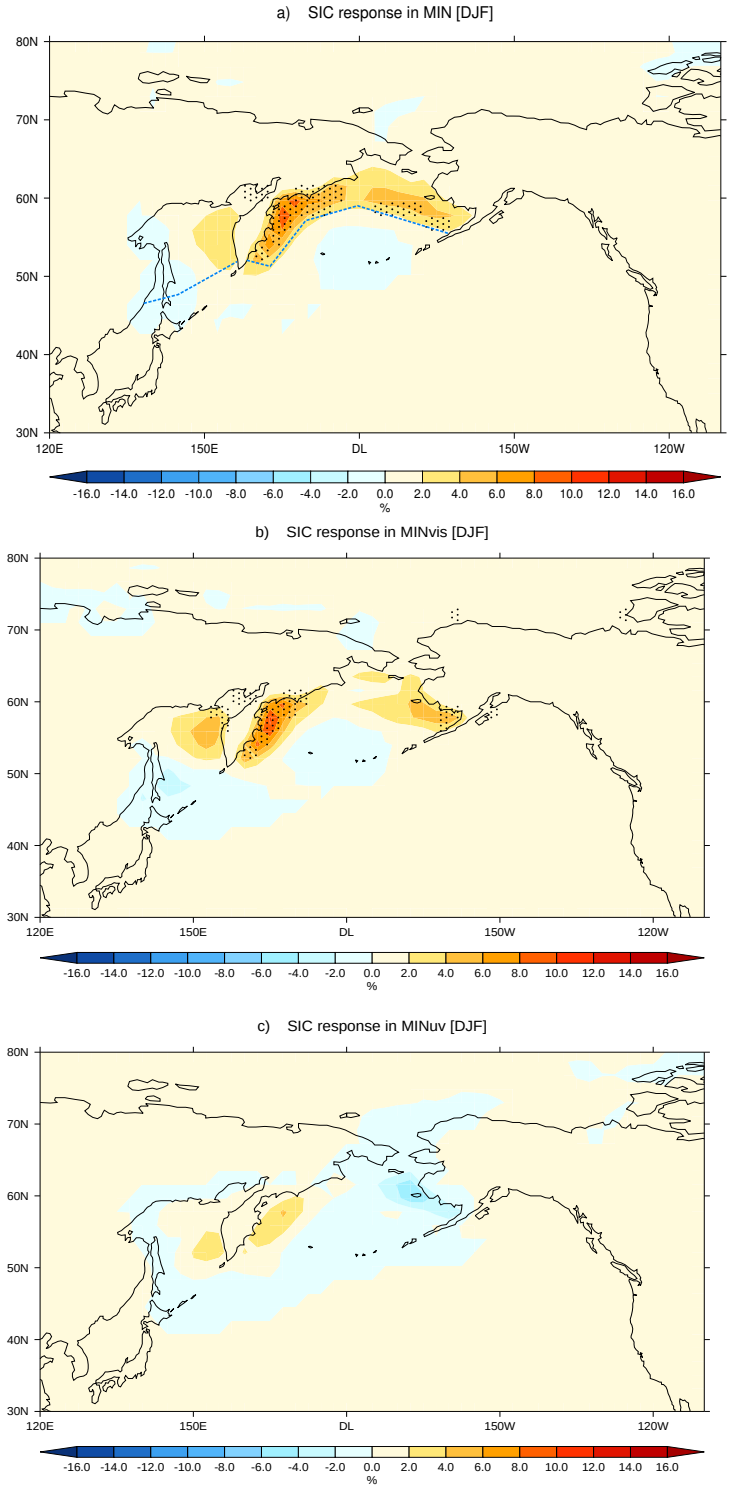

Figure 4: As in Fig. 2, for the sea ice concentrations (SIC) response in the NH Pacific sector. The sea-ice edge (estimated as a grid cell containing more than 30% of sea-ice) simulated in the RCP45 ensemble during the 2005-2015 period is represented by the blue stippled line. Contours are drawn every 2 units, corresponding to a 2 % change in winter mean SIC.

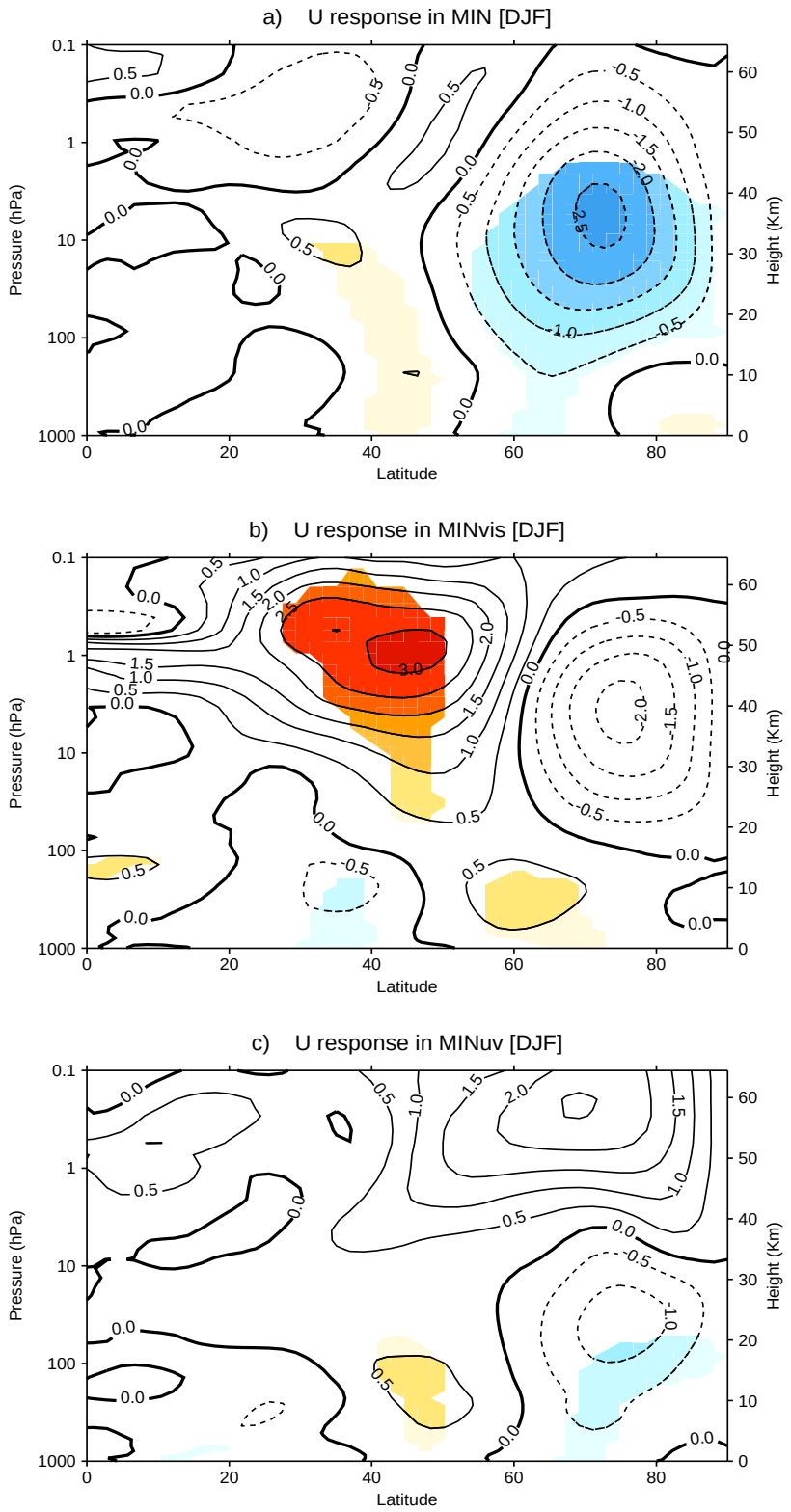

Figure 5: As in Fig. 2, for mean zonal wind MIN response in the first half of the simulated period (2005-2035). Colours highlight regions where differences are statistically significant at 95%. Contours are drawn every 0.5. Units m/s

Supplementary material

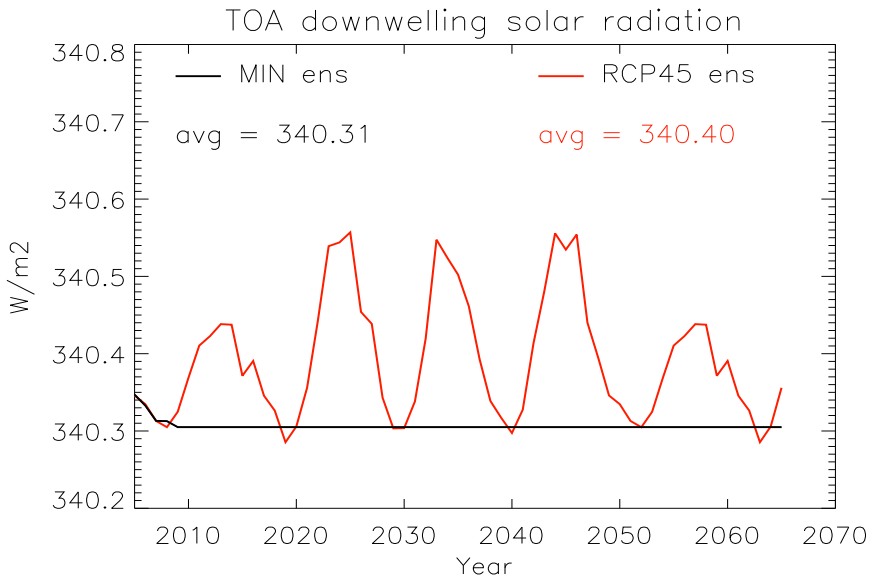

Figure S 1: Time series of the global average downwelling solar radiation at TOA in the MIN and RCP45 ensembles. The average values are shown for both ensembles. Units W/m^2.

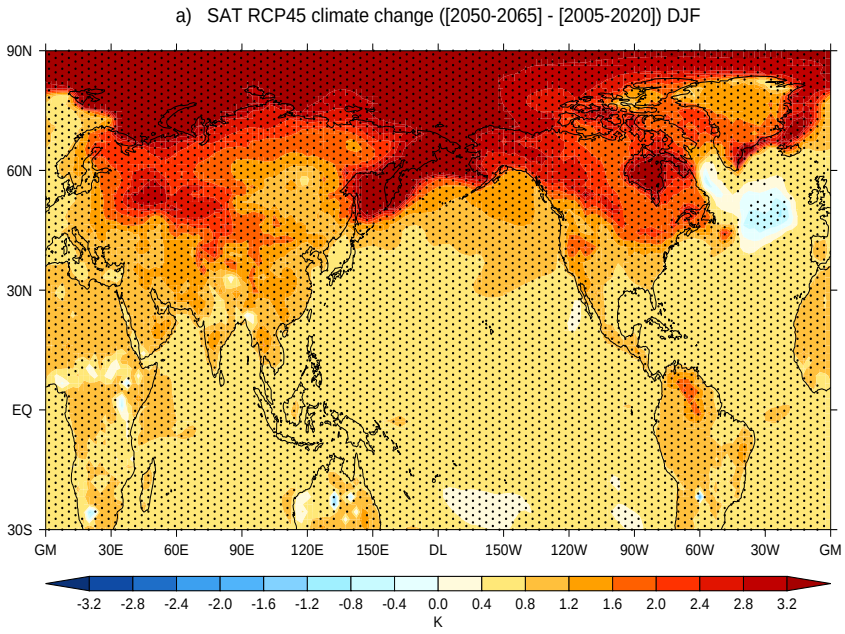

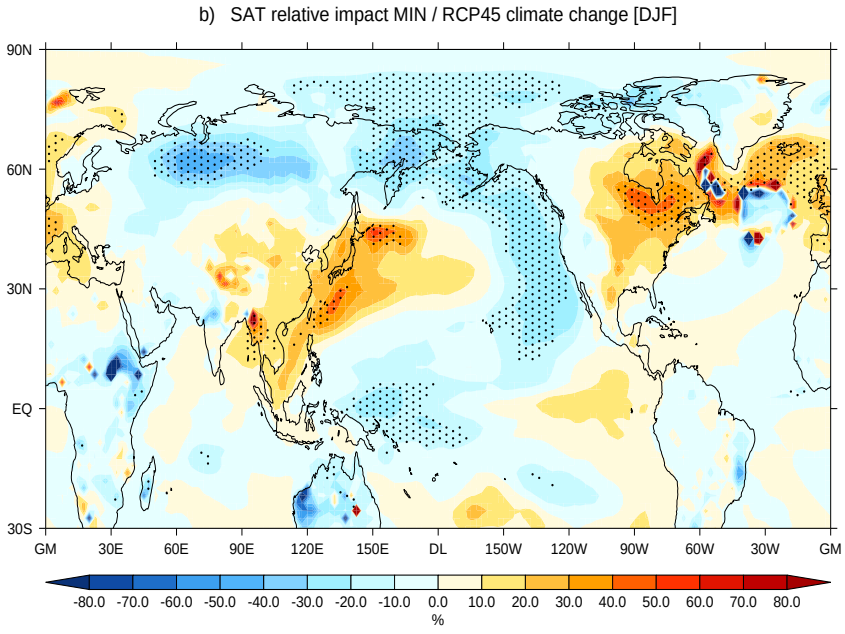

Figure S 2: a) Boreal winter (DJF) mean ensemble mean climate change response in surface air temperature in the RCP45 simulations, calculated as a difference of [2050-2065] minus [2005-2020] climatologies, units K.; (b) relative impact (in %) of the MIN forcing on boreal winter climate change, calculated as the fraction of the surface air temperature response in MIN (Fig. 2a) to the RCP45 climate change response shown in (a).

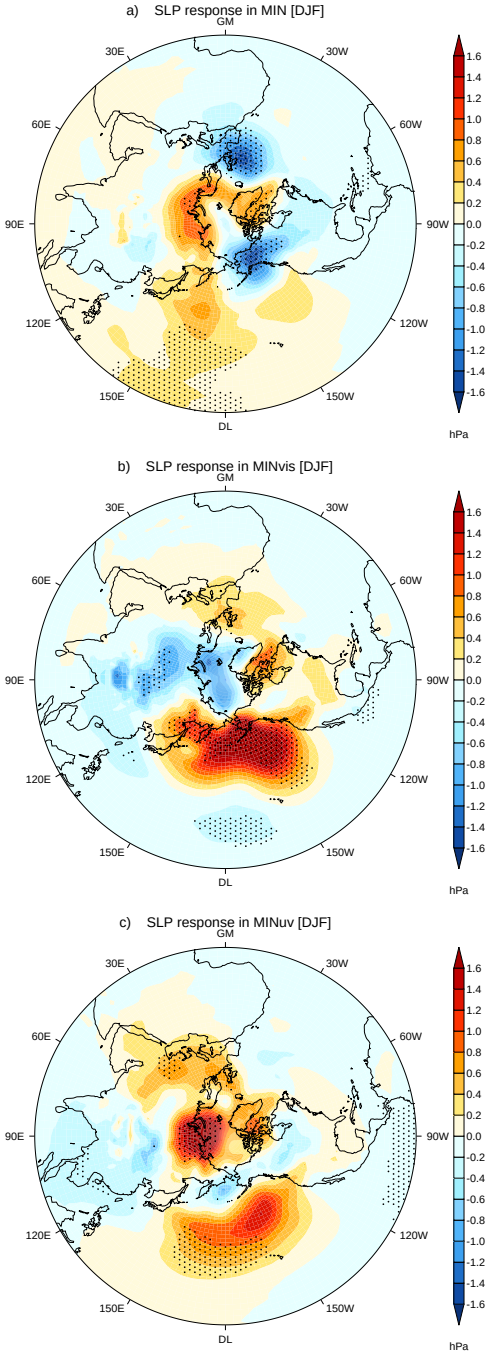

Figure S 3: As in Fig. 3, for the first half of the simulations (2005-2035). Differences are shown for (a) MIN minus RCP45, (b) MINvis minus RCP45, and (c) MINuv minus RCP45. Contours are drawn every 0.2. Units hPa

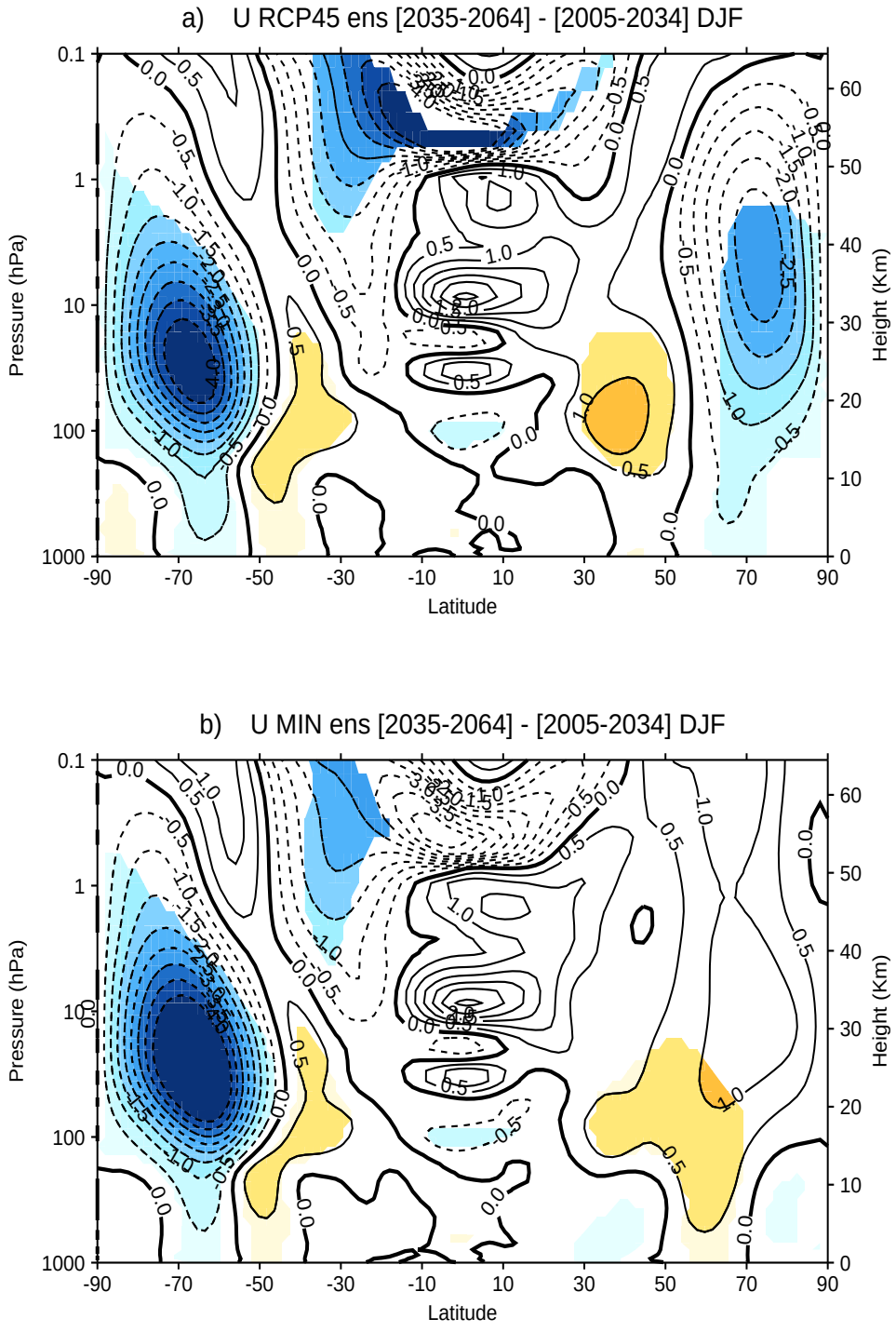

Figure S 4: Climate change response in boreal winter mean zonal wind, as simulated in the (a) RCP45 and (b) MIN ensembles, shown as climatological difference between the second and first half of the simulation (i.e., [2035-2064] minus [2005-2034] climatologies). Colours highlight regions where differences are statistically significant at 95%. Contours are drawn every 0.5. Units m/s

6 Summary and conclusions

In the first part of this thesis [*Chiodo et al.*, 2012], the atmospheric response to the 11-yr solar cycle is simulated in an ensemble of transient simulations from the WACCM3.5 model. The novelty of the study lies in the combination of realistic forcings used to drive the simulations over the 1960-2005 period. This allows for a direct comparison between the modeled solar signal and that observed from re-analysis and satellite datasets. In addition, as solar signals in models are usually analyzed based on individual simulations, the availability of four ensemble members allows for an improved estimation of the internal variability, thereby posing a more stringent statistical test of the putative signal.

The results have shown that WACCM3.5 simulates a significant 11-yr response in the tropical stratosphere, characterized by an increase in temperature and ozone during peaks of the solar cycle, which maximize in the upper stratosphere at 40-50 km. Compared to the previous WACCM version (WACCM3.1), WACCM3.5 provides much closer estimates to the observed solar signal in temperature and ozone in the tropical lower stratosphere at 20 km.

During winters with peak solar activity (solar maximum), a poleward and downward migration of a westerly wind anomaly is simulated, consistent with the modulation of the polar night jet reported in observations [*Kodera and Kuroda*, 2002]. It is shown that an increase in UV-absorption in the tropical stratopause region initiates the westerly wind anomaly in the subtropical upper stratosphere. Subsequently, changes in wave propagation and momentum deposition amplify the wind anomaly, and transfer it poleward and downward to the lower polar stratosphere. There is also a concomitant weakening of the Brewer Dobson circulation, which causes the temperature increase in the tropical lower stratosphere at 20 km. This winter response is not reproduced in the previous WACCM3.1 version, which is possibly due to its worse stratospheric polar jet and SSWs climatology. It is argued that for this reason, the tropical lower stratospheric response in WACCM3.5 is more realistic than in WACCM3.1.

WACCM3.5 also reproduces the apparent QBO-solar modulation of the polar vortex in late winter (February) reported by *Labitzke* [1987, 2004, 2005], whereby a cold and strong vortex is seen in QBO east conditions, while a warm and weak vortex is observed in QBO west winters. However, this behavior is not reproduced in all ensemble members, suggesting an influence of the initial conditions, and thus the lack of robustness of the modeled QBO-solar modulation. During boreal winter, there are also signals in tropospheric and surface climate, such as a positive NAO phase in the Atlantic sector, a weakening of the Hadley cell, and an increase in precipitation off the Equator. The tropospheric signals agree well with observations, and seem to be linked to the stratospheric polar vortex response to the 11-yr cycle.

Overall, the modeled response to the 11-yr solar cycle is close to observations, both in the tropical and extratropical stratosphere. The winter solar signal is found to be consistent with the conceptual model proposed by *Kodera and Kuroda* [2002], and provides evidence for the polar route within the stratospheric "top-down" pathway depicted in Section 1.3. For the first time, this mechanism is confirmed in model simulations using realistic forcings. It is argued that the model success in simulating a realistic solar signal

is closely tied to the improved polar vortex climatology and variability.

The second part of this thesis [*Chiodo et al.*, 2014] investigates the feasibility of separating the 11-yr solar signal from other natural sources of variability using regression methods in timely limited records, such as the simulations analyzed in the first study, and state-of-the-art observational data sets that only cover at most three solar cycles (1979-present). This study focuses on the tropical stratosphere, where a large portion of interannual variability is due to ENSO, QBO and major volcanic events, to investigate whether these sources of variability potentially map onto the quasi-decadal signal commonly attributed to the 11-year solar cycle. Simulations including all observed forcings are compared to idealized experiments excluding one of the non-solar forcings mentioned above. The solar signal is diagnosed using a novel MLR approach never used before in this field, which reduces collinarity between indices, and the autocorrelation in the model time series.

It is found that a large fraction of the apparent solar cycle response in both ozone and temperature in the tropical lower stratosphere (at about 20 km) is due to two volcanic eruptions (El Chichón in 1982 and Mt. Pinatubo in 1991). These eruptions map onto the 11-yr signal due to their alignment with the peaks of solar cycles number 21 and 22. In ozone, a minor contribution to the apparent solar signal is also due to the QBO. In addition, interannual variability in tropical upwelling may complicate the attribution of ozone changes. Consequently, the larger temperature and ozone response in the tropical lower stratosphere in WACCM3.5, and the apparent improved agreement with observations compared to WACCM3.1 evidenced in the first part of this thesis could be due to the inclusion in this model version of volcanic heating and QBO forcings.

Since signals from other sources of variability can overlap with the apparent 11-yr solar signal, unambiguous attribution of solar effects is challenging. Hence, it is important to determine the minimum number of years needed to detect a robust solar signal in observational records. In the upper tropical stratosphere (40-50 km), a robust solar cycle signal can be extracted using regression analysis of 10-15 years of data, suggesting that available observational records are long enough for accurate determination of the solar signal. However, in the tropical lower stratosphere (20-30 km) it is unfeasible to obtain a robust estimate of the solar signal from either the 25-years long typical re-analysis record, or from 45-years long simulation. This is due to the effects of El Chichón and Mt. Pinatubo eruptions. Excluding a two-year window corresponding to the post-eruption periods from the regression analysis ameliorates the attribution issue, but also drastically reduces the apparent solar signal in the tropical lower stratosphere. In this region, more observations of 11-yr cycles without concomitant major eruptions are still needed to clearly detect a solar signal in lower stratospheric temperature.

These results indicate that the portion of quasi-decadal variability, which can be unambiguously attributed to the solar cycle in the tropical lower stratosphere may be smaller than previously thought. This has implications for the interpretation of the "tropical route", which has been proposed as a possible pathway for the downward propagation of the solar signal. The present results suggest that the dynamical mechanisms associ-

ated with this pathway, which are described in *Haigh et al.* [2005]; *Haigh and Blackburn* [2006]; *Simpson et al.* [2009], and are based on dynamical adjustment in the tropospheric jet to heating in the tropical lower stratosphere, may be linked to volcanic heating rather than solar variability.

In the last part of this thesis, the impact of a future solar minimum under climate change conditions is investigated [*Chiodo et al.,* 2014, submitted]. The anomalous behavior of solar activity during the current solar cycle number 24 has shown that the 11-yr solar cycle is far from being a quasi-periodic forcing. Thus, the approach of IPCC models to repeat the last four 11-yr solar cycles may not be adequate. In addition, suggestions have been made for a near future descent into an extended phase of reduced solar activity levels. As long-range forecasts of solar activity are unfeasible, this represents one possible solar scenario that might be realistic.

An ensemble of three realizations of WACCM4 (as WACCM3.5 except that it is coupled to a deep ocean model) is forced with perpetual solar minimum conditions from 2005 to 2065. A realistic solar spectral irradiance forcing is calculated from data modeled by *Lean et al.* [2005] for the minima of cycles 20-23. This ensemble mean is compared with another forced with solar cycle variability by repeating the last four 11-yr solar cycles. Both ensembles are forced with a mid-range emission scenario of greenhouse-gases, the Representative Concentration Pathway 4.5 (RCP4.5), and thus only differ in the solar forcing. The design of the experiments allows using simple climatological differences to diagnose the impact of the solar minimum on surface climate, avoiding the problems in the detection of the solar signal associated with the regression analysis evidenced in the second part of this thesis.

While a solar minimum would not alter the global mean surface temperature rise of 1.5 K projected by 2065, results reveal that significant effects are found in boreal winter climate in the Northern Hemisphere. Cooling up to 1-1.5 K is simulated over two separate regions of Russia and the Bering Strait, which extends into a PDO-like pattern in the tropical Pacific, while warming is simulated in Eastern North America. Over the Northern Hemisphere high latitudes (60°N-90°N), the projected GHG-induced warming tendency is significantly reduced up to 30% during solar minimum conditions.

The cooling in the Pacific is primarily due to the minimum in visible wavelengths, directly affecting the surface that are amplified by surface feedbacks involving changes in sea-ice ("bottom-up" mechanism). The cooling simulated over Russia is driven by a "top-down" mechanism, whereby the minimum in ultraviolet radiation favors a more disturbed stratospheric polar vortex that affects surface circulation patterns. This is consistent with the boreal winter response to peaks of the 11-yr solar cycle shown in the first part of the thesis [*Chiodo et al.*, 2012]. However, the "top-down" contribution to surface anomalies is not obvious over the entire simulated period, as a climate change tendency in the polar vortex cancels out the effects of the minimum in the late stages of the simulations. Thus, the effect of a prolonged solar minimum on boreal winter surface climate is due to two different mechanisms, initiated by changes in irradiance in different regions of the solar spectrum.

Even though the modeled changes in surface climate are observed in geographically

limited regions, they have far-reaching implications for the assessment of global warming impacts in other compartments of the climate system, such as high-latitude ecosystems. The role of future solar activity as a potential source of uncertainty needs to be reconsidered in the design of CMIP6 model projections that will participate to the next assessment reports. One method would consist of designing solar forcing scenarios, such as the experiments performed in this study. Given that both changes in the visible and ultraviolet wavelengths are equally instrumental in creating surface temperature anomalies, the present results also stress the importance of using spectrally resolved solar scenarios.

7 Outlook

The thesis has provided answers to three different questions regarding the impact of the 11-yr solar cycle signal in climate. Still, many other aspects about the sun-climate relationship remain unclear.

One research question of high relevance to the climate community is the impact of the uncertainty in the UV forcing in light of the recent SORCE-SIM measurements, as discussed in Section 1.1. Over the descending phase of the solar cycle 23 (2004-2007), SORCE-SIM estimates show a larger UV variation compared to the data by *Lean et al.* [2005] that are widely used in modeling studies, including the WACCM simulations performed in this thesis. One recent study evidenced that a stronger UV forcing exacerbates the "top-down" mechanism, leading to a strong NAO response [*Ineson et al.*, 2011]. However, as SORCE-SIM data only extend over part of the solar cycle 23, they may not be representative of 11-yr variability, and must still be considered as provisional [*Garcia*, 2010]. Some discrepancies in the UV variability are also found in the longer term, if data from *Lean et al.* [2005] are compared with the empirical model of *Krivova et al.* [2006] (see Fig. 14). This suggests that the model by *Lean et al.* [2005] may be underestimating UV variability. A mismatch appears across the whole UV spectrum, albeit with much weaker amplitudes than when the Lean model is compared to SORCE-SIM. It is therefore clear that solar variability in these bands is uncertain. The impact of such uncertainty on the modeled climate is currently being explored in WACCM3.5 as an extension to this thesis work. This can be done by performing sensitivity experiments driven with an artificial increase of 1-3% in the mid UV (240-270 nm) and near UV (300-400 nm). These estimates represent the long term UV uncertainty, and thus, are more realistic than the extreme UV forcings used in previous studies (e.g. [*Haigh et al.*, 2010; *Ineson et al.*, 2011; *Merkel et al.*, 2011]). Since these bands are absorbed at different heights in the tropical stratosphere, they can potentially lead to different dynamical responses in the polar stratosphere.

Another open research question of great interest to the sun-climate community is related to the QBO-solar modulation discussed in Section 1.4. In the first part of the thesis, this feature was found not to be robust across ensemble members. However, one limitation of WACCM3.5 lies in its inability to generate a self-consistent QBO. Prescribing the observed tropical winds may inhibit the interactions between the solar cycle and the QBO, which are key to capturing

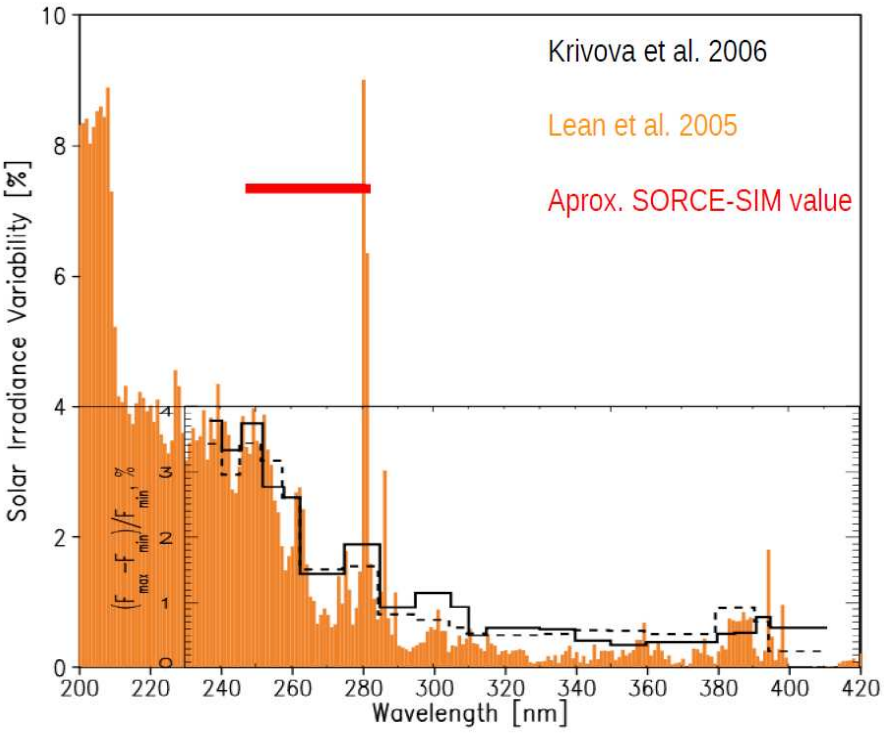

Figure 14: Relative 11-yr variation in solar spectral irradiance in data from empirical models [*Lean et al.*, 2005; *Krivova et al.*, 2006] and from SORCE-SIM [*Harder et al.*, 2009].

the extratropical response. For this reason, this topic can be explored in a model with an internally generated QBO such as the Hamburg Model of the Neutral and Ionized Atmosphere (HAMMONIA) [*Schmidt et al.*, 2010]. A set of transient experiments with the same set-up as in *Chiodo et al.* [2012] will be performed, albeit with an internally generated QBO. Since the modelled QBO is not in phase with the observed QBO, the role of the observed alignment between the QBO and solar cycle phases in the solar signal can be assessed, shedding light on the robustness of the QBO-solar relationship.

Resumen y conclusiones de la tesis

Introducción y métodos

Las variaciones en la actividad solar dan lugar a fluctuaciones en la irradiancia total recibida en la Tierra, o lo que es lo mismo, en la densidad de flujo de energía entrante en el tope de la Atmósfera. Desde el año 1979, los satélites han tomado medidas de la irradiancia total, la cual posee una variacin cuasi periódica, a la que se denomina ciclo solar de 11 años. Este ciclo está asociado a las manchas solares, que aumentan en fase con la irradiancia. Entre máximos y mínimos del ciclo de 11 años, hay una variación de 1 W/m^2, lo cual se traduce en un forzamiento radiativo despreciable para el sistema climático.

Sin embargo, la variación cíclica en las bandas del ultravioleta es mucho más grande (5-10%) que en la irradiancia total (0.1%) [*Fröhlich and Lean*, 2004]. Debido a que la radiación ultravioleta se absorbe en la estratosfera, el mayor impacto del ciclo solar ha de esperarse en esta región atmosférica, donde el ozono presenta su mayor concentración [*Mohanakumar*, 2008]. En línea con estas expectativas, durante máximos de actividad solar se observa un calentamiento de 1 K en la estratopausa tropical, y un aumento de ozono [*Soukharev and Hood*, 2006; *Randel and Wu*, 2007]. Por otro lado, los picos de actividad solar también se asocian con un calentamiento de la baja estratosfera tropical (20 km) y de las latitudes medias en la troposfera [*Frame and Gray*, 2010]. Además, se han observado cambios en el chorro polar estratosférico [*Kodera and Kuroda*, 2002], y troposférico [*Haigh et al.*, 2005] y otros estudios también sugieren una influencia solar sobre patrones de variabilidad como la Oscilación de Atlántico Norte (NAO) [*Gimeno et al.*, 2003] y los bloqueos [*Barriopedro et al.*, 2008]. La aparente respuesta al ciclo solar en estas regiones atmosféricas se debe a efectos indirectos que todavía no se conocen y que, por consiguiente, son actual objeto de investigación [*Gray et al.*, 2010].

Con objeto de dar una explicación de la señal observada en las bajas capas de la estratosfera y troposfera, se han propuesto diferentes mecanismos. Un posible mecanismo consiste en una propagación durante el invierno boreal de fluctuaciones en el chorro polar estratosférico [*Kodera and Kuroda*, 2002]. Otros estudios sugieren un ajuste dinámico del chorro troposférico a anomalías térmicas en la baja estratosfera tropical [*Haigh and Blackburn*, 2006; *Simpson et al.*, 2009]. Aunque estos mecanismos difieren en la causa que los provoca, tienen en común la importancia de la radiación ultravioleta en generar anomalías térmicas en la estratosfera, que desencadenan cambios en la interacción entre ondas atmosféricas y flujo medio.

A pesar de las numerosas evidencias de un aparente impacto del ciclo solar sobre el clima, existe un problema en la caracterización estadística de la señal en las observaciones. Para la atmósfera libre (5-50 km) sólo existen datos observacionales de los últimos 30 años (1979-presente). Esto dificulta la separación de la señal solar de otras fuentes de variabilidad climática, como la oscilación del Niño (ENSO), la oscilación cuasi bienal de los vientos de la estratosfera tropical (QBO), los volcanes, y la variabilidad interna. Debido a la corta longitud de los registros observacionales, la fiabilidad de técnicas estadísticas como la regresión múltiple son

cuestionables, a pesar de que su uso para extraer la señal de las observaciones esté bastante extendido (p.j., *Soukharev and Hood* [2006]; *Frame and Gray* [2010]).

En este contexto, el uso de modelos resulta provechoso para investigar los mecanismos que se han propuesto en la literatura, y para estudiar cuán robusta es la señal solar observada. La mayoría de las simulaciones hechas con modelos acoplados de química-clima han sido capaces de reproducir el calentamiento en la alta estratosfera tropical (50 km) observado durante picos de actividad solar [*Frame and Gray,* 2010]. Sin embargo, los modelos generalmente no reproducen la señal en la baja estratosfera tropical, y la señal invernal en altas latitudes [*Gray et al.*, 2010]. Por otro lado, las simulaciones que reproducen estos patrones han empleado condiciones de contorno idealizadas, como un patrón fijo de actividad solar y temperaturas del océano constantes [*Marsh et al.*, 2007; *Schmidt et al.*, 2010], excluyen la QBO [*Tourpali et al.*, 2003; *Rozanov et al.*, 2004; *Egorova et al.*, 2004], o con una amplitud del forzamiento de la radiación ultravioleta exagerada [*Ineson et al.*, 2011]. Por lo tanto, cabe preguntarse si:

- **Es posible reproducir la respuesta observada al ciclo solar en la baja estratosfera, usando un modelo de química-clima, con condiciones de contorno más realistas?**
- **Es posible extraer una seal robusta de las series observadas, teniendo en consideración su extensión limitada?**

Otra cuestión a destacar es la incertidumbre acerca de la evolución futura de la actividad solar, y de su posible impacto sobre el cambio climático futuro. Aunque la actividad solar sea poco predecible a escalas de tiempo decadales [*Solanki and Krivova,* 2011], muchos estudios apuntan a la posibilidad de que el Sol pueda entrar en una fase de inactividad prolongada [*Abreu et al.*, 2008; *Lockwood et al.*, 2011], parecida en duración y amplitud al mínimo de Maunder del siglo XVII [*Eddy,* 1976]. Los estudios de modelización que han investigado esta cuestión (p.j., *Anet et al.* [2013]; *Meehl et al.* [2013]), han empleado un forzamiento solar basado en reconstrucciones del mínimo de Maunder, como las de *Shapiro et al.* [2011], que sobrestiman la disminución de la irradiancia [*Feulner*, 2011]. Es por ello que entonces cabe cuestionarse:

- **Cuál es el impacto de un posible mínimo solar futuro en condiciones de cambio climático?**

Para abordar estas tres cuestiones, se realizan simulaciones climáticas con el modelo acoplado de química-clima WACCM3.5. Debido a la química interactiva, este modelo climático es capaz de simular la interacción entre la radiación ultravioleta y el ozono estratosférico. Además, por su alto tope atmosférico (140 km) y resolución vertical (66 niveles), es capaz de representar la dinámica estratosférica de manera adecuada, y es por tanto la herramienta ideal para investigar los mecanismos dinámicos que se han propuesto anteriormente para explicar la respuesta de la atmósfera al ciclo solar [*Gray et al.*, 2010]. WACCM3.5 representa una versión mejorada del

modelo WACCM3.1 empleado en estudios anteriores de modelización de la respuesta al ciclo solar (p.j., *Marsh et al.* [2007]) en cuanto a implementación del forzamiento solar, y variabilidad estratosférica [*CCMVal-2*, 2010].

Discusión de los resultados obtenidos, y conclusiones

En la primera parte de esta tesis [*Chiodo et al.*, 2012], se estudia la respuesta atmosférica al ciclo solar en un conjunto de simulaciones con el modelo WACCM3.5 aplicándole diferentes condiciones iniciales. La novedad del estudio está en el realismo de las condiciones de contorno empleadas para la simulación del clima en la época de 1960-2005. Las simulaciones incluyen las temperaturas observadas del océano, los efectos de las erupciones volcánicas, el ciclo solar de 11 años, el aumento de gases de efecto invernadero, y la QBO. Esto permite una comparación directa entre la señal de 11 años simulada con las observaciones de re-análisis y satélites. Además, la dimensión del conjunto (4 simulaciones independientes) es más grande que en estudios anteriores, lo cual permite una mejor caracterización de la variabilidad interna y de la significatividad de la señal solar. Los resultados muestran una respuesta significativa del modelo en la estratosfera tropical. Durante picos de actividad solar, ésta se caracteriza por un patrón de calentamiento y aumento de ozono, que alcanza valores máximos en las capas altas (50 km) y bajas (20 km) de la estratosfera tropical. En comparación con la antigua versión del modelo, WACCM3.1, la señal solar simulada por WACCM3.5 tanto en la temperatura, como en el ozono de la baja estratosfera tropical, está más cerca de los valores observados en *Frame and Gray* [2010] y *Soukharev and Hood* [2006].

Durante los inviernos boreales en condiciones de máximo solar, el modelo simula en el hemisferio norte una propagación hacia la estratosfera polar y sucesivamente hacia la troposfera, en coherencia con la modulación observada del chorro polar estratosférico [*Kodera and Kuroda*, 2002]. Durante máximos de actividad solar, el aumento de absorción de la radiación ultravioleta en la alta estratosfera tropical desencadena una aceleración del chorro estratosférico en latitudes subtropicales (30°N). Sucesivamente, cambios en la propagación y deposición de momento por parte de las ondas planetarias, amplifican las anomalías de viento zonal y dan lugar a su propagación hacia la baja estratosfera polar durante los meses de invierno. Una menor deposición de momento en la estratosfera polar causa, a su vez, un debilitamiento de la circulación de Brewer-Dobson, lo cual explica en parte el calentamiento de la baja estratosfera tropical (20 km). Ésta respuesta de la estratosfera polar no se reproduce en el modelo WACCM3.1, posiblemente debido al menor realismo en la climatología del chorro polar y en la variabilidad de los eventos súbitos estratosféricos. Consecuentemente, se sostiene que la respuesta en la baja estratosfera tropical es más realista en WACCM3.5 debido a las mejoras en la respuesta polar.

El modelo utilizado también reproduce la modulación de la señal de la QBO en la estratosfera polar durante los meses de invierno tardío (Febrero) [*Labitzke and Loon*, 1989; *Labitzke*, 2004, 2005; *Labitzke and Kunze*, 2009] según la cual, se observa un vórtice fuerte y frío en fases este de la QBO y máximo solar, y débil y cálido en fases oeste de la QBO y máximo solar. Sin embargo, esta respuesta no se reproduce en todos los miembros del conjunto de simulaciones,

lo cual indica que dicha modulación no es robusta. Durante el invierno boreal en fases de máximo solar, también se obtiene una señal en el clima troposférico y en la superficie, como la fase positiva de la NAO, el debilitamiento en la circulación de Hadley, y la supresión de la precipitación tropical.

En conclusión, se muestra concordancia entre la señal simulada y las observaciones, tanto en la estratosfera tropical como polar. La señal del invierno boreal es coherente con el modelo conceptual propuesto por *Kodera and Kuroda* [2002], y aporta evidencia a favor de la propagación de la influencia del ciclo solar desde la estratosfera hacia la troposfera y superficie. Por primera vez, este mecanismo se confirma en simulaciones forzadas con condiciones de contorno realistas. Se sostiene que el éxito del modelo en reproducir la señal observada se debe a las mejoras en la climatología y variabilidad del chorro polar estratosférico.

En la segunda parte de esta tesis [*Chiodo et al.*, 2014], se investiga la viabilidad de la caracterización de la señal del ciclo solar de 11 años mediante métodos de regresión en el análisis de registros limitados, como las observaciones y los datos de satélites. Este estudio se centra en la estratosfera tropical, donde una porción importante de la variabilidad interanual es debida a factores como ENSO, la QBO y las erupciones volcánicas, con el objetivo de investigar la posibilidad de que estos factores den lugar a la variabilidad cuasi-decadal que comúnmente se atribuye al ciclo solar. Se comparan simulaciones que incluyen todos los forzamientos observados con experimentos en los que se excluye cada uno de los factores mencionados anteriormente, a excepción del ciclo solar de 11 años. Se extrae la señal solar en cada conjunto a través de un método de regresión múltiple nuevo en este campo, que reduce la colinealidad entre predictores y la auto-correlación. La comparación entre las componentes de 11 años obtenidas en cada experimento, cuantifica el impacto de los otros factores sobre la detección estadística de la señal solar.

Se encuentra que una fracción importante de la aparente señal solar en temperatura y ozono de la baja estratosfera tropical se debe a dos erupciones volcánicas, cuyas cenizas alcanzaron la estratosfera tropical (El Chichón en 1982, y Mt. Pinatubo en 1991). Estas erupciones dan lugar a una señal de 11 años debido a su coincidencia con las fases de máximo de los ciclos 21 y 22. En ozono, una menor contribución a la aparente señal solar de 11 años se debe a la QBO, y a la variabilidad interna de la circulación estratosférica. En consecuencia, la mayor intensidad de la señal solar en la baja estratosfera tropical en el modelo WACCM3.5, y la aparente mejora en comparación con WACCM3.1 que se detalla en la primera parte de esta tesis, se deben en parte a la inclusión en esta versión del modelo del efecto de las erupciones volcánicas y de la QBO.

Debido a la presencia de otras fuentes de variabilidad, la atribución de la señal de 11 años en un registro de duración limitada, como las observaciones, es complicada. Como las simulaciones se pueden extender a periodos más largos que las observaciones, es posible cuantificar el número de años requerido para detectar una señal solar robusta, y consiguientemente determinar la viabilidad de la extracción de la señal solar en los registros existentes. En la alta estratosfera tropical (40-50 km), sólo se necesitan 15 años para una estimación fiable de la señal solar, que consiste en un calentamiento de 0.8 K y un aumento relativo de ozono de 2% en máximos

solares, relativo a mínimos del ciclo de 11 años. Sin embargo, en la baja estratosfera tropical (20-30 km), no es posible obtener una estimación robusta de la señal usando una ventana de 25 años, como la que abarcan los registros existentes. Esto se debe a los efectos de las erupciones de El Chichón y Mt. Pinatubo. Si se excluyen los años inmediatamente posteriores a estos eventos (1982,1983,1991,1992), se mitiga el problema de atribución. Por otro lado, también se reduce la amplitud de la aparente señal solar en la baja estratosfera tropical. Para una mejor detección de la señal solar en esta región, se necesitan más observaciones de ciclos solares sin erupciones volcánicas.

La porción de variabilidad cuasi-decadal de la baja estratosfera tropical que se puede atribuir al ciclo solar de 11 años, entonces, es más pequeña de lo que se creía con anterioridad. Estos resultados tienen implicaciones de cara a la interpretación de los mecanismos dinámicos que se han propuesto para explicar la repuesta troposférica a anomalías térmicas en la baja estratosfera tropical [*Haigh et al.*, 2005; *Haigh and Blackburn*, 2006; *Simpson et al.*, 2009]. Los resultados obtenidos sugieren que tales mecanismos están asociados a las erupciones volcánicas, en vez del ciclo solar de 11 años.

En la última parte de esta tesis [*Chiodo et al.*, 2014, submitted], se investiga el impacto de un futuro mínimo de actividad solar bajo condiciones de cambio climático. La debilidad del actual ciclo solar 24 demuestra que el ciclo solar de 11 años está lejos de ser un forzamiento cuasi-periódico. Por lo tanto, repetir los ciclos observados, o el último ciclo 23 para el futuro, como se ha hecho en la mayoría de los modelos del quinto informe del IPCC, no representa un método adecuado para representar la evolución futura del forzamiento solar. Estudios recientes han planteado la posibilidad de que el Sol entre en una prolongada época de actividad reducida [*Abreu et al.*, 2008; *Lockwood et al.*, 2011; *Zolotova and Ponyavin*, 2014] que se asemeje al mínimo de Maunder del siglo XVII [*Eddy*, 1976]. Como no es posible predecir la actividad solar a largo plazo, un mínimo solar representa un posible escenario futuro [*Solanki and Krivova*, 2011].

Se han realizado simulaciones del periodo 2005-2065 con el modelo WACCM4, cuya física es equivalente a la de la versión WACCM35 empleada en las simulaciones antes mencionadas, pero con la inclusión del acoplamiento a un modelo de océano. En un conjunto de simulaciones (MIN), se emplea un mínimo constante para el periodo 2008-2065, calculado a partir de los datos de irradiancia espectral de *Lean et al.* [2005] en las fases de mínimo de los ciclos observados. En otro conjunto, se repiten los 4 ciclos observados (RCP45). Ambos experimentos se fuerzan con el escenario futuro de rango medio de concentración creciente de gases de efecto invernadero empleado en el quinto informe del IPCC, denominado RCP4.5. La única diferencia entre ambos reside en el forzamiento solar y el diseño de los experimentos permite el uso de diferencias climatológicas para caracterizar el impacto del mínimo solar en el clima de la superficie, solventando así el problema de la detección de la señal solar asociado al uso de métodos de regresión, que se ha puesto en evidencia anteriormente [*Chiodo et al.*, 2014].

Los resultados muestran que un mínimo solar constante no tendría impacto sobre el calentamiento global de 1.5 K, simulado para el año 2065. Sin embargo, se encuentra un impacto

significativo en el clima invernal del hemisferio norte. En respuesta al mínimo solar, el modelo predice un patrón de enfriamiento de 1-1.5 K en Siberia y el Estrecho de Bering, que abarca todo el Pacífico en forma de herradura, formando un patrón parecido a la fase negativa de la oscilación decadal del Pacífico ("Pacific Decadal Oscillation", PDO). Por otro lado, el modelo simula un calentamiento en el este de Norte América, relativo al escenario RCP45. En promedio sobre la franja de altas latitudes del hemisferio norte, un mínimo solar reduciría la tendencia de calentamiento global en un 30%, y modularía su distribución espacial.

El patrón PDO se debe a una reducción de la radiación en las bandas del visible, que afecta el balance energético superficial. Además, el enfriamiento en las regiones del Estrecho de Bering se amplifica a través de una menor disminución del hielo marino comparado con el experimento de control (RCP45). Por otro lado, el enfriamiento sobre Siberia se debe a la propagación hacia la superficie de anomalías en el flujo zonal estratosférico, que indican un debilitamiento del vórtice polar, causado por una disminucin en la absorcin de la radiacin ultravioleta. Estos resultados son coherentes con la respuesta del chorro polar a picos de actividad solar, que se detalla en la primera parte de la tesis [*Chiodo et al.*, 2012]. Destacar que este efecto sólo se observa durante la primera época (2005-2035), debido a una respuesta no-lineal del vórtice polar estratosferico al aumento de la concentración de los gases de efecto invernadero. Por lo tanto, el efecto de un mínimo solar durante el invierno boreal se debe principalmente a dos mecanismos, desencadenados ambos por la radiación de diferentes regiones del espectro solar.

Aunque los cambios relativos a la tendencia de calentamiento global son pequeños y limitados geográficamente, una reducción de la actividad solar tendría impacto en zonas muy sensibles al cambio climático, como el límite del hielo marino en el Estrecho de Bering, y las regiones de tundra y permafrost en la Rusia continental. Los resultados de este estudio tienen implicaciones en la evaluación del impacto del calentamiento global sobre los ecosistemas de las zonas sub-árticas. El papel de la incertidumbre representada por la evolución futura del forzamiento solar se debería de tener en cuenta en los futuros informes del IPCC. Para ello, un método posible consistiría en diseñar escenarios solares, como los experimentos realizados en este estudio. Debido a que tanto la radiación en el ultravioleta como en el visible generan anomalías térmicas en diferentes regiones del hemisferio norte, estos resultados también indican que es fundamental emplear la irradiancia espectral en los escenarios solares futuros.

References

Abreu, J., J. Beer, F. Steinhilber, S. Tobias, and N. Weiss (2008), For how long will the current grand maximum of solar activity persist?, *Geophysical Research Letters*, *35*(20).

Anet, J., et al. (2013), Impact of a potential 21st century grand solar minimum on surface temperatures and stratospheric ozone, *Geophysical Research Letters*, *40*(16), 4420–4425.

Anstey, J. A., and T. G. Shepherd (2014), High-latitude influence of the quasi-biennial oscillation, *Quarterly Journal of the Royal Meteorological Society*, *140*(678), 1–21.

Austin, J., et al. (2008), "coupled chemistry climate model simulations of the solar cycle in ozone and temperature", *J. Geophys. Res.*, *113*(D11), 1–20, doi:10.1029/2007JD009391.

Bal, S., S. Schimanke, T. Spangehl, and U. Cubasch (2011), On the robustness of the solar cycle signal in the pacific region, *Geophysical research letters*, *38*(14).

Barriopedro, D., R. García-Herrera, and R. Huth (2008), Solar modulation of northern hemisphere winter blocking, *J. Geophys. Res.*, *113*(D14118), doi:10.1029/2008JD009789.

Box, G., and G. Jenkins (1980), *Time Series Analysis. Forecasting and Control*, Holder Day, San Francisco.

Brasseur, G. (1993), The response of the middle atmosphere to long-term and short-term solar variability: A two-dimensional model, *Journal of Geophysical Research: Atmospheres (1984–2012)*, *98*(D12), 23,079–23,090.

Calvo, N., M. Giorgetta, and C. Pena-Ortiz (2007), Sensitivity of the boreal winter circulation in the middle atmosphere to the quasi-biennial oscillation in MAECHAM5 simulations, *J. Geophys. Res.*, *112*(D10), D10,124.

Calvo, N., M. Giorgetta, R. Garcia-Herrera, and E. Manzini (2009), Nonlinearity of the combined warm ENSO and QBO effects on the Northern Hemisphere polar vortex in MAECHAM5 simulations, *J. Geophys. Res.*, *114*(D13), D13,109.

Camp, C. D., and K.-K. Tung (2007), The influence of the solar cycle and qbo on the late-winter stratospheric polar vortex, *Journal of the atmospheric sciences*, *64*(4), 1267–1283.

CCMVal-2 (2010), SPARC CCMVal Report on the Evaluation of Chemistry-Climate Models, edited by: Eyring, V., Shepherd, TG, and Waugh, DW, *Tech. rep.*, SPARC Report No. 5, WCRP-132, WMO/TD-No. 1526.

Charlton, A. J., L. M. Polvani, J. Perlwitz, F. Sassi, E. Manzini, K. Shibata, S. Pawson, J. E. Nielsen, and D. Rind (2007), A new look at stratospheric sudden warmings. part ii: Evaluation of numerical model simulations, *Journal of Climate*, *20*(3), 470–488.

Chiodo, G., N. Calvo, D. Marsh, and R. Garcia-Herrera (2012), The 11 year solar cycle signal in transient simulations from the whole atmosphere community climate model, *Journal of Geophysical Research: Atmospheres (1984–2012)*, *117*(D6).

Chiodo, G., D. Marsh, R. Garcia-Herrera, N. Calvo, and J. García (2014), On the detection of the solar signal in the tropical stratosphere, *Atmospheric Chemistry and Physics*, *14*(11), 5251–5269.

Chiodo, G., R. Garcia-Herrera, N. Calvo, J. Vaquero, and J. Añel (2014, submitted), The impact of a future solar minimum under a climate change scenario, *Nature Climate Change*.

Christoforou, P., and S. Hameed (1997), Solar cycle and the pacific centers of action', *Geophysical Research Letters*, *24*(3), 293–296.

Collins, W., et al. (2004), Description of the NCAR community atmosphere model (CAM 3.0), *NCAR Tech. Note NCAR/TN-464+ STR*.

Conley, A., J.-F. Lamarque, F. Vitt, W. Collins, and J. Kiehl (2012), Port, a cesm tool for the diagnosis of radiative forcing, *Geoscientific Model Development Discussions*, *5*(3), 2687–2704.

Eddy, J. A. (1976), The maunder minimum, *Science*, *192*(4245), 1189–1202.

Egorova, T., E. Rozanov, E. Manzini, M. Haberreiter, W. Schmutz, V. Zubov, and T. Peter (2004), Chemical and dynamical response to the 11-year variability of the solar irradiance simulated with a chemistry-climate model, *Geophys. Res. Lett.*, *31*(6119), 1–4, doi:10.1029/2003GL019294.

Eyring, V., et al. (2008), Overview of the new ccmval reference and sensitivity simulations in support of upcoming ozone and climate assessments and the planned sparc ccmval report, *SPARC Newsl*, *30*, 20–26.

Feulner, G. (2011), Are the most recent estimates for maunder minimum solar irradiance in agreement with temperature reconstructions?, *Geophysical Research Letters*, *38*(16).

Feulner, G., and S. Rahmstorf (2010), On the effect of a new grand minimum of solar activity on the future climate on Earth, *Geophys. Res. Lett.*, *37*, 5707–+, doi:10.1029/2010GL042710.

Frame, T., and L. J. Gray (2010), The 11-year solar cycle in era-40 data: an update to 2008, *J. Clim.*, *23*, 2213–2222, doi:10.1175/2009JCLI3150.1.

Fröhlich, C., and J. Lean (2004), Solar radiative output and its variability: evidence and mechanisms, *The Astronomy and Astrophysics Review*, *12*(4), 273–320.

Garcia, R. R. (2010), Atmospheric physics: Solar surprise?, *Nature*, *467*(7316), 668–669.

Garny, H., G. Bodeker, and M. Dameris (2007), Trends and variability in stratospheric mixing: 1979 - 2005, *Atmos. Chem. Phys.*, *7*(3), 6189–6228.

Gimeno, L., L. de la Torre, R. Nieto, R. Garcıa, E. Hernández, and P. Ribera (2003), Changes in the relationship nao–northern hemisphere temperature due to solar activity, *Earth and Planetary Science Letters*, *206*(1), 15–20.

Gray, L., S. Rumbold, and K. Shine (2009), Stratospheric temperature and radiative forcing response to 11-year solar cycle changes in irradiance and ozone, *J. Atmos. Sci.*, *66*(8), 2402–2417.

Gray, L., et al. (2010), Solar influences on climate, *Rev. Geophys.*, *48*(RG4001), 1–53, doi: 10.1029/2009RG000282.

Haigh, J. (1994), The role of stratospheric ozone in modulating the solar radiative forcing of climate, *Nat.*, *370*(6490), 544–546.

Haigh, J. (2003), The effects of solar variability on the Earth's climate, *Philosophical Transactions of the Royal Society of London. Series A: Mathematical, Physical and Engineering Sci.s*, *361*(1802), 95.

Haigh, J., and M. Blackburn (2006), Solar influences on dynamical coupling between the stratosphere and troposphere, *Space Sci. Reviews*, *125*(1), 331–344, doi:10.1007/s11214-006-9067-0.

Haigh, J., M. Blackburn, and R. Day (2005), The response of tropospheric circulation to perturbations in lower-stratospheric temperature, *J. Clim.*, *18*, 3672–3685.

Haigh, J. D., A. R. Winning, R. Toumi, and J. W. Harder (2010), An influence of solar spectral variations on radiative forcing of climate, *Nature*, *467*(7316), 696–699.

Harder, J. W., J. M. Fontenla, P. Pilewskie, E. C. Richard, and T. N. Woods (2009), Trends in solar spectral irradiance variability in the visible and infrared, *Geophysical Research Letters*, *36*(7).

Hathaway, D. H., R. M. Wilson, and E. J. Reichmann (2002), Group sunspot numbers: Sunspot cycle characteristics, *Solar Physics*, *211*(1-2), 357–370.

Holton, J., and H. Tan (1980), The influence of the equatorial quasi-biennial oscillation on the global circulation at 50 mb, *J. Atmos. Sci.*, *37*, 2200–2208.

Hood, L. (1997), The solar cycle variation of total ozone: Dynamical forcing in the lower stratosphere, *J. Geophys. Res.*, *102*(D1), 1355–1370.

Hoyt, D. V., and K. H. Schatten (1998), Group sunspot numbers: A new solar activity reconstruction, *Solar physics*, *181*(2), 491–491.

Huang, T., and G. Brasseur (1993), Effect of long-term solar variability in a two-dimensional interactive model of the middle atmosphere, *J. Geophys. Res.*, *98*(D11), 413–420, doi:10.1029/93JD02187.

Hurrell, J. W., J. J. Hack, D. Shea, J. M. Caron, and J. Rosinski (2008), A new sea surface temperature and sea ice boundary dataset for the community atmosphere model, *Journal of Climate*, *21*(19), 5145–5153.

Ineson, S., A. A. Scaife, J. R. Knight, J. C. Manners, N. J. Dunstone, L. J. Gray, and J. D. Haigh (2011), Solar forcing of winter climate variability in the northern hemisphere, *Nature Geoscience*, *4*(11), 753–757.

Jones, G. S., M. Lockwood, and P. A. Stott (2012), What influence will future solar activity changes over the 21st century have on projected global near-surface temperature changes?, *Journal of Geophysical Research: Atmospheres (1984–2012)*, *117*(D5).

Kinnison, D., et al. (2007), Sensitivity of chemical tracers to meteorological parameters in the MOZART-3 chemical transport model, *J. Geophys. Res.*, *112*, D20,302, doi:10.1029/2006JD007879.

Kodera, K. (2003), Solar influence on the spatial structure of the nao during the winter 1900–1999, *Geophysical Research Letters*, *30*(4).

Kodera, K. (2004), Solar influence on the indian ocean monsoon through dynamical processes, *Geophys. Res. Lett*, *31*(10.1029), doi:10.1029/2004GL020928.

Kodera, K., and Y. Kuroda (2002), Dynamical response to the solar cycle, *J. Geophys. Res.*, *107*(D24), 4749, doi:10.1029/2002JD002224.

Kodera, K., and K. Shibata (2006), Solar influence on the tropical stratosphere and troposphere in the northern summer, *Geophys. Res. Lett*, *33*(L19704), doi:10.1029/2006GL026659.

Krivova, N., S. Solanki, and L. Floyd (2006), Reconstruction of solar uv irradiance in cycle 23, *Astronomy & Astrophysics*, *452*(2), 631–639.

Labitzke, K. (1987), Sunspots, the qbo, and the stratospheric temperature in the north polar region, *Geophys. Res. Lett.*, *14*(5), 535–537, doi:10.1029/GL014i005p00535.

Labitzke, K. (2004), On the signal of the 11-year sunspot cycle in the stratosphere and its modulation by the quasi-biennial oscillation, *J. Atmos. Sol. Terr. Phys.*, *66*(13-14), 1151–1157, doi:10.1016/j.jastp.2004.05.011.

Labitzke, K. (2005), On the solar cycle-QBO relationship: a summary, *J. Atmos. Sol. Terr. Phys.*, *67*(1-2), 45–54, doi:10.1016/j.jastp.2004.07.016.

Labitzke, K., and M. Kunze (2009), On the remarkable arctic winter in 2008/2009, *Journal of Geophysical Research: Atmospheres (1984–2012)*, *114*(D1).

Labitzke, K., and H. Loon (1989), Association between the 11-Yr Solar Cycle, the QBO, and the Atmosphere. Part III: Aspects of the Association, *J. Clim.*, *2*(6), 554–565, doi:http://dx.doi.org/10.1175/1520-0442(1989)002⟨0554:ABTYSC⟩2.0.CO;2.

Labitzke, K., M. Kunze, and S. Broennimann (2006), Sunspots, the QBO and the stratosphere in the North Polar Region-20 years later, *Met. Zeit.*, *15*(3), 355–364, doi:http://dx.doi.org/10.1127/0941-2948/2006/0136.

Laken, B. A., E. Pallé, J. Čalogović, and E. M. Dunne (2012), A cosmic ray-climate link and cloud observations, *Journal of Space Weather and Space Climate*, *2*, A18.

Le Mouël, J.-L., M. G. Shnirman, and E. M. Blanter (2007), The 27-day signal in sunspot number series and the solar dynamo, *Solar Physics*, *246*(2), 295–307.

Lean, J. (2000), Evolution of the Sun s spectral irradiance since the Maunder Minimum, *Geophys. Res. Lett*, *27*(16), 2425–2428.

Lean, J., J. Beer, and R. Bradley (1995), Reconstruction of solar irradiance since 1610: Implications for climate change, *Geophysical Research Letters*, *22*(23), 3195–3198.

Lean, J., G. Rottman, H. Kyle, T. Woods, J. Hickey, and L. Puga (1997), Detection and parameterization of variations in solar mid-and near-ultraviolet radiation (200–400 nm), *J. Geophys. Res.*, *102*(D25), 29,939, doi:10.1029/97JD02092.

Lean, J., G. Rottman, J. Harder, and G. Kopp (2005), Sorce contributions to new understanding of global change and solar variability, *The Solar Radiation and Climate Experiment (SORCE)*, pp. 27–53, doi:10.1007/0-387-37625-9_3.

Lee, H., and A. Smith (2003), Simulation of the combined effects of solar cycle, quasi-biennial oscillation, and volcanic forcing on stratospheric ozone changes in recent decades, *J. Geophys. Res.*, *108*(4049), 16, doi:10.1029/2001JD001503.

Lin, S. (2004), A vertically lagrangian finite-volume dynamical core for global models, *Mon. Weather Rev.*, *132*, 2293–2307, doi:http://dx.doi.org/10.1175/1520-0493(2004)132⟨2293:AVLFDC⟩2.0.CO;2.

Lockwood, M., M. Owens, L. Barnard, C. Davis, and F. Steinhilber (2011), The persistence of solar activity indicators and the descent of the sun into maunder minimum conditions, *Geophysical Research Letters*, *38*(22).

Lu, H., M. P. Baldwin, L. J. Gray, and M. J. Jarvis (2008), Decadal-scale changes in the effect of the qbo on the northern stratospheric polar vortex, *Journal of Geophysical Research: Atmospheres (1984–2012)*, *113*(D10).

Marsh, D., and R. Garcia (2007), Attribution of decadal variability in lower-stratospheric tropical ozone, *Geophys. Res. Lett.*, *34*(21), L21,807, doi:10.1029/2007GL030935.

Marsh, D., R. Garcia, D. Kinnison, B. Boville, F. Sassi, S. Solomon, and K. Matthes (2007), Modeling the whole atmosphere response to solar cycle changes in radiative and geomagnetic forcing, *J. Geophys. Res.*, *112*(D23306), doi:10.1029/2006JD008306.

Marsh, N. D., and H. Svensmark (2000), Low cloud properties influenced by cosmic rays, *Physical Review Letters*, *85*(23), 5004.

Matthes, K., K. Kodera, J. Haigh, D. Shindell, K. Shibata, U. Langematz, E. Rozanov, and Y. Kuroda (2003), Grips solar experiments intercomparison project: Initial results, *Papers in Meteorology and Geophysics*, *54*(2), 71–90.

Matthes, K., U. Langematz, L. Gray, K. Kodera, and K. Labitzke (2004), Improved 11-year solar signal in the freie universitaet Berlin climate middle atmosphere model (FUB-CMAM), *J. Geophys. Res.*, *109*(D06101), 15, doi:10.1029/2003JD004012.

Matthes, K., Y. Kuroda, K. Kodera, and L. U. (2006), Transfer of the solar signal from the stratosphere to the troposphere: Northern winter, *J. Geophys. Res.*, *111*(D6), D06,108, doi: 10.1029/2005JD006283.

Matthes, K., D. Marsh, R. Garcia, D. Kinnison, F. Sassi, and S. Walters (2010), Role of the QBO in modulating the influence of the 11 year solar cycle on the atmosphere using constant forcings, *J. Geophys. Res.*, *115*(D18), D18,110, doi:10.1029/2009JD013020.

Matthes, K., K. Kodera, R. R. Garcia, Y. Kuroda, D. R. Marsh, and K. Labitzke (2013), The importance of time-varying forcing for qbo modulation of the atmospheric 11 year solar cycle signal, *Journal of Geophysical Research: Atmospheres*, *118*(10), 4435–4447.

Meehl, G., J. Arblaster, K. Matthes, F. Sassi, and H. van Loon (2009), Amplifying the Pacific climate system response to a small 11-year solar cycle forcing, *Sci.*, *325*(5944), 1114–1118, doi:10.1126/science.1172872.

Meehl, G. A., and J. M. Arblaster (2009), A lagged warm event-like response to peaks in solar forcing in the pacific region, *Journal of Climate*, *22*(13), 3647–3660.

Meehl, G. A., J. M. Arblaster, and D. R. Marsh (2013), Could a future grand solar minimum like the maunder minimum stop global warming?, *Geophysical Research Letters*, *40*(9), 1789–1793.

Merkel, A. W., J. W. Harder, D. R. Marsh, A. K. Smith, J. M. Fontenla, and T. N. Woods (2011), The impact of solar spectral irradiance variability on middle atmospheric ozone, *Geophysical Research Letters*, *38*(13).

Misios, S., and H. Schmidt (2012), Mechanisms involved in the amplification of the 11-yr solar cycle signal in the tropical pacific ocean, *Journal of Climate*, *25*(14), 5102–5118.

Misios, S., and H. Schmidt (2013), The role of the oceans in shaping the tropospheric response to the 11 year solar cycle, *Geophysical Research Letters*, *40*(24), 6373–6377.

Mohanakumar, K. (2008), *Stratosphere troposphere interactions*, Springer.

Pittock, A. B. (1978), A critical look at long-term sun-weather relationships, *Reviews of Geophysics*, *16*(3), 400–420.

Randel, W., and F. Wu (2007), A stratospheric ozone profile data set for 1979–2005: Variability, trends, and comparisons with column ozone data, *J. Geophys. Res*, *112*, D06,313, doi:10.1029/2006JD007339.

Richter, J., F. Sassi, and R. Garcia (2009), Towards a physically based gravity wave source parameterization in a general circulation model, *J. Atm. Sci.*, *67*, 136–156, doi:http://dx.doi.org/10.1175/2009JAS3112.1.

Rienecker, M. M., et al. (2011), Merra: Nasa's modern-era retrospective analysis for research and applications, *Journal of Climate*, *24*(14), 3624–3648.

Rottman, G., L. Floyd, and R. Viereck (2003), Measurements of the solar ultraviolet irradiance, *Solar Variability and Its Effects on Climate*, pp. 111–125.

Roy, I., and J. D. Haigh (2010), Solar cycle signals in sea level pressure and sea surface temperature, *Atmospheric Chemistry and Physics*, *10*(6), 3147–3153.

Roy, I., and J. D. Haigh (2012), Solar cycle signals in the pacific and the issue of timings, *Journal of the Atmospheric Sciences*, *69*(4), 1446–1451.

Rozanov, E., M. Schlesinger, T. Egorova, B. Li, N. Andronova, and V. Zubov (2004), Atmospheric response to the observed increase of solar uv radiation from solar minimum to solar maximum simulated by the university of illinois at urbana-champaign climate-chemistry model, *J. Geophys. Res.*, *109*(D18), 01,110, doi:10.1029/2003JD003796.

Schmidt, H., G. Brasseur, and M. Giorgetta (2010), Solar cycle signal in a general circulation and chemistry model with internally generated quasi biennial oscillation, *J. Geophys. Res.*, *115*(D00I14), 16, doi:10.1029/2009JD012542.

Schrijver, C., W. Livingston, T. Woods, and R. Mewaldt (2011), The minimal solar activity in 2008–2009 and its implications for long-term climate modeling, *Geophysical Research Letters*, *38*(6).

Shapiro, A., W. Schmutz, E. Rozanov, M. Schoell, M. Haberreiter, A. Shapiro, and S. Nyeki (2011), A new approach to the long-term reconstruction of the solar irradiance leads to large historical solar forcing, *Astronomy & Astrophysics*, *529*, A67.

Shindell, D. T., G. A. Schmidt, M. E. Mann, D. Rind, and A. Waple (2001), Solar forcing of regional climate change during the maunder minimum, *Science*, *294*(5549), 2149–2152.

Simpson, I. R., M. Blackburn, and J. D. Haigh (2009), The role of eddies in driving the tropospheric response to stratospheric heating perturbations, *Journal of the Atmospheric Sciences*, *66*(5), 1347–1365.

Smith, A., and K. Matthes (2008), Decadal-scale periodicities in the stratosphere associated with the solar cycle and the QBO, *J. Geophys. Res.*, *113*, D05,311, doi:10.1029/2007JD009051.

Solanki, S. K., and N. A. Krivova (2011), Analyzing solar cycles, *Science*, *334*(6058), 916–917.

Soukharev, B., and L. Hood (2006), Solar cycle variation of stratospheric ozone: Multiple regression analysis of long-term satellite data sets and comparisons with models, *J. Geophys. Res.*, *111*(D20314), doi:10.1029/2006JD007107.

Steinhilber, F., et al. (2012), 9,400 years of cosmic radiation and solar activity from ice cores and tree rings, *Proceedings of the National Academy of Sciences*, *109*(16), 5967–5971.

Stocker, T. F., et al. (2013), Climate change 2013: The physical science basis, *Intergovernmental Panel on Climate Change, Working Group I Contribution to the IPCC Fifth Assessment Report (AR5)(Cambridge Univ Press, New York)*.

Thomason, L., L. Poole, and T. Deshler (1997), A global climatology of stratospheric aerosol surface area density deduced from stratospheric aerosol and gas experiment ii measurements: 1984–1994, *Journal of Geophysical Research: Atmospheres (1984–2012)*, *102*(D7), 8967–8976.

Tiao, G., G. Reinsel, D. Xu, J. Pedrick, X. Zhu, A. Miller, J. DeLuisi, C. Mateer, and D. Wuebbles (1990), Effects of autocorrelation and temporal sampling schemes on estimates of trend and spatial correlation, *J. Geophys. Res.*, *95*(D12), 20,507–20,517, doi:10.1029/JD095iD12p20507.

Tilmes, S., R. Garcia, D. Kinnison, A. Gettelman, and P. Rasch (2009), Impact of geoengineered aerosols on the troposphere and stratosphere, *J. Geophys. Res.*, *114*(D12305), doi:10.1029/2008JD011420.

Tourpali, K., C. Schuurmans, R. Van Dorland, B. Steil, and C. Brühl (2003), Stratospheric and tropospheric response to enhanced solar uv radiation: A model study, *Geophys. Res. Lett.*, *30*(1231), 4, doi:10.1029/2002GL016650.

Tsutsui, J., K. Nishizawa, and F. Sassi (2009), Response of the middle atmosphere to the 11-year solar cycle simulated with the Whole Atmosphere Community Climate Model, *J. Geophys. Res.*, *114*(D2111), doi:10.1029/2008JD010316.

Tung, K.-K., and J. Zhou (2010), The pacific's response to surface heating in 130 yr of sst: La niña-like or el niño-like?, *Journal of the Atmospheric Sciences*, *67*(8), 2649–2657.

van Loon, H., and G. A. Meehl (2008), The response in the pacific to the sun's decadal peaks and contrasts to cold events in the southern oscillation, *Journal of Atmospheric and Solar-Terrestrial Physics*, *70*(7), 1046–1055.

Vaquero, J. M., M. Gallego, I. G. Usoskin, and G. A. Kovaltsov (2011), Revisited sunspot data: a new scenario for the onset of the maunder minimum, *The Astrophysical Journal Letters*, *731*(2), L24.

Wang, Y.-M., J. Lean, and N. Sheeley Jr (2005), Modeling the sun's magnetic field and irradiance since 1713, *The Astrophysical Journal*, *625*(1), 522.

White, W., and Z. Liu (2008), Non-linear alignment of el nino to the 11-yr solar cycle, *Geophys. Res. Lett*, *35*(L19607), doi:10.1029/2008GL034831.

White, W. B., J. Lean, D. R. Cayan, and M. D. Dettinger (1997), Response of global upper ocean temperature to changing solar irradiance, *JOURNAL OF GEOPHYSICAL RESEARCH*, *102*(C2), 3255–3266.

Wilks, D. S. (2011), *Statistical methods in the atmospheric sciences*, vol. 100, Academic press.

Yousef, S. M. (2000), The solar wolf-gleissberg cycle and its influence on the earth, in *Proceedings of the international conference on the environmental hazards mitigation, Cairo University, Cairo*.

Zolotova, N. V., and D. I. Ponyavin (2014), Is the new Grand minimum in progress?, *Journal of Geophysical Research (Space Physics)*, *119*, 3281–3285, doi:10.1002/2013JA019751.

Zwiers, F. W., and H. von Storch (1995), Taking serial correlation into account in tests of the mean, *Journal of Climate*, *8*(2), 336–351.